constant as previously considered in the absence of measurements of N_L for twins and ε platelets [5.6]. Since the growth of a twin corresponds to the propagation of Shockley dislocations on every plane, it is reasonable to assume a constant aspect ratio for twins i.e. thickness to diameter ratio. If $\bar{t} = c\,\bar{D}$ then f should equal $4c\ N_L^2/N_A$. Fig. 3 illustrates the variation of N_L^2/N_A with the volume fraction. There is some scatter in the data for large volume fractions which is due to the difficulty of determining N_A, the number of twins per unit area, under these conditions. However a regression analysis of the results shows that the hypothesis does hold with $\bar{D}/\bar{t} = 26$ independently of temperature. This yields in particular for the diameter of the first twins to form $d_o = 47$ and 26μm at 293K and 473K respectively.

IV. The Nucleation Model

The formation of a twin can be considered as achieved by the propagation of stacking faults in neighbouring planes as for ε platelets. Most of the models proposed for the nucleation of a twin from a single stacking fault are in fact growth models [see e.g. 12]. Recently Mahajan and coworkers have proposed that fcc twin nuclei (or hcp martensite

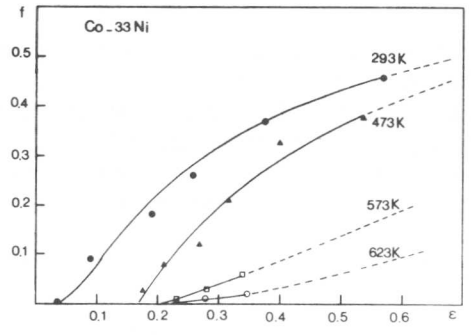

Fig. 1

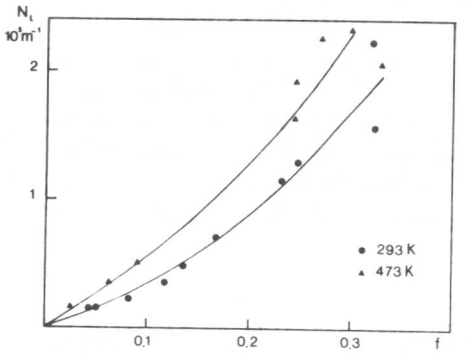

Fig. 2

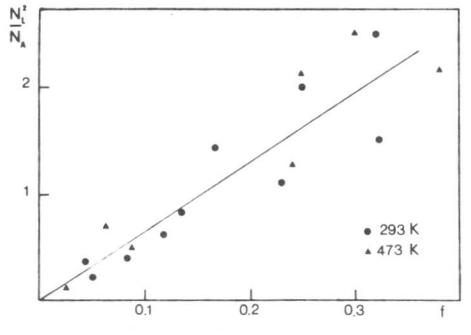

Fig. 3

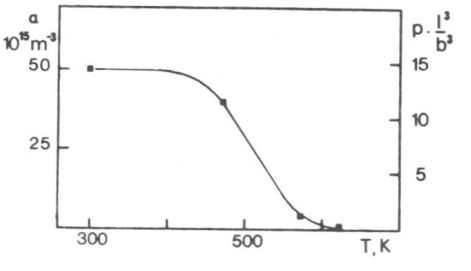

Fig. 4

nuclei) can be three layer microtwins (six layer hcp platelets) [13,14]. These microtwins (or hcp platelets) may evolve from the interaction of two perfect dislocations; these dislocations may be coplanar slip dislocations as considered by these authors or also dislocations of different slip planeswith the primary plane of one dislocation being the cross slip plane of the other. However the twin nuclei evolve from the interaction of perfect slip dislocations with suitable Burgers vectors for a resolved shear stress higher than a critical value. The existence of a critical stress for the occurrence of fcc twinning is strongly borne out by single crystal experiments [12, 15]. Accordingly in the case of polycrystals twinning will only occur for a critical strain ε_c which corresponds on the average to the critical stress level.

Accordingly the number of macroscopic twins which form per unit volume of matrix can be assumed to be proportional to the number of dislocations which interact n_i. For an applied strain increase $d\varepsilon p$ the number of twins per unit volume of specimen increases from N_V to N_V+dN_V with :

$$dN_V = (1 - f)\ p\ dn_i \qquad (2)$$

where p is a constant independent of the strain level which is the efficiency of dislocation interactions in nucleating twins and which should vary with SFE.

The number of dislocations per unit volume n_V can be obtained by considering dislocations as rods of length $k \times \rho^{-1/2}$with ρ the dislocation density per unit area and k a constant around 16 as obtained for cell size by Staker and Holt [16], which yields $n_V = (2/k)\ \rho^{3/2}$. It can be shown from stereology that the number of dislocation interactions per unit volume of the matrix n_i is proportional to the square of n_V :

$$n_i \simeq \frac{2}{3}\ \pi\ l^3\ \ n_V^2 \qquad (3)$$

with l the distance of interaction between total dislocations which should be of the order of b the Burgers vector for perfect dislocations but in the present case l could be higher thanks to the low value of SFE. In the following this distance will be treated as constant and independent of temperature. The number of dislocation interactions is therefore directly related to the matrix strain ε since the dislocation density has been shown to be proportional to the strain in a low SFE austenitic stainless steel with a proportionality constant $K \sim 2.4\ 10^{15}\ m^{-2}$ [17]. In the following the matrix strain is identified with applied strain, which has been shown to be a reasonable approximation [6].

On the other hand the increment of number of twins per unit volume dN_V can be written as :

$$dN_V = d\ (\frac{f}{\bar{v}}) \qquad (4)$$

with $\bar{v}$ the mean twin volume. The average volume can be expressed as a function of f taking into account Eq. (1) and the constant aspect ratio, by :

$$v = v_o(1-f)^q \qquad (5)$$

where q = 3n and V_o the volume of the first twins to form is 2.75 10^{-15} and 0.60 10^{-15} m^3 at 293K and 473K respectively. Substituting Eqs (4), (5) and (3) into Eq. (2) one obtains a differential equation relating f and ε. This equation can be easily integrated remembering the boundary condition $\varepsilon = \varepsilon_c$ for f = 0, which gives :

$$\Phi(f) = \alpha(\varepsilon^3 - \varepsilon_c^3) \qquad (6a)$$

with $$\Phi(f) \equiv \frac{1}{v_o} \cdot \frac{1}{q(q+1)} \cdot \{ \frac{1+(q^2-1)f}{(1-f)^{q+1}} - 1 \} \qquad (6b)$$

and $$\alpha = p \cdot (8\pi/3) \cdot l^3 K^3 / k^2 \qquad (6c)$$

Accordingly the volume fraction of twins is expressed as a function of strain through an implicit function which depends upon two parameters ε_c and α. ε_c is related to the existence of a twinning stress which depends upon the SFE see e.g.[12]. α which has the dimension of the inverse of a volume, is proportional to p the efficiency of dislocation interactions in nucleating twins. In Eq. (6c) all the constants are known except l the distance of interaction of dislocations which is some multiple of the Burgers vector.

V. Discussion

The nucleation model as defined by Eq. (6) has been fitted to the data of Fig. 1 assuming that the growth process of twins was described by Eq. (5) at 573K and 623K with the same constants as at 473K. One can check in Fig. 1 that the kinetic curves so obtained, as indicated by solid lines before necking and dotted lines for higher strains, are in good agreement with experimental results at the various temperatures.

The values of the critical strain ε_c at the onset of twinning are given in Table I with the corresponding critical shear stress for twinning estimated from the tensile stress using Taylor's theory [6] .

Table I Estimation of the twinning stress from the critical strain ε_c at the onset of twinning

Temperature (K)	ε_c	twinning stress ($10^{-3}\mu$)	mJ/m^2	SFE	$10^{-3}\mu b$
293	.035	0.8	15		0.80
473	.17	1.8	24		1.32
573	.20	2	29		1.67
623	.22	2.1	31.5		1.85

μ and b are shear modulus and Burgers vector of slip dislocation respectively.

The large temperature dependence of the twinning stress shown in Table I is simply the result of the large increase of intrinsic SFE with increasing temperature. This behaviour is in good agreement with most results obtained on both single and polycrystals with fcc structure [see e.g.7,12].

The variation of the α parameter is reported in Fig. 4 as a function of temperature. However this parameter has the drawback to be not dimensionless and of no direct physical meaning. So we have also given in the same diagram the constant $p\ l^3/b^3$ to which α is proportional. A direct estimation of p is unfortunately beyond the present possibilities of dislocation description of the deformed state. This would require first a good theory of deformation by both slip and twinning not yet available and a statistical evaluation of the proportion of total dislocation interactions giving rise to twin nuclei. In addition l the distance of interaction between two dissociated dislocations is needed as the ratio of the density of mobile dislocations to the overall density, assumed here constant. Remembering these limitations, both α and $p\ l^3/b^3$ vary with decreasing temperature as a the probability function of a gaussian distribution with respect ot temperature i.e. with respect to SFE which is linearly related to temperature above 293K. The mean and standard deviation of this distribution are 513 and 47K for temperature or 26 and 2.5 mJm^{-2} for SFE. This behaviour is in good agreement with that expected from the model : the efficiency of events of dislocation interactions giving rise to twin nuclei increases when the SFE decreases and low enough values of SFE.

Finally it is worth noting the strong partitioning effect which is due to the fact that twins are strong obstacles to the propagation of twinning dislocations as discussed previously [7,18]. The lower values of the dimensions of the first twins to form at 473K as compared to 293K and their lower dependence upon the amount of transformation can be explained as follows : at 473K twinning appears at a higher critical stress and thus higher strain. Accordingly twinning partials have to propagate into a denser dislocation array which impedes their growth.

References

1 T. Angel, J. Iron Steel Inst., 177 (1954), 165.
2 P.I. Mangonon and G. Thomas, Met. Trans., 1 (1970), 1587.
3 W.W. Gerberich, G. Thomas, E.R. Parker and V.F. Zackay, Proc. 2nd Int.Conf. on the Strength of Metals and Alloys, Asilomar, U.S.A. (1970).
4 G.B. Olson and M. Cohen, Met. Trans., 6 (1975), 791.
5 L. Rémy, Met. Trans. A, 8A (1977), 253.
6 L. Rémy, Acta Met., 26 (1978), 443.
7 L. Rémy, Thesis, Orsay - Paris XI, (1975).
8 L. Rémy, Acta Met., 25 (1977), 173.
9 L. Rémy, A. Pineau and B. Thomas, Mat. Sci. Eng., 36 (1978), 47.
10 V. Raghavan and M. Cohen, Met. Trans., 2 (1971), 2409.
11 R.L. Fullman, Trans. A.I.M.E., 197 (1953), 447.
12 J.A. Venables, in Deformation Twinning, Gordon and Breach, New York (1964), 77.
13 S. Mahajan and G.Y. Chin, Acta Met., 21 (1973), 1353.
14 S. Mahajan, M.L. Green and D. Brasen, Met. Trans. A, 8A (1977), 283.
15 G.Y. Chin, W.F. Hosford and D.R. Mendorf, Proc. R. Soc. London, Ser. A, 309 (1969), 433.
16 M.R. Staker and D.L. Holt, Acta Met., 20 (1972), 569.
17 J. Piqueras and R. Lagneborg, Mém. Scient. Revue Métall., 66 (1969), 713.
18 L. Rémy, Acta Met., 25 (1977), 711.

Obsevation of Early Stages of Martensite Formation in Fe-Ni-Mn Alloy

Setsuo Kajiwara

In an attempt to understand the nucleation mechanism of the martensitic transformation, early stages of the martensite formation in an Fe-Ni-Mn alloy were observed by a 500 kV electron microscope. The observed results show that the invariant plane strain condition is the controlling factor for the martensite formation even in its nucleation stage.

I. Introduction

Observation of early stages of martensite formation is a vital step toward the understanding of nucleation mechanism of martensitic transformation, but no successful attempts have been made so far although a few scattered observations were reported [1-2]. The main reason for the failure of such an observation was due to the fact that martensite plates usually grow to their final sizes once they have nucleated. Recently the present author found by optical microscope that the martensite plate formed isothermally in Fe-Ni-Mn alloys is not a single plate but consists of small, fragmented plates which are aligned along the habit plane [3]. This fact suggests a possibility that very small martensite plates which are considered as early stages of martensite formation may be observed by electron microscope. In the present work such observations were performed using 500 kV electron microscope and the results are discussed in connection to current nucleation models.

II. Experimental Method

Rolled sheets of Fe-22.88Ni-3.81Mn (wt.%) with 0.3 mm thickness were heated in evacuated silica capsules at 1423 K for 20 min and quenched into water. In this heat treatment the specimens were enveloped by a sheet of Fe-Mn alloy to prevent the sublimation of Mn atoms. After removing a surface layer of 0.05 mm, the specimens were quenched to 77 K or to 143 K, and kept there for 1 month (at 77 K) or 1 week (at 143 K). At these low temperatures the martensitic transformation from fcc to bcc ocurred isothermally. Thin foils prepared from these specimens were observed by a 500 kV electron microscope.

III. Experimental Results

The essentially same results were obtained for both the specimens transformed at 77 K and 143 K. Figs. 1(a) and (b) show a group of martensite platelets typically observed in this study. Micrographs (a) and (b) in these figures are at different diffracting conditions. Each martensite plate has a straight edge parallel to direction A. It was found that this direction coincides with the projection of a $\langle 110 \rangle_f$

National Research Institute for Metals
2-3-12 Nakameguro, Meguro-ku, Tokyo 153, Japan

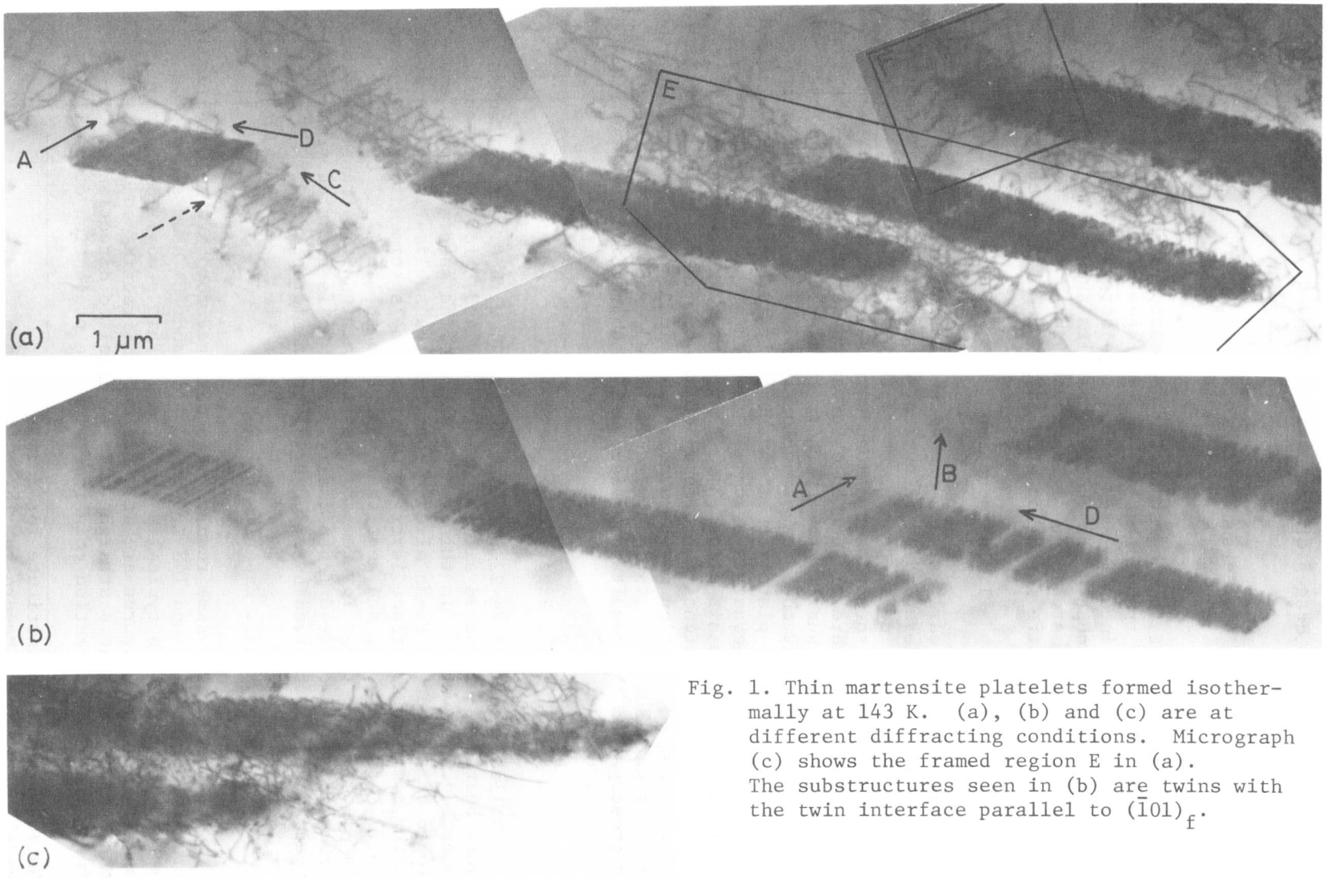

Fig. 1. Thin martensite platelets formed isothermally at 143 K. (a), (b) and (c) are at different diffracting conditions. Micrograph (c) shows the framed region E in (a). The substructures seen in (b) are twins with the twin interface parallel to $(\bar{1}01)_f$.

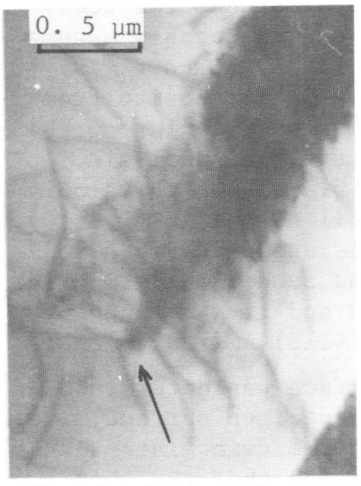

Fig. 3. Nucleating stage of martensite. The micrograph is an enlarged one of area F in Fig. 1(a).

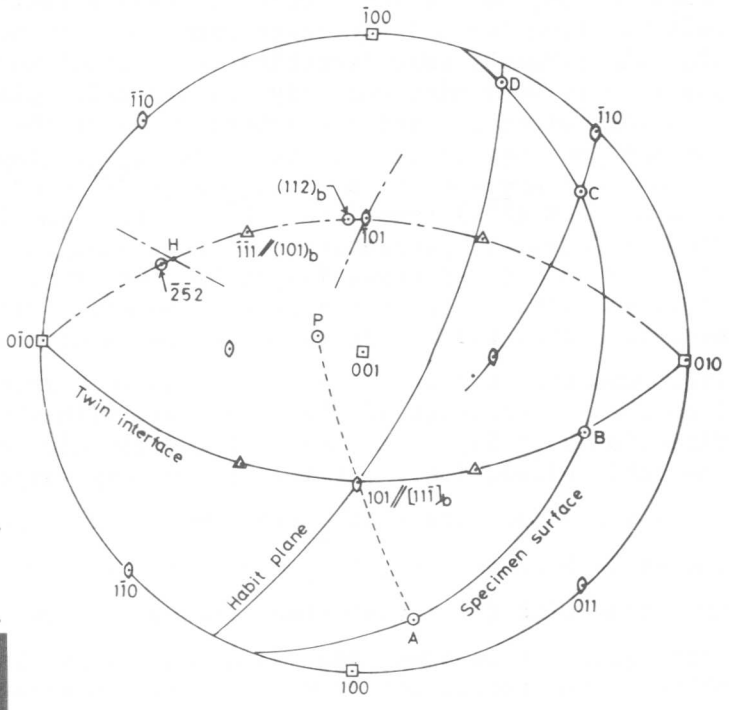

Fig. 2. Stereographic analysis of crystallographic features of thin martensite plate.

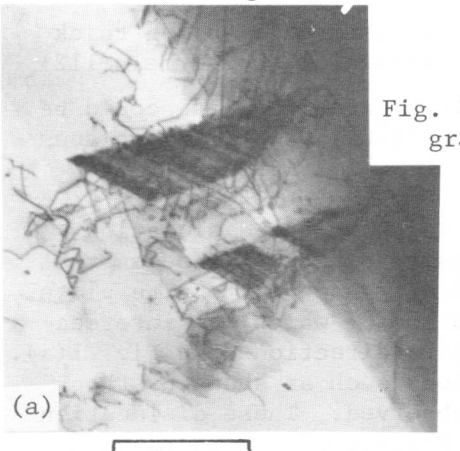

1 μm

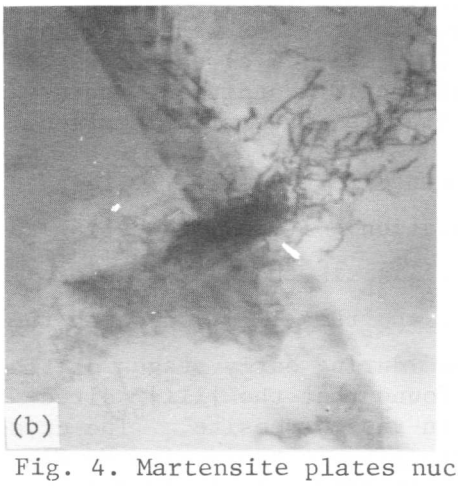

Fig. 4. Martensite plates nucleating from a grain boundary.

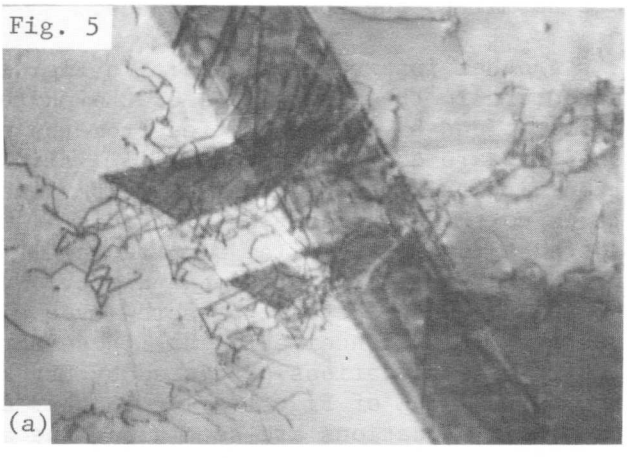

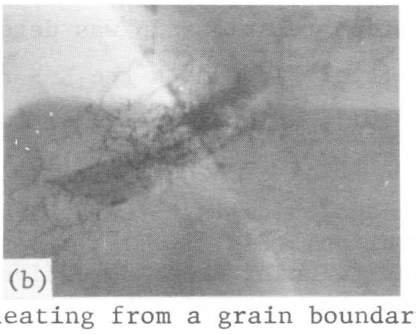

Fig. 5. The same martensite plates as in Fig. 4, but at a different diffracting condition.

direction on the specimen surface. (The subscript f stands for fcc.) This was true for all the cases examined. So we can reasonably assume that the straight edge direction is parallel to $\langle 110 \rangle_f$. Then it is possible to determine uniquely the the habit plane of martensite from this edge direction and the intersection of the martensite plate with the specimen surface. This is equivalent to the two face analysis. The habit plane thus determined was $(\bar{0}.375\ \bar{0}.837\ 0.375)$, which is only 3° away from $(\bar{2}\bar{5}2)$ toward the $(\bar{1}\bar{1}1)$ pole. The foil normal is $[\bar{1}\ \bar{3}\ 10]$. The stereographic presentation of such analysis is shown in Fig. 2 together with other crystallographic features. As seen clearly in Fig. 1(b), the martensite plates contain substructures and it was found by electron diffraction that these are twins with a $(112)_b$ mirror plane. (The subscript b stands for bcc.) The twin interface was determined from the intersection of the twin plate with the specimen surface, i.e., direction B in Fig. 1(b), and the intersection of the twin plate with the habit plane, i.e., $[101]_f$. It is very surprising that the twin interface is not the $(112)_b$ plane but a plane parallel to $(\bar{1}01)_f$ plane. The angle between the $(112)_b$ and $(\bar{1}01)_f$ is about 5° as shown in Fig. 2. The twins with $(\bar{1}01)_f$ interface are usually seen for thin martensite platelets, but in some cases such twins were observed also for thick plates. The transition from the $(\bar{1}01)_f$ interface to the normal $(112)_b$ twin interface in the lateral growth of the martensite plate could be identified by a micrograph in which both the $(\bar{1}01)_f$ and $(112)_b$ planes are normal to the specimen surface.

Another interesting feature in Fig. 1 is about the dislocation structure in the austenite near the martensite plates. It seems that dislocations have been emitted from the edge of each martensite plate and they are confined to the $(\bar{1}\bar{1}1)_f$ slip plane of which the intersection with the specimen surface is parallel to direction C in Fig. 1(a). It is worth noting that straight dislocations such as shown by the dotted arrow in Fig. 1(a) are frequently observed. These dislocation lines are parallel to the edge direction, $[101]_f$, of the martensite plate and hence they are of screw type with the $a/2\cdot[101]_f$ Burgers vector. It is conceivable that these screw dislocations were originally interface dislocations predicted by Frank [4]. Fig. 1(c) shows the framed region E of Fig. 1(a) at another diffracting condition, where tangled dislocations are seen along the austenite-martensite inerface.

The orientation relationship was determined to be $(\bar{1}\bar{1}1)_f \,//\, (101)_b$, $[101]_f // [11\bar{1}]_b$ (Fig. 2), namely the K-S relation. It is interesting to note that the $[101]_f$ which is parallel to $[11\bar{1}]_b$ is the zone axis of the habit plane, the twin interface $(\bar{1}01)_f$, and the $(\bar{1}\bar{1}1)_f$ on which the the slip in the austenite is first activated during early stages of the martensite formation. (Fig. 1(a)) It was found that the $[11\bar{1}]_b$ direction is also the twinning shear derection in the martensite. The crystallographic features presented by the stereographic projection of Fig. 2 were confirmed for all the cases oberved, in some completely and in others partly.

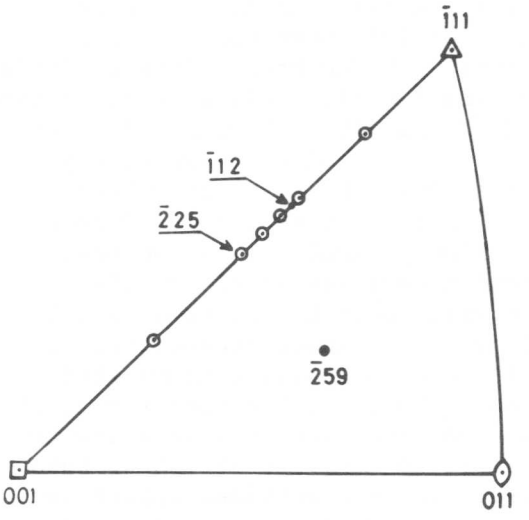

Fig. 6. Habit planes of thin martensite plates.

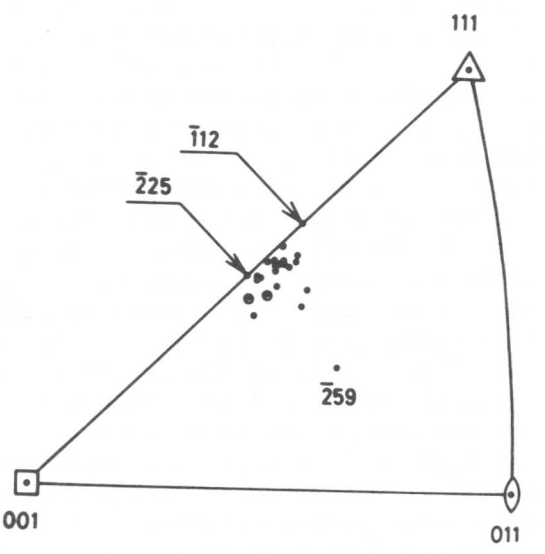

Fig. 7. Habit planes of fully grown martensite plates.

Fig. 3 is an enlarged photo of the framed area F of Fig. 1(a). The region indicated by the arrow in Fig. 3 may be regarded to be in the nucleating stage of martensite formation. The estimated size of this small martensite plate is about 100 nm in diameter and probably the smallest size ever observed with bulk specimens. Tangled dislocations are seen around this martensite. Figs. 4 and 5 show thin martensite plates nucleating from a grain boundary. The grain boundary in these figures is identical and micrographs (a) and (b) show thicker and thinner parts of the same foil specimen, respectively. Figs. 4 and 5 are at sightly different diffracting conditions. Many dislocations are seen around these thin martensite plates. It seems that dislocations were pushed out also toward the other side of the boundary. Twins are contained even in these very thin martensite plates. (Fig. 4(a)) The habit plane of these martensite plates was determined to be $(\overline{0.415}\ 0.415\ 0.809)$ which is 6° away from $(\bar{2}25)$.

Fig. 6 shows habit plane normals for thin martensite plates with 50-180 nm thickness, which were determined by the same method as described for Fig.1. A main source of experimental error in this method comes from inaccuracies in the determination of the specimen foil orientation, although this could be much improved by use of high voltage electron microscope. Fig. 7 shows habit plane normals for fully grown martensite plates determined by the two face analysis of bulk specimens [3]. It is clear from these figures that the haibit plane of very thin martensite plates which are in the early stage of martensite formation is essentially the same as that for the fully grown martensite plate, that is, the $\{225\}$ habit for both cases.

IV. Discussion

The results described in the preceding section are discussed in reference to a nucleation model of martensite proposed recently by Olson and Cohen [5]. One of the basic assumptions of this model is that the martensite forms on a $(111)_f$ plane at the very early stage of the fcc to bcc transformation. The results in the present work are

incompatible with this basic assumption; the (111) habit was never observed. The crystallographic features of thin martensite plates shown in Fig. 2 are in complete agreement with the predictions by Bowles and Mackenzie which are drawn based on the invariant plane strain condition with the dilatation parameter $\delta=\sqrt{2/3}\cdot a/a'$ [6]. Here a and a' are lattice constants of the austenite and the martensite, respectively. Therefore it is more reasonable to assume that the invariant plane strain condition is the controlling factor for the martensite formation even at its earliest stage. The dilatation parameter δ in the Bowles-Mackenzie theory is 1.0188 for the present case (a=0.3581 nm, a'=0.2870 nm), which means that the martensite crystal must be uniformly and isotropically dilated by 1.88% in the plane of the austenite-martensite interface. This strain is too large to be elastically accommodated and hence the plastic deformation must occur. However, the flow stress of the martensite may be much higher than the austenite at such a low temperature as in the present experiment. It is very probable that this strain is accommodated in the austenite. The dislocations around the martensite plates observed in the present study are considered to have generated from this accommodation. The edge of the martensite plate with such strain may be a point of high stress concentration, and therefore, dislocations are emitted into the austenite as seen in Fig. 1(a).

The origin for the isotropic dilatation at the austenite-martensite interface is considered as follows. The directions, $[101]_f$ and $[11\bar{1}]_b$, which are parallel with each other in the K-S relationship, lie in the $(\bar{2}5\bar{2})$ habit plane. Since the interatomic distance along this direction is greater by 1.84% for the austenite than for the martensite, the martensite crystal must be dilated by 1.84% in this direction to keep the coherency between the atoms at the habit plane. The spacings of $(\bar{1}\bar{1}1)_f$ and $(101)_b$ planes are different by 1.83%, that of the austenite being again greater. So the intersections of these planes with the habit plane, namely $[101]_f$ and $[11\bar{1}]_b$ atom rows, differ also by 1.83% in their inter-atomrow spacings. Therefore, if the planes $(\bar{1}\bar{1}1)_f$ and $(101)_b$ are to be kept coherent at the habit plane, the martensite crystal must be dilated by 1.83% in the direction normal to $[11\bar{1}]_b$ within the habit plane. Thus the martensite must be isotropically dilated by about 1.8% at the habit plane to keep atomic coherencies at the austenite-martensite interface. The amount of the dilatation for {225} habit assumed by the Bowles-Mackenzie theory is surprisingly in good agreement with that drawn from the above simple atomistic considerations.

In conclusion, the plastic deformation for the relaxation of the stress imposed by the dilatation parameter δ is the controlling factor in the early stage of martensite formation and probably in the nucleation stage too.

References

[1] S. Dash and N. Brown: Acta Met., 14(1966), 595.
[2] K. Shimizu, M. Oka, and C. M. Wayman: Acta Met., 18(1970), 1005.
[3] S. Kajiwara: to be published.
[4] F. C. Frank: Acta Met., 1(1953), 15.
[5] G. B. Olson and M. Cohen: Met. Trans., 7A(1976), 1905.
[6] J. S. Bowles and J. K. Mackenzie: Acta Met., 2(1954), 224.

A Macroscopic Model for Predicting Thermoelastic Growth

H. C. Ling and W. S. Owen

On the assumption that thermoelastic growth is possible only when no macroscopic plastic deformation accompanies the thickening of an isolated plate of martensite, a model is presented from which the aspect ratios at which significant plastic flow will occur at M_s can be estimated. It is demonstrated that the model clearly differentiates between alloys which behave thermoelastically (ordered Fe_3Pt and Au-47.5 Cd and those which do not (disordered Fe_3Pt and Fe-30 Ni). Further, it is demonstrated that whereas the change in the anisotropy ratio on cooling has little influence on the driving force at M_s in ordered Fe_3Pt (typical of fcc$\rightleftarrows$bcc transformations), it has a large effect on Au-47.5 Cd (typical of β-alloys) and probably accounts for the unusually small transformation driving-force in the latter alloy.

I. Introduction

In two previous papers [1,2], we have developed macroscopic models for predicting thermoelastic growth; starting with the assumption that the only necessary condition for thermoelastic growth of an isolated plate of martensite is that the transformation shape change be accommodated by the matrix without plastic deformation [3]. In the second paper [2], strain field calculations were based on a continuum model derived from Eshelby's treatment of the elastic strain fields surrounding an inclusion [4]. The model is three-dimensional and, unlike the first model proposed [1], it takes into account the dilatation strains. It was assumed [2] that the matrix and the plate of martensite are elastically isotropic with the same modulus. Because in a continuum model there is always a region of the matrix near the periphery of an ellipsoidal plate where the von Mises criterion for yielding is satisfied, the critical aspect ratio for thermoelastic growth was assumed to be that for which the plastic zone is less than 1% of the plate radius.

Recently, the single-crystal elastic constants of Fe_3Pt have been measured as a function of temperature and the order and the polycrystalline elastic moduli of Fe_3Pt martensite have been determined [5]. These data encouraged us to extend the model to take account of the differences in elastic properties of the matrix and the martensite plate and also to attempt computations of the elastic strain fields using anisotropic elastic constants. A new, and we think more realistic, criterion for thermoelastic growth is proposed.

II. Extension of the Model

The new stress field calculations utilized the Eshelby model, as described earlier [2]. In the first extension of the model, the matrix

---

Department of Materials Science and Engineering, M.I.T., Cambridge, MA 02139

and the martensite were assumed to be elastically isotropic but with different elastic moduli. The martensite plate is assumed to be a thin, ellipsoidal coherent particle of radius r and semithickness c lying in the x-y plane with the transformation shear in the x direction ($e^T_{13} \neq 0$). Plastic flow will occur within a volume enclosed by a surface at which the von Mises criterion for yielding is satisfied. The relevant parameters are listed in Table I for ordered and disordered Fe_3Pt, Fe-30 Ni and Au-47.5 Cd. The two thermoelastic alloys, ordered Fe_3Pt and Au-47.5 Cd, have a much smaller shear modulus and a larger yield stress than the non-thermoelastic alloys. Furthermore, Au-47.5 Cd has an unusually small lattice shape strain. All the calculations were made for alloys at their M_s temperature. The stress fields in the matrix of Fe_3Pt at M_s were calculated as a function of the aspect ratio c/r for various degrees of atomic order S. Figures 1 and 2 show the shear stress σ^c_{13} in the plane of the plate (along the x-axis) and normal to the plate (along the z-axis) for S = 0.6. Along these two axes, σ^c_{13} is the only non-zero stress component. In the plane of the plate, curves of σ^c_{13} for various aspect ratios always exceed the critical shear stress, $\sigma_{crss} = \sigma_y/\sqrt{3}$, at some distance from the edge of the plate. Along the z direction, σ_{crss} is exceeded only for plates with an aspect ratio larger than 0.04 (Figure 1).

The extent of the plastic zones are shown in Figure 3. The shear modulus of the martensite phase and the transformation shape strain remain nearly constant in the four cases considered. Hence, changes in the size of the plastic zone with the degree of order of the austenite reflects the combined effect of changes in the elastic properties and flow stress of the austenite. In the disordered case, the plastic zone disappears entirely from the broad interface for plates with a small aspect ratio. By calculating the aspect ratio at which this plastic zone vanishes, an upper limit to the chemical driving force at M_s, Δg_c, for thermoelastic growth can be deduced.

At M_s, a martensite plate grows rapidly in the radial direction till it hits a barrier; then it thickens. Under thermoelastic equilibrium, the thickening stops when a balance between the chemical driving force and the elastic strain energy is reached. Then [6]

$$\Delta g_c + 2A \left(\frac{c}{r} \right) = 0 \qquad (1)$$

where $A = \frac{\pi(2-\nu)\mu}{8(1-\nu)} (2e^T_{13}{}^2)$. Thus, thermoelastic growth is generally associated with the thickening of a plate, i.e., the movement of the broad interface between martensite and austenite. We now postulate that the criterion for thermoelastic growth is that there should be no plastic zone along this broad interface. The plastic zone which always exists at the tapered edges of the plate extends into the barriers blocking the radial growth. The interaction of this zone with the barrier probably presents a restraining force in the final stages of the reverse transformation, but it is not an essential factor in determining whether or not the growth is thermoelastic.

Using this new criterion, a quantitative measure of the size of

the plastic zone is the distance along the thickening direction [001] at which the yield stress is exceeded. Figure 4 shows this parameter, r_p, as a function ratio at different points along the [100] direction for Fe_3Pt, S = 0.6. At x = 0.75r, the plastic zone disappears at an aspect ratio of 0.03. The elastic strain energy of such a plate is 59 cal/mole (247 J/mole) and from Equation 1, the upper limit of Δg_c is 118 cal/mole (494 J/mole). For S = 0.4 and 0.2, the critical aspect ratios are 0.025 and 0.02 respectively. The upper limit of Δg_c is 108 cal/mole (451 J/mole) in both cases. Since the chemical driving force decreases with ordering, it can be concluded that Δg_c does not exceed 108 cal/mole (451 J/mole) in the ordered states. A theoretical calculation of Δg_c [5] based on the Olson-Cohen nucleation model [7] yields similar values for ordered Fe_3Pt.

Fe-30 Ni behaves similarly to disordered Fe_3Pt. With $\Delta g_c \approx 300$ cal/mole, Equation 1 predicts an equilibrium aspect ratio of 0.038 at M_s if a thermoelastic condition is attainable in this alloy. Figure 5a shows the plastic zone associated with a plate of this size. Clearly elastic accommodation is impossible. The situation with Au-47.5 Cd is entirely different. With a transformation shear of 0.07 [8] and Δg_c (M_s)~10 cal/mole (42 J/mole) [9], an equilibrium aspect ratio of 0.02 is predicted at M_s. Yet at an aspect ratio four times as large (c/r = 0.08), there is still only a small plastic zone near the periphery of the plate (Figure 5b).

III. The Influence of Anisotropy

So far, the problem of elastic accommodation has been discussed in the context of isotropic elasticity. However, it is known that thermoelastic alloys are highly anisotropic at M_s. Since in most alloys both the habit plane and the shape strain direction do not have simple indices, the effect the increasing anisotropy with decreasing temperature of the austenite on the elastic accommodation of the transformation strain can not be predicted from qualitative arguments. A calculation using the measured anisotropic elastic constants was undertaken to determine the elastic strain energy and the stress field in the matrix for ordered Fe_3Pt. It was found that [5] for small aspect ratios, the anisotropic elastic energy varies linearly with c/r and it does not deviate significantly from the isotropic model discussed earlier in which the average shear modulus was used. The factor A in the elastic energy term in Equation 1 is not altered to any significant extent for the particular orientation of the martensite plate under consideration. It was not possible to do extensive calculation of the stress fields in an anisotropic matrix because of the amount of computing time involved. However, sufficient data was obtained to indicate that the resolved shear stress on the nearest slip system, $\{1\bar{1}1\}\langle 011\rangle$ in the austenite in the direction normal to the habit plane does not exceed the critical shear stress for slip for a plate with aspect ratio of 0.02. If this is taken to be the lower limit to the critical aspect ratio, the corresponding Δg_c (M_s) is 100 cal/mole (418 J/mole). Hence, an anisotropic calculation has not changed significantly the estimate of Δg_c for thermoelastic growth in ordered Fe_3Pt. It appears, then, the increasing anisotropy of the austenite on cooling does not

play an important role in the minimization of strain energy of a growing plate.

The increasing anisotropy of the austenite is expected to have a greater effect on the nucleation process in β-alloys than in ferrous alloys. Transformation in β-alloys involves $\{110\}\langle\bar{1}10\rangle_\beta$ shear followed by $\{112\}\langle\bar{1}11\rangle_\beta$ shear. The elastic constants corresponding to these two shear modes exhibit softening on cooling [10,11]. The softening is most drastic in $C' = 1/2\ (C_{11} - C_{12})$, which measures the resistance to $\{110\}\langle\bar{1}10\rangle_\beta$ shear. This is reflected in a large increase in the anisotropy ratio ($= C_{44}/C'$). In the fcc→bcc transformation, such as in the ferrous alloys, $\{111\}\langle 110\rangle_\gamma$ and $\{111\}\langle 112\rangle_\gamma$ shears are involved [7]. Resistance to both of these shears is determined by the elastic constant $1/3\ (C_{11} - C_{12} + C_{44})$. Compare ordered Fe_3Pt (representative of fcc⇄bcc alloys) and Au-47.5 Cd (representative of β-alloys). In both alloys, C' softens and reaches nearly the same value at M_s (0.33×10^{11} dyn cm^{-2}). In Fe_3Pt, $1/3\ (C_{11} - C_{12} + C_{44})$ also softens on cooling and reaches a value of 2.7×10^{11} dyn cm^{-2} at M_s. However, between 200°C and M_s, C' changes by a factor of ten, whereas $1/3\ (C_{11} - C_{12} + C_{44})$ decreases by only a factor of two, and at M_s the value of the former is much smaller than that of the latter. Since the shears in the transformation of Fe_3Pt are controlled by $1/3\ (C_{11} - C_{12} + C_{44})$ and in Au-47.5 Cd by C', it is expected that the effect of elastic anisotropy on the transformation in Au-47.5 Cd is much greater than in Fe_3Pt and that the chemical driving force of the β-alloy at transformation is much smaller. The latter is observed experimentally.

IV. Acknowledgement

This work was supported by the National Science Foundation under Grant DNR 7422719.

References

[1] G.B. Olson and W.S. Owen, Symposium on "New Aspects of Martensitic Transformations," Japan Institute of Metals (1976), 105.
[2] H.C. Ling and W.S. Owen, Proceedings of ICOMAT Conference, Kiev (1977), 108.
[3] G.V. Kurdjumov and L.C. Khandros, Dokl. Akad. Nank. SSSR, 66(1949), 211.
[4] J.D. Eshelby, Progress in Solid Mechanics, 7(1961), 90.
[5] H.C. Ling, Sc. D. Thesis, M.I.T. (1978).
[6] G.B. Olson and M. Cohen, Scripta Met., 9(1975), 1247.
[7] G.B. Olson, Sc.D. Thesis, M.I.T. (1974).
[8] R.V. Krishnan and L.C. Brown, Met. Trans. 4(1973), 423.
[9] H. Warlimont and L. Delaey, Progress in Materials Science, 18(1974).
[10] A. Nagasawa and Y. Ueda, J. Phys. Soc. Japan, 45(1978), 1249.
[11] S. Zirinski, Acta Met., 4(1956), 164.
[12] M.J. Schmutz, Sc.D. Thesis, M.I.T. (1978).
[13] J. Nilles, Ph.D. Thesis, Cornell Univ. (1970).
[14] N. Nakanishi, Shape Memory Effects in Alloys, Plenum Press (1975), 147.

Table I Relevant parameters in the macroscopic model for predicting thermoelastic growth

	ordered Fe_3Pt(S=0.6)	disordered Fe_3Pt(S=0)	Fe-30 Ni	Au-47.5 Cd
M_s	-196°C	0°C	-30°C	50°C
Transformation shear	0.2	0.2	0.2	0.07 [8]
Volume change	~0	1.4%	2.3%	~0
Shear modulus μ ($\times 10^{-11}$ dyn/cm^2)	2.50	5.93	6.50	1.67 [11]
Poisson's ratio ν	0.43	0.21	0.25	0.42
Flow stress σ_y (MPa)	700 [12]	220 [13]	270 [12]	500-700 [14]
Anisotropy ratio ($=C_{44}/C'$)	32	3.4	4	14
Shear modulus of martensite ($\times 10^{-11}$ dyn/cm^2)	5.77	5.40	5.5	

Figure 1. The shear stress σ_{31} along z-axis. Fe_3Pt. S=0.6

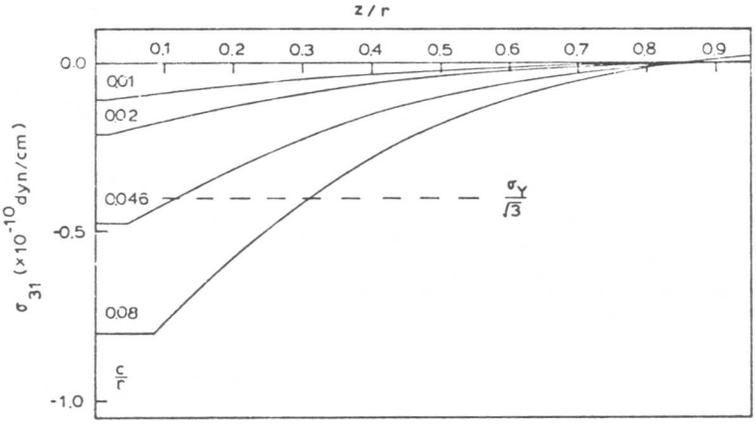

Fig. 2. The shear stress σ_{31} along the x-axis due to an ellipsoidal plate lying in x-y plane with shear in the x direction. Fe_3Pt. S=0.6.

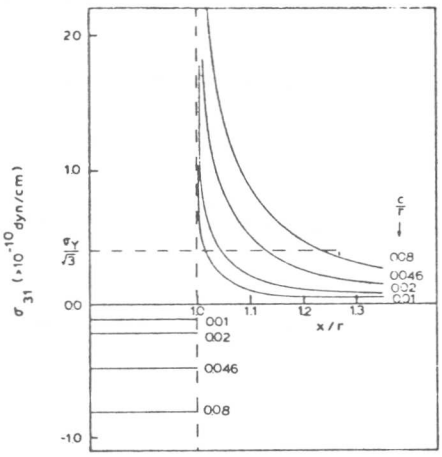

Fig. 3. Matrix yield stress contours of an ellipsoidal plate lying in x-y plane with shear in x direction. Fe_3Pt. Aspect ratios 0.02 (—), 0.04 (--), 0.08 (-·-)

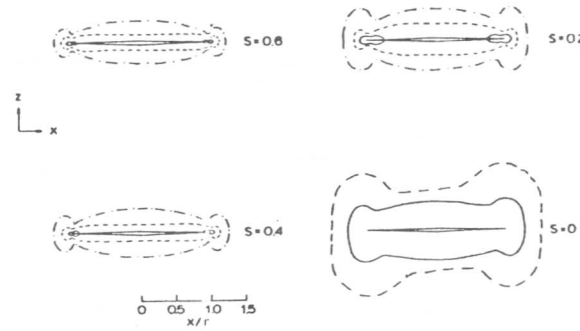

Fig. 4. The radius of yield stress envelop, r_p, along [001] measured at various points x in [100] direction. Fe_3Pt. S=0.6

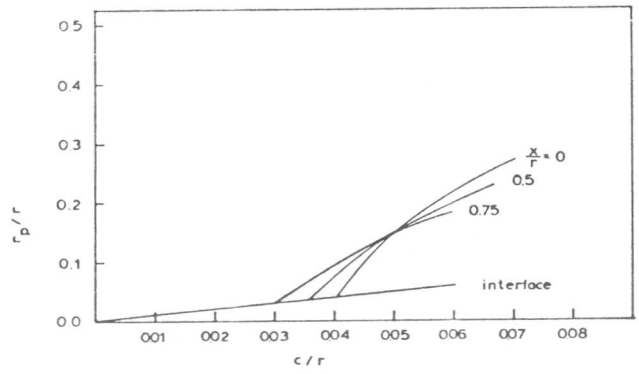

Fig. 5. Matrix yield stress contours of (a) Fe-30 Ni, aspect ratio 0.038, (b) Au-47.5 Cd, aspect ratio 0.08

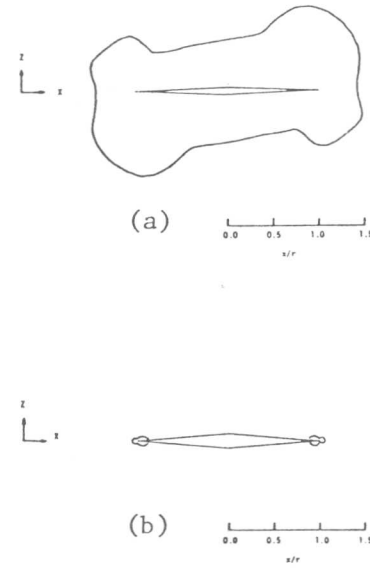

ON THE THERMODYNAMICS OF THE MARTENSITIC GROWTH-ARREST IN A BURST TRANSFORMATION*

G. A. Knorovsky+ and Morris Cohen++

ABSTRACT

The thermodynamic driving force required to propagate a martensitic plate during a burst transformation has been determined by means of thermal-gradient and concentration-gradient experiments. In the iron-nickel single crystals under investigation, the martensitic plates are arrested when the driving force is less than about 905 J/mole if the arrest is gradual (isothermal), and less than about 760 J/mole if the arrest is sudden (adiabatic). The former value corresponds to $-\Delta G^{A\rightarrow M}$ at the temperature or composition of growth-arrest, whereas the latter value corresponds to $-\Delta H^{A\rightarrow M}$ at the temperature or composition of growth-arrest.

---

*This research was part of a doctoral thesis submitted by G. A. Knorovsky in February 1977 to the Department of Materials Science and Engineering at the Massachusetts Institute of Technology, Cambridge, MA, USA. The work was sponsored by the National Science Foundation under Contract No. DMR-7622993.

+Sandia Laboratories, Albuquerque, NM 87185, USA.

++Massachusetts Institute of Technology, Cambridge, MA 02139, USA.

Electric and Optic Kinetic Study of the Martensitic Burst in an Fe-32wt% Ni Alloy

M. Robin*, G. Lormand** and P.F. Gobin*.

If a sample of Fe-32Ni, not subjected to a d.c. current, is cooled in the martensitic range, electric transient signals are detected at its ends. In other samples of the same alloy, we have shown that an electric transient signal is always superimposed to the signal due to variations of d.c. electrical resistance directly induced by the first martensitic burst. We give thus evidence that an electric emission is related to the martensitic growth in that type of alloy. It is proposed to relate this emission to interaction between highly mobile austenite-martensite interfaces and the conduction electrons of the alloy. In order to evaluate directly the duration of martensitic bursts, we have designed an optoelectronic device to measure the time of formation of martensitic relief : the intensity of light reflected onto the surface of a previously polished Fe-32Ni sample is measured with a fast response photodiode. The reflecting power of the sample decreases suddenly with the successive bursts. The durations of the electric emission and of the reflectivity decrease due to the first burst are of the same order ($\simeq 5\mu s$); these values are consistent with the estimation generally done for the rate of growth of martensite plates.

I. Introduction

The martensitic transformation $\gamma \rightarrow \alpha'$ in Fe-29$\sim$34%Ni alloys has a peculiar kinetic : on continuous cooling, the transformed volume fraction f increases by jumps - or bursts - and its value may attain 0.8 [1-3]. We have tried to measure the duration of a martensitic burst and the growth rate of lenticular martensite plates by two methods very different and nevertheless well suited for the study of fast phenomena.

Chemical Composition (in wt%) of the Alloy used						
Ni	C	Si	Mn	Cr	Mo	Fe
32	0.010	<0.010	<0.027	<0.021	<0.011	balance

*Groupe d'Etude de Métallurgie Physique et de Physique des Matériaux, E.R.A. n°463 Bâtiment 502, INSA de Lyon 69621, Villeurbanne Cédex, FRANCE.

**Laboratoire d'Etude des Matériaux, E.R.A. n°602 Bâtiment 303, INSA de Lyon 69621 Villeurbanne Cédex, FRANCE.

II.Electrical Study.

(1)Experimental procedure.

The alloy is reduced by wiredrawing at room temperature from 1.8mm down to 0.35mm diameter and annealed 24 hours at 1500K in hydrogen. The samples, 8mm in length, have then the bamboo structure. The sample is immersed in stirred petroleum ether and submitted to a cooling-heating cycle at $5Kmn^{-1}$ between room temperature and 190K. The electrical tension between ends of the samples is measured by a pen recorder (riseti-me 0.4s) and a transient recorder (time resolution 10ns).

(2)Results.

In a first series of tests, the sample is submitted to a d.c. current of 100mA kept constant within 4.10^{-3} whatever the amplitude and rate of variation of the resistance of the sample may be. Figure 1 shows the relative tension change $y=V(T)/V_Y(273K)$, obtained by the pen recorder, with temperature T of the cooling liquid. The graph is composed with :
-two linear and reversible parts AB and DE corresponding respectively to the resistivities of the sample before and after transformation.
-an irreversible jump BC corresponding to a big decrease of tension which duration is less than 0.4s. Point B corresponds to the time t_o at which the sample reaches the transformation triggering temperature Mb and point C to the time t_o+5s [4]. Mb=200±5K, in good agreement with measurements by Delorme [5] on other samples from the same melt.

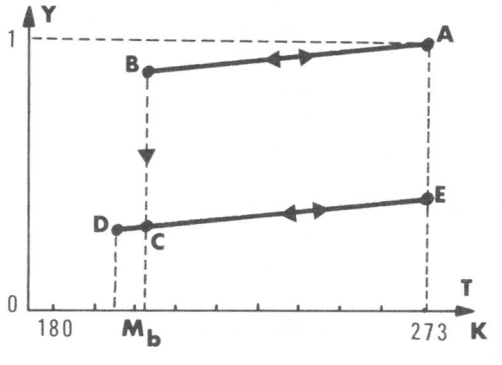

Figure 1. Pen recording of tension changes during a thermal cycle.

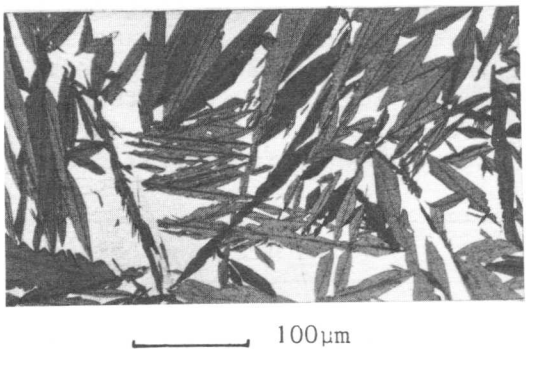

Figure 2. Longitudinal section of a transformed sample.

Figure 2 shows a longitudinal cut of a transformed sample. By studying several analogous micrographs, we could estimate the mean number N_p of plates per sample and the transformed volume fraction f. For the group of 6 samples previously mentionned $N_p \sim 300$ and f=0.74±0.03.

Figure 3 shows the typical aspect of the electrical signal obtained

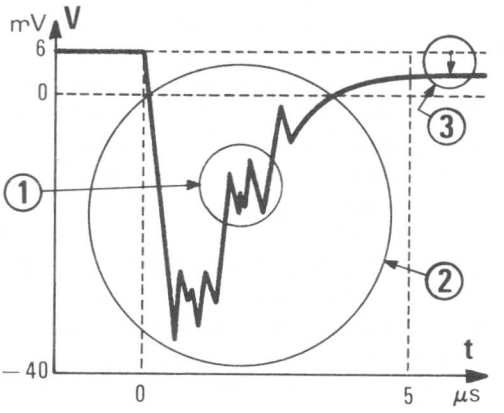

Figure 3.Typical aspect of electrical signal with d.c. current.

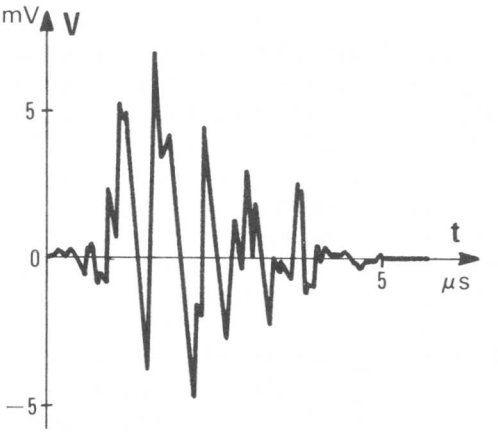

Figure 4.Typical aspect of electrical signal without d.c. current.

by the transient recorder when the temperature of the cooling liquid reaches M_b. The total duration t_1-t_0 of the signal is about 5μs. Between t_0 and t_1, the signal is formed by an oscillation packet (1) and a negative peak (2) with the same duration as the packet. After t_1, an offset (3) of the trace remains in the same direction as the jump BC in figure 1, but with a slightly smaller amplitude due to the adiabatic heating induced by the burst [4]. The oscillations (1) have an apparently random aspect, a peak-to-peak value of about 20mV and their mean number per signal is between 20 and 40. If a magnetic field of 5.10^3Oe (this one is greater than the saturation values for γ and α') and parallel to the sample's axis is applied, peak (2) is suppressed but oscillations (1) and offset (3) remain.

In a second series of tests, the d.c. current has been suppressed. When the temperature reaches M_b, the pen recorder does not measure any tension, but the transient recorder takes the signal shown in figure 4. With respect to the signal of figure 3, the packet of oscillations (1) remains alone, with the following characters : zero mean value, duration between 2 and 8μs, number per signal between 20 and 50, peak-to-peak value between 5 and 40mV.

(3)Discussion.

Some characteristics of the transient signal obtained with a d.c. current (Fig.3) can be simply explained by assuming that this signal lasts at least as the burst [4]. As the offset (3) is proportionnal to the current and to the variation of resistance of the sample induced by the transformation, we must expect that (3) is zero when the current is suppressed. The peak (2) is probably due to the ferromagnetic properties of γ and α' phases [6]; it is similar to the "anomalies" already observed by Kimmich and Wachtel [7].

When no d.c. current passes through the sample, the occurrence of electrical signals during the transformation has already been observed [8,9] but not specifically studied. All our observations give evidence that, in the alloy studied, the martensitic transformation triggers an electric emission characterized by oscillations (1) . In the transformed volumes, growth of martensite causes expansion, magnetic perturbations and adiabatic heating. The electrical effects associated with these phenomena cannot explain the observed signal [6]. On the other hand, the movement of austenite-martensite interfaces induces transient variations of the ionic density of charge to which the electron gas almost immediately responds. This mechanism implies a momentum transfer between ions and electrons. We can estimate the signal amplitude by inversion [10] of the reasonings made in order to explain defects resistivities and electromigration phenomena [11]. If n is the electron density, a tension $U=\rho_s ne\, v$ is induced during the displacement of an interface of specific resistivity ρ_s and velocity v. Giving to v a reasonable value and taking for ρ_s a value measured for iron grain boundaries [12], we find that U is included between 1 and 100mV which is an order of magnitude consistent with our measurements.

In our samples, several interfaces are moving during the martensitic burst in all directions and almost at the same time. Thus, the magnitude and sign of the measured tension must vary in an apparently random fashion, as we have observed. An electronic origin seems then probable for oscillations (1) ; a detailed interpretation will be published elsewhere [13]. As the total duration of the burst must be at least equal to the time of formation of the biggest plate, we estimate that the mean velocity for propagation of a γ-α' interface would be greater than $10^2 ms^{-1}$, which agrees with values previously proposed by other workers [14,15].

III.Optical Study.

(1)Experimental procedure.

A 1.8mm diameter wire is laminated at room temperature down to 0.3mm in thickness, then annealed at 1373K for 24h in argon gas. A fast response photodiode placed on the eye piece of a metallographic microscope measures the intensity of light reflected by an area of about $1mm^2$ of a previously polished sample. The sample is submitted to a cooling-heating cycle at $25Kmn^{-1}$ between room temperature and 77K in a cooling stage under vacuum. The tension delivered by the photodiode can be measured by the pen recorder or the transient recorder previously used.

(2)Results

Figure 5 shows the typical aspect of the dependance of reflectivity

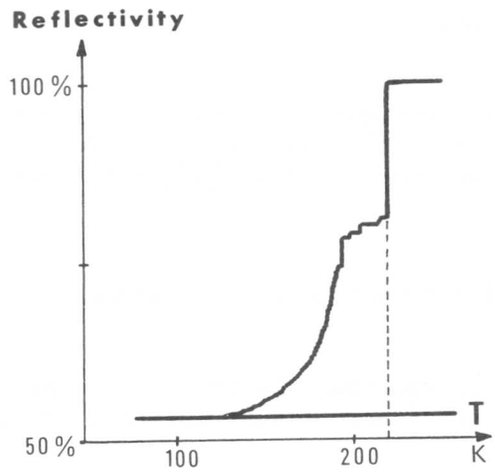

Figure 5.Pen recording of reflectivity during a thermal cycle.

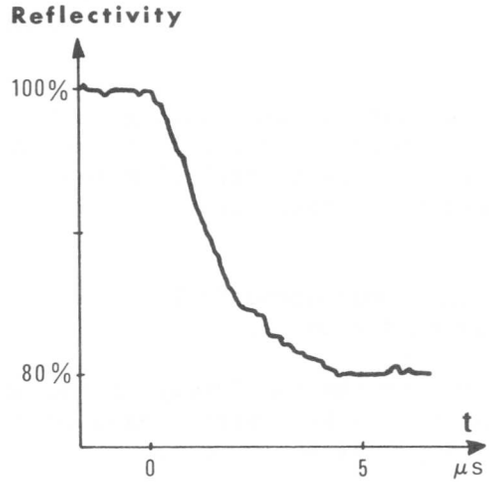

Figure 6.Typical aspect of a transient optical signal.

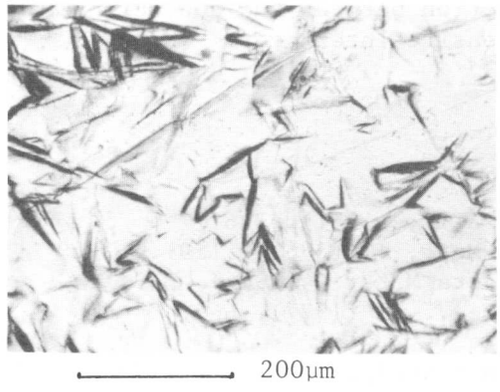

Figure 7.Superficial relief on a transformed sample.

with temperature, as measured with the pen recorder. We can see several jumps of decreasing amplitude. Figure 6 shows the dependence of reflectivity on time during the first jump, as measured by the transient recorder. Figure 7 shows the superficial martensitic relief formed after the first jump.

(3)Discussion.

The jumps in figure 5 correspond to successive martensitic bursts of decreasing values. These samples have a different form and a smaller grain size than those used for the electrical study ; the bursts have thus a less greater extent. As in the case of the electrical study, the mechanism of the burst is too complex to enable us to distinguish, on figure 6, in what sequence the different plates form. However, the total duration of the reflectivity decrease, and thus of the first burst, is of the same order as in the preceeding study. A detailed description of these optical experiments will be done elsewhere [16].

IV.Conclusion.

We have measured with good accuracy the duration of the first martensitic burst on cooling of a Fe-32%Ni alloy. We have developed for this purpose an electrical method first proposed in 1940 [17] but rarely used since this date.

These measurements have been verified by a new optical method fairly simple to use.

Due to the complexity of the burst phenomenon, the growth rate of single martensitic plates have only been estimated : we think that it is at least equal to $10^2 ms^{-1}$.

In the alloy studied, we have shown that an electric emission takes place during the martensitic burst and we described it. We propose to attribute that emission to an interaction between the conduction electrons and the moving austenite-martensite interfaces.

References.

[1] E.S. Machlin and M. Cohen : Trans. AIME, (1951), 746.
[2] J.C. Bokros and E.R. Parker : Acta Met., 11 (1963), 1291.
[3] R.L. Patterson and C.M. Waymann : Acta Met., 14(1966), 347.
[4] M. Robin and P.F. Gobin : Scripta Met., 11 (1977), 669.
[5] J.F. Delorme, thèse, Lyon (1971).
[6] M. Robin, G. Lormand and P.F. Gobin : Scripta Met., 12 (1978), 399
[7] H. Kimmich and E. Wachtel : Arch. Eisenhütt., 35 (1964), 1193.
[8] H. Beisswenger and E. Scheil : Arch. Eisenhütt., 27 (1956), 413.
[9] E.E. Lahteenkorva : Ann. Ac. Sc. Fenn. AVI. 87 (1961), 3.
[10] L. Turban, P. Nozières and M. Gerl : J. Physique, 37 (1976), 159
[11] J.N. Pratt and R.G.R. Sellors : "Electrotransport in Metals and Alloys", Trans. Tech. (1973).
[12] S. Arajs, B.F. Oliver and J.T. Michalak : J. Appl. Phys.,38 (1967), 1676.
[13] M. Robin, thèse, Lyon (to be published).
[14] R.F. Bunshah and R.F. Mehl : Trans. AIME, (1953), 1251.
[15] K. Mukherjee : Trans. AIME, 242 (1968), 1495.
[16] G. Lormand and M. Robin : to be published
[17] F. Förster and E. Scheil : Z. Metall., 32 (1940), 165.

Inhibition of the Martensitic Transformation of Small Austenite Particles in Low-Alloy Steels

J. M. Rigsbee*

Abstract

Annealing of various low-alloy steels in the intercritical ferrite plus austenite region produces a ferrite matrix with individual small particles of austenite. Upon cooling to room temperature, austenite particles smaller than ca. 1 μ in diameter do not transform to martensite. These retained austenite particles, which can comprise as much as 10 vol. % of the material, are extremely stable and do not transform even when cooled to liquid helium temperature. Analysis of chemical partitioning shows that carbon and manganese are partitioned to retained austenite and silicon to ferrite. High resolution TEM techniques show good compatability between the austenite and ferrite phases since the interphase interface is semicoherent. Size of individual retained austenite particles was shown to be very important in their relative stabilities since the average untransformed retained austenite particle size decreases with increasing mechanical strain. The respective roles of chemistry, interfacial structure and particle size are discussed with regard to inhibition of the martensitic transformation of discrete retained austenite particles.

Introduction

Research in the general area of high-strength steels has accelerated during the past five years because of the extensive vehicle weight reduction programs initiated in the automotive industry. Much high-strength steel research in the steel industry has centered about development of a class of steels, termed "dual-phase," which exhibit strength/formability combinations superior to current HSLA steels [1-4]. During development of "dual-phase" steel microstructure-mechanical property relationships [5-7], transmission electron microscopy and X-ray diffraction techniques revealed that surprisingly large amounts of austenite (ca. 5 to 10 vol. %) are typically retained in these low-alloy steels at room temperature. The retained austenite, which appears in the form of discrete submicron sized particles, is contained in a ferrite matrix and is extremely stable since it does not transform to martensite when quenched in liquid helium [8] or when relatively unconstrained in a TEM foil. The objective of this work was to develop an understanding of the origin of the austenite stability by: examination of the chemistry of the austenite with energy dispersive and wavelength dispersive X-ray analysis techniques;

---

* Republic Steel Corporation Research Center, 6801 Brecksville Road, Cleveland, Ohio 44131.

examination of the interfacial structure at the austenite/ferrite interface with high resolution weak-beam dark-field (WBDF) transmission electron microscopy; and examination of austenite particle sizes in both the unstrained condition and as a function of tensile strain.

Experimental Technique

Material and Heat Treatment

The nominal chemistry for the commercial alloys used in this study is: Fe, balance; C, 0.15 wt %; Mn, 1.45; Si, 0.47; Cb, 0.02; V, 0.05; and Al, 0.04. The hot-rolling schedules involved finishing temperatures of ca. 890°C (1635°F) and coiling temperatures of ca. 650°C (1200°F). The as-hot-rolled microstructures typically consisted of equiaxed ferrite grains with banded regions of pearlite (pearlite banding is caused by Mn segregation with higher than average alloy Mn composition present in the pearlite bands). Intercritical annealing of the as-hot-rolled steels to produce a "dual-phase" microstructure involved reheating the materials to ca. 845°C (1550°F), holding at this temperature for 2-4 minutes, and cooling to room temperature.

Microstructural Analysis

Optical and scanning electron microscopy involved the use of an etch (2 gms $(NH_4)_2S_2O_8$, 2 ml HF, 50 ml CH_3COOH and 150 ml H_2O) which, through differing rates of attack, made it possible to distinguish the various microconstituents. Carbon and manganese partitioning to austenite particles was analyzed using SEM wavelength-dispersive and energy-dispersive procedures, respectively. TEM imaging (bright- and dark-field and WBDF) and diffraction (selected area and convergent beam diffraction) modes were used for detailed analysis of the microstructure. Details on TEM sample preparation techniques and on the application of WBDF imaging techniques for high resolution analysis of interphase interfacial structure are discussed in reference [9]. Quantitative analysis of retained austenite volume fractions was done using a standard X-ray diffraction procedure [10] discussed in detail in reference [5].

Results

General Microstructure

Intercritically annealing material with the previously discussed time/temperature conditions produces a microstructure consisting of equiaxed ferrite grains with particles of austenite nucleated, predominately, at ferrite grain boundary carbides. Figure 1 shows a typical microstructure after cooling from the intercritical annealing temperature. The "second-phase" austenite generated by intercritical annealing now appears to be divided into two distinct classes: particles which etch darker than the ferrite and are, on the average, greater than 10^{-6} m in diameter; and particles which etch lighter than the ferrite and are, on the average, smaller than the darker etching class of particles. It has previously been shown [5] using quantitative

metallography, X-ray analysis, and TEM techniques that the darker etching particles are martensite (i.e., austenite that transformed upon cooling) and the lighter etching particles are retained austenite.

High magnification SEM examination of etched samples revealed the source of the etching contrast differences between the retained austenite and martensite particles. The retained austenite particles shown in Figure 2(a) have smoother surfaces than the ferrite and, because of their higher surface reflectivity, would therefore appear lighter in an optical micrograph than the ferrite background. Conversely, the larger martensite particle shown in Figure 2(b) has a rougher surface than the ferrite and would appear darker in an optical micrograph than the ferrite background. The general lack of internal structure for the retained austenite and the profuse amount of internal structure for the martensite (discussed next in the TEM section) would favor the martensite being most rapidly attacked by the etchant.

Figure 3(a) and 3(b) show low and high magnification views of a typical martensite particle. As evident from Figure 3(a), this martensite particle is composed of a complex arrangement of several transformation variants. The higher magnification TEM micrograph shown in Figure 3(b) illustrates the internal transformation twin structure of two adjacent martensite variants. All martensite regions observed in this investigation exhibited the internally twinned structures characteristic of high-carbon, low-transformation temperature plate martensite [11, 12] and most martensite regions contained more than one martensite transformation variant. As previously reported [5, 6] for "dual-phase" steels, TEM examination showed a high dislocation density in the ferrite regions directly adjacent to many of the martensite particles. This result is explained by the ca. 2 to 3% volume expansion [13] accompanying the austenite to martensite phase transformation.

Figure 4(a) is a bright-field TEM micrograph showing a particle of retained austenite surrounded by the ferrite matrix. The convergent beam electron diffraction pattern shown in Figure 4(b) quantitatively identifies the particle as austenite. The important points of interest in this micrograph are (a) the faceted nature of the austenite/ferrite interphase boundary at all positions (note dashed lines) around the retained austenite particle and (b) the linear structures lying approximately normal to the interphase boundary extinction fringes. The relevance of the interfacial faceting and boundary structure to the coherency of the austenite/ferrite interface will be detailed in the Discussion section.

Austenite Chemistry

SEM point analyses and line scans across retained austenite/martensite* (A/M) particles revealed significant partitioning of carbon

* Although it was not possible in the SEM to unambiguously determine whether the particles examined were retained austenite or martensite, no drastic chemical differences are expected between the two particle types.

and manganese to austenite and silicon to ferrite. Figure 5(a) shows a wavelength dispersive (WDX) carbon line scan across two A/M particles along the path denoted by the horizontal line. Carbon partitioning to the two particles (relative to the ferrite matrix) is clearly shown by the peaks in the count rate versus beam position curve. Although the peak signal from the smaller of the two A/M particles appears less than that from the larger particle, the difference most probably results from the fact that the electron beam sampling volume (ca. 1 μm diameter for the kV used) included a portion of ferrite. Figure 5(b) shows an energy dispersive (EDX) manganese line scan across two A/M particles. The partitioning of Mn to A/M and its relative depletion in the ferrite matrix is clearly shown by the respective peaks and valleys in the count rate curve. Preliminary TEM thin foil EDX point analyses of austenite particles (identified by electron diffraction) and the ferrite matrix have also shown Mn to be partitioned to austenite and Si to be partitioned to ferrite.

Austenite/Ferrite Interphase Structure

Figure 6(a) and (b) are WBDF TEM micrographs (obtained using a ferrite <020> reflection with a deviation of ca. 0.015 Å^{-1} from the exact Bragg diffraction condition) which show interfacial structures typically found at the interface between a retained austenite particle and its ferrite matrix. Figure 6(a) is a lower magnification micrograph which shows the entire austenite particle and the surrounding ferrite matrix. The wide projected width of the austenite/ferrite (γ/α) interface results from the interface being nearly parallel (within 10°) to the plane of the foil and allows a clear presentation of the complex interfacial structure. The faceted nature of the γ/α interface is indicated by the three dashed regions labeled 1, 2, and 3. The spacing and arrangement of the interfacial features varies from facet to facet. The primary interphase structures evident in Figure 6(a) are the growth ledges which lie nearly perpendicular to the γ/α interface extinction contours at facets 2 and 3 and which are nearly semicircular at facet 1. The ledge nature of these features (which apparently nucleate at some position on facet 1) are proven by the extinction contour deflections which they produce. Figure 6(b) shows additional linear features which are spaced ca. 30 Å apart and lie along the indicated direction only at facet 1.

Strain Induced Austenite to Martensite Phase Transformation

Samples strained in tension from 0 to 20% showed steadily decreasing amounts of retained austenite with increasing strain [5]. The percent austenite transformed to martensite per unit strain also showed a maximum at the lowest strains and decreased with increasing strain. The key result of metallographic analysis of the strained materials showed that the average untransformed retained austenite particle size decreased rapidly with increasing strain.

Discussion of Results and Conclusions

It is proposed that chemical partitioning, γ/α interphase structure and austenite particle size each play roles, not independent of one another, in austenite stabilization. C and Mn, which were shown to partition to austenite, are well-known to stabilize austenite by depressing the M_S temperature [14]. However, complete partitioning of C and significant partitioning of Mn to austenite would not reduce M_S below 0°C. The experimental results on the faceting and interfacial structure of the γ/α interphase boundaries support previous detailed computer modeling [15] and TEM analyses [9] of f.c.c.:b.c.c. boundaries which show that it is possible for a partially coherent interface to exist between ferrite and austenite which would be an effective barrier to growth. Such an interface would be effective in mechanically constraining the particle and would serve to increase the degree of chemical partitioning by reducing the growth of the austenite. The increase in stability with decreasing particle size can be explained by the probable higher level of chemical partitioning and by the increased effectiveness of the interface (relative to the volume of the particle) in constraining the particle against the required particle shape changes accompanying a martensitic transformation.

References

[1] R. A. Grange, Proceedings of the Second International Conference on the Strength of Metals and Alloys, 3, Pacific Grove, California, 861 (1970).

[2] T. Katsuoka and K. Yamamori, Met. Trans., 6A, 1613 (1975).

[3] S. Hayami and T. Furukawa, Proceedings of the Symposia Micro Alloying 75, IIA, Washington, D.C., 78 (1975).

[4] M. S. Rashid, Proceedings of the AIME (Chicago 1977) Symposia Modern Developments in HSLA Formable Steels, in press.

[5] J. M. Rigsbee and P. J. Vander Arend, ibid.

[6] J. M. Rigsbee, J. W. Pickens, A. T. Davenport, J. E. Franklin and J. K. Abraham, Proceedings of the AIME (New Orleans 1979) Symposia Structure and Properties of Highly Formable Dual-Phase HSLA Steels, to be published.

[7] W. R. Cribb and J. M. Rigsbee, ibid.

[8] A. R. Marder, private communication (1977).

[9] J. M. Rigsbee and H. I. Aaronson, Acta Met., in press.

[10] H. R. Erard, Tech. Paper 5A-TR20-2409, Springfield Armory, Springfield, Massachusetts (1964).

[11] G. Krauss and A. R. Marder, Met. Trans., 2, 2343 (1971).

[12] G. Thomas, Met. Trans., 2, 2373 (1971).

[13] J. M. Moyer and G. S. Ansell, Met. Trans., 6A, 1785 (1975).

[14] K. W. Andrews, JISI, 203, 721 (1965).

[15] J. M. Rigsbee and H. I. Aaronson, Acta Met., in press.

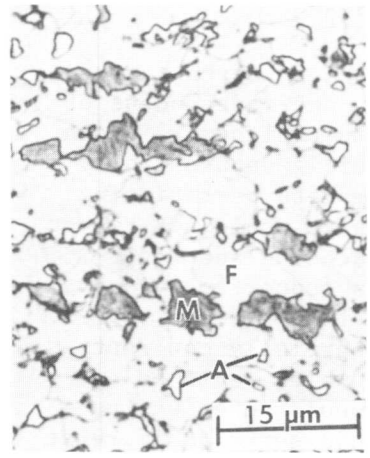

Fig. 1: Optical micrograph; F = ferrite, M = martensite, A = retained austenite.

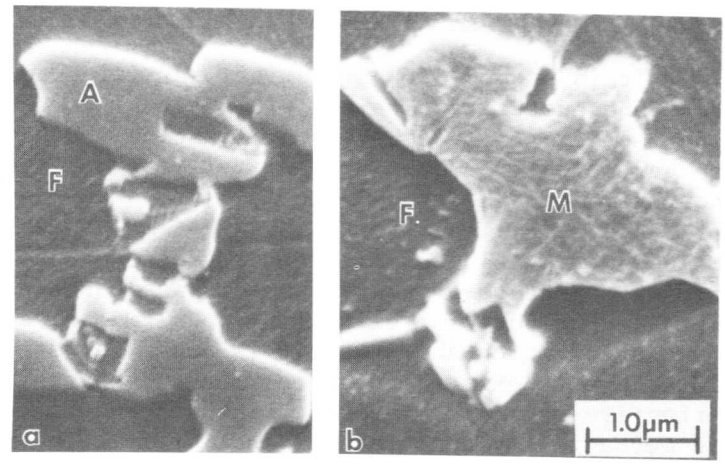

Fig. 2: Scanning electron micrographs; (a) retained austenite particles, (b) martensite particle.

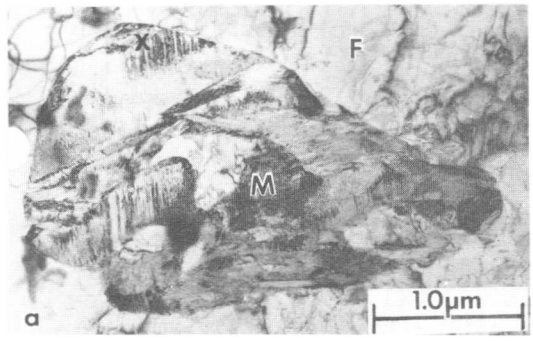

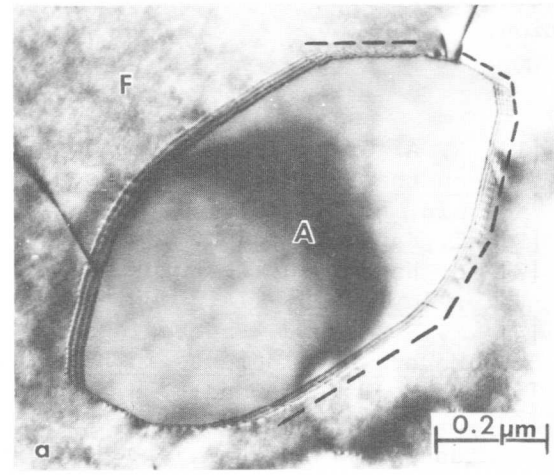

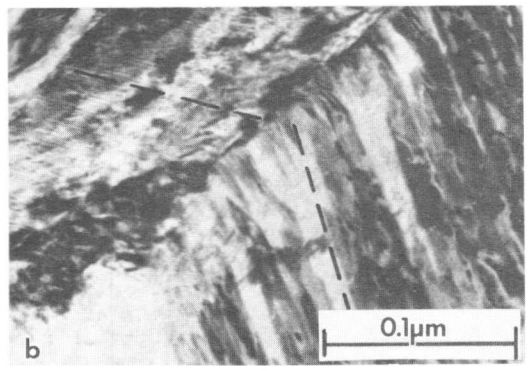

Fig. 3: Transmission electron micrographs, martensite particle; (a) low magnification, (b) high magnification of area "X" of 3(a).

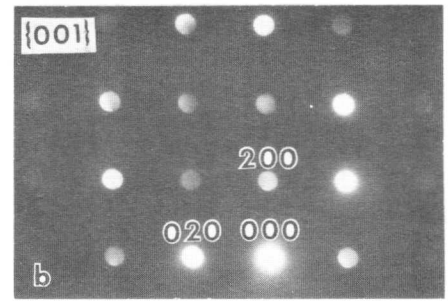

Fig. 4: Transmission electron micrographs, retained austenite; (a) bright-field, (b) {001} convergent beam diffraction pattern.

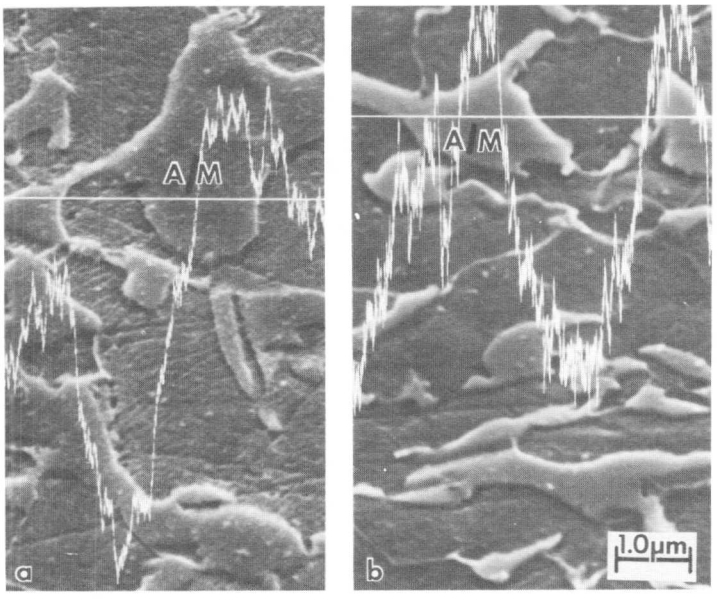

Fig. 5: Scanning electron micrographs showing concentration profiles across retained austenite/martensite particles of (a) carbon and (b) manganese.

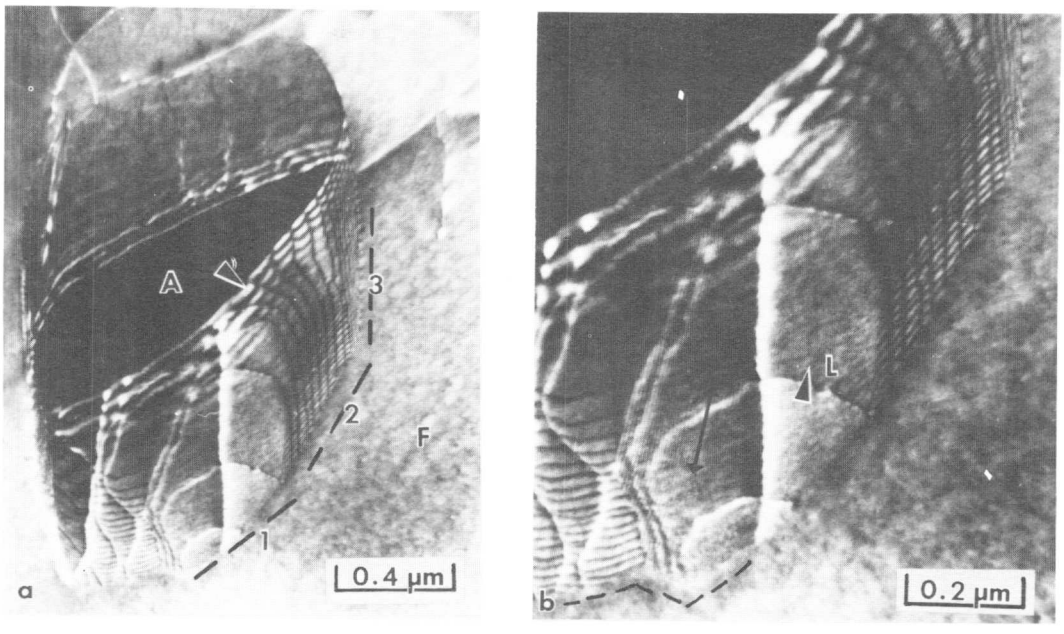

Fig. 6: Weak-beam dark-field transmission electron micrographs ($\bar{g}_{020}$, $|S| \simeq 0.015$ Å^{-1}) showing retained austenite/ferrite interphase interface structure; (a) entire austenite particle (1, 2, 3 indicate facets), (b) higher magnification micrograph of the same boundary (L indicates growth ledge).

Martensitic Transformation in High Magnetic Fields

M. K. Korenko* and M. Cohen**

The kinetics of the isothermal martensitic transformation in Fe-29.6Ni and Fe-22.5Ni-4Mn alloys were investigated as a function of constant magnetic fields, ranging up to 140 KOe (11 x 10^6 ampere/m). The principal role of the applied magnetic field is to increase the free-energy difference between the product and parent phases in these iron-based alloys, and so the transformational driving force for a given composition can be varied even at a fixed temperature. In the Fe-Ni alloy, the isothermal transformation rate is increased by raising the magnetic field as well as by lowering the temperature, leading in either case to the entré of burst characteristics. The Fe-Ni-Mn alloy does not transform perceptibly without an applied field, but exhibits isothermal C-curve kinetics in fields above 60 KOe (4.8 x 10^6 ampere/m). There is some tendency for the morphology to become less lath-like and more plate-like with increasing field strength at a given transformation temperature, and likwise with increasing temperature at a given driving force. Evidently the prevailing view that martensite becomes more plate-like with decreasing transformation temperature is not a pure thermal effect as such, but is rather a consequence of the attendant increase in driving force.

I. Introduction

In typical steels, the martensitic phase is ferromagnetic while the austenite is paramagnetic. Under these conditions, the application of a magnetic field can induce an additional free-energy difference between the parent and product phases.

In 1929, Herbert [1] found that magnetizing a quenched steel caused an increase in hardness. This effect was not linked to the martensitic transformation until 1960, when Sadovskiy et al. [2] reported that they induced extensive martensitic transformation in a Fe-23Ni-1.5Cr-0.5C steel at 77°K with a pulsed field of 350 KOe. Since that time, work in this area has flourished [e.g., 3-10]. Much of this effort has been carried out by Russian investigators using up to 500 KOe pulsed magnetic fields on athermally transforming iron-nickel-chromium alloys. Typically, the effect of the field is to raise M_s in a linear fashion by some 0.1 to 0.3°C/KOe.

There have been comparatively few magnetic studies on alloys which undergo isothermal martensitic transformations [11-14]. Estrin [12] showed that the application of a steady field caused an increase in the rate of transformation. More recently Peters, Bolton and Miodownik [14] described the transformation of an Fe-26Ni-2Mn alloy induced by steady fields up to 20 KOe over a temperature range of -60 to -80°C. They changed the field strength during the course of the reaction, and adopted

* Hanford Engineering Development Laboratory, Richland, WA 99352, USA
** Massachusetts Institute of Technology, Cambridge, MA 02139, USA

the Kaufman-Cohen (K-C) model [15] to evaluate the shift in activation energy for nucleation due to the magnetic field, as well as the temperature dependence of the critical-embryo size.

In the present investigation, the magnetic field is used as a thermodynamic variable to investigate the kinetics of martensitic transformations. Since the effective driving force can be raised by increasing the field strength or by lowering the temperature, it becomes possible to separate the interdependent roles of temperature and chemical driving force.

II. Experimental Procedure

The two alloys investigated, Fe-29.6Ni-0.009OC and Fe-22.5Ni-4.0 Mn-0.0055C, had a final grain size of 41 and 22 μm respectively. Electrical resistivity specimens were prepared by spot welding nickel-wire leads onto swaged wire stock and then carbon doping the surfaces to prevent preferential surface nucleation.

The magnetic fields were generated at the MIT Francis-Bitter National Magnet Laboratory by passing up to 25 Kamps through special axial-flow helical solenoids. The fields varied from 20 to 140 KOe for times up to 3-5 hours in a 2.1-inch bore magnet. Subzero temperatures were held to $\pm$0.2°C over a temperature range of +10° to -140°C.

The isothermal transformations at subatmospheric temperatures were followed by changes in electrical resistance, measured with a Kelvin double bridge. The fractional resistance change corresponding to a 1 percent transformation from austenite to martensite (calibrated by quantitative metallography) was found to be 6.96×10^{-3} and 3.10×10^{-3} for the iron-nickel and iron-nickel-manganese alloys, as referred to 25°C.

The magnetization of the austenitic and martensitic phases in each alloy was measured at the temperatures of interest as a function of field strength, using a vibrating-sample magnetometer in a suitable dewar.

III. Results and Discussion

The Fe-22.5Ni-2.0Mn alloy does not detectably transform by isothermal holding at any temperature. However, by applying magnetic fields in the range of 60 to 140 KOe, it is possible to transform this alloy up to 50% martensite. This illustrates quite clearly that applying a field is very different from lowering the temperature. Figure 1 demonstrates the effect of applying higher and higher fields at constant temperature, whereas Fig. 2 illustrates the effect of varying the temperature at constant field. The transformation is definitely isothermal over the whole temperature range and exhibits a C-curve behavior, which is typical of Fe-Ni-Mn alloys. The higher Mn content of the present alloy (4% Mn) shifts the C-curve out of the experimentally detectable range, unless the kinetics are accelerated by high magnetic fields.

Shih, Averbach and Cohen [16] empirically correlated the nose temperature versus percent Mn. According to their correlation, the nose temperature of the present composition should be below -140°C, approximately 20°C lower than the 140 KOe field-induced nose temperature.

Thus, the magnetic field apparently shifts the C-curve to shorter times and to higher temperatures.

The zero-field martensitic transformation curves for the Fe-29.6Ni alloy are shown in Fig. 3. Isothermal transformations can be observed within convenient times at temperatures below about -8°C. As the reaction temperature is lowered, the kinetics are accelerated but remain fully isothermal down to approximately -20°C, where the transformation may be described as a very fast initial reaction (or burst) followed by a relatively slow isothermal stage. With further lowering of the transformation temperature, the burst is more pronounced and the subsequent isothermal stage becomes smaller. The total amount of transformation observed in these runs increases with decreasing temperature.

The effect of magnetic fields on the transformation kinetics at constant temperature (-2 and +9°C) is illustrated in Figs. 4 and 5. Higher fields are necessary to +9°C than at -2°C to obtain comparable results because of the smaller chemical driving force prevailing at the higher temperature. In comparing Figs. 3, 4 and 5, it is interesting to note that the magnetic field makes it feasible to observe the martensitic transformation at higher temperatures than would otherwise be possible. As the field is increased , the reaction rate in this Fe-Ni alloy is enhanced in somewhat the same manner as lowering the temperature; however, as will be demonstrated shortly, lowering the temperature is different from increasing the magnetic field, even when the same effective driving force is achieved.

Under zero-field conditions at temperatures from -9° to -18°C, the structure is lath-like having a loose-packet morphology as shown in Fig. 6(a). As the temperature is lowered from -9° to -13°C the amount of this lath martensite increases; however, the structure of the individual martensite units remains unchanged. As the temperature is lowered further, however, the structure changes to a mixture of {259} plates with definite midribs and irregular interfaces surrounded by the higher-temperature lath structure, as shown in Fig. 6(b). The temperature at which the plates are first observed is -20°C, where the reaction kinetics change from isothermal to bursting in Fig. 3. As the temperature is lowered even further, the plate morphology begins to predominate. Since these morphological changes (shown in Fig. 6) occur at constant nickel content, we are led to conclude that alloy composition is not the only variable dictating the morphology.

If temperature were the major determining factor in the morphological transition, then the field-induced transformation runs (which are at higher temperatures) should be lath-like in nature. Fig. 7 shows instead that these specimens go through the same transition in morphology as those of Fig. 6. We can, therefore, conclude that temperature is not the only parameter controlling the morphology.

It was possible to compare the structures of several sets of specimens which transformed under nearly the same Gibbs free-energy change; some were produced simply by lowering the temperature and others by a combination of lowering the temperature and increasing the magnetic field. The morphology and kinetics of specimens transformed under con-

ditions of similar driving forces may be quite different.

Likewise, when specimens are compared having the same activation energy ΔWa, it is found that the field-induced specimens display faster transformation rates and have the greater tendency to form the plate morphology. The reason for this is rather straight-forward. The magnetic field accelerates the reaction not only by increasing the Gibbs free-energy difference between the phases but also by allowing the reaction to occur at higher temperatures, thereby taking advantage of the additional thermal energy. For a thermally activated process, like the martensitic phase transformation, the temperature per se is just as important as the magnitude of the activation energy.

Finally, when a comparison is made among specimens having the same $\Delta Wa/T$, or the same transformation rate, it is found that they have nearly identical structures. Thus, the rate of transformation governs the morphology or vice versa. Since $\Delta Wa/T$ is obviously inversely proportional to the temperature, we are forced to make the controversial deduction that high temperature favors {259} martensite, in direct contrast to the usual experimental observation in which we see plate martensite only at lower temperatures. This is not a contradiction, however, since at the lower temperatures we have a higher chemical driving force and lower ΔWa which, up to the present use of magnetic fields, has invariably masked the intrinsic effect of temperature in martensitic transformations.

This work was supported by the National Science Foundation.

References

[1] E.G. Herbert: Iron and Steel Inst., 120(1929), 239.
[2] V.D. Sadovskiy et al.: Phys. Metals Metallogr., 12(1961), 131.
[3] E.A. Zavadskii and I.G. Fakidov: Phys.Metals Metallogr.,19(1965),101.
[4] Ye.A. Fokina and E.A. Zavadskii: Phys. Metals Metallogr.,16(1963), 128.
[5] M.A. Krivoglaz and V.D. Sadovskiy: Phys. Metals Metallogr., 21(1964), 119.
[6] Ye.A. Fokina et al.: Phys. Metals Metallogr., 19(1965), 101.
[7] L.V. Voronchikhin and I.G. Fakidov: Phys. Metals Metallogr., 21(1966), 110.
[8] L.V. Voronchikhin et al.: Phys. Metals Metallogr., 26(1968), 183.
[9] P.A. Malinen and V.D. Sadovskiy: Phys. Metals Metallogr., 28(1969), 54.
[10] K.R. Satyanarayan and A.P. Miodownik: Inst. of Metals, Monograph and Report Series No. 33 (1969), 162.
[11] Ye.A. Fokina, L.V. Smirnov and V.D. Sadovskiy: Phys. Metals Metallogr.,19(1965), 73.
[12] E.I. Estrin: Phys. Metals Metallogr., 19(1965), 117.
[13] P.A. Malinen et al.: Phys. Metals Metallogr.,24(1967), 101.
[14] C.T. Peters et al.: Acta Met., 20(1972), 881.
[15] M. Cohen: Trans. AIME, 212(1958), 171.
[16] C.H. Shih et al.: Trans. AIME, 202(1955), 183.

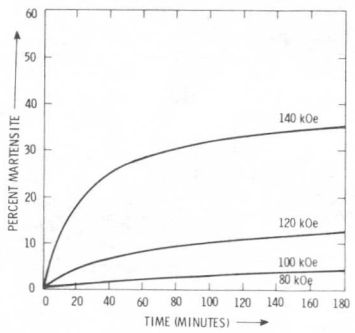

FIG. 1 FIELD-INDUCED TRANSFORMATION KINETICS OF Fe22.5 Ni 4.0 Mn AT -81°C

HEDL 7904-004.2

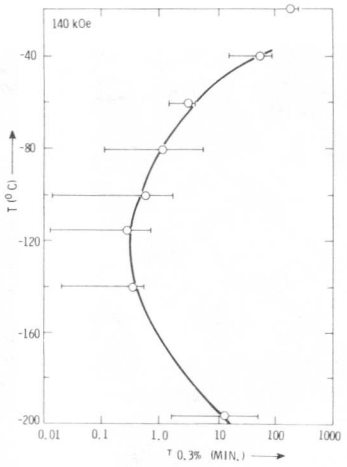

FIG. 2 TIME TO TRANSFORM TO 0.3% MARTENSITE AS A FUNCTION OF TEMPERATURE AT A MAGNETIC FIELD OF 140 kOe.

HEDL 7904-004.5

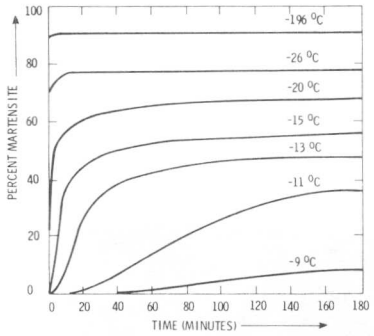

FIG. 3 TRANSFORMATION KINETICS OF Fe 29.6 Ni UNDER ZERO-FIELD CONDITIONS

HEDL 7904-004.1

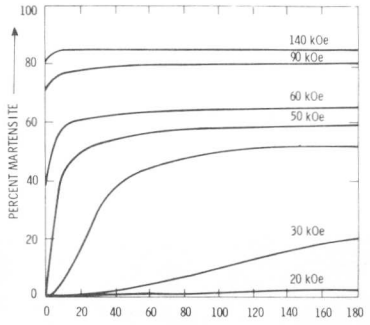

FIG. 4 FIELD-INDUCED TRANSFORMATION KINETICS OF Fe 2.. 6 Ni AT -2° C

HEDL 7904-004.3

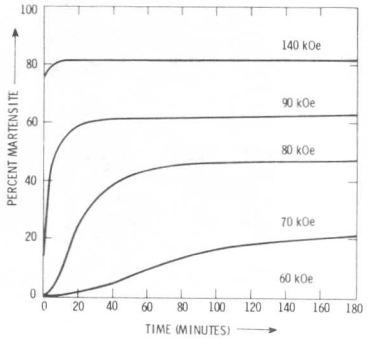

FIG. 5 FIELD-INDUCED TRANSFORMATION KINETICS OF Fe 29.6 Ni AT + 9° C

HEDL 7904-004.4

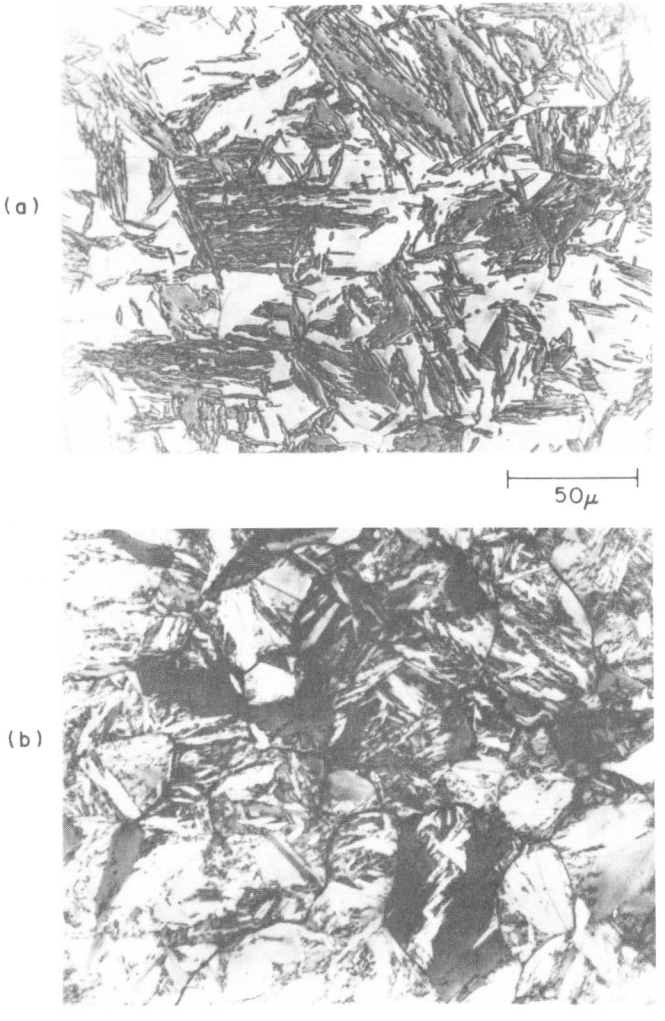

FIG. 6 Morphological transition in Fe-29.6Ni under zero-field conditions. (a) Laths at -13°C, (b) mixture of plates and laths at -196°C.

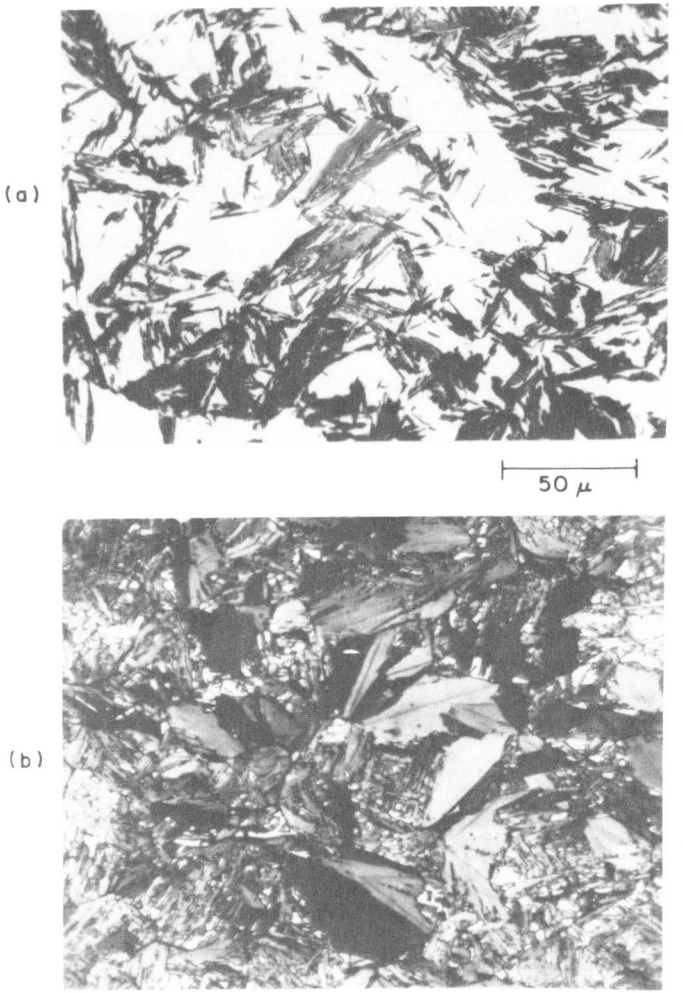

FIG. 7 Field-induced morphological transition in Fe-29.6Ni at -2°C. (a) Laths at 40 KOe, (b) mixture of plates and laths at 140 KOe.

Sequence in Variation of Kinetico-Morphological Characteristics of Transformation from "Normal" to "Martensitic" with Rise in Driving Force of the Process

E.V. Safonov and A.V. Shalimova

As a result of the investigation of the processes taking place in rhodanic ammonium single crystals it was found four kinetico-morphological types of transformation upon heating. For the first time it was possible to follow the subsequent changes of almost all the varieties of transformation of one substance from "normal" to "martensitic", that were described in the literature. The change of the kinetico-morphological type of transformation upon heating occurs so that the orientation influence of the matrix increases with rise in temperature. The martensitic transformation takes place at the highest deviation from the phase equilibrium temperature, T_o. Lower deviation from T_o corresponds to more inert kinetic. A detailed study of the transformation kinetics reveals the spasmodic character of the phase boundary which consists of the displacement and halt in all types of transformations. In the course of transformation of one type of transformation to another the displacement value does not essentially change; only the expectation time between separate boundary movement acts varies considerably. In martensitic transformation the expectation time tends to zero. The experimental data obtained supports the conclusion of the heterogeneous structure transformation theory that there exists apparently a single stable phase formation mechanism for all polymorphous transformations.

At the present time there is a great deal of experimental data in literature showing that the shift of kinetico-morphological transformation from normal to martensitic is due to varying the rate of heating or cooling. The essential distinction in the kinetics of these transformation as observed in many cases leads to the conclusion that there exist two different mechanism in forming a new phase: civil (corresponding to normal transformation) and military (cooperative martensitic transformation). However, there exists another generally recognized point of view that no matter how great the difference in the kinetics and morphology of normal how great the difference in the kinetics and morphology of normal or martensitic transformations may be, it need not necessarily be counted as a

---

Central Scientific Research Institute of Ferrous Metallurgy, Moscow

result of a strict difference pertaining to their particular mechanism. It can be regarded as a result of relaxation of the internal stresses occurring in the ordered contact of phases [1]. The relaxation processes obscuring the ordered picture of transformation peculiar to the martensitic kinetic, decrease the degree of crystallographic interaction of the phases and bring about the occurrence of a whole spectrum of diverse kinetico-morphological types of one and the some polymorphic transition.

To check the above-mentioned conception the simulation method for processes occurring in metals on optically transparent crystals was used, as this method proved to be highly appreciable in elaborating the theory of crystallization. Rhodanic ammonium was the material to be investigated, the kinetico-morphological peculiarities of transformation development of this compound was described in [3, 2].

By generalizing the experimental data obtained in these studies, corresponding to certain isothermic exposition temperatures, it was possible to descern the following development of the process:

I. The T = 79°C - transformation starts with the formation of one or two nuclei on the sample faces to be followed by crystal growth. Their interphase boundary of irregular shape leaves behind a high temperature phase single crystal during its movement. No relief is observed on the sample faces at the site of the rise of the new phase. The rate of the interphase boundary movement is given in Fig. 1, curve a.

II. The T = 83°C - character of the onset of transformation does not change. The nucleation of a new phase appears on the sample faces as previously, but a polycrystalline structure starts to form behind the front of the growing crystal. The interface of the phase represents a well-pronounced broken shape. The sample does not exhibit any relief on its faces or any change in shape. The rate of the movement on such a boundary increases noticeably (Fig. 1, curve b).

III. T = 80°C - growth of the high temperature phase, nucleated on the sample face, proceeds at the expense of the interphase boundary of rectilinear shape passing through the whole sample. The growing domain preserves a polycrystalline structure. An essential distinction of this type of transformation from the previous one, with the exception of the boundary rectilinearity, is the dramatic change in sample shape. The boundary movement rate is illustrated in Fig. 1, curve c.

IV. T = 93°C - beginning with this temperature one witnesses a dramatic martensitic transformation characterized by a high speed of transformation of high tempe-

rature phase crystals strictly oriented relative to the lattice of the low temperature phase, by the change in the shape of the sample and athermic kinetic. The growth of the new phase proceeds at the expense of formation of new crystals, but not owing to the growth earlier formed crystals. The transformation ends with the formation of a high-temperature phase single crystal.

The peculiarities of the transformations behaviour described above, shows that not all the external features of development of the process change simultaneously in the transition of one type of transformation to another. For instance, the shape of the interphase boundary of the first and second types of transformation preserve the same irregular shape in spite of the substantial structural change of the high-temperature phase the change from single crystal to polycrystal. The transition of the second to the third type of transformation leads to smoothing out of the interphase boundary front, but the polycrystalline nature of the structure which has undergone a domain transformation, remains invariable. A considerable change in the shape of the sample accompanying the third type of transition is one of the most characteristic features of martensitic transformation. A more vivid inheritable character of transition of types of formation manifests itself in the analysis of the orientational influence of the matrix on the growth of crystals of a new phase.

The mutual position of the lattices of the growing crystals and matrices was determined using the polarizationally-optical technique for angles of total extinction in a crossed polaroid. By turning the sample in the plane perpendicular to the axis under observation it is possible to get in line the direction of the axis of the optical indicatrice of the crystal and the mutually-perpendicular axes of the analyser and polarizer. This corresponds to a condition of an absolute extinction in the circular polarizer. In the formation of new phase crystals the birefringence conditions changes and by revolving the microscope table the position of absolute extinction is restored. The required angle for this rotation is referred to as an absolute extinction angle. Different rotation angle values relative to the original position of absolute extinction correspond to different orientations of the daughter crystals. The experimental results for transformations "I" and "II" are illustrated in the diagram in Fig. 2. The extinction angle values from -45 to +45° relative to the position of absolute extinction of the matrix are plotted as coordinates. The chosen range covers the entire high temperature phase orientation spectra and its further expansion is unreasonable due to the limitation superimposed by the polarizationally-optical procedure symmetry. The measurement accuracy of the angle is $\pm 0.5°$. The encountering frequency of one and the same angle values is laid off along the X-axis.

As is seen from the data obtained for transformation I (Fig. 1a), one may practically notice all possible (taking account of the measurement accuracy data) disorientation angle values of the growing phases and matrices. However, some of these directions are more preferable than others. For example, the angle values 2°, 6°, -33° occur twice more often than the mean repetition number, equal to 5. On the other hand six values occur only once, whereas five are not registered at all. The difference between the minimal and maximal quantity of repetition of the extinction angle values is more than an order. A well-defined tendency of formation of high-temperature phase orientation in certain groups (Fig. 2b) is noticeable in transformation II. Here, the repetition of the extinction angle values is slightly higher since a large number of grains of similar orientation occurs simultaneously in polycrystal structures.

Transformation III is characterized by the formation of a complex polycrystalline structure wherein the achievement of an absolute extinction position for the majority of the high-temperature phases was a failure. The orientation of such sites, where absolute extinction is possible, varies within $\pm 6°$ relative to the extinction angle value, equal to 13°.

Finally, as a result of the martensitic transformation IV strictly oriented relative to the matrix system of mutually-perpendicular crystals of a high-temperature phase forms. This system has one extinction angle value, equal to -13°.

A more detailed analysis of the kinetic process has produced interesting results regarding the genetic relationship of different types of transformation. The cinematographic films analysis of the process reveals an interrupted character of the boundary movement (Fig. 3) inherent in all the types of transformation under investigation consisting of intrinsic displacement and cessation. When the superheating enhances, the jump value does not change effectively, only the expectation time changes noticeably between the individual acts of movement, which frequency rising with its increasing (Fig. 3a, b, c). The extrapolation of the dependence of the expectation time on the superheating tending to zero offers a critical superheat value close to the onset the martensitic transformation (Fig. 4). The path of the travelling boundary for one act of movement for transformations II and III are significantly less than the size of separate grains of high-temperature phase polycrystal structures. The normal movement of the boundary for all types of transformation is realized at the expense of swelling its separate sites and subsequent pulling the rest parts to a normal level.

The analysis of the obtained experimental data has shown that a more satisfactory explanation is found in the framework of the theoretical conception based on the relaxation mechanism.

The enhancement of the orienting influence of the matrix with a rise in the driving force of the process during heating cannot be convincingly accounted for from the position of admitting the existence of two mechanisms of civil and military transformation. The action of the first one is traditionally associated with the high mobility of atoms. With the rise in temperature the action of this mechanism should lead to the weakening of the orienting influence of the matrix. The experimental data are indicative of an opposite tendency which is, as in the case of the interrupted character of the boundary movement, well explained by the action of diverse relaxation mechanisms accompanying the interphase boundary movement in solids [4]. The tendency of the expectation time between individual boundary movement acts toward zero when approaching the time of onset of the martensitic transformation, confirms the presence of a genetic relationship between different types of polymorphic transformation.

Thus, the unique case of observation under normal pressure on one surstance of a successive interchange of almost all the known kinetico-morphological types of transformation in the aggregate with the basic experimental data on the character of the interphase boundary movement and orientational relationship of the phases allows one to make an assumption on the possibility of there existing a single mechanism for all types of polymorphous transformation. The visual observing discrepancy between morphology can be apparently connected with diverse degree of proceeding of the relaxation mechanisms on interphase boundary during its movement.

References

1. A.L. Roitburd, Col. Problems of Modern Crystallography Nauka (1975), 345 (in Russian), Moscow.
2. A.L. Roitburd, E.V. Safonov, T.M. Syritskaya, A.V. Shalimova, Kristalografia, 22 (1977), p. 307.
3. E.V. Safonov, A.V. Shalimova, International Conference. Martensitic Transformations, abstracts of papers, Kiev (1977), 140.

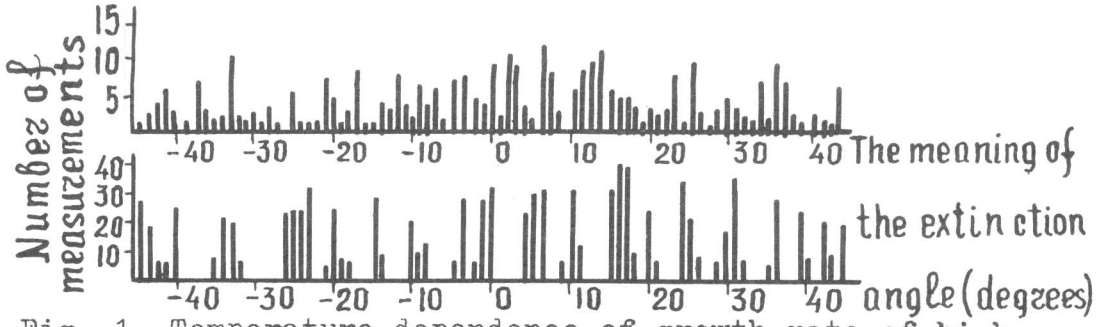

Fig. 1. Temperature dependence of growth rate of high- - temperature phase in a rhodanic ammonium single crystal for normal transformation of types I and II

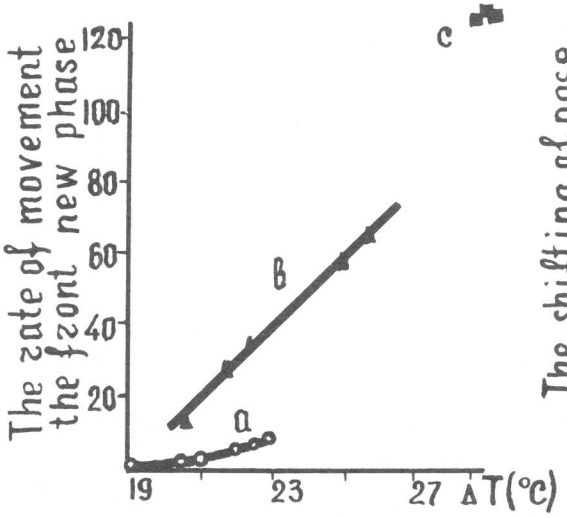

Fig. 2. Orientation relationships diagram for different types of normal transformation in rhodanic ammonium crystals: a - transformation I; b - transformation II

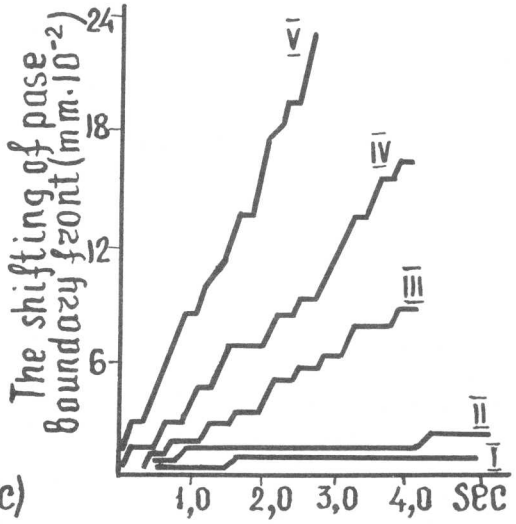

Fig. 3. Interrupted character of interphase boundary movement for different types of polymorphic transformation in rhodanic ammonium single crystals: I, II - T = 79 °C; III, IV - T = 83 °C, V - T = 90 °C

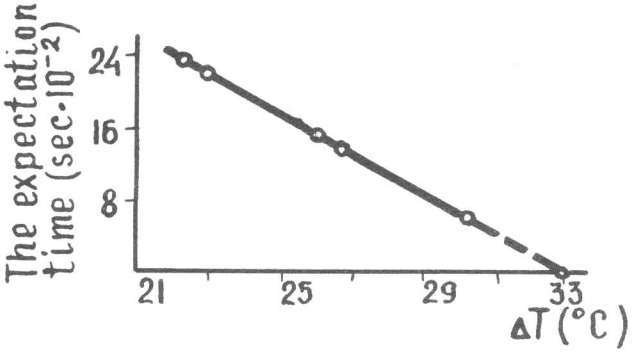

Fig. 4. Influence of superheating on the length of the steps between separate acts of interphase boundary movement

Premartensitic Phenomena

L. Delaey[x], P.F. Gobin[o], G. Guenin[o] and H. Warlimont[xx]

Various phenomena which are regarded as "premartensitic" in the literature are reviewed and schematically represented for comparison. Two main aspects of these phenomena are considered : the anomalous evolution of bulk lattice properties and the occurrence of microregions having a structure and properties different from those of the parent phase. The pertinent aspects of the elastic constants, phonon dispersion and electron microscopic observations are emphasized. Some phenomena have a direct effect on the martensite formation, others are just competitive and still others may be regarded as an intermediate stage.

A main conclusion is that "premartensitic" phenomena should be differentiated with respect to those which are bulk properties and those which occur in conjunction with lattice defects and interfaces, in particular with free surfaces. Based on the bulk properties of the parent phase in the temperature range above M_s, the martensitic alloys can be classified into three main groups. In each group the lattice stability or instability has a different degree of influence on the transformation characteristics (structure morphology, mechanism and nucleation). The effects associated with defects and interfaces permit, on the other hand to analyse some of the changes of structure and properties pertinent to the bulk "premartensitic" phenomena and to the martensitic transformations.

I. Introduction

A number of phenomena which do not comply to the normal behaviour of metals and alloys occur in alloys which transform martensitically. These phenomena observed mainly in the temperature range above M_s are a softening of elastic constants, inelastic neutron scattering, resistivity anomalies, anomalous magneto-resistance effects, calorimetric effects, diffuse and extra diffraction effects, the occurrence of an ω-phase and similar structural transitions, contrast effects and shimmering or streaming effects in transmission electron microscopy, changes in internal friction, hardness, magnetic susceptibility and in Mössbauer effects, anisotropy of the Debye-Waller factor and anomalous effects observed by positron annihilation. These effects are referred to in the literature as "premartensitic", "premonitory", "precursory", "pretransition", "intermediate", "soft mode effects", "elastic softening", "phonon softening" "lattice instabilities", triggering effects", "dispersion anomaly" and even "unidentified fluctuation observations (UFO)".

---

[x] Department of Metallurgy, Katholieke Universiteit Leuven, Belgium

[o] Department of Physical Metallurgy, Institut National des Sciences Appliquées de Lyon, Villeurbanne (France)

[xx] Vacuumschmelze GmbH, Research and Development, Hanau (W. Germany)

Some of these observations concern bulk properties, others concern thin foil observations and still others are concerned with the appearance of martensite plates already above the "macroscopic" M_s, i.e. the transformation temperature obtained by conventional macroscopic property measurements.

In connection with these observations several theories have been developed to explain the phenomena and the underlying processes. In several interrelated theories lattice instabilities are calculated taking into account anharmonic terms of elastic or strain free energy. In these theories plane waves of large amplitude phonons are assumed to exist in the pretransformation region and are assumed to trigger the martensitic transformation. These theories are known in the literature as "localized soft phonon", "strain spinodal", "heterophase fluctuation", "condensation of phonons", "phonon nucleation" theory, etc.

In 1965 at the conference on "The Physical Properties of Martensite and Bainite" [1] only two papers [2, 3] have been concerned with the relation between the elastic properties of the parent phase (the lattice instability with respect to shear modes, as first explained by Zener [4]) and the transformation temperature and nucleation. The study of shape memory alloys brought the problem of "the premartensitic phenomena" to the foreground of the discussions, because it is in those alloys that most of the anomalous phenomena are observed. In 1975 at the conference on "Shape Memory Effects in Alloys" [5] eight papers out of thirty-four treated the premartensitic phenomena. The localized soft mode theory had already been introduced at that time [6]. It was shown that there is an intimate relation between the softening of the elastic constants and the thermoelastic and pseudoelastic behaviour [7, 8]. The elastic softening in the β-Hume Rothery alloy systems was explained by the temperature dependence of the repulsive ion core interaction [9]. The crystallographic relation between vibrational modes, static displacements and martensite formation was also discussed [10]. Some of those points were reconfirmed in 1976 at the Kobe symposium [11, 12, 13]. The existence of some new intermediate phases in steel was reported [14] and the nucleation of stress-induced martensite was attributed to large amplitude lattice waves [15]. At the ICOMAT 1977 Conference in Kiev [16] the concept of lattice instabilities prior to the martensite transformation was further analysed[74].Based on earlier work [17], calculations of lattice stability with respect to a bcc → ω, bcc → 9R and fcc → bcc transition using third order elastic coefficients were presented. However, attention was drawn to the heterogeneous nature of the nucleation of martensite nucleation and to the finite and often large undercooling required to nucleate martensite; these features common to all martensitic transformations are not required for phase transitions which proceed by infinite lattice softening [18].

Since many alloys show no lattice softening, others a moderate but not infinite softening at M_s and still others - a limited number - exhibit a drastic softening, the alloys which transform martensitically will be treated according to these groups throughout the present paper.

II. Mechanical Lattice Stability

The mechanical lattice stability is a direct consequence of the interatomic bonds. This stability may be studied using two different approaches : a static approach treating the conditions are determined for a lattice to be stable when submitted to small static or quasistatic homogeneous strains, and a dynamical approach treating the dynamical characteristics that a lattice should possess in order to be mechanically stable. The former approach leads to the elastic constants whereas the latter, which is more universal, leads to the study of phonons.

The static approach : the free elastic energy density may be expressed by

$$F = F_o + \frac{1}{2!} \sum_{ij} C_{ij}\, \varepsilon_i\, \varepsilon_j + \frac{1}{3!} \sum_{ijk} C_{ijk}\, \varepsilon_i\, \varepsilon_j\, \varepsilon_k + \ldots \quad (1)$$

C_{ij} are the second order constants, C_{ijk} the third order elastic constants, ε_i the homogeneous strains and F_o the free energy of the unstrained lattice.

For a lattice to be stable when submitted to small homogeneous strains, the free elastic energy density must increase for all possible strains. The quadratic form $\Sigma C_{ij}\varepsilon_i\varepsilon_j$ must therefore be positive because the other forms can then be neglected. Mathematically this is expressed by saying that all the eigenvalues of the C_{ij}-matrix must be positive or all the determinants of successive minors of the C_{ij}-matrix must be positive. In the case of cubic crystals these conditions reduce to $C_{44}>0$, $C_{11}-C_{12}>0$ and $C_{11} + 2C_{12}>0$.

These stability conditions can be modified in the strained regions of the lattice because of the existence of the anharmonic terms (third and higher order elastic constants [6, 19, 20]). Schematically this can be understood as follows : formula (1) can be simplified as

$$F = F_o + \frac{1}{2} C_2\, \varepsilon^2 + \frac{1}{6} C_3\, \varepsilon^3 \quad (2)$$

The restoring force against a strain ε is then given by

$$\frac{\partial^2 F}{\partial \varepsilon^2} = C_2 + C_3\, \varepsilon \quad (3)$$

In the general case C_2 is a combination of second order elastic constants (C_{ij}) and C_3 is a combination of second and third order elastic constants (C_{ij}, C_{ijk}). Formula (3) shows that this restoring force may increase or decrease with strain depending on the sign of $C_3\, \varepsilon$.

The dynamic approach : Born and Huang [21] have shown that the above criteria are not sufficient to ensure complete stability, in particular for heterogeneous strains such as those produced during short wave length propagation of vibrations. Born and Huang established that a crystal will be stable for all kinds of small strains if all the normal modes exhibit real frequencies ($\omega^2 > 0 \;\forall\; Q = 1/\lambda$). The study of complete instability is therefore done through the examination of phonon dispersion curves. The tendency towards mechanical instability is seen when a particular vibrational mode ($q = q_o$), either optic or acoustic, at $q = 0$ or elsewhere in the Brillonin zone becomes unstable :

$\omega \to 0$ for an optic mode at $q = q_o$ (q_o)
$\omega \to 0$ for an acoustic mode at $q = q_o$ ($q_o \neq 0$)
$d\omega/dq \to 0$ for an acoustic mode at $q_o = 0$.

The particular mode becoming unstable is called a "soft mode". A structural transition is called a soft mode transition when, at a temperature T_c, a particular mode is unstable leading to a spontaneous distortion of crystal. The structure of the new phase is uniqually determined by the eigenvector is simply the arroy of atomic displacements accompanying the exitation of that mode. In that case the transition is second order.

In most real cases the martensitic transition in metals and alloys occursbefore any vibrational mode being completely unstable ($\omega \neq 0$ or $d\omega/dq \neq 0$), the structural transition is thus first order.

III. Schematic Representation of the Observed Phenomena

In table 1 a number of characteristic alloys are classified according to their lattice mechanical instability.

Table 1 Classification of various martensitic alloys according to the magnitude of lattice softening.

Group A no lattice mechanical instability	Group B moderate lattice mechanical instability	Group C drastic lattice mechanical instability
Fe-C	Cu-, Ag-, Au- and Ni-	In-X alloys
Fe-Cr-Ni	β Hume-Rothery phases	(X = Tl, Cd, Hg ....)
Fe-Mn-C	U.	A15 compounds (V_3Si,
Co	Fe-Ni (Ni% > 30%)	Nb_3Sn)
Co-Ni	Fe-Pt (near Fe_3Pt)	antiferromagnetic alloys
Fe-Ni (Ni% < 30%)		(Mn-Cu, Mn-Ni, ...)

On fig. 1 are drawn some selected C' and C_{44} measurements representative for a wide variety of martensitic alloys are plotted. Table 2 shows some data for comparison extracted from figure 1 and literature. The common features are a large or very large elastic anisotropy A in the vicinity of the transformation, which is mainly due to a low value of C', and an anomalous positive temperature coefficient, $dC'/dT > 0$. From these data, in particular $(1/C')\,(dC'/dT)$, it is obvious that groups B and C should be differentiated. Some typical dispersion curves are given for the same alloys, if available, in figure 2. In the case of Fe-Ni no special behaviour is observed [30], for the ordered Fe_3Pt [31] and the β-phase alloys [32, 33, 34] we notice that the entire TA_2 [ξξo] branch, the slope of which at the origin corresponds to C', is low or very low in energy qualitative and for some cases (e.g. Cu-Zn-Al) in quantitative, and decreases with decreasing temperature, which is in agreement with the ultrasonic measurements. In the case of Au-Cu-Zn and Cu-Zn-Al an anomaly is observed at $q = 2/3\ q_{max}$, but there is no critical behaviour at M_s. By contrast, in the case of Nb_3Sn [35, 36] a soft mode on TA_2 [ξξo] branch is located at q = o, the remaining branch being "normal" as M_s is approached.

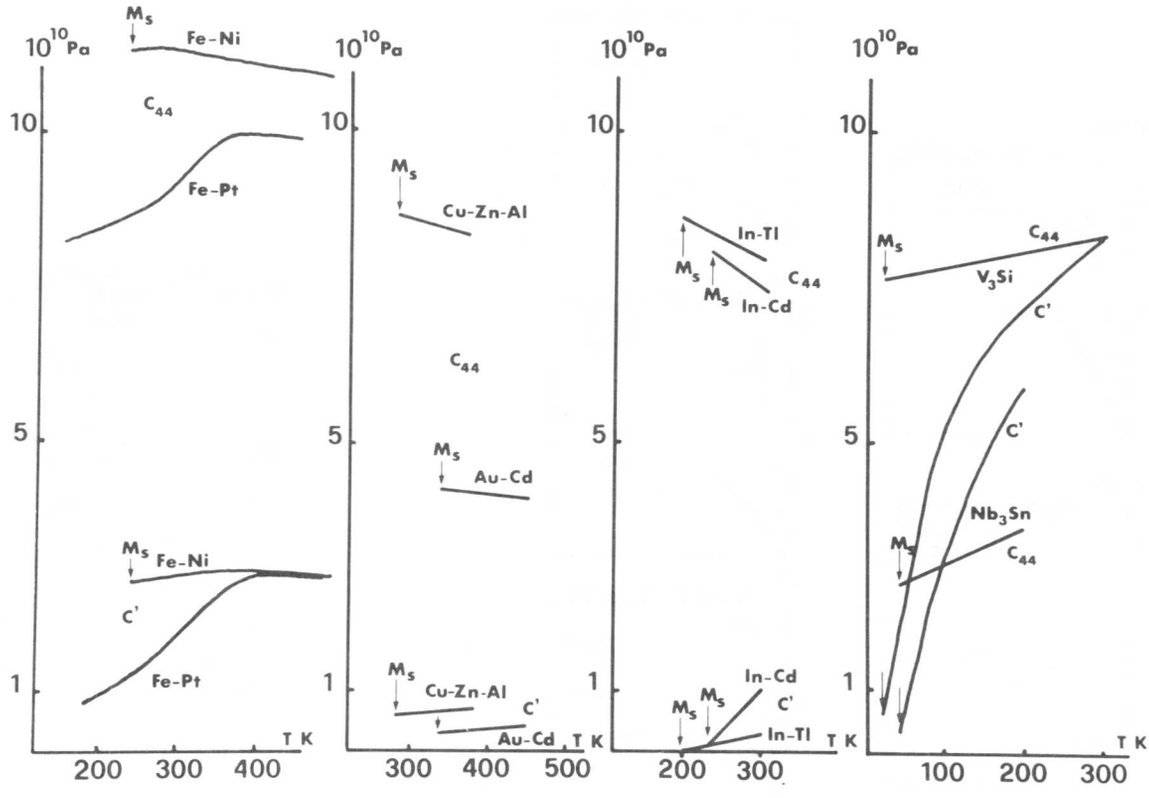

Figure 1 : C' and C_{44} measurements
Fe-Ni 31.5 % (22), Fe-Pt (23), Cu-Zn-Al (24), Au-Cd (25), In-Tl (26), In-Cd (27), Nb_3Sn (28), V_3Si (29).

Table 2 Data on elastic constants (C' and C_{44}) and the elastic anisotropy A at M_s and their temperature dependence.

	10^{10}Pa C_{44} at M_s	10^{10}Pa C' at M_s	A at M_s	$\frac{1}{C_{44}}\cdot\frac{dC_{44}}{dT}$ 10^{-4}	$\frac{1}{C'}\cdot\frac{dC'}{dT}$ 10^{-4}	reference
Nb_3Sn	2.73	0.27	> 10	+ 25	∿ 2800	(32)
V_3Si	7.6	0.61	> 12.5	+ 2.4	∿ 960	(31)
InTl	7.9	0.03	287	- 8.6	∿ 700	(26)
InCd	8.06	0.10	67	- 9.1	∿ 1300	(27)
AuCd	4.1	0.29	14	- 3.6	27	(25)
CuZnAl	8.6	0.58	15	- 4	4.3	(80)
AuCdZn	5.6	0.7	7.5	- 5.3	7	(78)
NiAl	13.5	1.47	9	- 5.7	6	(81)
CuAlNi	10.2	.76	13	- 3.5	3.9	(78)
Fe_3Pt	8.1	1.16	7	11	47	(23)
$FeNi_{33.8}$	10.4	1.8	5.6	1.4	11	(22)
$FeNi_{31.5}$	11.2	2.8	4.1	- 0.4	3.3	(22)

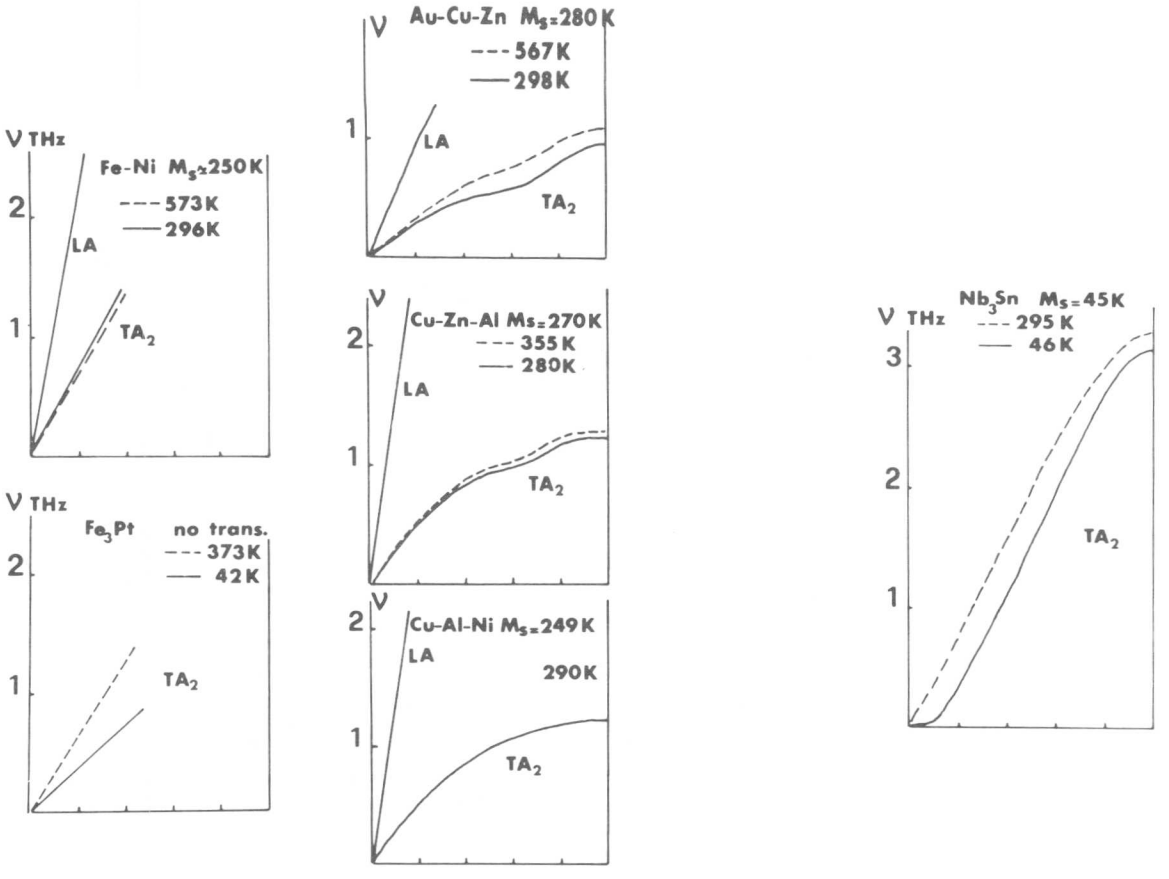

Figure 2 : $[\xi\xi_0]$ phonon branches (LA and TA_2)
Fe-Ni (30), Fe-Pt (31), Au-Cu-Zn (32), Cu-Zn-Al (33),
Cu-Al-Ni (34), Nb_3Sn (35)(36).

The observations referred to as "premartensitic" in the literature will now be analysed in more detail.

Group A In this group no lattice softening is observed. The low temperature electron microscopic observations of Oshima and Wayman [35] and Fujita and coworkers [14] appear, to the authors' knowledge, to be the only observations in iron base alloys which are interpreted as "intermediate"structures. Based on a six layer structure, which explains the diffraction patterns, Fujita proposes a new path of the martensitic transformations in steel. His model which is based on thin film observations appears to be compatible with other bulk phenomena. On approaching M_S a gradual increase in the distance between two partial dislocations was observed for a Fe-Cr-Ni alloy [36]. This corresponds to a decrease of the stacking fault energy. This observation was used by Olson and Cohen [37] to support their nucleation model which involves the appearance of defects and intermediate phases, the first step being a stacking fault or group of stacking faults.

Group B The alloys which have received most attention regarding "premartensitic" phenomena are the β-Hume Rothery phases and the ferromagnetic Fe-Ni and Fe-Pt alloys.

The β-Hume-Rothery phases have a body centered cubic structure which

usually undergoes a disorder-order transformation prior to the martensite transition [85]. High temperature diffuse scattering is observed in X-ray as well as electron diffraction which is explained by high amplitude vibrational modes leading to entropy stabilisation at high temperatures [38, 39]. The β-phases are characterised by a high equilibrium and quenched-in vacancy concentration (up to $10^{-4} \sim 10^{-3}$). Upon cooling the metastable and even the stable β-phases, the C'-shear elastic constant and Young's modulus become progressively more anomalous. The magnitude deceases ($C' < 10^{10}$ N/m^2, $E < 7000$ kg/mm^2) and the temperature coefficient turns positive, $\partial C'/\partial T > 0$, $\partial E/\partial T > 0$. At the same time the elastic anisotropy increases, values for $A = 2C_{44}/(C_{11} - C_{12})$ as high as 18 are reported. C' and E become minimum but not zero at M_S whereas A reaches a maximum. The elastic shear constant C' is strongly affected by uniaxial stresses as shown in figure 3 [20, 40], whereas the other elastic constants are not much affected. The transverse acoustic TA_2-branch is low in energy, a local softening at q = 2/3 [110] on approaching M_S is observed only in alloys which transform to a 9R-type martensite and not to a 2H-martensite. Apart from the softening of $(C_{11} - C_{12})/2$ at least two other types of elastic mode have been shown to become soft prior to the martensite transformation [66, 67, 77].

In thin foil observations anomalous diffraction and contrast effects are found, which have been explained by various structural transitions such as the β - ω transitions, or others such as proposed by Sato, Naga-

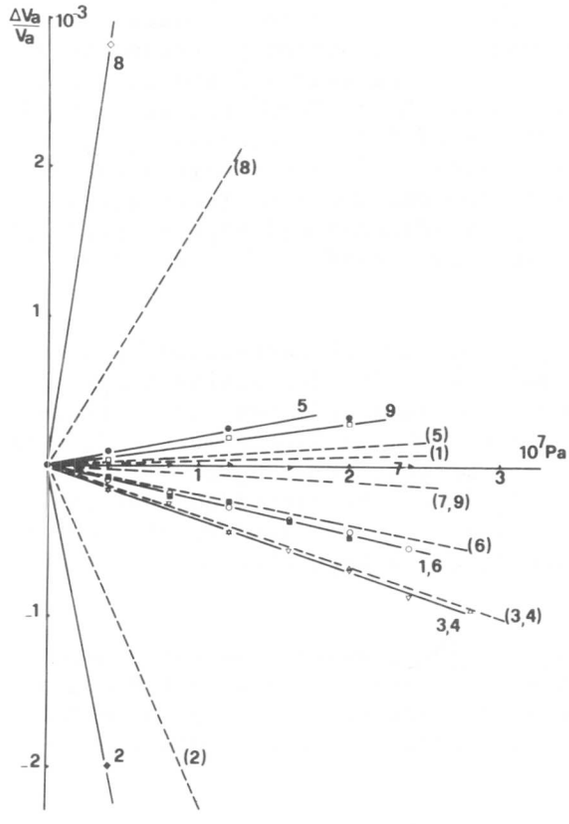

Fig. 3 : Ultrasonic velocity dependence on static uniaxial stress for Cu-Zn-Al —— (40) and Cu-Zn --- (20) curves 2 and 8 relative to (110) [1$\bar{1}$0] velocity measurements when stressed in the [001] and [1$\bar{1}$0] directions respectively. Other curves are relative to other velocity measurements corresponding to C_{44}, C_{11} and C_L (see ref. 40).

sawa, Delaey et al. [41, 42, 43, 44, 45, 62, 69] and Prasetijo et al. [77]. Even reflections from the martensite structure are observed far above M_s [43, 46]. From diffuse electron scattering experiments it was concluded that low frequency transverse acoustic phonon modes, [110] [110] existed in the pretransformation region. In the following paper, the attention will be drawn to the fact that these anomalous diffraction spots are due, at least in Cu-Zn-Al, to finely dispersed 9R martensite with the habit parallel to the foil surface [48]. This phase has thus to be considered as "concurrent" instead of "premartensitic".

Lattice softening has been predicted to occur also in the martensite phase upon heating and prior to the reverse transformation [49]. Such a behaviour has been found in a Cu-Zn-Al martensite single crystal as shown in [50, 19].

The ferromagnetic Fe-Ni and Fe-Pt alloys show pronounced elastic softening prior to martensitic transformation [22, 23]. But it is observed only if the Curie temperature T_c is above M_s (Ni % > 30 %). Phonon dispersion [31] and specific heat [51] measurements corroborate that the elastic anomalies of these systems are lattice properties associated with their large invar effects; however, a "central peak" in the phonon dispersion of Fe_3Pt is not yet completely understood [31]. In Fe_3Pt alloys with $Tc > M_s$ a tetragonal distortion of the austenite was observed by X-ray and electron diffraction above M_s [68]. It has been attempted to show by Mössbauer spectroscopy that the area of the resonance absorption peak, f', which depends on the mean square atomic displacement $\langle X^2 \rangle$ as $f' = \exp\left(-(4\pi^2/\lambda^2)\langle X^2\rangle\right)$, indicates an increase in displacements on approaching M_s [52, 53]. The evidence is not strictly conclusive at present but it may point to an effect beside magnetic softening. An increase in magneto resistance, 5 to 6 K above M_s in Fe-Ni has been found and interpreted in terms of the occurrence of "strain embryos" [54]. Recently, diffuse electron and X-ray scattering in Fe-Ni alloys was studied. It was interpreted as indicating the existence of fluctuation waves of displacements characterized by two-dimensional regions parallel to {110} with polarization vectors <110> and interference effects of these [55].

The titanium- and zirconium-based alloys are characterized by a low shear elastic constant C' [56] which decreases with decreasing temperature. Low frequencies are also observed by inelastic neutron scattering [57]. Moreover, an ω-transition, athermal and isothermal, occurs in these alloys prior to martensite transformation. From measurements on the hexagonal low temperature phase [73] it can be concluded that the martensite phase is probably characterized by a low shear modulus which decreases anomalously upon approaching A_s and a high elastic anisotropy which increases upon approaching A_s.

Hexagonal metals such as Ti, Zr, ... [58], which transform martensitically to the bcc-phase upon heating, all show a positive temperature coefficient of $A = C_{44}/C_{66}$ in the hexagonal phase; the hexagonal metals which do not transform to bcc high temperature phases all show a negative temperature coefficient.

The low temperature phase transition in alpha uranium shows anoma-

lies in the thermal expansion, Hall coefficient, electrical resistivity and thermoelasticity power. The C_{11}-constant is strongly affected by the transition and the lattice instability is believed to be a result of the nature of certain interatomic bonds [59].

Group C For these alloys the transition is characterized by a tetragonal or orthorhombic distortion of the cubic high temperature structure at a critical temperature T_d. It remains to be analysed conclusively whether the entire volume is distorted simultaneously at $T < T_d$ or the low temperature phase forms by nucleation and growth. The lamellar microstructures observed may arise from stress relaxation in the former and from martensitic growth in the latter case.

The In-X alloys transform from fcc to fct. Both parent and martensite phase show a low elastic shear constant (C' in the parent phase and C_{55}, which corresponds to C', in the twinned martensite). Both decrease drastically on approaching the transformation temperature [26, 27]. To the authors knowledge no intermediate or "premartensitic" phases are observed.

The A 15 compounds (V_3Si and Nb_3Sn) have at high C' constant at room temperature leading to a nearly elastically isotropic behaviour. On cooling to low temperatures C' is diminished drastically when approaching the transition temperature. The martensit phase is a tetragonal distortion of the cubic structure of the parei : phase. This soft mode is localized at q = 0 (see figure 2). Although no premartensitic phase is observed, it was suggested that local distortions occur around point defects [60, 61]. This would lead to locally extremely small regions with tetragonal symmetry above the bulk transformation temperature.

In the Mn-X (X = Cu, Ni) magnetostrictive antiferromagnetic alloys the antiferromagnetic ordering is frequently accompanied by a distortion of the crystal lattice. Young's modulus exhibits a sharp decrease and often a minimum at or slightly below the Néel temperature T_N. Single crystal measurements on a Mn-Ni alloy have shown that C' decreases sharply, but because of extreme attenuation effects magnitude of the decrease is unknown [82, 83, 84]; the onset of all the elastic anomalies is above T_N.

IV. Discussion

A. Bulk properties. The reasons for the widely observed softening of the C' mode are certainly different from one alloy to the other as suggested by the large quantitative discrepancies.

The elastic anomalies in the ferromagnetic alloys can be fully accounted for by the magnetic anomalous contributions to the elastic constants [22, 23].

But apart from the "premartensitic" effects which are strictly magnetic in origin, others are possibly related to a lattice instability. Since heat treatments which lead to ordering in Fe_3Pt and to unknown structural changes in Fe-Ni stabilize the austenite, i.e. lower M_s, the

question, whether the observed non-magnetic premartensitic effects are related or competitive to the martensitic transformation is still open. On the other hand a reduction of the elastic stiffness of the parent phase, even if it is caused magnetically, will reduce the nucleation free energy of a martensitic transformation. Lattice defects and interfaces will modify the nucleation conditions as shown e.g. by the surface nucleation effects and thickness effects on the variation of M_S [70, 71].

The elastic anomalies in the β-Hume Rothery alloys have been discussed by Zener [4], Nakanishi [72], Rusovic et al. [9, 12], Swartz et al. [20]. The β-phases, when considered as hard sphere bcc structures, are mechanically instable, the lattice stability is mainly provided by a particular balance between the ion core repulsion, electrostatic and Fermi energy contributions. Some results point to a major significance of the temperature dependency of the ion core repulsion [9, 12, 74] and others to a dominating effect of the Fermi energy contribution [75].

The soft mode observed in InTl is attributed by Gunton and Saunders [26] to the electrostatic and band structure contributions to the total free energy. Labbe and Friedel [86, 87] explained the soft mode in V_3Si and Nb_3Sn in terms of an Jahn-Teller electronic instability.

For the alloys of group A the martensitic transformation appear to be essentially unrelated to the lattice mechanical stability. In the case of the alloys of group C the transitions at T_d are nearly of second order because in the vicinity of the transformation temperature the C' modulus of the parent phase is very small and decreases catastrophically. Consequently large lattice vibrations occur with low frequencies inducing large displacements correlated over large distances (critical fluctuations). Since C' goes to very low values but not exactly to zero/the trhansition from the cubic to the non-cubic structure requires very low stress; its magnitude depends in addition on the temperature dependence of the change in lattice parameter on passing T_d. Assuming that the latter is low, too, very small strains associated with internal stresses or with lattice defects will suffice to "nucleate" the new phase and to permit rapid spontaneous growth. If the misfit between the high and low temperature structures is low such that elastic accommodation without discrete interfacial dislocations is possible, the phase interface will be diffuse, not identifiable and will move rapidly across an entire crystal or crystallite. Whatever the mechanism in detail, the soft mode like behaviour of C' is the "cause" of the transformation and the parent phase becomes unstable at a very small temperature decrement below T_d, leading to a quasi-instantaneous transformation. This is the essential feature that differentiates this group of alloys from the other two. Moreover, the soft mode is also the path from the parent to the martensite structure. Indeed the cubic to tetragonal transformation can be understood as the frozen-in of two equal shear C' phonons (for example $(110)[1\bar{1}0] + (101)[10\bar{1}]$ at q = 0 (i.e. a homogenous shear).

For the alloys of group B, in spite of a low C' and a high elastic anisotropy at the transition temperature, the temperature variation of C' is smooth (see table 2). This means that the parent phase has not lost its inherent mechanical stability completely at temperatures even

far below M_s. The lattice is rather thermodynamically unstable with regard to a different more stable structure (i.e. another phase), as is also the case for group A. However, the lower C' can affect the "path" of the transformation and widely help the nucleation and growth for two reasons : - it reduces the strain energy terms in the energy balances controlling both the nucleation and the growth of martensite [7]; - it is associated with large amplitude vibrations which contribute to overcoming the remaining energy barrier. If, moreover the volume change at the transformation is small, a low value of C' will essentially contribute to the occurrence of thermoelasticity, pseudoelasticity and shape memory effects.

Another prominent anomalous stability effect of these group B alloys (at least for β-Hume Rothery phases) is the high sensitivity of C' with respect to uniaxial stress. This denotes a high corresponding anharmonicity. Consequently, local strained regions near lattice discontinuities (surface, dislocations, vacancies, ...) exhibit much lower C' than in the bulk [19]. As will be shown in another contribution [19], C' may even become zero locally. The role that plays the low magnitude of C' plays in determining the path of the transformation is thus greatly enhanced in the immediate vicinity of lattice defects. This may lead to local nucleation of martensite or orther concurrent or intermediate phases.

B. Discussion of the electron microscopic observations.

Many electron microscopic and X-ray diffraction investigations clearly show that in the temperature range above M_s, contrast and diffraction effects are present, which cannot be attributed to either the matrix phase or the martensite phase. Although nearly all the observed diffraction phenomena can be fully explained by a phase whose crystal structure can be interpreted as intermediate between that of the parent and martensite phase, no direct experimental evidence of any geometrical correlation between the intermediate particles and the onset or nucleation of the martensite phase has been given until now. The mottled structure shown in figure 9 of ref. [39] is perhaps the only direct indication that a correlation exists; the mottling in the β-Cu-Zn phase is associated with a linear contrast structure in the habit plane between the β and a 9R martensite plate. All these observations have a common merit of proposing new transformation models consisting of a combination of shuffling mechanism or lattice wave displacements which result in that intermediate structure and a dislocation type shear of the intermediate structure which results in the martensite phase.

The low temperature electron microscopic observations of Oshima and Wayman [35] and Fujita [14] appear, to the authors' knowledge, to be the only observations in iron base alloys which are interpreted as identifying "intermediate" structures. Based on a six layer structure which explains the diffraction patterns, Fujita [14] proposes a new path of the martensitic transformations in steel. His model is however based on thin film observations but appears compatible with other bulk phenomena.

Most of the other investigations pertain to the β-Hume Rothery phases (Cu-, Ag-, Au- and Ni-alloys). They all show diffraction patterns with streaks, which are continuous or contain diffraction maxima, along di-

rections at or close to $\langle 110 \rangle_\beta$. Since the observation that the diffraction pattern can fully be explained by surface martensite (see the following contribution [48]), the explanations given in the literature should be reanalysed. It is shown [48] that only high angle tilt ($\pm 60°$) experiments on the same sample area fully reveals the true crystal structure of the so-called premartensitic phases : the extra-spots in the [110]-zone patterns and which were believed to originate from a ω-structure [88, 85, 77, 39] or an orthorhombic structure [41, 45] or a hexagonal phase [90, 91] are explained by a 9R-finely dispersed martensite phase with its habit plane parallel to the (110) foil surface. By high tilting experiments a [100] diffraction pattern such as used by Nagasawa et al. [42 - 44] and also observed in Ni-Ti [92] is formed.

Unless complete sets of electron diffraction patterns taken of the same sample area by high angle tilting experiments are available, it remains uncertain whether all the thin foil observations should be interpreted either as "premartensitic" or as "thin-foil" or "surface martensite". The structure of this thin foil martensite needs not necessary to be the same as that observed in the bulk. The structure may even be different from foil orientation to foil orientation. This would explain the diversity of the [100]-zone and [111]-zone diffraction patterns in which the stacking sequence effects the exact position of the extra spots. The extra spots appearing in the [110] zone patterns are however unaffected [48] by the stacking sequence.

As shown for Fe-Ni [71] the M_S-temperature in thin foils may be considerably higher than in the bulk. Care is thus recommended in interpreting thin foil results.

It can be concluded that the thin foil observations are due to transformation products which compete with the subsequent martensitic phases [90] or to phases resulting from a still unknown effect of free surface and sample geometry on the lattice stabilities; rather than due to "premartensitic phenomena". The"intermediate" or "competitive" phases may even stabilize the matrix against martensitic transformations, as has been studied e.g. in the Cu-Sn system [89].

V. Conclusion

Many so-called "premartensitic" phenomena should be considered as intimately linked with the lattice instability of the parent phase rather as precursory phenomena determined by the martensite phase. In terms of the lattice mechanical instability three groups may be differentiated.

In the first group (A) only observations such as those made by Fujita can be interpreted as "intermediate" martensite.

In the second group (B), the anomalously low value and temperature evolution of C' in the parent phase, implies the path of the transformation or predisposes a limited number of specific deformations of the lattice leading to the martensite phase. Thus C' is primarly a property of the parent phase with a "predisposing" effect on the martensitic transformation process, and thus also on the thermoelastic, pseudoelastic and shape memory behaviour. Other phases such as surface martensite, ω, etc.

should be regarded as "concurrent" phase transformations which are also predisposed by the low value of C'.

In the last group (C), the soft mode of the parent phase reflects both the final structure of the martensite phase and the path of the transformation already at temperatures above M_s. The soft mode behaviour of this group may therefore be regarded as a genuine "premartensitic" phenomenon.

References

[1] Physical Properties of Martensite and Bainite", Special Report 93, The Iron and Steel Institute, England (1965).
[2] W.D. Robertson, in ref. [1].
[3] H. Warlimont, in ref. [1].
[4] C. Zener "Elasticity and anelasticity of Metals" 37, University of Chicago Press (1948).
[5] "Shape Memory Effects in Alloys" ed. J. Perkins, Plenum Press (1975).
[6] P.C. Clapp, Phys. Stat. Sol. (b) 57 (1975) 561.
[7] L. Delaey and H. Warlimont, in ref. [5].
[8] N. Nakanishi, in ref. [5].
[9] N. Rusović and H. Warlimont, in ref. [5].
[10] S. Yatanayon and R.F. Heheman, in ref. [5].
[11] "New Aspects of Martensitic Transformation" suppl. Trans. JIM, ed. Japan Inst. Met. 17 (1976).
[12] H. Warlimont, G. Hausch, A. Praesetyo and F. Reynaud, in ref. [11].
[13] N. Nakanishi, in ref. [11].
[14] F.E. Fujita et al., in ref. [11].
[15] T. Suzuki, in ref. [11].
[16] Proceedings of the Int. Conf. "Martensitic Transformations, Icomat 77", Kiev (1978).
[17] V.V. Kondrat'yev, in ref. [11].
[18] M. Cohen, oral discussion in ref. [16].
[19] G. Guenin and P.F. Gobin, in this conference.
[20] K.D. Swartz, W. Bensh and A.V. Granato, Phys. Rev. B 12 (1975) 2125.
[21] M. Born and K. Huang, Dynamical Theory of crystal lattices, Oxford Univ. Press London (1966).
[22] G. Hausch and H. Warlimont, Acta Met. 21 (1973) 401.
[23] G. Hausch, J. Phys. Soc. of Japan, 37 (1974) 819 and 824.
[24] G. Guenin, M. Morin, P.F. Gobin and L. Delaey, Scripta Met. 11 (1977) 1071.
[25] S. Zirinsky, Acta Met. 4 (1956) 164.
[26] D.J. Gunton and G.A. Saunders, Solid State Comm. 14 (1974) 865.
[27] M.R. Madhava and G.A. Saunders, Phil. Mag. 36 (1977) 777.
[28] L.R. Testardi and T.B. Bateman, Phys. Rev. 154 (1967) 1402.
[29] K.R. Keller and J.J. Hanak, Phys. Rev. 154 (1967) 628.
[30] E.D. Hallman and B.N. Brockhouse, Canadian J. of Phys. 47 (1969) 1117.
[31] K. Tajima, Y. Endoh, Y. Ishikawa and W.G. Stirling, Phys. Rev. Letters 37 (1976) 519.
[32] M. Mori, Y. Yamada and G. Shiranz, Sol. State Comm. 17 (1975) 127.
[33] G. Guenin, S. Hautecler, R. Pynn, P.F. Gobin and L. Delaey, Scripta Met. 13 (April 1979).

[34] S. Hoshino, G. Shirane, M. Suezawa and T. Kajitani, Jap. J. Appl. Phys. 14 (1975) 1233.
[35] R. Oshima and C.M. Wayman, Scripta Met. 8 (1974) 223.
[36] F. Lecroisey and A. Pineau, Met. Trans. 3 (1972) 387.
[37] G.B. Olson and M. Cohen, Met. Trans. 6A (1975) 791.
[38] G. Honjo, S. Kodera and N. Kitamura, J. Phys. Soc. Jan. 19 (1964) 351.
[39] L. Delaey, J. Perkins and T.B. Massalski, J. Mater. Sci. 7 (1972) 1197.
[40] G. Guenin and P.F. Gobin, Scripta Met. 12 (1978) 351.
[41] K. Takezawa and S. Sato, J. Japan Inst. Metals 37 (1973) 793.
[42] A. Nagasawa, J. of Phys. Soc. of Japan 40 (1976) 1021.
[43] A. Nagasawa, K. Mizunoya, N. Nakanashi, K. Enami and S. Nenno, Scripta Met. 12 (1978) 409.
[44] K. Enami, J. Hasunuma, A. Nagasawa and S. Nenno, Scripta Met. 10 (1976) 879.
[45] Y. Murakami, L. Delaey and G.S. Dullenkopf, Trans. JIM 19 (1978) 317.
[46] Y. Murakami, S. Kachi, Trans. Jap. Inst. Metals 20 (1979).
[47] K. Otsuka, C.M. Wayman and H. Kubo, Met. Trans.
[48] L. Delaey, G. Van Tendeloo, Y. Murakami and J. Van Landuyt, this conference.
[49] N. Nakanishi, Mem. of Kônan University, Science Series No. 15, Art. 77 (1972) and in ref. [5].
[50] G. Guenin, D. Rios Jara, Y. Murakami, L. Delaey and P.F. Gobin, Scripta Met. 13 (1979) April.
[51] R. Caudron, F.F. Meunier and P. Costa, Solid State Comm. 14 (1974) 975.
[52] Ye. Ye. Yurchikov and A.Z. Menshikov, Phys. Met. Metallogr. 32 (1971) 169.
[53] M. Shimotemai, R.R. Hasiguti and K. Karasawa, in ref. [11].
[54] H. Livingstone and K. Mukerjee, J. Appl. Phys. 43 (1972) 4544.
[55] Yu.D. Tyapkin, V.G. Pushin, R.R. Romanova and N.N. Buynov, Phys. Met. Metallogr. 41 (1976) 123.
[56] E.S. Fisher and D. Dever in "The Science, Technology and Application of Titanium", ed. R.I. Jaffée and N.E. Promisel Pergamon Press (1966) 373.
[57]
[58] E. S. Fisher and D. Dever, Trans. AIME 239 (1967) 48.
[59] E.S. Fisher and H.J. Mc Skimin, Phys. Rev. 124 (1961) 67.
[60] C.S. Barrett, Trans. Jap. Inst. Met. 17 (1976) 465.
[61] S.T. Chui, Phys. Rev. B, 11 (1975) 3457.
[62] C.M. Varma, J.C. Phillips and S.T. Chui, Phys. Rev. Letters 33 (1974) 1223.
[63] V. Krasevec, Phys. Stat. Sol. a 29 (1975) 563.
[64] U. Hocke and H. Warlimont, J. Phys. F. 7 (1977) 1145.
[65] V. Krasevec, in ref. [16].
[66] A. Nagasawa and Y. Ueda, Journ. of Phys. Soc. of Jap. 45 (1978) 1249.
[67] A. Nagasawa et al. this conference.
[68] M. Foos, C. Frantz and M. Gantois, Scripta Met. 12 (1978) 795.
[69] A. Nagasawa, A. Gyobu, K. Enami, S. Nenno and N. Nakanashi, Scripta Met. 10 (1976) 895.
[70] J.A. Klosterman, Ph. Thesis, T.H. Twente (1970).

[71] H. Warlimont, Trans. AIME 221 (1961) 1270 and Met. Trans. 2 (1971) 1847.
[72] N. Nakanishi, Trans. J.I.M. 6 (1965) 222.
[73] E.S. Fisher and C.J. Renken, Phys. Rev. 135 (1964) A482.
[74] E.H. Estrin, in ref. [16].
[75] V.R. Panin et al., this conference.
[76] J. Labbé and Friedel, J.J.Phys. 27 (1966) 153, 303 and 708.
[77] A. Prasetyo, F. Reynaud and H. Warlimont, Acta Met 24 (1976), 1009.
[78] M. Suizawa and K. Sumino, Scripta Met. 10 (1976) 789.
[79] N. Nakanishi, M. Takano, H. Morinoto, Y. Murakami and S. Kachi, in ref. [83] p. 339.
[80] G. Guenin, M. Morin, P.E. Gobin, W. Dejonghe and L. Delaey, Scripta Met. 11 (1977) 1071.
[81] K. Enami, J. Hasunuma, A. Nagasawa and S. Nenno, Scripta Met. 10 (1976) 879.
[82] H. Warlimont, A. Schnolz, unpublished work.
[83] G. Hausch and E. Torôk, Proceedings of the International Conference on Internal Friction and Ultrasonic Attenuation in Solids et. Hasiguti and Mikoshiba, Univ. of Tokyo Press (1977) 731.
[84] K. Sugimoto in ref. [83] p. 725.
[85] H. Warlimont and L. Delaey, "Martensitic Transformations in Copper-Silver- and gold-based alloys" Progr. Mat. Science vol. 18 (1974).
[86] J. Labbé and J.J. Friedel, J. Phys. Radium 27 (1966) 708.
[87] R.N. Bhatt, Physical Review B 16 (1977) 1915.
[88] F. Reynaud, J. Microsc. Spectrosc. Electron 2 (1977) 381.
[89] N.F. Kennon and T.M. Miller, Trans. Jap. Inst. Metals 13 (1972) 322.
[90] K. Otsuka, H. Sakamoto and K. Shimizu, to be published Trans. JIM
[91] C.M. Wayman et al. this conference.
[92] S.R. Lÿlstra, J. Beijer and J.A. Klostermann, J. of Mat. Science 9 (1974) 145.

Premartensitic Phenomena: Manifestations, Genesis and Role In Crystallographic Transformations

K. Mukherjee*

In recent years there has been a great deal of interest in premartensitic and/or precursor phenomena associated with diffusionless transformation. Much scattered information related to anomalous behavior of observable physical properties preceding and sometimes during the actual crystal structure change, has been cited in the literature. A whole host of such effects ranging from precipitous drop in elastic modulus, anomalous sound propagation, galvanomagnetic effects, resistivity anomaly, x-ray diffraction peak broadening and splitting, "shimmering" of image preceding transformation under transmission electron microscope, diffuse electron diffraction patterns are a few of the reported observations. In this paper some specific experimental observations, related to premartensitic and very early stages of martensitic transformation in Au-Cd and Ti-Ni are presented. These results are discussed in terms of the nature and any possible role of the precursor phenomena in martensitic transformation.

I. Manifestations

In recent years, considerable interest has been generated in the field of "premartensitic" phenomena [1-10]. Manifestations of pretransformation effect include mottling and diffuse electron diffraction [1-5,11,12], electrical resistivity anomaly [2,6], nonlinear magnetoresistance [4], x-ray peak broadening and splitting [1], anomalous microhardness [13], anomalous changes in elastic moduli and sound wave velocity [14-17] and "streaming" or shimmering effects [18] at temperatures approaching the Ms.

II. Genesis

What gives rise to such anomalous effects is not clearly understood. It has been suggested, for example, that the mottling is produced by a spinodal decomposition in a thin foil [19]. Whether, such a spinodal reaction in a highly ordered alloy such as Au-Cd, for example, is possible, is not immediately obvious. Further, in Au-Cd the mottling and associated r e l r o d effects appear as the Ms temperature is approached and disappear at a few degrees above it. More importantly, mottling as well as diffuse diffraction effects precede stress induced martensite (SIM) formation in this alloy.

Likewise, the pronounced electrical resistivity anomaly in Ti-Ni alloy [2-6] does not have a simple explanation. Clearly, the resistivity peak in this case is accentuated as a sample is cycled between Mf and Af temperatures a few times. As the Ti-Ni virgin sample is thermally cycled, its Ms temperature also decreases. It can be argued that, initially, the resistivity peak is masked by the decrease of resistance

* Department of Physical and Engineering Metallurgy, Polytechnic Institute of New York, New York 11201, U.S.A.

due to martensitic transformation. However, as the Ms is lowered, the pretransformation temperature range becomes separated. Question then still remains, what is the cause and what is the effect.

The answer to the above question might be sought by looking at other physical property changes associated with the thermal cycling of Ti-Ni. One such observation is the hardening of the parent phase induced by transformation cycling [13]. What is observed, is that as the sample is cycled, the parent phase becomes harder and the Ms temperature becomes lower. A linear relation between the transformation induced hardening of the parent phase and the shift in Ms temperature exists [13]. Direct electron microscopic observation shows that the dislocation density of the parent phase increases with increasing number of transformation cycling [20]. The hardening or the excess dislocation debris must produce a kinetic barrier (stress field of dislocations, barrier to interface motion, etc.) for the martensitic transformation. Thus a larger driving force is now necessary for transformation, i.e., Ms shifts to an even lower temperature relative to the thermodynamic equilibrium temperature T_o. When this happens the temperature regime, within which the system is thermodynamically unstable, is expanded.

Meaning of thermodynamic instability can be broadened to include such a phenomenon as the charge density waves [21,22]. A charge density modulation can be either commensurate or incommensurate with the lattice periodicity. This charge density modulation causes each lattice ion to see a different potential, resulting in the displacement of ions in a new equilibrium position. The actual ion displacements are quite small; of the order of a few tenths of an angstrom. An incommensurate charge density wave can be locked-in by impurities with an attractive potential or by structural imperfections (such as dislocations) at which lattice relaxation is relatively easier. Lock-in or stabilization of such waves will produce changes in all thermodynamic and transport properties of the crystal at or near T_o. Electrical resistivity may be drastically changed due to a change in carrier density as well as elimination of some Fermi surface sections (thus produces a change in scattering). In Ti-Ni, the dislocation debris produced by transformation cycling, may provide such a lock-in mechanism. Furthermore, if Ms is suppressed by thermal cycling one is able to approach a temperature well below T_o at which the charge density wave becomes more dominant. Such a charge density wave can also explain the anomalous magneto-resistance preceding martensitic transformations in Fe-Ni and Au-Cd alloys reported by us [4]. Elimination of some Fermi surface sections will affect the second order galvanomagnetic effects such as magnetoresistance [23,24].

III. Premartensitic-Martensitic Transformation

A commensurate charge density wave will give rise to a periodic modulation of the lattice resulting in a mottled contrast akin to a spinodal decomposition. Such a mottling of the β-phase in Au-Cd alloy is observed prior to martensitic transformation. Figure 1 shows a sequence of martensitic nucleation in a Au-47.5 at.% Cd alloy. Clearly the very early stages of plate formation is crystallographically related

to the mottled substructure. In Fig. 1(b) is shown (arrow) a dislocation loop like feature in the mottled region, which coarsens as the transformation proceeds. Figure 2 shows another example of the parallelism between the mottled substructure and the growing martensitic plate.

In the Ti-Ni alloy pronounced changes in x-ray diffraction pattern are observed in the temperature range at which the electrical resistivity peak exists. Figure 3 shows a systematic broadening and splitting of (110) B_2 reflection in this range. The intensity profile of the (110) reflection at 16.5° C corresponds to the resistivity peak. Thereafter, splitting and peak separation continues. Even at 13°C , the integrated intensity of the split reflection is, within experimental error, equal to that at 18°C. New diffraction lines corresponding to martensitic phase occur after the integrated intensity of this split (110) peak begins to drop. It would, therefore, appear that a continuous distortion of the β lattice and development of unequal sets of (110) d-spacing gradually merge into the final martensitic structure in this alloy. It is of particular interest to note that stacking modulated martensitic structures can be constructed, in this alloy, by appropriate stacking shifts along sets of (110) planes of the β -phase.

IV. Nucleation and Early Stages of Martensitic Growth in Au-47.5 at.% Cd alloy.

Figures 4(a) - (d) show the sequence of nucleation of martensitic plates in a Au-47.5 at.% Cd alloy. Arrow in Fig. 4(a) shows an ill-defined contrast area in the mottled β-background. This region grows along both directions as indicated by the arrows in Fig. 4(b). In Fig. 4(c), although this region has now been converted to a recognizable martensitic plate, its upper boundary as well as its internal structure are poorly defined. The plate boundary becomes better defined after an adjacent plate ("B" in Fig. 4(d)) forms. Figure 5 shows a higher magnification electron micrograph of this nucleation region. Two sets of faults, one parallel to the growth direction and the other at an angle of $\sim$72.5° to this direction, are clearly visible. The arrow corresponds to $[\bar{1}10]$ direction and arrow 2 corresponds to a $[\bar{1}12]$ direction in this micrograph. It is suspected that the time dependent refinement of internal structures of a freshly formed martensite is responsible for the aging necessary for obtaining rubber-like behavior of the martensitic phase in this alloy. It is proposed that the driving force for this adjustment of internal structures (twin interfaces) is the order parameter. Small displacements (fractional lattice spacing) of atoms occur at these interfaces to optimize unlike-pair contact distances. As a corollary, stronger ordering forces will require shorter or zero aging time and weaker ordering forces (as in a non-stoichiometric alloy) will require longer aging times before this interface adjustment (and thus rubber-like behavior) can occur.

References

[1] K. Mukherjee, M. S. Chandrasekaran and F. Milillo, Shape Memory Effects in Alloys, Plenum Press, N.Y. p. 177 (1975).

[2] G. D. Snadrock, A. J. Perkins and R. F. Heheman, Met. Trans., 2, 2769 (1971).

[3] K. Mukherjee and P. Ferraglio, Fizika, 2, Sup. 2, 27.1 (1970).

[4] H. Livingston and K. Mukherjee, J.App.Phys., 43, 4944 (1972).

[5] F. E. Wang, S. J. Pickert and H. A. Alpern, J.Appl.Phys., 43, 97 (1972).

[6] C. M. Wayman and I. Cornelis, K. Simizu, Scripta Met., 6, 115 (1972).

[7] L. Delaey, J. VanPaemel and T. Struyeve, Scripta Met., 6, 507 (1972)

[8] N. Nakanishi, Shape Memory Effects in Alloys, Plenum Press, N.Y., p. 147 (1975).

[9] N. Rusovic and H. Warlimont, Shape Memory Effects in Alloys, Plenum Press, N.Y., p. 467 (1975).

[10] This conference (See for example nearly two dozen papers on this subject.)

[11] E. Hornbogen and H. Warlimont, Act. Met., 15, 943 (1967).

[12] K. Otsuka, C. M. Wayman and H. Kubo, Met. Trans., 9A, 1075 (1978).

[13] K. Mukherjee, F. Milillo and M. Chandrasekaran, Mat. Sc. & Eng., 14, 143 (1974).

[14] S. Zirinsky, Acta Met., 4, 164 (1956).

[15] R. J. Wasilewski, Trans. AIME, 233, 1691 (1965).

[16] S. Spinner and A. G. Rozner, J. Acoust. Soc. Amer., 40, 1009 (1966).

[17] D. Bradley, J. Acoust. Soc. Amer., 37, 700 (1965).

[18] H. C. Tong and C. M. Wayman, Phys. Rev. Lett., 32, 1185 (1974).

[19] H. Kubo and C. M. Wayman, To be published.

[20] J. Perkins, G. R. Edwards et al., Shape Memory Effects in Alloys, Plenum Press, N. Y., p. 273 (1975).

[21] J. A. Wilson et al., Adv. in Phys., 24, 117 (1975).

[22] F. J. Disalvo, Electron Phonon Interactions, Plenum, (1977).

[23] C. K. Sidrov, Izv. Akad Nauk, SSSR, Ser. Fiz., 11, 511 (1947).

[24] B. Wiener et al., J. Appl. Phys., 26, 609 (1955).

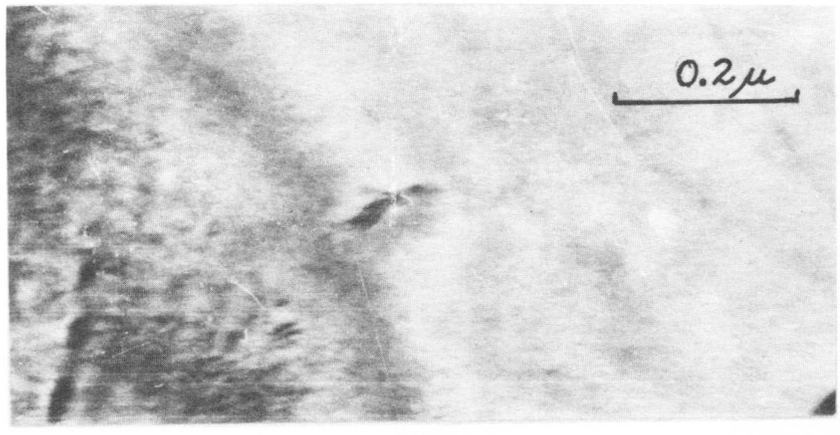

(a)

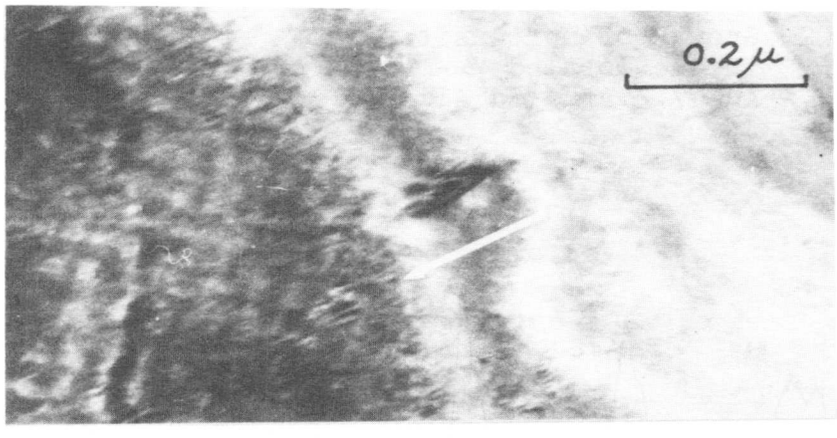

(b)

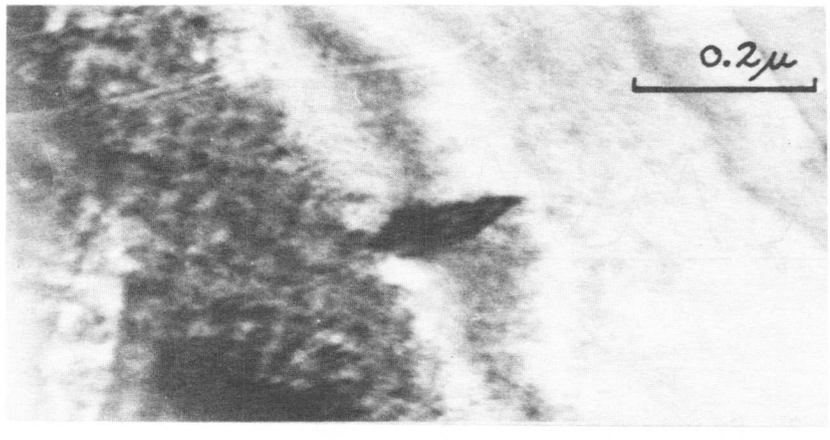

(c)

Fig. 1. Martensitic nucleation in the mottled β matrix of a Au-47.5at.%CD alloy.

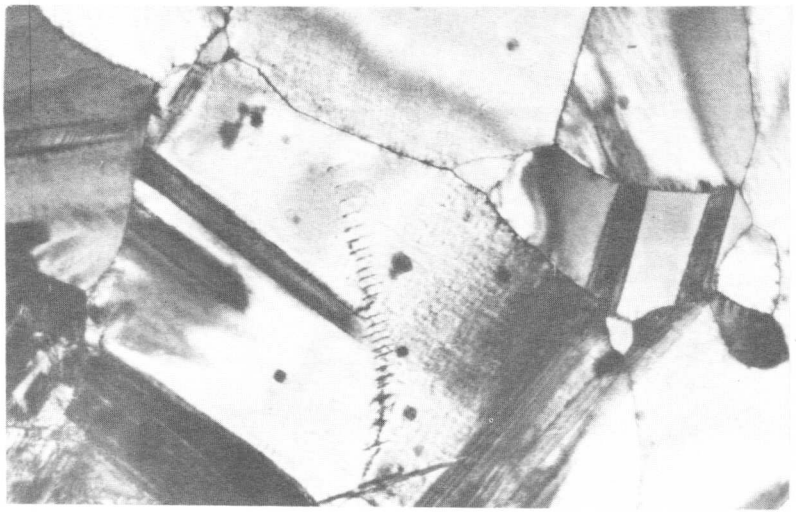

Fig. 2. Growth of martensit plates in the mottled β-matrix of Au-47.5.at.% Cd alloy.

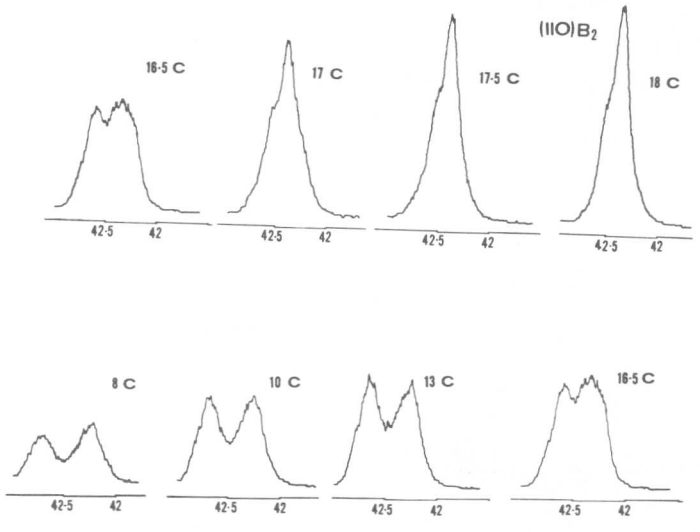

Fig. 3. Broadening and splitting of (110) reflection in the pre-transformation range in Ti-Ni

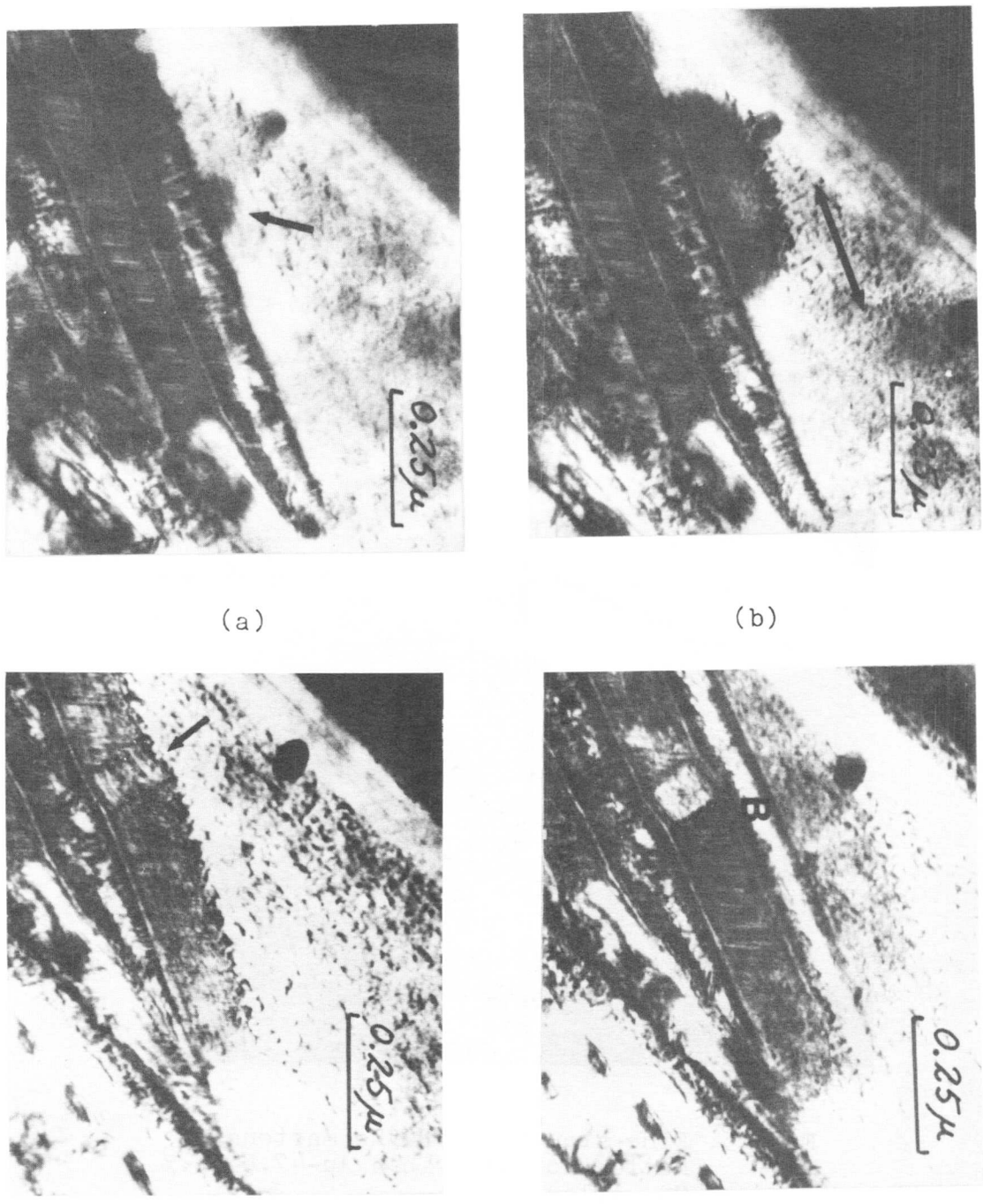

Fig. 4. Nucleation and growth of thermoelastic martensite in a Au-47.5 At.% Cd alloy.

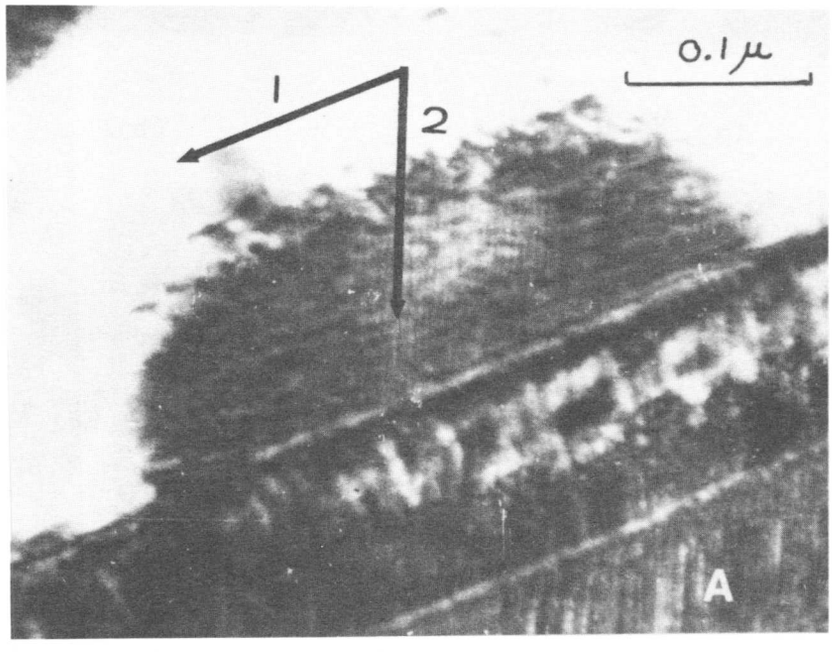

Fig. 5. Fine structure of the martensitic nucleation site in a Au-47.5 at.% Cd. alloy.

Elastic Soft Modes and Mechanism of Martensitic Phase Transformation in β Phase Alloys

Akira Nagasawa, Norihiko Nakanishi*, Yoshie Matsuo and Kazuyuki Enami**

Besides the C' softening, several kinds of elastic anomalies occur as the preceding phenomena of the martensitic phase transformation in the β phase alloys. The elastic constants C' and C_{44} exhibit cooperatively non-linear changes near the M_s point. Due to such changes, another kind of the lattice softening is induced. This softening, named the special mode softening, is responsible to the formation of the close packed planes in the martensite. From a view point of the softenings of C' and the special mode, we discuss dynamical mechanisms of the martensitic phase transformation in the β phase alloys. The origin of the lattice softenings are also discussed.

I. Introduction

Before the martensitic phase transformation in the β phase alloys, the β_1 phases exhibit many anomalies known as the preceding phenomena. Among them, elastic, structural and phonon anomalies are typical. The elastic anomaly, i.e., the softening of C', is found in such alloys as AuCd[1], Au-Cu-Zn[2], Cu-Al-Ni[3], NiAl[4] and others. As already reported by us[5-7] and others[8], the X-ray, electron and neutron diffraction studies reveal that the structural anomaly is also induced in the β_1 phase as a premartensitic phenomenon. This is due to an enhanced lattice wave with wave and polarization vectors, q and e, of the [110] and $[\bar{1}10]$ directions. The phonon anomaly is softening of a TA phonon mode with q=[110]/3 and e// $[\bar{1}10]$ as observed in Au-Cu-Zn alloy[8].

When the martensite is formed in the β phase alloys, on the other hand, two kinds of shears are necessary to occur in the β_1 phase. The one is the $(110)[\bar{1}10]$ type of the periodic shear propagating along the [110] direction and the other is the $(112)[11\bar{1}]$ shear. This geometrical relationship is known as the Burgers relation[9]. It must be noted here that all the anomalies mentioned above relate commonly only to the $(110)[\bar{1}10]$ shear in the β_1 phase. Any anomaly has not concerned the $(112)[11\bar{1}]$ shear process. This situation is unusual.

The present study is planned to solve this problem. We will show firstly the existence of elastic anomalies concerning the $(112)[11\bar{1}]$ shear. Secondly, nature of such anomalies will be elucidated. Based on the obtained results, we will finally discuss the dynamical mechanism of the martensitic phase transformation in the β phase alloys.

Department of Physics, Nara Women's University, Nara 630, Japan.
*Department of Chemistry, Konan University, Kobe 658, Japan.
**Department of Materials Science and Engineering, Osaka University, Osaka 565, Japan.

II. Elastic Waves and Special Mode

The elastic properties of a crystal are represented by the elastic stiffness constants. To survey immediately the elastic behaviours in the crystal, however, velocity surfaces of elastic waves are more adequate than the constants. The three kinds of the wave velocity surfaces are obtained by substituting the constants in the elastic wave equation and they are named the L, T_1 and T_2 modes. L and T represent longitudinal and transverse types of the waves, respectively. On any velocity surface, there are some extremum points along the several directions. Among them, the two points are important for the present problem. The one is the minimum point corresponding to a transverse wave (T_1 mode) with q and e parallel to the [110] and [$\bar{1}$10] axes respectively on the (001) plane. This gives the elastic constant C'. The other, which has so far escaped from our notice, relates to another transverse wave (T_2 mode) along a special direction on the (110) plane.

On the (110) plane in any cubic crystal, the velocity surface section for the T_2 mode is given by the following equation:

$$\rho v^2 = \frac{1}{2}[D_1 - \frac{1}{2}(D_2 - D_3)\sin^2\theta] - \frac{1}{2}[\{D_2 - \frac{1}{2}(D_2 - D_3)\sin^2\theta\}^2 - 2(D_2 + 2D_3)(D_2 - D_3)\sin^2\theta\cos^2\theta]^{1/2} \quad , \qquad (1)$$

where ρ is the density of the crystal, θ the angle of q from the [001] direction, $D_1=C_{11}+C_{44}$, $D_2=C_{11}-C_{44}$ and $D_3=C_{12}+C_{44}$.

Fig.1 shows the velocity surface section of the T_2 mode on the (110) plane in the case of Cu-Al-Zn alloy; the behaviour of the T_1 mode on the (001) plane is also shown for convenience. It is clear that the velocity of the T_2 mode becomes minimum along a special direction close to the [112] axis.

The angle θ_s of the special direction is expressed as

$$\theta_s = \sin^{-1}[2(D_2 + D_3)/(3D_2 + 5D_3)]^{1/2} \quad . \qquad (2)$$

The minimum velocity v_s or the corresponding elastic constant C_s at this angle is given as

$$\rho v_s^2 = C_s = C' + \frac{1}{2}(C_{44} - C')\sin^2\theta_s \quad . \qquad (3)$$

The wave given by this equation is named the special mode[10].

The eq.(3) indicates that the behaviours of the special mode depend mainly upon the characteristics of both C' and C_{44}. As typical features of the β phase alloys, C' becomes soft while C_{44} hard during cooling. We can expect, however, that the special mode softening will occur ac-

cording to a correlation between C' and C_{44}. In fact, we have found the special mode softening to occur really in the β phase alloys such as NiAl, AuCd, Cu-Al-Zn, Au-Ag-Cd and others[10,11]. Fig.2(a) and (b) are examples in the cases of Cu-Al-Zn and Au-Ag-Cd alloys. As is seen in the figures, the special modes exhibit the softening in the temperature ranges above the M_s points. The detailed experimental results will be reported in another paper of this symposium.

III. Nature of Specila Mode Softening

When the β_1 phase undergoes the martensitic transformation, the $(112)[11\bar{1}]$ shear is necessary to occur as one of the formation processes of the martensite. We emphasize here that this process is originated from the special mode softening. The reason is as follows. The direction of q of the special mode, obtained by the eq.(2) as θ_s, is close to the [112] axis. This is common for all of the alloys examined by the present study. The polarization vector e is the eigenvector in the wave equation. In the case of the special mode of the β phase alloys, e lies commonly on a direction close to the $[11\bar{1}]$ axis. Therefore it is evident that the special mode corresponds closely to the $(112)[11\bar{1}]$ shear, although the special mode is a quasi-transverse wave. Since any elastic constant is resistance to the corresponding strain, the fact that the special mode becomes soft proves existence of the mechanism to cause easily the $(112)[11\bar{1}]$ shear. That is, the origin to form the close packed planes in the martensite is no more than the special mode softening.

A detailed examination on the elastic behaviours in the β_1 phase is important to understand nature of the special mode softening. Fig.3 (a) and (b) show temperature changes of C' and C_{44} in Cu-Al-Zn alloy. In many β phase alloys, C' decreases while C_{44} increases with decreasing temperature. As shown in Fig.3, however, it is noticed that both C' and C_{44} exhibit non-linear changes, which begin to occur cooperatively at the temperature near the M_s point.The non-linearities are essential for the present problem. Because the special mode softening starts immediately after such phenomena, as are comfirmed by comparing Figs.2 (a), 3(a) and 3(b) with each other. This is just the prediction of the eq.(3). Consequently, we can conclude that an interaction between the lattice waves corresponding to C' and C_{44} is the origin of the special mode softening. That is, the special mode softening is due to an anharmonic effect in the β_1 phase. The β phase alloys such as Au-Ag-Cd [11], NiAl and others exhibit also the non-linear phenomena. Detailed results will be reported in another paper of this symposium.

The structural anomaly is also remarkable as the preceding phenomenon of the martensitic transformation in the β phase alloys. The anomaly appearing on the diffraction pattern is characterized by some periodic extra spots with diffuse streaks along the [110] direction. As analysed by us[5-7] and others[8], such an anomaly relates to the periodic stacking modulation of the (110) planes in the β_1 phase. This means existence of an enhanced lattice wave corresponding to the C' softening. Another type of structural anomaly has recently found by us in the case of NiAl. Fig.4 shows an example of anomalous electron diffraction patterns. We can see the [112] diffuse streaks. This implies

existence of an enhansed transverse lattice wave propagating along the [112] direction. Such a situation can be interpreted by a term of the special mode softening.

IV. Transformation Mechanism

The Burgers relation[9] is known as a geometrical model of the martensitic transformation in the β_1 phase. It requires the $(110)[\bar{1}10]$ and $(112)[11\bar{1}]$ shears in the course of the transformation. From a dynamical point of view, however, one of the most important problems is what mechanism plays essential role to induce such shears.

During cooling, the C' mode softening is firstly induced in the β_1 lattice. This is responsible to the lattice distortion with stacking modulation of the (110) plane. As reported previously[5,6], the modulated or distorted lattice has the same symmetry as that of the final product, i.e., the martensite. In the case of the Heusler type lattice, for an example, the symmetry of the β_1 phase changes as follows:

$$O_h^5\ (\beta_1) \begin{cases} \longrightarrow D_{2h}^{13}\ (DL) \longrightarrow D_{2h}^{13}\ (M;2H) \\ \longrightarrow C_{2h}^{1}\ (DL) \longrightarrow C_{2h}^{1}\ (M;18R) \end{cases}$$

where DL and M mean respectively distorted lattice and martensite. That is, the symmetry change due to the transformation is completed before the formation of the martensite.

On the other hand, any lattice distortion causes an increase of strain energy. Hence the distortion can be realized if the symmetry change is attended with so sufficient decrease of crystal energy that its decrement exceeds the increment of the strain energy. A possible and reasonable mechanism is that a certain kind of degenerate energy state is split by the symmetry change and the crystal energy decreases with the lattice distortion. The structural phase transformation in the β-W type alloys is just due to such a mechanism known as the band Jahn-Teller effect[12,13]. It is attractive to suppose that the lattice instability related to the C' softening is also originated from the band Jahn-Teller effect. Thus we can suppose that characteristics of the degenerate energy state will firstly design a direction of the symmetry change. Along the direction, the β_1 lattice will begin to fluctuate. This is the lattice instability observed as the C' softening.

Further cooling of the β_1 phase causes the cooperative and nonlinear changes of both C' and C_{44} and then the special mode softening is induced. This stage of the lattice instability is responsible to the formation of the close packed planes. The $(112)[11\bar{1}]$ shear corresponding to the special mode softening is not related to the symmetry change and hence the origin of this softening is quite different from that of the C' softening. The $(112)[11\bar{1}]$ shear will be a mechanism to lower the crystal energy, because the close packed arrangement of atoms is more stable than that on the (110) plane. The special mode softening is originated from an anharmonic effect.

References

[1] S.Zirinsky: Acta Metall. 4(1956)164.
[2] N.Nakanishi,Y.Murakami and S.Kachi: Scripta Metall. 5(1971)433.
[3] M.Suezawa and K.Sumino: Scripta Metall. 10(1976)789.
[4] K.Enami et al.: Scripta Metall. 10(1976)879.
[5] A.Nagasawa: J.Phys.Soc.Jpn. 40(1976)1021.
[6] A.Nagasawa et al.: Scripta Metall. 10(1976)895.
[7] A.Nagasawa et al.: Scripta Metall. 12(1978)409.
[8] M.Mori,Y.Yamada and G.Shirane: Solid State Commun. 17(1975)127.
[9] W.G.Burgers: Physica 1(1934)561.
[10] A.Nagasawa and Y.Ueda: J.Phys.Soc.Jpn. 45(1978)1249.
[11] A.Nagasawa et al.: J.Phys.Soc.Jpn., to be published.
[12] E.Pytte: Phys.Rev.Lett. 25(1970)1176.
[13] E.Pytte: Phys.Rev. B4(1971)1094.

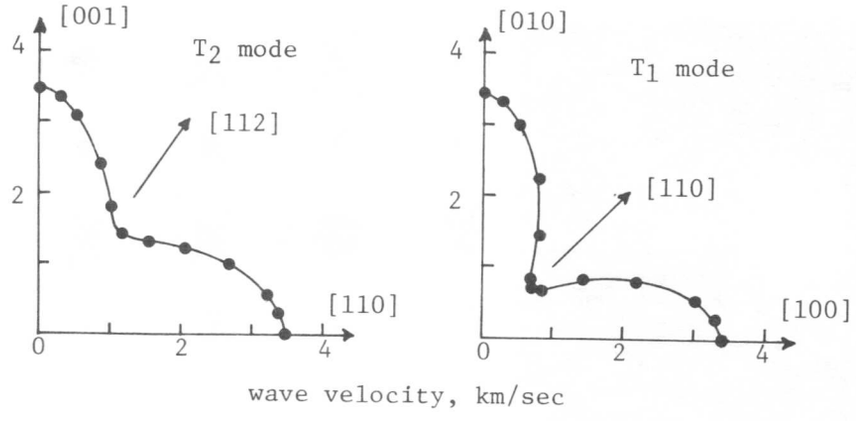

Fig.1. Velocity surface sections in Cu-17.1Al-13.8Zn alloy at 300K.

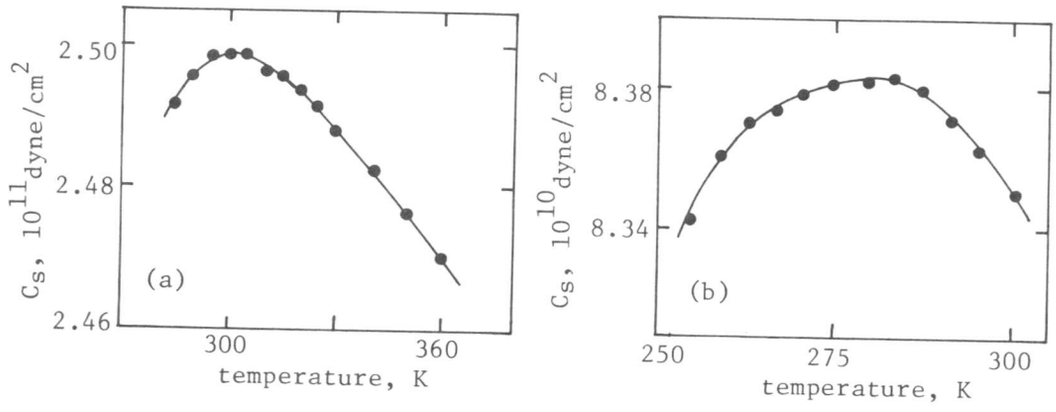

Fig.2. Examples of special mode softenings. (a): Cu-17.1Al-13.8Zn alloy. (b): Au-10.0Ag-47.5Cd alloy cooled slowly.

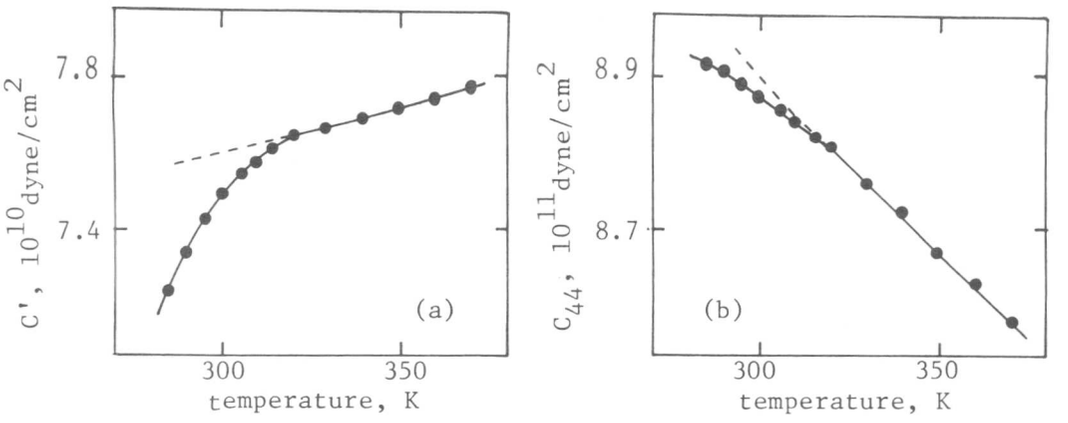

Fig.3. Temperature changes of c' and C_{44} in Cu-17.1Al-13.8Zn alloy.

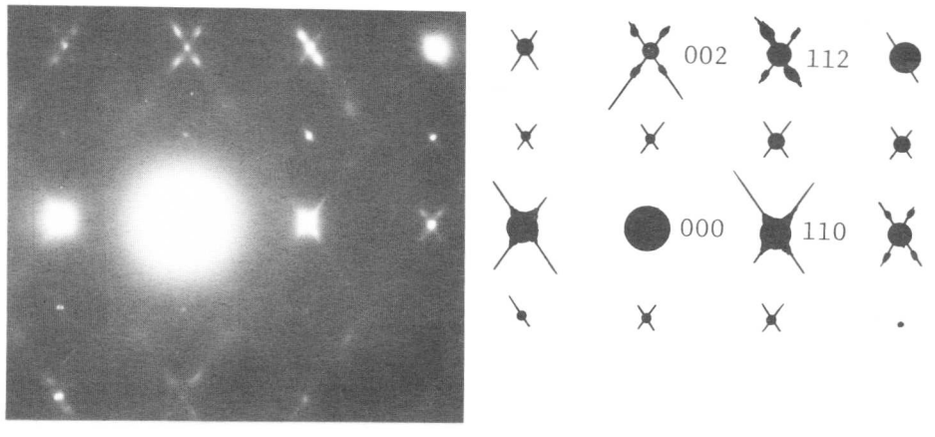

Fig.4. Electron diffraction pattern of Ni-36.4Al alloy, taken at about 390K. Beam // $[1\bar{1}0]$ zone axis.

Elastic Softening of Special Mode Preceding Martensitic Phase Transformation in NiAl, Cu-Al-Zn and Au-Ag-Cd Alloys

Akira Nagasawa, Norihiko Nakanishi*, Toshiharu Suzuki,
Kazuyuki Enami** and Soji Nenno**

Elastic anomalies in NiAl, Cu-Al-Zn and Au-Ag-Cd alloys are studied in detail mainly from a view point of the special mode softening. The special mode softening is responsible to the $(112)[11\bar{1}]$ shear, i.e., to the formation process of the close packed planes. It is essencial for the dynamical transformation mechanism in the β phase alloys. Such a softening is due to non-linearities occurring cooperatively in C' and C_{44}. Ultrasonic attenuation show also non-linear anomaly, which relates closely to the special mode softening. The above mentioned anomalies depend strongly on the heat treatments of the alloys. Base on the softening phenomena, we discuss the elastic properties of metals and alloys.

I. Introduction

The martensitic transformation in the β phase alloys is structurally characterized as the change of the β_1 phase to the martensite with the close packed layer structure. The β_1 phases have the order structures such as the CsCl, Fe_3Al and Heusler type ones. In the transition process, the $(110)[\bar{1}10]$ and $(112)[11\bar{1}]$ shears are necessary to occur as expected by the Burgers relation[1]. However, this geometrical model does not give any indication on the dynamical mechanism of the phase transformation. Present interests are to solve the problem what plays essencial role for the transformation mechanism.

Recent studies on the premartensitic anomalies have presented some important informations concerning the problems. Firstly, as observed in AuCd[2], Au-Cu-Zn[3], Cu-Al-Ni[4], NiAl[5] and others, the shear constant C' becomes soft as a precursor of the transformation. This is responsible to the $(110)[\bar{1}10]$ shear. The C' softening, on the other hand, relates closely to the structural and phonon anomalies[6-8] and, as just reported by us in this symposium, it is originated from the mechanism to reduce crystal energy by the symmetry change. Secondly, another kind of the lattice softening, named special mode softening, occurs in the β phase alloys as observed recently by us[9,10]. This concerns with the $(112)[11\bar{1}]$ shear. Therefore, in order to understand the essential nature of the martensitic transformation, it is necessary to investigate the special mode softening in detail. This is a main subject of the present paper. In addition, the elastic properties of metals and alloys are discussed in this paper from a view point of the elastic softenings.

Department of Physics, Nara Women's University, Nara 630, Japan.
*Department of Chemistry, Konan University, Kobe 658, Japan.
**Department of Materials Science and Engineering, Osaka University, Osaka 565, Japan.

II. Experimental

Specimens examined by the present study are single crystals of Ni-36.8Al[5], Cu-17.1Al-13.8Zn[11] and three kinds of Au-Ag-47.5Cd[10] alloys. Composition are shown in at%. Au-Ag-47.5Cd alloys contain 10, 28 and 35%Ag. Procedures such as specimen preparations, heat treatments, determination of crystal orientations and others are abbreviated; for details refer to the paper cited above.

The single crystals with the (100) and (110) surfaces were examined in a wide range of temperature by the ultrasonic measurements using the MATEC 6000 and 6600 systems. The elastic constants were obtained by the wave velocity data determined by the overlapping pulse-echo method with 5MHz ultrasonic wave. We pay a special attention to the measurements in a temperature range near the M_S point, because the anomalies are very enhanced in the range. The ultrasonic attenuations were also measured in Au-Ag-Cd alloys.

III. Results and Discussion

The elastic shear constant C' of all alloys examined by the present study exhibits softening behaviour as expected. This softening means decrease of resistance to the $(110)[\bar{1}10]$ shear and hence it is responsible to the periodic stacking modulation of the (110) planes in the β_1 lattice. On the other hand, the structural anomalies[6,7,11] and the phonon softening[8] have been already found as the premartensitic phenomena. Since these anomalies are due to an enhanced lattice wave with wave and polarization vectors, q and e, parallel to the [110] and $[\bar{1}10]$ axes, the origin of them is same as that of the C' Softening.

Besides the C' softening, the β phase alloys show another kind of lattice softening, i.e., the special mode softening[9,10]. This softening is commonly observed in all alloys examined by the present study. Fig.1(a) and (b) show examples of the softening behaviours of C' and C_S; C_S is the elastic constant corresponding to the special mode. The special mode is a quasi-transverse wave with q and e nearly parallel to the [112] and $[11\bar{1}]$ directions. This means that the C_S softening is related closely to the $(112)[11\bar{1}]$ shear, which is necessary for the close packed planes in the martensite to be formed. These situations lead us to the conclusion that the C' and C_S softenings give a dynamical meaning for the geometrical model known as the Burgers relation[1] to the martensitic transformation in the β phase alloys.

As just reported by us in another paper of this symposium, property of the special mode depends mainly upon characteristics of both C' and C44. In addition, Fig.1 indicates clearly that the special mode softening occurs near the M_S point. Therefore, to examine in detail the behaviours of C' and C_{44} near the M_S point is useful. Fig.2(a) and (b) show the temperature changes of C' and C_{44} in the two kinds of Au-Ag-Cd alloys. It is clear that they exhibit non-linear changes, which begin to occur cooperatively near the M_S point. It is also noticed that the C_S softening is induced immediately after such cooperative non-linearities start. Thus we can understand that the origin of the C_S softening is an interaction between the C' and C_{44} modes, i.e., an anharmonic effect.

The non-linearities of C' and C_{44} are also considered to result from the enhanced anharmonicity in the β_1 lattice near the M_s point. These phenomena occur commonly in all the alloys studied. The case of Cu-Al-Zn alloy has been already reported in another paper.

The stage at which the special mode becomes soft corresponds to a heavily fluctuated state of the β_1 phase. At this stage, we can expect a certain kind of anomaly of the ultrasonic attenuation to occur. Fig.3 shows an example of the attenuation curve of the C' mode in Au-Ag-Cd alloy; the C' curve is drawn for convenience. The attenuation curve exhibits a non-linear anomalous feature as expected. That is, it begins to increase rapidly at about 190K. Then it attains the peak closely near the M_s point. By comparing the two curves in Fig.3 with each other, we can find that the attenuation anomaly relates closely to the non-linear change of C'. This relation suggests strongly that the origin of the attenuation anomaly is same as that of the special mode softening. In other words, the attenuation mechanism at this stage is the enhanced anharmonicity of the β_1 phase.

Properties of the β phase alloys depend strongly upon history of heat treatments of the alloys. In the case of Au-Ag-Cd alloy, the CsCl to Heusler type of the phase transformation occurs; T_c is about 500K. The β_1 phases cooled slowly and quenched from a temperature range above the T_c point have respectively the Heusler (higher ordering) and CsCl (lower ordering) type structures. These two kinds of the β_1 phases will exhibit different behaviours, though they have the same compositions. Fig.4(a) and (b) show the C_s softenings of the slowly cooled and quenched β_1 phases. It is clear that the softening in (b) is steeper than that in (a). Besides the C_s softenings, both the C' and C_{44} curves of the quenched alloy behave in different manners from those of the slowly cooled one. The features of C' and C_{44}, of course, influence the characteristics of the C_s softening. These situations are common for the other Au-Ag-Cd alloys.

It is possible to interpret this problem from two different points of view. The one is as follows: Before the martensite is formed, certain kinds of embryos will nucleate in the β_1 phase. If lattice defects facilitate such nucleations and if the formation of embryos is related to the lattice softening or the locarized soft mode[12], the quenched β_1 phase wiil exhibit more considerable softening than the slowly cooled one. Because the quenched alloy is lower ordering and has many quenched vacancies. The other interpretation is a converse one: The M_s point of the quenched alloy is genarally lower than that of the slowly cooled one. This implies that the lattice defects act as obstructions to the phase transformation. Therefore, for the transformation to occur in the quenched alloy, the softening of the β_1 phase must proceed so markedly that the lattice instability exceeds a threshold formed by the lattice defects, as seen in Fig.4. The two interpretations are inconsistent with each other. Question which of them is appropriate remains to be solved in future.

With respect to the elastic softenings, we will finally discuss the elastic properties in metals and alloys with the cubic symmetry. Many materials do not undergo any phase transformation. Elastic behaviours of

them are normal. That is, the elastic constants increase with decreasing temperature. Therefore, all the velocity surfaces of the elastic waves expand over whole directions with the lowering temperature, as schematically shown in Fig.5(a). We classify them into the first group. The β-W type alloys such as Nb_3Sn and others undergo the structural phase transformation, which is similar to the martensitic one. Elastic behaviours of them are also typical. That is, all the velocity surfaces contract continuously with decreasing temperature. They are belonging to the second group as classified in Fig.5(b). In the alloys, the C' mode shows perfect softening, i.e., C'=0 at the transition temperature. This corresponds to freezing of a TA phonon mode at the Γ point in the Brillouin zone[13,14]. The β phase alloys undergoing the martensitic transformation belong the third group. As shown in Fig.5(c), the temperature dependency of the velocity surfaces exhibits complicated phenomena. That is, the C' and C_S modes shows imperfect softenings while the others become hard. Any material will belong to one of the three kinds of groups, or at least to a modified one.

References

[1] W.G.Burgers: Physica 1(1934)561.
[2] S.Zirinsky: Acta Metall. 4(1956)164.
[3] N.Nakanishi,Y.Murakami and S.Kachi: Scripta Metall. 5(1971)433.
[4] M.Suezawa and K.Sumino: Scripta Metall. 10(1976)789.
[5] K.Enami et al.: Scripta Metall. 10(1976)879.
[6] A.Nagasawa: J.Phys.Soc.Jpn. 40(1976)1021.
[7] A.Nagasawa et al.: Scripta Metall. 12(1978)409.
[8] M.Mori,Y.Yamada and G.Shirane: Solid State Commun. 17(1975)127.
[9] A.Nagasawa and Y.Ueda: J.Phys.Soc.Jpn. 45(1978)1249.
[10] A.Nagasawa et al.: J.Phys.Soc.Jpn., to be published.
[11] A.Nagasawa et al.: Scripta Metall. 10(1976)895.
[12] P.C.Clapp: Phys.Status Solidi(b) 57(1973)561.
[13] K.R.Keller and J.J.Hanak: Phys.Rev. 154(1967)628.
[14] G.Shirane and J.D.Axe: Phys.Rev.Lett. 27(1971)1803.

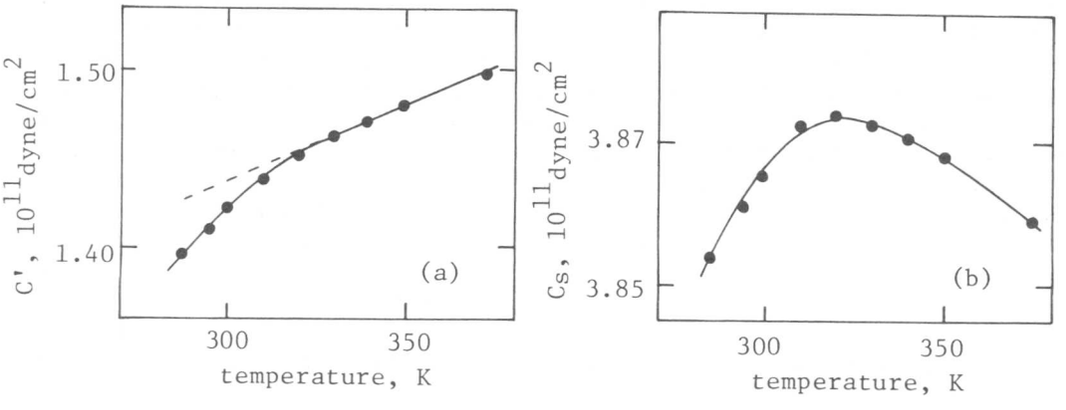

Fig.1. Elastic softenings of C' and C_S in Ni-36.8 alloy.

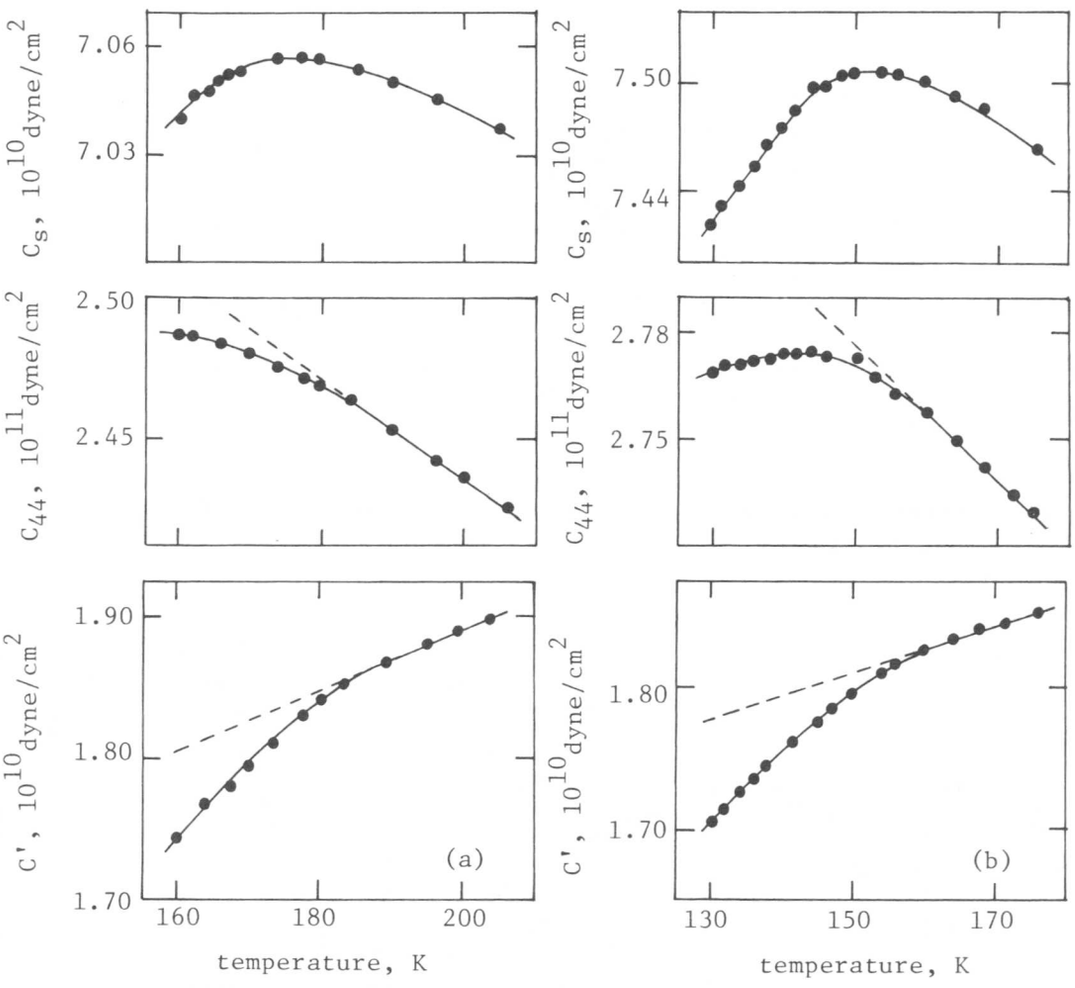

Fig.2. Temperature changes of C', C_{44} and C_s in Au-Ag-Cd alloys. (a): 28% Ag alloy cooled slowly. (b): 35% Ag alloy quenched from about 870K.

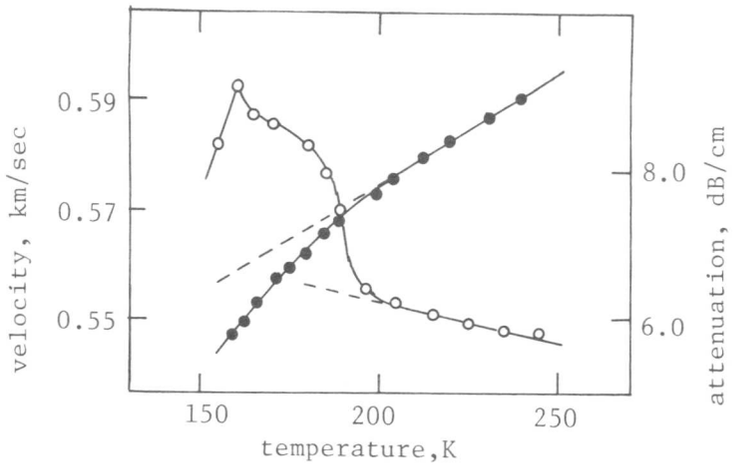

Fig.3. Attenuation(open circles) and wave velocity(full circles) of C' mode in quenched 28% Ag alloy.

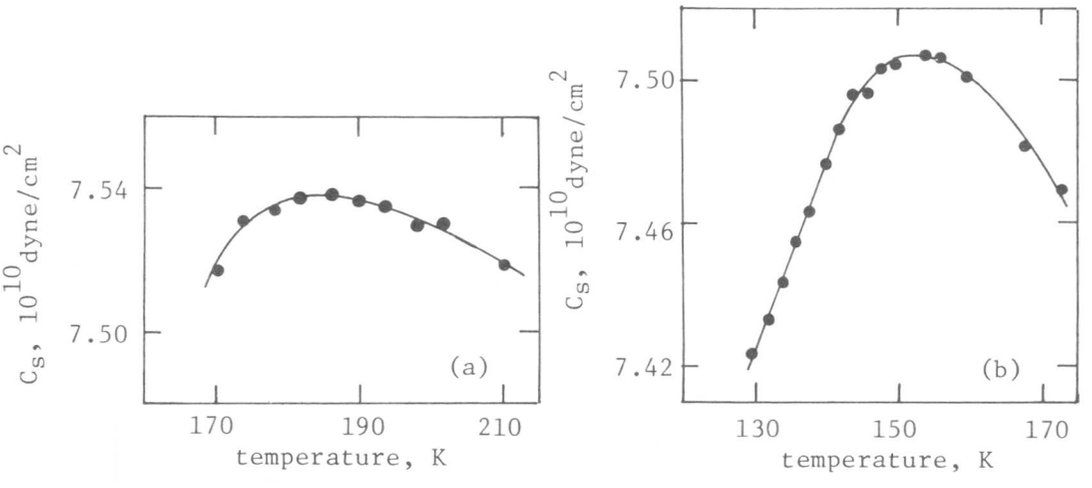

Fig.4. C_s softening in 35% Ag alloy. (a): slowly cooled. (b): quenched from about 870K.

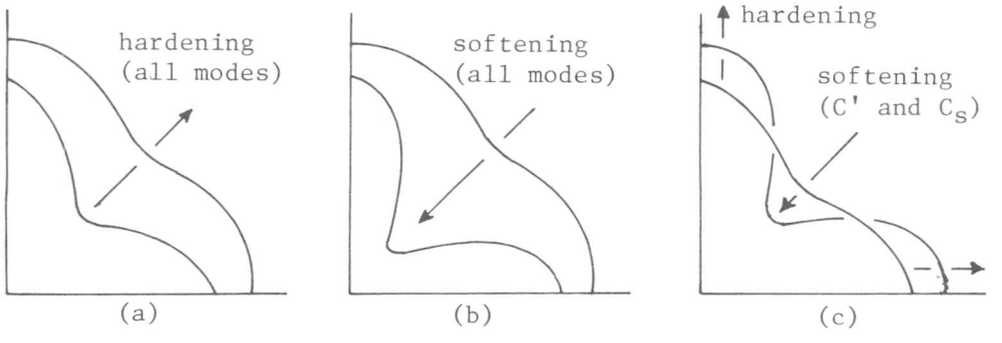

Fig.5. Schematical classification of elastic behaviours of metals and alloys with cubic symmetry.

On Nature of Premartensite Shear Instability in 3/2 Electron Compounds

V.E.Panin, I.I.Naumov and M.F.Zhorovkov

The pseudopotential method is applied to investigate the temperature and composition dependences of the shear elastic constant $c' = \frac{c_{11} - c_{12}}{2}$ in 3/2 electron compounds such as β-brass. The noted dependences are shown to be explained in terms of "interaction" between Fermi surface and Brillouin zone facets. The theory is in qualitative agreement with experiment.

It is well known that above M_S the pure shear elastic constant c' in β-brass type alloys shows the anomal temperature dependence ($\frac{dc'}{dT} > 0$). Moreover, there is correlation between M_S and c' as the functions of z (z-electron-atom ratio): M_S greater for lower c' and vice versa.

As suggested by [1-3] the true interpretation of c'(T) and c'(z) may be possible only in case of taking into account the Born-Mayer ion repulsion. As to c'(T), it is as follows. The repulsion between the nearest ions leads to a negative contribution to c'. As the distance between them decreases with temperature the repulsion increases and c' drops, that is it shows the anomal temperature behaviour.

In spite of its elegance and simplicity this mechanism of temperature lattice softening doesn't seem to be plausible. If so, the temperature anomaly must be observed at all concentrations of quenched β-phases. This fact is in contradiction with experiment. For instance, in some stoichiometric composition systems (CuZn, AgMg, NiAl) $\frac{dc'}{dT} < 0$. Incorporation the interaction between second nearest neighbours doesn't solve the problem. Moreover, in this case, as may be easily shown, the probability of lattice softening becomes rather small, especially in alloys with different atom size components.

The above mentioned gives the possibility to think that the Born-Mayer forces don't determine the behaviour of c'(T) above M_S. At the same time the explanation of the

Siberian Physico-Technical Institute, Tomsk,
Pl. Revolutsii I, U S S R

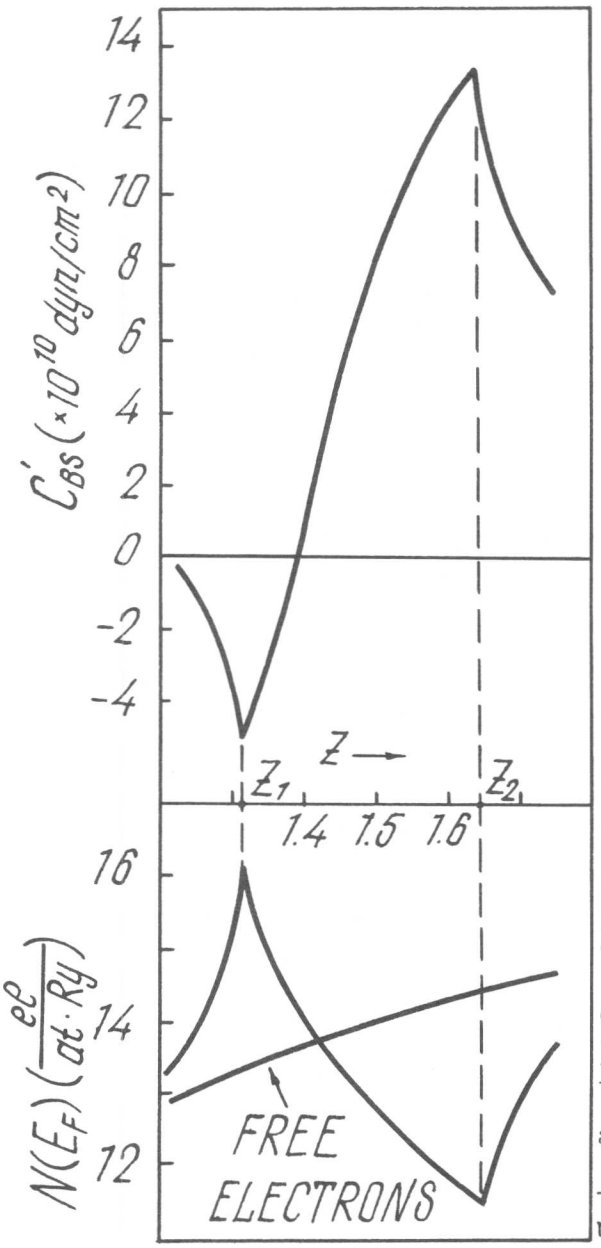

Figure 1. Elastic constant c' and density of states $N(E_F)$ calculated in β-CuZn as functions of z

temperature as well as the concentration change of c' may be reached by consideration of c'_{bs}, i.e. the contribution to c' from the band structure energy E_{bs}. To describe E_{bs} we use the pseudopotential model [4], which takes into consideration the "real" (instead of sphere) Fermi surface.

As the analysis shows, the peculiarity of the shape of $c'_{bs}(z)$ is determined by its singular terms, corresponding to the set of reciprocal vectors $\{h^*\}$ such as $\frac{2\pi}{a}\langle 110\rangle$. The singularity in question (Kohn anomaly) arises as a result of "interaction" between the Fermi surface and the Brillouin zone boundaries (110). For the measure of this interaction one may take the band energy gap $\Delta E = 2\,V(q)/_{q=h^*}$, where $V(q)$ is the screened form factor of pseudopotential.

The calculated curve $c'(z)$ for $V(h^*) \approx 0.9$ev is shown in Fig.1 (the atomic volume Ω doesn't depend on z and equals to one for β-CuZn of stoichiometric content: $\Omega = 86.15$at. un.). This curve has a

almost linear and great enough increase of c'(z) with z; it is in agreement with experiment [3,6-8].

As has been noted in literature (see, for example, [9]) there is a direct junction between the lattice softening and the behaviour of density of states N(E) in the vicinity of the Fermi level E_F. The calculated dependence $N(E_F)=f(z)$ is shown in Fig.1. At $z=z_1$ and $z=z_2$ it has the well known van Hove singularities of M_1- and M_2-type respectively. That is why the minimum of c' corresponds to the peak of $N(E_F)$ and vice versa. Such correlation take place, for example, in the case of the superconductive BCC-metals (V, Nb, Ta, Cr, Mo, W) and their alloys. The low values of their shear constant c' correspond to the high density of states at the Fermi level.

Let us investigate the sign of the derivative $\frac{dc'}{dT}$ with different z values. Like Zener [10], we shall assume that the dependence c'=c'(T) is due to the temperature lattice expansion solely, that is

$\frac{dc'}{dT} = \frac{dc'}{d\Omega} \cdot \frac{d\Omega}{dT}$ (quasiharmonic approximation). The change c' wuth Ω is illustrated by Fig.2. The decreasing of volume Ω leads to compressing of c'(z) along the axis z and to the stretching of it along the axis c'. This, there are three areas ($z < x_1, x_2 < z < x_3$ and $z > x_4$) of the usual change of c', where $\frac{dc}{dT} < 0$. Two areas ($x_1 < z < x_2$ and $x_3 < z < x_4$) correspond to the anomal temperature dependence of c' ($\frac{dc'}{dT} > 0$). The former of the two areas (a broader one) appears to be in accordance with experiment, which testifies that the anomaly change of c'(T) mostly takes place to the left of z=3/2. As to the second area, it is to the right of z=3/2 and, perhaps, outside of the β-phases contents.

The curves c'(z) corresponding to different Ω may also be interpreted as the ones corresponding to different pressures. In quasiharmonic approximation the sign of the derivative $\frac{dc'}{dP}$ is opposite to the sign of $\frac{dc'}{dT}$ automatically. The simultaneous measures of $\frac{dc'}{dT}$ and $\frac{dc'}{dP}$ in Ag-47,5at % Cd [11] show that $\frac{dc'}{dT} > 0$ and $\frac{dc'}{dP} < 0$; it is in agreement with quasiharmonic approximation. However, in the case of CuZnAl it was found [12] that $\frac{dc'}{dP}$ was above zero as well as $\frac{dc'}{dT}$. It follows that describing c'(T) and c'(P) seems to be not exact enough in quasiharmonic approximation. In more correct approach alongside the quasiharmonic effects it is necessary to take into account the self unharmonic ones.

It should be noted that there two alternative approa-

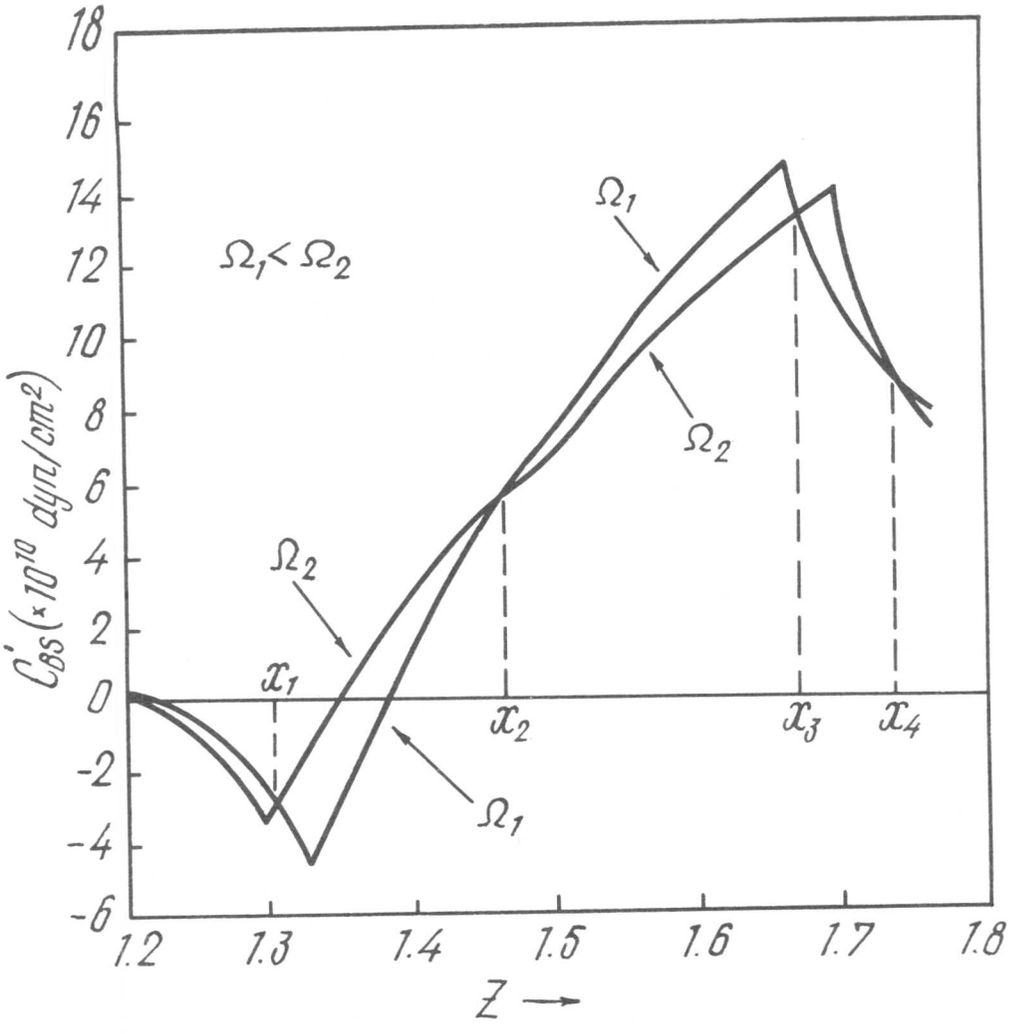

Figure 2. Dependences c'(z) calculated in β-CuZn for two different atomic volumes; Ω_1 = 86.15at.un., Ω_2 = 96.15at.un.

z-like form with two sharp peaks (minimum and maximum) at the points z_1 and z_2 respectively. The former point indicates the value z when the Fermi surface first touches the Brillouin zone plane and the latter-when the overlap first occurs. From the view point of long-wave limit such a form of the curve is due to Kohn anomaly in phonon spectra and there is "anomaly down" for $z < z_1$ and "anomaly up" for $z > z_2$ [5]

It is of interest that in vicinity of the point $z=z_1$ c' not only minimal, but negative as well. In other words, c'_{BS} on its own account predicts the absolute instability of lattice. The compositions of 3/2 electron phases are within $[z_1 \div z_2]$, where the Fermi surface is in contact with the energy gap plane. There the theory predicts an

ches to the problem of understanding of the lattice softening in 3/2 electron compounds dealing with the Born-Mayer repulsion and band structure energy respectively. No final choice between alternatives is possible at present. In this connection the further investigations of the elastic constants in the frame of microscopic theory are highly desirable.

References

[1] N.Nakanishi: Trans.Japan Inst.Met., 6 (I965), 222
[2] N.Rusovic and H.Warlimont: Proc.Int.Symp.Shape Memory Effects, Plenum Press, N.Y. (I976), 467.
[3] N.Rusovic and H.Warlimont: Phys.Stat.Sol., A 44 (I977), 609.
[4] A.R.Williams and D.Weaire: J.Phys., C 3 (I970), 387.
[5] W.A.Harrison: Pseudopotentials in the Theory of Metals N.Y. (I966).
[6] S.Zirinsky: Acta Met., 4 (I956), I64.
[7] Y.Murakami and S.Kachi: Japan J.Appl.Phys., 13 (I974), 1728.
[8] A.Prasetyo: Untersuchungen des vormartensitischen Zustands von -Hume-Rothery-Phasen an $Cu_{3-x}Mn_xAl$ und CuZn. Diss.Dokt.Naturwiss.Univ.Stuttgart (1976).
[9] M.Veger and I.Goldberg: Solid State Physics, 28 (I973), 2.
[10] C.Zener: Phys.Rev., 7I (I947), 7I.
[11] Y.Gefen, J.Makovsky and M.Rosen: J.Phys.Chem.Solids, 38 (1977), 647.
[12] G.Guenin and P.F.Gobin: Scr.Met., 12 (1978), 351.

Temperature and Pressure Dependence of the Elastic Constants of β-AuCd Near M_s and Mode Softening in C'

T.D. Kohan,* D.E. Schuele,** R.F. Hehemann,* and W.L. Gordon**

The adiabatic elastic stiffness constants, C_n, C_{44}, and C' of Au-47.5 at.% Cd and Au-50 at.% Cd were determined using the ultrasonic pulse echo technique. These constants were measured as a function of temperature and pressure in the vicinity of the martensite phase transformations of this system. The volume independent temperature derivative reveals the strong anharmonic character of the C' mode, and this mode softens with decreasing temperature and increasing pressure as the transformation temperature is approached. This is opposite to the behavior of the other modes, which behave normally. A determination has been made of the crystalline directions in which this mode softening appears. Both of the low temperature phases were stabilized by increasing pressure, with the transformation temperature rising 1.7 ± .2°C/kbar and 1.0 ± .2°C/kbar for 47.5% Cd and 50% Cd respectively. Hydrostatic weighing confirms a volume decrease on transformation during cooling. The structural change in 47.5% Cd is consistent with acoustic mode softening resulting from a zone boundary mode instability while the 50% Cd does not lend itself to this direct interpretation.

I. Introduction

Two martensitic transformations which occur in β-AuCd are of interest here: β(B2) to β'(B19) and β to ζ' (trigonal or hexagonal) [1]. More recent work indicates trigonal symmetry [2]. The composition ranges over which these transformations appear are shown in Fig. 1 which illustrates the dependence of M_s on composition [3].

Hehemann and Vatanyon [2] have used crystallographic relationships of the parent and product phases of the gold-cadmium alloy to predict static displacement waves which carry the parent phase into the product phase. For the 47.5% crystal this static displacement wave consists of zone boundary shear modes. For the 50% crystal the static modes necessary to carry the parent phase into the product phase are longitudinal modes which occur at a wave vector of 2/3 [111] and [110] to the zone boundary. It is customary to relate such static displacements to one or more soft lattice modes which, according to their analysis, should be different in the two transformations.

The work reported here tests for indications of softening at low wave vector through elastic constant measurements in two compositions, Au-47.5 at.% Cd and Au-50 at.% Cd. While the wave vectors of the above static displacement waves are well beyond those involved here, the

*Department of Metallurgy and Material Science; **Department of Physics, Case Western Reserve University, Cleveland, Ohio 44106 U.S.A.

behavior of the low wave vector region can be expected to show trends such as a general softening of a dispersion curve. The shear elastic constant $C' = (C_{11}-C_{12})/2$ is known to be small and to show a positive temperature coefficient for both of these compositions [4]. Elastic constants and their pressure derivatives have been obtained in this study in order to determine the temperature and volume dependence of the acoustic mode frequencies above M_s.

II. Experimental Procedure

Single crystal samples of Au-47.5 at.% Cd and of Au-50 at.% Cd alloys were grown from high purity starting materials by a Bridgman method in sealed quartz crucibles and annealed for several days at 550°C. Sample compositions and the absence of vertical concentration gradients were confirmed by resistance measurement of M_s and compared with the results of Nakanishi and Wayman [2]. Elastic stiffness measurements by a standard pulse-echo method at 10 MHz required samples with parallel (110) faces on which 1/2" diameter x-cut or y-cut quartz transducers could be mounted. Orientation of the sample faces was less than ½ degree from the desired axis. Sucrose was used as the bond material and, while surface relief in 47.5% samples due to the transformation occasionally caused bond deterioration, an adequate bond could eventually be obtained. Surface relief caused no problems in the 50% samples. High presure measurements (1-2 kbar) were carried out with octoil as the pressure transmitting fluid.

III. Results and Discussion

Atmospheric pressure values of elastic stiffnesses are presented in Table I and illustrated in Fig. 2. Both C_{44} and C_n (longitudinal) behave in the usual manner with negative $(dC/dT)_P$, while $(dC'/dT)_P$ is positive. The low value of C' is illustrated by the anisotropy ratio, $A = C_{44}/C'$, of 13 and 10 for 47.5% and 50% samples. When extending the results below M_s in Fig. 2, we note that these data do not correspond to the same modes as above because of the non-cubic structure of the low temperature phases. However, this does demonstrate some of the changes occuring at the transformation including hysteretic behavior and dramatic changes in ultrasonic velocities. The plots also indicate that with the transducer oriented to observe C_n above M_s a signal could be followed continuously through the transformation, whereas the other two modes could not due to attenuation or crystal orientation.

Table II lists the experimentally determined temperature and pressure derivatives of the elastic stiffnesses. Again, the C' mode stands out with both temperature and pressure derivatives of opposite sign to the other modes.

The logarithmic volume derivative (Gruneisen parameter, γ) of the normal mode frequency is tabulated for the three acoustic modes in the [110] propagation direction. It is seen that both the 47.5% crystal and the 50% crystal have negative Gruneisen parameters for the C' shear mode whereas the C_{44} shear mode and the longitudinal mode both show positive Gruneisen parameters which is the usual case. Examination of the explicit temperature dependence of the normal mode frequency, which is a

direct measure of the anharmonicity of this mode, shows, also from Table II, that it is the C' mode for both crystals which is highly anharmonic.

Fig. 3 schematically depicts the range of propagation directions over which negative pseudo-transverse acoustic mode γ values occur within the unit cell of the cubic phase. Shear modes whose polarizations lie in the (001) plane change from pure C' at [110] to pure C_{44} at [100] but are not far from pure C' out from [110] as far as the range of softness extends. In moving from [110] toward [111], softness persists to [111] where the two transverse modes are degenerate.

The static displacement wave found by Hehemann and Vatanyon [2] to explain the 47.5% crystal displacement transformation is consistent with the softening of the C' acoustic shear mode. However in the 50% crystal we find no softening of the acoustic longitudinal modes which one would expect from the analysis of Hehemann and Vatanyon. According to the ultrasonic measurements one would have expected the transformation characteristics of the 47.5% crystal and the 50% crystal to be essentially the same since both exhibit a C' acoustic mode softening. However, examination of Fig. 1 shows that at approximately 48.5% the transition goes over from the β phase to the trigonal phase while below 47.5% the transition is to the orthorhomic phase. The changeover on the M_s vs. T diagram is not smooth and the possibility exists that the mechanism of transformation for the two compositions is different. Thus the soft mode theory may only be applicable to one of the transformations. There is a possibility that the soft mode for the β to ζ transformation may be associated with an optical mode. However, a direct test of the dynamic soft mode theory by neutron diffraction methods cannot be done in this system.

An alternative explanation for C' softening in the β phase as M_s is approached is that of the formation of a coherent second phase (ω-like). The measured C' is no longer that of the pure β phase but of a mixture and is dependent on the properties and relative amounts of each component. For example, the simultaneous appearance of ω phase and C' softening has been documented in β CuZn [5]. In such a case, it is not clear whether C' softening is a result of the formation of the second phase alone or whether soft modes also appear in the β lattice. While definite evidence of an ω phase has not been reported in AuCd, diffuse diffraction effects are present in both 47.5% and 50% Cd alloys [3]. These diffuse <111> streaks which appear about 200°C above M_s are correlated with ω formation in systems in which the ω phase is documented.

Temperature dependent resistance measurements on representative samples yielded dM_s/dP values consistent with those found in elastic constant results: $1.7 \pm .2$°C/kbar for 47.5% and $1.0 \pm .2$°C/kbar for 50% samples. Hydrostatic weighing was used in determining the temperature dependence of the density, necessary to the reduction of the elastic constant data. Water was adequate for the 50% sample but tetrabromoethane was used with the 47.5% sample to avoid bubble formation in the higher temperature range. The volume reduction on transformation to the lower temperature phase was $(0.20 \pm .05)$% for the 47.5% sample and $(0.11 \pm .05)$% for the 50% sample. These results yield a heat of transformation of

104 ± 10 and 85 ± 10 cal/mole for 47.5% and 50% crystals, respectively - significantly lower than the values estimated by Gefen and Rosen [6].

Supported by an NSF-MRL grant to Case Western Reserve University under DMR 74-01878.

References

[1] H. M. Ledbetter and C. M. Wayman: Met. Trans. 3 (1972), 2349.
[2] N. Nakanishi and C. M. Wayman: Trans. AIME, 227 (1963), 500.
[3] S. Vatanayon and R. F. Hehemann: Proc. Int. Symposium on Shape Memory Effects (1975) Plenum Press, N.Y. (1976).
[4] S. Zirinsky: Acta. Met., 4 (1956), 164.
[5] A. Prasetyo, F. Reynaud, and H. Warlimont: Acta. Met. 24 (1976), 1009.
[6] Y. Gefen, A. Halwany, and M. Rosen: Phil. Mag., 28 (1973), 1.

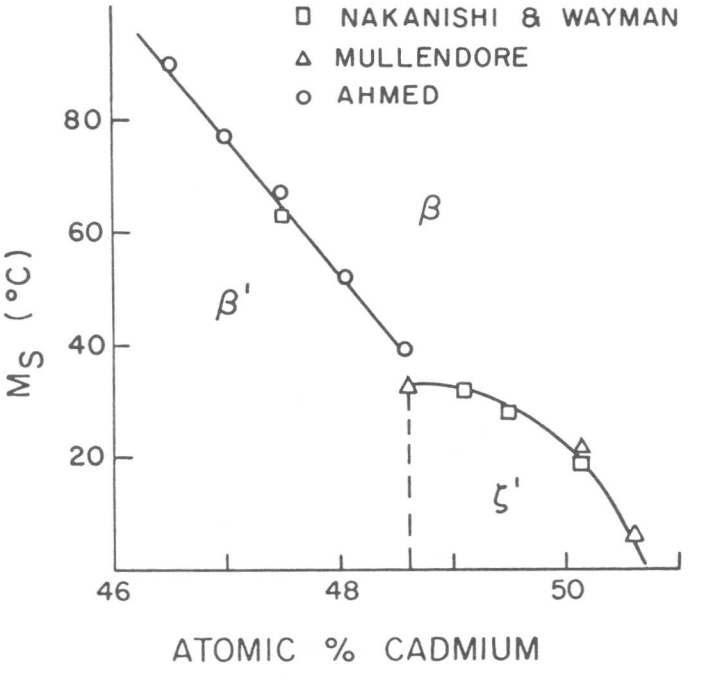

Figure 1

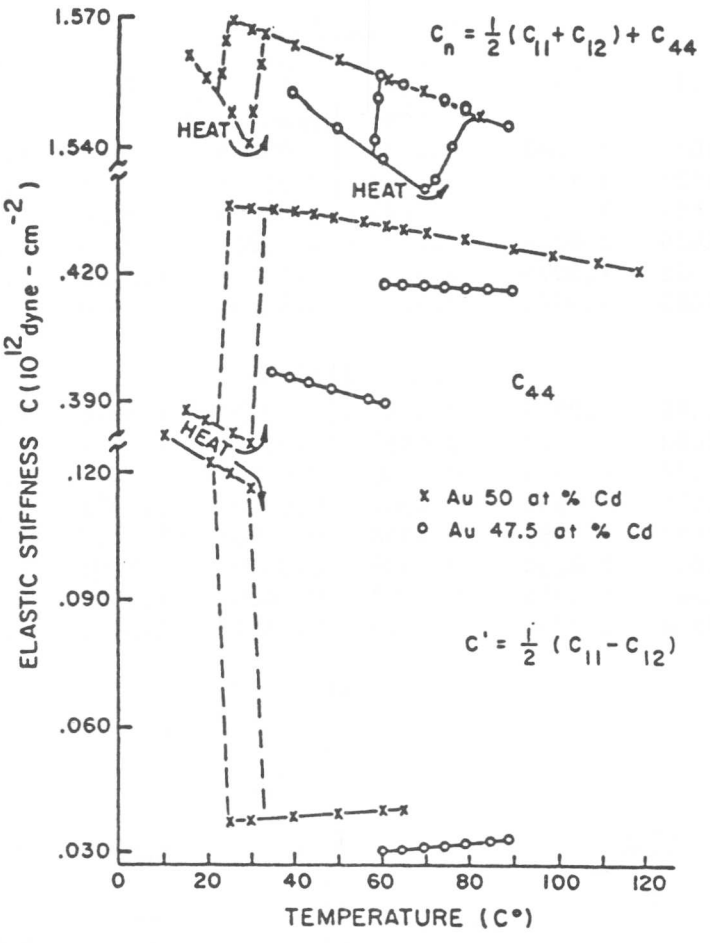

Figure 2

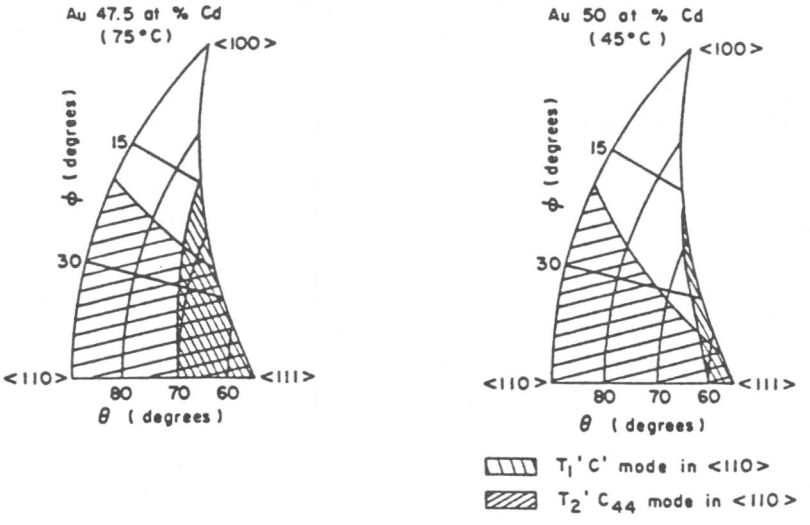

Figure 3

Au 47.5 at.% Cd

Temp. (°C)	C_{11}	C_{12}	C_{44}	C'	C_n	B_s	B_T
			(10^{12} dynes-cm^{-2})				
65	1.1675	1.1062	0.4179	0.03065	1.5548	1.1266	1.0554
70	1.1622	1.1040	0.4177	0.03111	1.5528	1.1247	1.0528
75	1.1651	1.1020	0.4175	0.03156	1.5510	1.1230	1.0504
80	1.1639	1.0999	0.4171	0.03202	1.5490	1.1212	1.0480
85	1.1628	1.0979	0.4166	0.03248	1.5470	1.1195	1.0456
90	1.1618	1.0960	0.4162	0.03291	1.5450	1.1179	1.0433
			Au 50 at.% Cd				
30.2	1.1688	1.0942	0.4361	0.03733	1.5676	1.1191	1.0546
35.0	1.1683	1.0927	0.4355	0.03781	1.5661	1.1179	1.0527
39.8	1.1677	1.0913	0.4350	0.03824	1.5645	1.1168	1.0508
44.5	1.1670	1.0996	0.4344	0.03867	1.5627	1.1154	1.0488
49.3	1.1663	1.0881	0.4338	0.03909	1.5610	1.1142	1.0468
56.1	1.1654	1.0860	0.4328	0.03968	1.5585	1.1125	1.0440
60.7	1.1644	1.0844	0.4322	0.04004	1.5566	1.1111	1.0419
65.2	1.1638	1.0830	0.4314	0.04042	1.5548	1.1099	1.0402

Table I

		Mode				
	Units	C_{11}	C_{12}	C_{44}	C'	C_n
$\left(\frac{dC}{dP}\right)_T$		5.00 5.87	5.15 6.02	2.44 2.61	-0.051 -0.073	7.54 8.56
$\left(\frac{dC}{dT}\right)_P$	$\frac{10^8 \text{dynes}}{\text{cm}^2\text{-deg.}}$	-2.58 -1.37	-4.38 -3.09	-0.40 -1.51	0.90 0.86	-3.88 -3.74
$\beta B_T \left(\frac{dC}{dP}\right)_T$	$\frac{10^8 \text{dynes}}{\text{cm}^2\text{-deg.}}$	3.32 3.85	3.42 3.95	1.62 1.71	0.034 0.048	5.01 5.61
$\left(\frac{dC}{dT}\right)_V$	$\frac{10^8 \text{dynes}}{\text{cm}^2\text{-deg.}}$	0.74 2.48	-0.96 0.54	1.22 0.20	0.87 0.82	1.13 1.87
$\left(\frac{d\ln C}{dT}\right)_V$	$\frac{10^{-4}}{\text{deg.}}$	0.64 2.13	-0.87 0.50	2.92 0.46	28.4 20.2	0.73 1.20
$\left(\frac{d\ln \omega}{dT}\right)_V$	$\frac{10^{-4}}{\text{deg.}}$	0.32 1.07	-0.44 0.25	1.46 0.23	14.2 10.1	0.37 0.60
$\left(\frac{d\ln \omega}{d\ln V}\right)$		2.09 2.46	2.29 2.72	2.91 2.98	-1.04 -1.11	2.39 2.70

By rows, values represent: Au-47.5 at.% Cd
Au-50 at.% Cd

Table II

Premartensitic Elastic Anomalies and Thermoelastic Properties in $Au_{52.5-x}Ag_xCd_{47.5}$ Pseudobinary Alloys

Norihiko Nakanishi, Mikio Takano, Hiroshi Morimoto, Sei Miura* and Akira Nagasawa**

We have studied a phase relation in $Au_{52.5-x}Ag_xCd_{47.5}$ pseudobinary alloys in which the transition temperatures of the Heusler- and martensitic transformations were measured as a function of Ag content. It is to be noted that in the case of Heusler-ordering, the $T_o(=\frac{1}{2}(M_S + A_S))$ temperature gradually decreases with increasing Ag content and exhibits a minimum at about 30 at% Ag, and then a maximum at about 35 at% Ag. While in the case of CsCl-ordering, T_o shows a minimum at about 35 at% Ag and a maximum at about 47 at% Ag. Temperature dependence of the elastic constants was measured by the ultrasonic pulse-echo method in the temperature range above and near M_S, using single crystals. Elastic softenings of $C'=\frac{1}{2}(C_{11}- C_{12})$ and C_S, corresponding to respectively the shear waves along $(110)[1\bar{1}0]_{bcc}$ and close to $(112)[11\bar{1}]_{bcc}$, were thus found in the premartensitic range. These shear waves appear to be very important for the transformation mechanism. Thermoelastic properties of the alloys were summarized as follows; (1) the temperature difference, $T_o-M_S \cong 4$ K, is very small and also in the concentration range over 23 at% Ag, $A_S-M_S \leq 0$ is observed on the curves of electrical resistivity, (2) the difference in enthalpy change between cooling and heating, $\Delta H_C-\Delta H_h$, is close to zero, (3) the so-called pseudoelastic behavior is observed in stress-strain relations, and (4) the entropy change associated with the martensitic transformation becomes nearly constant regardless of Ag content, e.g. $\Delta S=0.8\sim1.3$ J/mol·K.

I. Introduction

We have recently found the following characteristics, such as thermoelastic martensitic properties, pseudoelastic behavior and premartensitic elastic softening of $C'=\frac{1}{2}(C_{11}- C_{12})$ [1], in an $Au-Cu-Zn_{45\sim49}$ pseudobinary alloy. As just reported by Nagasawa et al. in this symposium, the so-called premartensitic elastic anomalies of the shear elastic constants, such as C' ($(110)[1\bar{1}0]$ type) and C_S (close to $(112)[11\bar{1}]$ type), were observed in the temperature range above M_S, and it was suggested that these anomalies (or softening) may be responsible for dynamical mechanisms of the nucleation process of martensite [2].

In the present study, the followings are reported in single crystals of $Au_{52.5-x}Ag_xCd_{47.5}$ pseudobinary alloys; (1) an influence of the CsCl and the Heusler orderings upon the martensitic transformation temperatures, (2) premartensitic elastic properties and (3) the thermoelasticity of martensite and related pseudoelastic behavior. The results obtained are compared with those obtained in the $Au-Cu-Zn_{45\sim49}$ alloys.

Department of Chemistry, Konan University, Kobe. *Department of Mechanical Engneering, Doshisha University, Kyoto. **Department of Physics, Nara Women's University, Nara, Japan.

II. Experimental Method

To complete the Heusler ordering the alloys were slowly cooled for 36 hrs from 993 to 373 K. The CsCl ordering was attained by rapid quenching from 993 to 273 K. Transition temperatures and related enthalpy changes were measured by differential scanning calorimetry. The electrical resistivity measurements were made by using the standard four-terminal technique. Measurements of elastic constants were carried out by the overlapping pulse-echo method (using a MATEC 6000 system) with a frequency of 5 MHz. Tensile tests were performed on an Instron-type testing machine. The strain rate mainly employed was 8.3×10^{-4}/sec.

III. Experimental Results and Discussion

In Fig.1 the critical temperature(T_c) of the Heusler-ordering was found around 480 K, being about 200 K lower than that of the $Au_1Cu_1Zn_2$ alloy[3]. This may be due to some difference in the strength of ionic-bondings between Au-Ag and Au-Cu pairs in the Heusler lattice. In the figure are also shown the martensitic transformation temperatures T_0 against Ag content. The T_0 lines were obtained by the measurements of enthalpy change, electrical resistivity change and stress-temperature curves, in which the critical stresses for inducing the martensite were extrapolated to zero and temperatures thus reached were thought to be the M_S temperatures. It must be noted that in the present alloys only the CsCl-order can be frozen by rapid cooling from the β_1 region, thus thermally formed martensite is holding the CsCl atomic arrangement. While the Heusler lattice can be developed during slow-cooling from the β_1 region and therefore the martensite lattice formed by further cooling holds the Heusler arrangement. As is seen in the figure, in the case of quenching the T_0 temperature gradually decreased with increasing Ag content and a peak appeared at about 47 at% Ag. While in the case of slow-cooling, T_0 also decreased with the increase of Ag content and exhibited a minimum at about 30 at% Ag, and then a maximum at about 35 at% Ag. Here we have two significant questions; (a) the reason why the transition temperature of the Heusler-ordered martensite behaves differently from that of the CsCl-ordered martensite, and (b) the reason why the T_0 temperature becomes minimum near the Heusler composition ($\sim$30 at% Ag), while T_0 did show a maximum at the Heusler composition in the AuCuZn alloy. Although the answers to these questions are not clear at present, it is of interest to note that in both the alloys the T_0 temperatures exhibit a similar tendency, i.e. both T_0's have the minimum at lower Ag and Cu concentrations and then the maximum at higher Ag and Cu concentrations. Now, we discuss dynamical models for premartensitic nucleation according to some data of the shear elastic constants in the temperature range above and near the M_S temperature.

Fig.2 shows the temperature change of C' above and close to M_S in 10 and 35 at% Ag alloys. The softening occurred above M_S and dC'/dT values were nearly equal (2.82 and 2.44 $\times 10^7$ dyn/cm^2.deg. were respectively obtained). It is noticed that the curvature becomes steeper near M_S (not linear) and the ultrasonic wave disappeared at slightly lower temperatures than M_S. On the other hand, an ultrasonic attenuation began at temperatures several ten degrees higher than M_S and showed a sharp

peak at M_S. As reported already in Au-Cd[4], Au-Cu-Zn[3] and Cu-Al-Ni [5] alloys, the shear wave (C') became soft, but could not reach zero at M_S. The values recently obtained in $AuCuZn_{47}$ alloys are dC'/dT =5.20 and 4.53 x 10^7 dyn/cm^2·deg. in the temperature range above M_S's of 30 at% and 33 at% Cu, respectively[6]. Nagasawa[7] and Yamada et al.[8] suggested that the existence of $1/3\langle 110\rangle\langle 1\bar{1}0\rangle$soft phonon could be responsible for the formation of metastable structures, as the distorted lattice or another model, in the premartensitic nucleation process. Moreover, the shear movements on the (110) plane with the $[1\bar{1}0]$ direction play an important role to make a stacking modulation of the close packed plane in the formation process of martensite lattice. Since the softening of C' observed is related to phonons with q=0, the information expected from the softening of shear elastic constants is still incomplete. This suggests that the phonon dispersion relations must be required. The fact that the ultrasonic attenuation corresponding to the C' softening began to increase at temperatures much higher than M_S may suggest an early preparating process for the martensitic nucleation.

In Fig.3 is shown the temperature change of the shear constant C_{44} of $(110)[001]$ type, which has a close relation to another important shear mode C_S ($(112)[11\bar{1}]$ type). The values of dC_{44}/dT were negative above M_S and C_{44} increased gradually from higher temperature toward M_S. However, a detailed observation showed that this increase is saturated at temperatures a few degrees above M_S , then the curves become flat, and finally rather slightly decrease just above M_S. This shear wave disappeared just below M_S. A marked difference obtained by comparing the case to C' is that the attenuation was fairly small and even any increase did not occur in the temperature range above M_S. dC_{44}/dT = -8.62 and -15.80 x 10^7 dyn/cm^2·deg. were obtained in 10 and 35 at% Ag alloys, respectively, and these values are not so different from those obtained in $Au\text{-}Cu\text{-}Zn_{47}$ alloys.

Fig.4 shows the temperature dependence of the special mode C_S, which has been found by one of the authors (A.N.) in NiAl alloys[9], and so far observed in many β-phase alloys, such as Au-Cd[9], $Au\text{-}Cu\text{-}Zn_2$ [10], Cu-Al-Ni[10] and also Nb_3Sn[9]. This mode corresponds closely to the $(112)[11\bar{1}]$ type shear, which is responsible for the formation of the close packed planes in the martensite phase. In other words, it corresponds to the change of atomic angle on the close packed plane ((110) $//(0001)$) from $70^\circ 32'$ to 60° , which first suggested by Burgers[11] as a mechanism of the martensitic transformation in Zr. It is necessary to understand the special mode softening as a correlation effect with the non-linear change of C' and C_{44} modes. When the shear, close to (112) $[11\bar{1}]$ type, operates together with the C' shear ((110) $[1\bar{1}0]$ type), a static model from bcc to close packed structure can be developed. This implies that the origin of the special mode softening is an anharmonic effect in the lattice waves. Therefore, the higher order elastic constants will play an essential role for the transition mechanism in the β-phase alloys. Experimental results showed that the decrease in C' begins at temperatures considerably higher than M_S and the special mode C_S and the mode C_{44} subsequently begin to decrease near M_S.

In Fig.5 is shown the temperature dependence of the elastic anisotropy values C_{44}/C'. Of course, the values increased up to M_S and the

slope became a little steeper below M_S. The values of 19.40 and 15.08 are obtained at their M_S's; 260 K (10 at% Ag) and 175 K (35 at% Ag), respectively. The fact that fairly large values of the anisotropy were obtained at temperatures near M_S may have a close relation to the dislocation stability in an anisotropic elastic field and accordingly to the formation of the martensitic nuclei, in view of the movements of the transformation dislocations.

It is certainly clear that the so-called thermoelastic martensitic transformation has occurred in the present alloys, because of the following experimental facts; (1) the difference of enthalpy change ΔH associated with the transformations on cooling and heating was almost zero, suggesting that the elastic strain energy which generated in the temperature range from M_S to M_f can be stored in the specimen and almost the same amount of the strain energy can be released between A_S and A_f during the reverse transformation, (2) the elastic strain energy associated with the transformation which can be calculated by a simple thermodynamic method was considerably small, ΔG_{el} =12 J/mol, and (3) the temperature hysteresis connected with the forward and reverse transformations was very small, A_S-M_S =1$\sim$8 K, as will be shown.

The temperature change of the longitudinal wave C_{11} exhibited an increase at M_S on cooling and a decrease at A_S on heating, thus making a hysteresis loop (Fig.6(a)). This tendency is similar to the change in electrical resistivity observed in Fig.6(b).

Fig.7 shows the Ag content vs. ΔH and ΔS in the cases of slow-cooling (Heusler) and quenching (CsCl). It is of very interest that ΔH gradually decreased with the increase of Ag content, which is quite analogous to the T_o vs. Ag content relation. Accordingly ΔS exhibited to be constant regardless of Ag content; ΔS =1.0 J/mol·K. This value obtained here is almost similar to 0.84$\pm$ 0.42 in AuCd, 1.30$\pm$ 0.04 in CuZn [12] thermoelastic martensitic alloys, and quite different from the case of Fe-C steel[13] where ΔS =5.86 J/mol·K.

The so-called pseudoelastic behavior has been understood as one of the typical properties of the thermoelastic martensitic transformation. This is the present case. For example, in Fig.8(a) are shown the stress-strain curves obtained in the case of quenching the single crystal of 35 at% Ag. (1) At 77 K which is below M_S (=145 K), two-stage yieldings were observed, which are similar to the curves obtained in Au-47.5 Cd binary alloys[14], and the second yield appears to correspond to the martensite-martensite transformation, (2) at 156$\sim$164 K, (slightly above M_S), superelastic loops having two-stage yieldings appeared and (3) at higher temperatures (175$\sim$195 K), the superelastic loops having only one yielding appeared. Fig.8(b) shows the critical stress vs. temperature relation obtained from the stress-strain curves, which exhibited correlations among the β_1, thermally formed martensite and stress induced martensite regions.

References

[1] S. Miura, S. Maeda and N. Nakanishi: Phil. Mag., 30(1974), 565.

[2] A. Nagasawa, N. Nakanishi, M. Takano, H. Morimoto, Y. Matsuo and T. Suzuki: To be published.
[3] N. Nakanishi, Y. Murakami and S. Kachi: Scripta Met., 5(1971), 433.
[4] S. Zirinsky: Acta Met., 4(1956), 164.
[5] M. Suezawa and K. Sumino: Scripta Met., 10(1976), 789.
[6] N. Nakanishi, M. Takano, H. Morimoto, Y. Murakami and S. Kachi: ICIFUAS-6 (1977).
[7] A. Nagasawa: J. Phys. Soc. Japan 40(1976), 1031.
[8] M. Mori, Y. Yamada and G. Shirane: Solid State Commum., 17(1975), 127.
[9] A. Nagasawa and Y. Ueda: J. Phys. Soc. Japan 45(1978), 1249.
[10] A. Nagasawa and N. Nakanishi: To be published.
[11] W. G. Burgers: Physica 1(1934), 561.
[12] P. L. Young and A. Bienenstock: J. Appl. Phys., 42(1971), 3008.
[13] H. Warlimont, L. Delaey, R. V. Krishnan and H. Tas: J. Mat. Sci., 9(1974), 1545.
[14] N. Nakanishi, T. Mori, S. Miura, Y. Murakami and S. Kachi: Phil. Mag., 28(1973), 277.

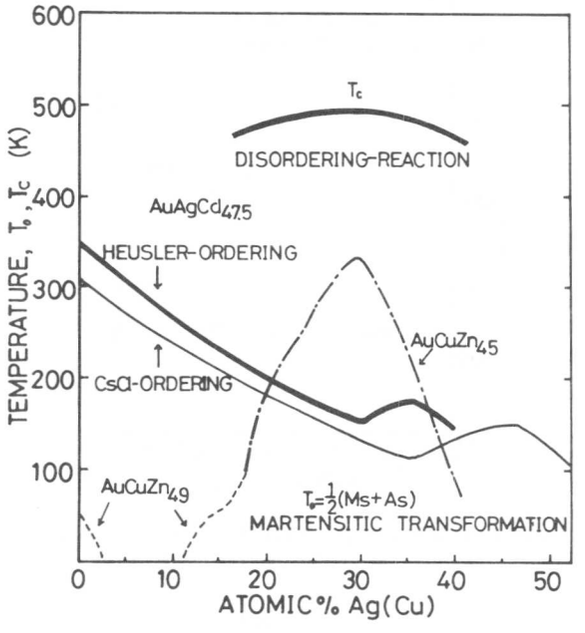

Fig.1: Phase diagram in Au-Ag-Cd pseudobinary alloys.

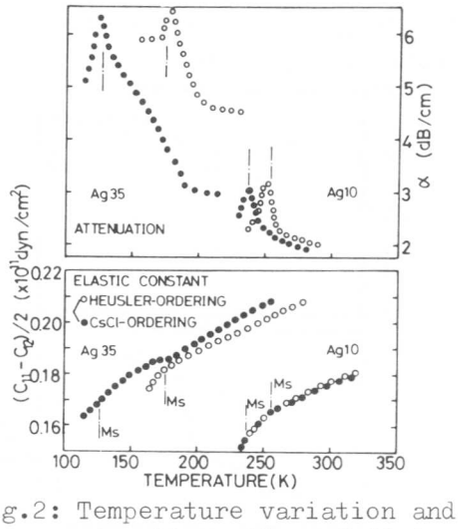

Fig.2: Temperature variation and ultrasonic attenuation of C' in 10 and 35 at% Ag alloys.

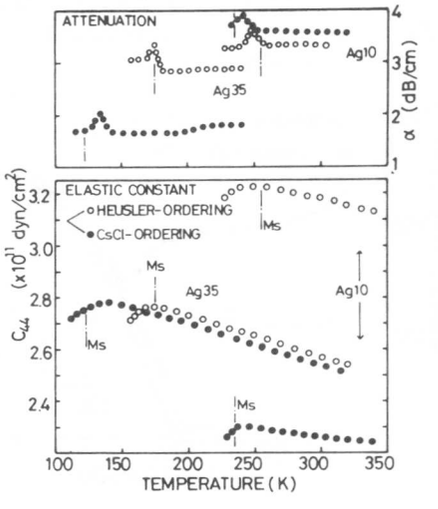

Fig.3: Temperature variation and ultrasonic attenuation of C_{44}.

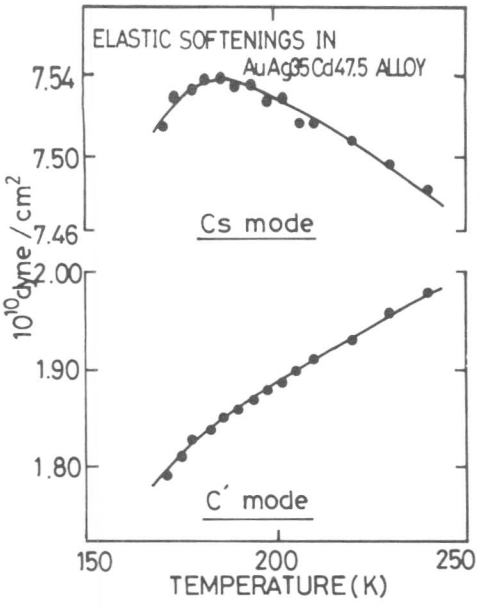

Fig.4: Temperature variation of shear waves, C' and C_S.

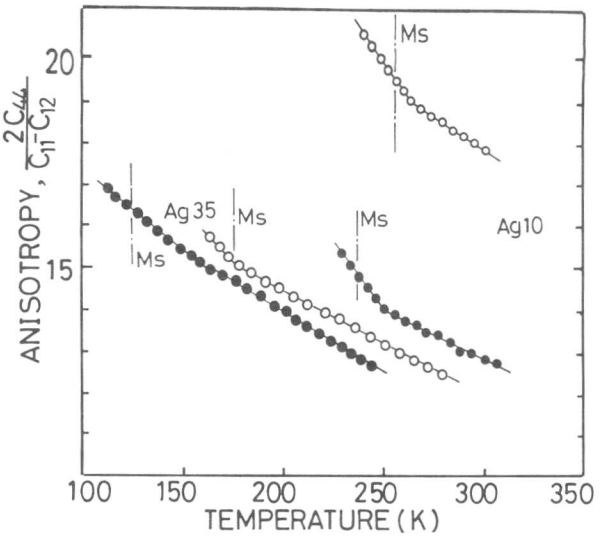

Fig.5: Temperature variation of the elastic anisotropy.

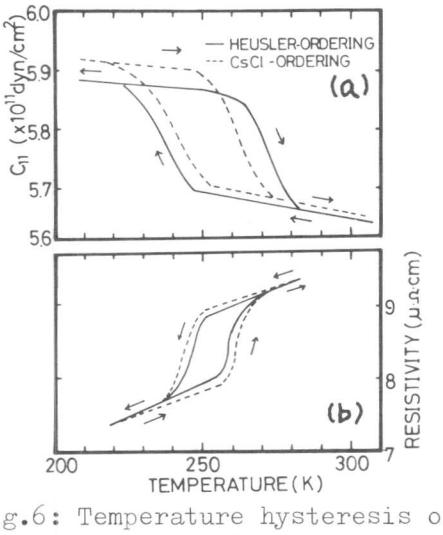

Fig.6: Temperature hysteresis of C_{11} and electrical resistivity in 10 at% Ag.

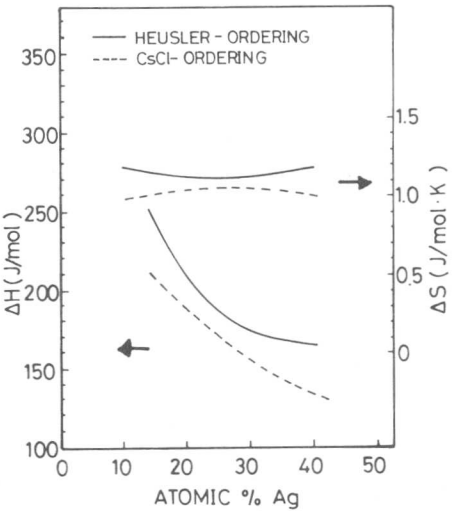

Fig.7: Enthalpy and entropy changes as a function of Ag content.

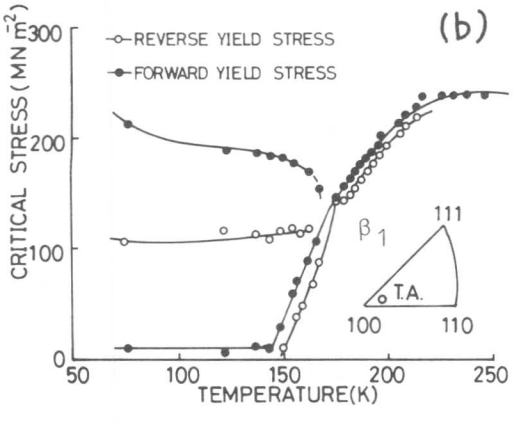

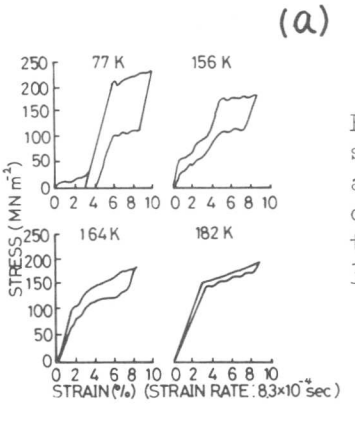

Fig.8: Stress-strain curves and the critical stress vs. temperature in 35 at% Ag.

Dispersion Anomaly of Ultrasonic Waves in the Cu-Zn Alloy Single Crystals

Kenichi Kojima, Taijiro Miyazaki, Masayuki Kikuchi and Tetsuro Suzuki

The dispersions of ultrasonic waves in Cu-Zn alloys are observed at the temperature range between 373 K and 78 K in the frequency of MHz. Not only TA_2 wave but also LA wave corresponding to shear elastic constants C' and longitudinal elastic constants C_L respectively, showed the dispersion. It seems that these dispersions mainly depend on the modulated structure.

I. Introduction

The quenched Cu-Zn alloys undergo the martensitic trnsformation at lower temperature. The temperature dependence of the shear elastic constants C' of the alloys shows the well known anomalous behavior, which has been interpreted in terms of the vibrational entropy of the B.C.C.-type lattice. Prasetyo, Reynaud and Warlimont [1] have pointed out the possibility that the anomalous temperature dependence of the shear elastic constants may be related to the presence of the modulated structure of ω-like phase.

Because the presence of the modulated structure can lead to the dispersion of ultrasonic waves with appropriate wavenumbers, the dispersion of ultrasonic waves in the quenched Cu-Zn crystals has been measured by use of a new technique.

II. Experimental Procedure

Single crystals of β brass with a diameter of 25 mm and a length of 70 mm were grown by the Bridgeman technique. These crystals were cut parallel to a (110) plane to investigate the elastic constants and the dispersion of ultrasonic wave velocity in the frequency range of 1 -100 MHz. The chemical analysis of these crystals shows Cu-46.5at.%Zn as the composition of used alloys. The dimensions of specimens for ultrasonic experiments are 5 mm thickness and 10x10 mm^2 area. These specimens are homogenized at 1073 K for 24 hr and then quenched into water at 273 K.

The block diagram for the equipment used in the ultrasonic dispersion experiment is shown in Fig.1. An electric pulse is sent from the pulse generator to one of the transducers. The longitudinal or shear waves are transmitted through a specimen and received at another transducer. These repeated signals are trnsformed by a sampling oscilloscope into a single wave train which sweeps at very slow rate.

Department of Physics, Yokohama City University, Seto 22-2, Kanazawa-ku Yokohama 236, Japan.

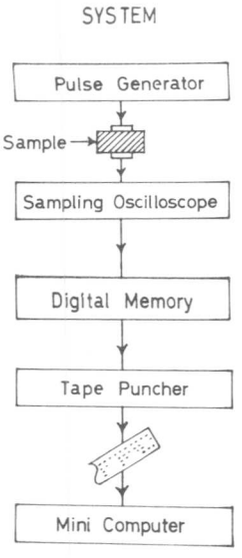

Fig.1 Experimental Arrangements

The output of it is fed into a slow digital wave memory device, which has a capacity of recording up to 1024 words of digitally converted data of the ultrasonic response. The ultrasonic response of the specimen with a dulation of 1 μs can be recorded with an effective time resolution of 1 ns. These digitally recorded data are transmitted to a computer by use of a standard ASC II paper tape or a magnetic tape. These data are analyzed by the computer to obtain the dispersion of an ultrasonic wave.

Since the details of the method of analysis have been already published [2,3], the basic principles are briefly summirized here: The first echo $u_1(t)$ and second one $u_2(t)$ are recorded digitally on a tape. The Fourier transforms of each echo is given by equations (1) and (2):

$$U_1(\omega) = \sum_n u_1(n\Delta t)e^{i\omega n\Delta t}\Delta t \qquad (1)$$

$$U_2(\omega) = \sum_n u_2(n\Delta t)e^{i\omega n\Delta t}\Delta t \qquad (2)$$

where Δt is the sampling interval time, ω is the angular frequency and n is the interger. The transfer function $H(\omega)$ corresponding to a passage of the ultrasonic wave through the specimen is defined by $H(\omega) = U_2(\omega)/U_1(\omega)$. Aprediction filter h(t) which predicts the second echo $u_2(t)$ from $u_1(t)$ is determined according to Winner's theory [2,3]. Once the prediction filter h(t) is obtained, the transfer function $H(\omega)$ is given by equation (3) as the Fourier transforms of h(t):

$$\widehat{H(\omega)} = \sum_n h(n\Delta t)e^{i\omega n\Delta t}\Delta t. \qquad (3)$$

Taking the time shift τ_0 into account, the phase of the transfer function $\widehat{H(\omega)}$ gives the deviation of the phase referred to $\omega\tau_0$,

$$\delta\varphi = \varphi - \omega\tau_0 \qquad (4)$$

where

$$\delta\varphi = \mathrm{Arg}(\widehat{H(\omega)}). \qquad (5)$$

The nonliniearity of phase shift $\delta\varphi$ with respect to ω shows the dispersion of ultrasonic waves.

III. Results and Discussion

The variation of the elastic constants C_{44}, C' and C_L of the Cu-46.5at.%Zn alloys in the temperature range from 373 K to 78 K is shown in Fig.2. The behavior of C_{44} and C_L with the increasing temperature is normal. In contrast, C' is abnormal because the slope is positive. This behavior is known as the chracteristics of many quenched β-type alloys such as Ag-Zn, Au-Zn, Au-Cd [4] and Cu-Al-Ni

[5] and others.

The deviation of the phase shift in Cu-Zn alloy for the ultrasonic waves corresponding to C_L, C_{44} and C' as a function of temperature was measured in the frequency range 1 -100 MHz. Hereafter, the ultrasonic waves corresponding to C_L, C_{44} and C' are degignated as LA, TA_1 and TA_2 waves, respectively. Fig.4 shows that the typical deviation of a phase shift of LA wave. Above 10 MHz, the phase shift decreases with increasing frequency and reaches the maximum around 30 MHz and then stay constant with weak fluctuations. The maximum phase shift near 30 MHz decreases as the temperature decreases. This result indicates that the delay of phase velocity of a given frequency will depend on the temperature. The curves of phase shift of TA_1 show the weak periodic fluctuations around zero in the frequency range above 10 MHz. This small amount of phase shift is comparable with errors so that we can expect that the delay of phase velocity of TA_1 is quite small. On the other hand, the behavior of the phase shift of TA_2 wave is quite different from LA and TA_1 waves as shown in Fig.3. In the higher frequency range than 10 MHz, the amount of the phase shift successively increases with the increasing frequency at every temperature. There is a weak temperature dependence of the magnitude of the phase shift. Hence, it is possible the phase shift increases near martensitic transformation temperature. In the lower frequency range (<10 MHz), the more detailed experiment is being carried out.

The relative delay of the phase velocity ($\delta v/v_0$) can be estimated by equation (6):

$$\delta v/v_0 = v_0 \delta\varphi/2\pi fL \qquad (6)$$

where f, v_0, $\delta\varphi$ and L are the frequency, the signal velocity, the phase shift and the propagation distance, respectively. The results for LA and TA_2 waves are shown in Fig.5 and Fig.6. The delay of phase velocity of LA wave rapidly increases at ~10 MHz and reaches the maximum which depends on a temperature i.e. 0.9% at 373 K and 0.2% at 78 K. Above 40 MHz, $|\delta v/v_0|$ decreases slowly. This result points out the phase velocity of the higher friquency is faster than that of the lower frequency. On the other hand, a $|\delta v/v_0|$ of TA_2 successively increases with the increasing frequency. This shows that the phase velocity is slower with the increasing frequency. Although a temperature dependence on $|\delta v/v_0|$ is quite small, the delay of the phase velocity increases at lower temperature. These results of LA and TA_2 waves can suggest that a dispersion relationship of ultrasonic wave exists even in small wave numbers.

A dispersion of ultrasonic waves is expressed by

$$\delta k/k_0 = v_0 \delta\varphi/2\pi fL \qquad (7)$$

where k_0 is the wave number of v_0 and δk is the deviation of wave number k_0. An expression of eq.(7) is identical with eq.(6) with respect to the frequency so that the dispersion curves of LA and TA_2 waves show the same behavior as $\delta v/v_0$ of them. A characteristic of the dispersion curve of LA wave has a small dip near 30 MHz,

which is getting small with the decreasing temperature. In contrast, it should be noticed that the dispersion behavior of TA_2 wave is anomalous, i.e. (1) the amount of dispersion increases with the increasing wave numbers and (2) the dispersion indicates a decreases at lower temperature.

In general, the dispersion of ultrasonic waves in a solid may be mainly caused by (1) the scattering of waves by densely distributed fine inhomogeneities in the material (scattering dispersion) and (2) the absorption or dissipation of wave energy into heat and other forms of energy in an irreversible process (dissipative dispersion). Prasetyo, Reynaud and Warlimont [1] showed that precipitates are several tens nm in diameter and 100 -200 nm long inthe alloy which has the same composition and same heat treatment as we used. Hence, the scattering effects of ultrasonic wave can be one of the important factors of dispersion in this alloy. This suggests that such a dispersion is a characteristic of martesitic transformation. Although drastic instability of TA_2 wave was not observed in this wave number range until 78 K, the softening could be expected at temperature near transition.

Acknowledgement

We thank Drs. S.Kobori and K.Ohori of Institute of Mitsubishi Metal and Mining Co., for preparing Cu-Zn alloys.

Refereces

[1] A. Prasetyo,F Renaud and H. Warlimont: Acta Met., 24(1976), 1009.
[2] M. Kikuchi, K. Kojima and T. Suzuki: "Internal Friction and Ultrasonic Attenuation in Solids:, Ed. R.R. Hashiguchi and N. Mikoshiba, University of Tokyo Press,(1977),333.
[3] M. Kikuchi: Phys. Earth and Planet. Inter.,19(1979),in print.
[4] Y. Murakami and S. Kachi: Japanese J. of Appl. Phys.,13(1974), 1728.
[5] M. Suezawa and K. Sumino: Scripta Met.,10(1976),789.

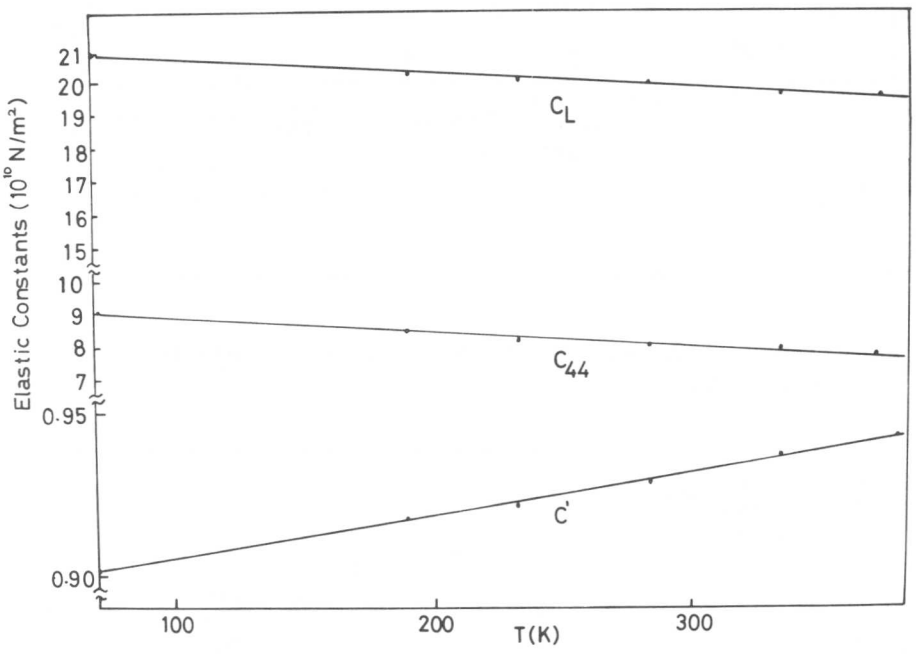

Figure 2 A temperature dependence of a longitudinal elastci constants C_L and two shear elastic constants C_{44} and C'.

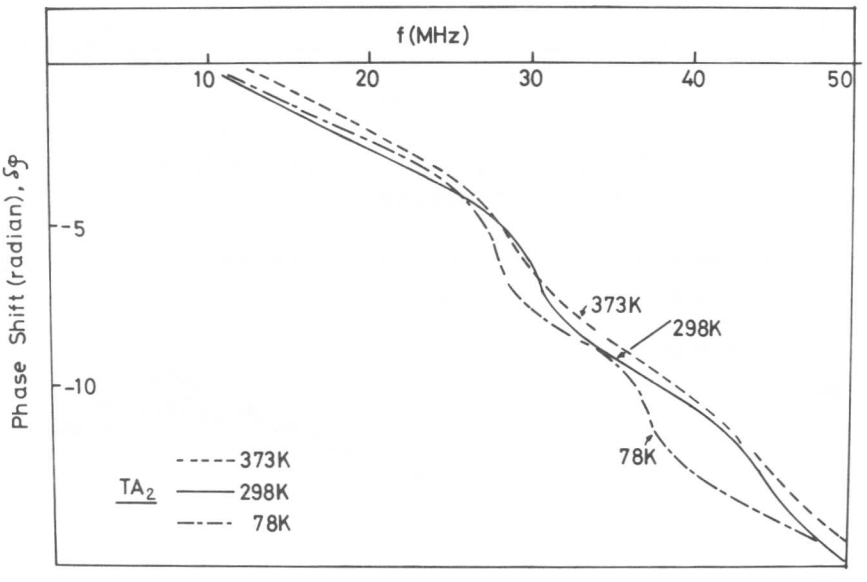

Figure 3 A phase shift of TA_2 wave at various temperatures.

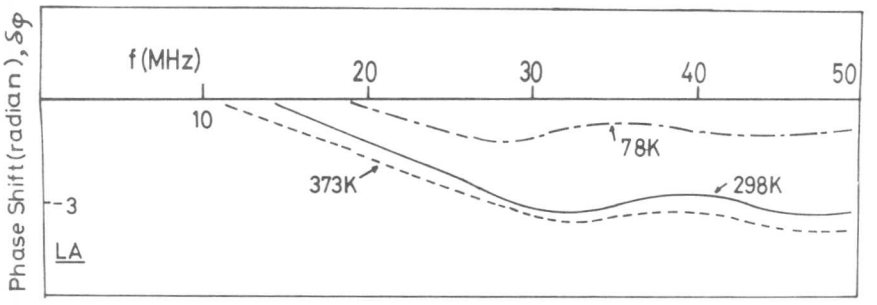

Figure 4 A phase shift of LA wave at various temperatures.

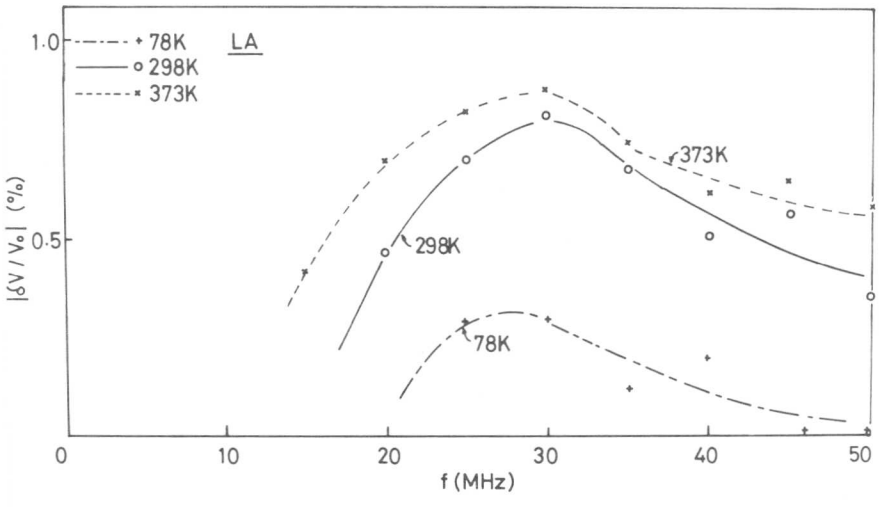

Figure 5 A delay of phase velocity of LA wave as a function of frequencies.

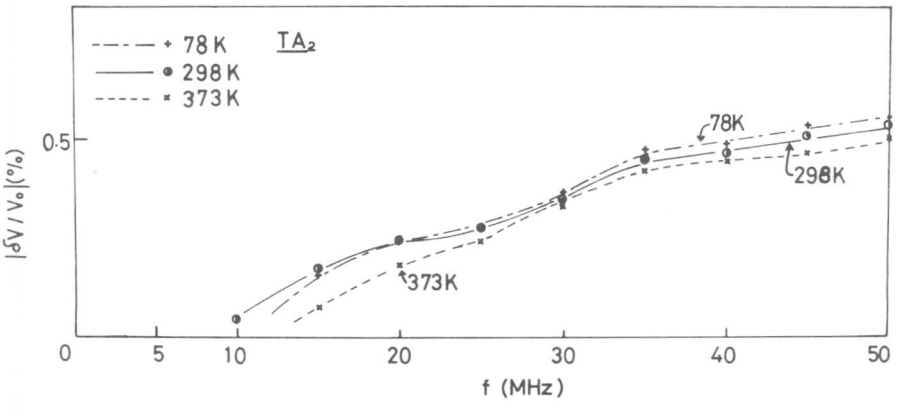

Figure 6 A delay of phase velocity of TA_2 wave as a function of frequencis.

Softening of Young's Modulus of Polycrystalline Nb_3Sn

D. O. Welch, J. F. Bussière, and M. Suenaga

Ultrasonic measurements show that the shear modulus $(C_{11}-C_{12})/2$ softens dramatically as single crystals of Nb_3Sn approach the martensitic transition near 50K. It is expected that Young's modulus of polycrystals will also soften, but previous ultrasonic measurements, which suffer from severe damping, fail to show the expected effect. We have measured Young's modulus of polycrystalline Nb_3Sn between 4.2K and 300K by static beam deflection methods, and observe marked softening. A value of $14.3\pm.5\times10^{11}$ dyne cm^{-2} was obtained at 300K by the deflection of thin Nb_3Sn-Nb-Nb_3Sn composite strips by external stress. The variation of the modulus with T was obtained from the change in the radius of curvature of internally stressed Nb_3Sn-Nb composite strips. (This method is made possible by the near perfect match between the thermal expansion coefficients of Nb and Nb_3Sn.) The modulus is found to be proportional to lnT between 50K and 300K and is temperature independent below the superconducting T_c, resulting in a decrease by a factor of ~2 between 300K and 18K. The observed softening is somewhat less than that predicted by a polycrystalline average of the experimental single crystal elastic constants, but is much larger than that observed with ultrasonic measurements.

I. Introduction

Nb_3Sn undergoes a reversible cubic $\rightleftarrows$ tetragonal martensitic phase transition near 50K. This transition is sensitive to the degree of order, presence of defects, and other microstructural properties; a summary of the characteristics of the transition in Nb_3Sn and other A15 compounds can be found in [1]. The temperature dependence of the elastic constants of single crystals and its relation to the phase transition have been studied in detail, both theoretically and experimentally [1,2]. A most striking feature is the vanishing of the shear modulus $(C_{11}-C_{12})/2$, and hence of Young's modulus in the [100] direction, at the transition.

Since technological applications of Nb_3Sn as a superconductor utilize polycrystals, their elastic behavior and its temperature dependence are of interest. Measurements on polycrystals, however, are scarce and inconsistent with single crystal data. Old and Charlesworth [3] found a value for Young's modulus at 300K of 17.9×10^{11} dyne cm^{-2} using an ultrasonic "critical angle" technique, while the published sound velocity data of Testardi et al. [4] lead to a value of 23.6×10^{11} dyne cm^{-2}. These values are considerably higher than is obtained by a Voigt-Reuss-Hill polycrystalline average [5] of single crystal constants [6,7], 13.7×10^{11} dyne cm^{-2}. Furthermore the Young's modulus derived from sound velocity data [4] softens much less than the modulus derived from single crystal data [7], as may be seen in Figure 1.

Brookhaven National Laboratory, Upton, NY 11973.

Such discrepancies do not occur for the A15 compound V_3Si, for which the softening predicted by polycrystalline averaging agrees with that from ultrasonic data [4]; dynamic resonance experiments on V_3Si polycrystals also show substantial softening [8]. In order to determine whether or not polycrystals of Nb_3Sn show substantial softening of Young's modulus as the temperature approaches that of the martensitic phase transition, we have measured the static deflection of bimetallic (Nb+Nb_3Sn) composite strips under the influence of internal and external stress and derived the Young's modulus of Nb_3Sn in the range of 4.2 to 300K.

II. Experimental Procedure

Nb_3Sn/Nb/Nb_3Sn composite strips were made by a solid state diffusion process (the "bronze process"). Initially, a Cu-13wt%Sn bronze is cast around a 3.2mmx40mmx150mm plate of pure niobium. The bronze/niobium composite is then rolled to obtain a tape of niobium (~25μm thick) with ~50μm of bronze on each side, which is then slit into 12mm x50mm pieces and reacted at 725°C for 50h. This results in Nb_3Sn layers of ~3-4μm thickness at the interface between the niobium and the bronze.

Because the thermal expansion coefficient of the bronze substantially exceeds that of the Nb and Nb_3Sn, cooling from the reaction temperature, 725°C, results in an internal stress. With bronze layers of the thickness in these experiments, the internal stress is sufficient to cause plastic flow in the unreacted Nb during cooling. Thus, an internal stress remains in the Nb_3Sn/Nb/Nb_3Sn composite which is obtained by etching away the bronze layers in dilute nitric acid. It is possible to remove this internal stress by annealing the composite strip (without bronze) at 725°C for 1/2 hour.

The temperature dependence of Young's modulus was determined with internally stressed composite strips (unannealed). The presence of the internal stress is made manifest by etching away <u>one</u> of the Nb_3Sn layers in 4 parts HNO_3, 2 parts H_2O, and 1 part HF, a solution which etches Nb_3Sn much faster than it does Nb. The resulting Nb_3Sn/Nb asymmetric composite curls with the Nb on the inside diameter, indicating that the Nb_3Sn was initially in compression. As described below, the thermal expansion coefficients of Nb and Nb_3Sn are very well matched; thus changes in the radius of curvature of the curled composites with temperature can be used to deduce the temperature dependence of the Young's modulus of Nb_3Sn.

The match between the thermal expansion of Nb_3Sn and Nb was determined by measuring the radius of curvature of a composite, annealed at 725°C for 1/2 hour (without the bronze matrix), where one layer of Nb_3Sn is removed. These measurements indicate that the mismatch in $\Delta L/L$ of the two materials between 725°C and room temperature is less than 10^{-5} and less than 5×10^{-6} between 300K and 4.2K. Thus any curvature in unannealed composites can be attributed to mismatch due to plastic flow in the Nb and this mismatch, Δ, is independent of temperature below room temperature.

With isotropic elasticity theory, it is straightforward to derive the resulting radius of curvature, R, of the bimetallic composite [9, 10]. The result is of the form:

$$\Delta = R^{-1}F(E_1,E_o,\nu_1,\nu_o,l_1,l_o) \tag{1}$$

where E is Young's modulus, ν is Poisson's ratio, l is the layer thickness, and the subscripts one and zero refer to Nb_3Sn and Nb, respectively. Because Δ is independent of temperature, the temperature dependence of the radius of curvature is of the form:

$$R(T)/R(300K) = F(300K)/F(T) \tag{2}$$

where the temperature dependence of F comes primarily from that of the Young's moduli; we shall neglect the temperature dependence of Poisson's ratio (a source of ~10% error). Explicitly writing F yields the relation between the temperature dependence of R and E [9]:

$$\frac{E_1'}{E_1} = \frac{RE_o'}{R'E_o} \cdot \frac{2}{a}\left\{1+\left[1-4k^{-2}a^{-2}L^2(R/R')^2\right]^{1/2}\right\}^{-1} \tag{3}$$

where:

$$L \equiv \frac{l_1}{l_o} \qquad k \equiv \frac{E_o l_o (1-\nu_1)}{E_1 l_1 (1-\nu_o)}$$

$$a \equiv k^{-2}\{(1+k)(L^2+k)+3k(1+L)^2-k(R/R')(4+6L+4L^2)\}$$

and the primed and unprimed symbols refer to values at low temperatures and room temperature respectively; the subscripts one and zero refer to Nb_3Sn and Nb, respectively.

The temperature dependence of R was measured by enclosing a Nb_3Sn/Nb composite strip in a cryostat with windows through which the strip could be photographed at temperatures between 4.2 and 300K. The radius of curvature was obtained by measuring the negatives in an optical comparator. These values, when inserted in Eq. (3) together with elastic data for Nb, yield the temperature dependence of E for Nb_3Sn.

III. Results and Discussion

The radii of curvature of two curled Nb/Nb_3Sn bimetallic strips, with characteristics summarized in Table I, were measured between 4.2 and 300K; changes were of the order of ~40%. These results were used, as described above, to derive the data shown in Fig. 1. For simplicity, the Poisson's ratios of Nb and Nb_3Sn were taken to be equal and temperature independent (resulting in an error of ~10%); a Voigt-Reuss-Hill average of the single crystal data of [11] was used for the temperature dependent Young's modulus of Nb. Fig. 1 shows that E_{Nb_3Sn} softens by about a factor of two between 300K and 50K, in marked contrast with the sound velocity data of [4]. The softening is somewhat sample dependent and is somewhat less than that predicted by a Voigt-Reuss-Hill polycrystalline average of single crystal data. The modulus

is essentially proportional to ln T between 50 and 300K and becomes temperature independent at the onset of superconductivity (~18K).

Three-point bending measurements were made on annealed Nb_3Sn/Nb/Nb_3Sn composites to obtain Young's modulus at 300K. An average of the results of such measurements on five samples, to be described elsewhere [9], yields a value of $14.3\pm.5 \times 10^{11}$ dyne cm^{-2}, in good agreement with 13.7×10^{11} dyne cm^{-2} obtained by a Voigt-Reuss-Hill average of single-crystal data [6,7], and in disagreement with the result of Old and Charlesworth [3], 17.9×10^{11}, and the value 23.6×10^{11} derived from the data of Testardi et al. [4].

*Work supported by the U.S. Department of Energy.

References

[1] M. Weger and I. B. Goldberg: in Solid State Physics, F. Seitz and D. Turnbull, Eds., vol. 28, p. 1, Academic Press, New York (1973).
[2] L. R. Testardi: Physical Acoustics, W. P. Mason and R. N. Thurston, Eds., vol. X, p. 193 (1973); vol. XIII, p. 29 (1977), Academic Press, New York.
[3] C. G. Old and J. P. Charlesworth: Harwell Report AERE-R7903 (Dec. 1974).
[4] L. R. Testardi, R. R. Soden, E. S. Greiner, J. H. Wernick, and V. G. Chirba: Phys. Rev. 154 399 (1976).
[5] H. B. Huntington: in Solid State Physics, F. Seitz and D. Turnbull, Eds., vol. 7, p. 213, Academic Press, New York (1958).
[6] W. Rehwald: Phys. Lett. A27, 287 (1968).
[7] K. R. Keller and J. J. Hanak: Phys. Rev. 154, 628 (1967).
[8] E. R. Vance and T. R. Finlayson: J. Appl. 19,1980 (1968).
[9] J. F. Bussière, D. O. Welch, and M. Suenaga: to be published.
[10] S. T. Timoshenko: The Collected Papers, p. 403, McGraw-Hill, New York, (1953).
[11] K. A. Jones, S. C. Moss, and R. M. Rose: Acta Met. 17, 365 (1969).

Table I Characteristics of the Curled Nb/Nb_3Sn Strips Used to Obtain $E_{Nb_3Sn}(T)$.

Sample	Nb Thickness (μm)	Nb_3Sn Thickness (μm)	Radius of Curvature at 300K (mm)	Maximum Compressive Strain in Nb_3Sn, 4.2K (%)
1	17.2	3.1	7.5	.11
2	14.9	3.6	9.5	.04

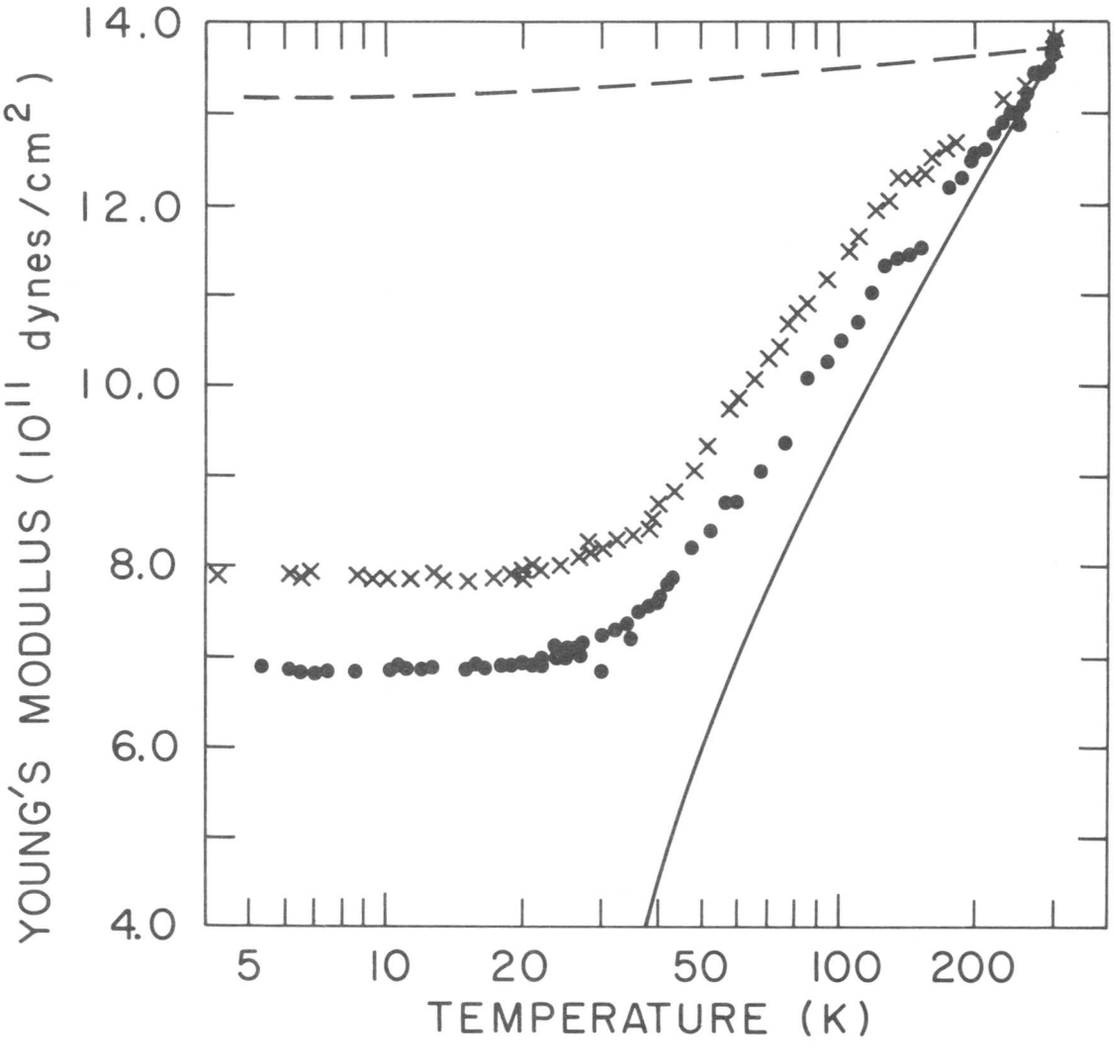

Figure 1. Temperature Dependence of the Young's Modulus of Nb_3Sn. x - Sample #1*, • - Sample #2*.

- - - Sound velocity data of ref. 4, normalized* at 300K.

_____ Voigt-Reuss-Hill average of single-crystal data of ref. 7.

*Data are normalized to the V-R-H average value:

$$E_{Nb_3Sn}(300K)=13.7\times10^{11} \text{ dyne cm}^{-2}.$$

Electron-Energy Spectrum of TiNi in Visinity of Martensitic Transformation

A.I.Lotkov, S.A.Shabalowskaja, I.I.Sasowskaja*, A.A.Baturin

By the methods of positron annihilation and metal optic the electronic structure of the intermetallic compound TiNi in austenite B2 and martensite B19' and also on the stages preceeding the beginning of the direct and indirect martensitic transformation (MT) are investigated. The optical constants n and k are measured in the energy region (0.07-4.5) ev. Basing on the analyses of optical conductivity it is established that by MT the infra-red part of TiNi the spectrum is mainly changed. In the structure B2 in the infra-red regions the intense interband absorbtion is observed, which testifies to the high density of states in immediate proximity to E_F. In the structure B2 the gap is formed around E_F which reaches 0.52ev wide. The changes of the electronic structure on the stages preceeding MT testify to the change of the Fermi surface near the transition. The probable nature of the structure B2 instability which is connected with the peak $N(E_F)$ is under discussion.

I. Introduction

The intermetallic compound TiNi CsCl ordered in the narrow region of concentration around room temperature undergoes some changes[1], both of the first order and those close to the second, going according to martensite-like mechanism. The transformation of B2-R (R-rombohedric distortion B2) was treated as the stage preceeding MT B2-BI9 for a long time. In all the investigations of the changes of electronic structure by MT made these transformations were not divided. Therefore it seems impossible to say something definite about the electronic structure, its changes and its role in various MT. The aim of this investigation is to get the information about the electronic structure in the phases B2 and B19, about its significance in the realization of MT.

Sibirian Physico-Technical Institute, USSR, Tomsk
*Institute of Metal Physics, Ural Scientific Centre, Academy of Sciences of the USSR, Sverdlovsk

II. Methods

TiNi alloy of the equiatom like composure is prepared out of electrolytic nickel and iodide titanium by electron -beam melting in helium atmosphere. Before taking the measurements the samples cut out of one ingot were annealed in vacuum (not lower than 10^{-4}mm mercury column at 800°C in the course of one hour),than they were cooled together with the furhace. To get the smooth surface the samples were mechanically- and then electropolished. The optical constants n and K were measured by the Bitty polarimeter methods to within 2-3%[2]MT being over,on the smooth surface of the samples was constantly appearing by the heating a small relief in the way that the smoothness was preserved but its quality grew worse. The spectrum received on the relief surface duplicated on the smooth surface in the alloy (Ti-5I at % Ni), which was in the same structural state. The relief appeared to bring only to the reduce of optical absorbtion in the whole investigated interval by 4-5 units. The investigations of positron annihilation were made in the apparatus with the angular resolution of 1 mrad. MT in the alloy of the given composure in the first cycles goes without rombohodral distorted of the initial B2 structure. The temperatures of MT are Ms=78°C, Mf=45°C and As=130°C. The angular distributions of the annihilated photons (ADAP) are received in martensite at room temperature and in austenite at the T=170°C and also on the stages preceeding the direct MT at 90°C and indirect MT at 75°. The optical experiment were made at the same temperatures with the exception of austenite state. To avoid the oxidation of the surface the measurements in austenite were made at the temperature T=I30° with the preliminary heating to 150°C.

III. Results and Discussion

1. Positron Annihilation

The analyses of ADAP (fig.I a,b) show that they consist of 2 contributions both in the structure B2 and in the structure Bl9. One of them is satisfactory described by the gaussiana G_1,reaching 17 mrad. The second fraction within the limits of an experimental mistake could be described in two ways: either by the gaussiana G_2 or like a superposition of the parabola P and transitional function φ (fig.I b). This dual description of the second fraction proves the fact that it was caused by both the annihilation of the stringly bonding electrons and free electrons. From the analyses of ADAP in the systems TiFe,TiCO,

TiNi follows the fact that the two fractions in ADAP reflect the positron annihilation with two groups of electrons of bonding (G_1) and antibonding (G_2) types. The last group is absent in the electronic spectrum of TiFe according to the calculation[3] correspondingly ADAP is described by one gaussiana. By the MT B2-B19 the redistribution between the two fractions is observed in the way that in the more closely packed structure B19 the fraction from the parabola in ADAP is increased to 3%. The width of impulse distribution doesn't change by this and constitues 9,8mrad in the half of the maximal intensity. The changes observed are the consequences of the increasing number of free electrons and testify to the strengthening of the metallic character of the bonding forces in the structure B19. In table I the fractions in various states in ADAP are given. ADAP on the stages preceeding MT undergo considerable changes. In martensite at 75° (fig.I a) ADAP is changed by this in the way that one can describe it by the superposition of the gaussian and the parabola without the transitional function. The width of ADAP is decreased to 9,2mrad The fraction of gaussian is increased by this considerably owing to P and φ (see table I) and reaches the quantity typical of the phaze B2. ADAP on the stage preceeding the direct MT (at 90°C) is transformed so that it may be described by one gaussiana. These changes of ADAP on the stages preceeding MT testify to the considerable redistribution of the electrons in the valency spectrum and reconstruction of the Fermi surface long before MT.

2. Optical Measurement

In fig.2 the spectrum of optical conductivity $\sigma = nK\nu$ (ν -light frequency) for 2 structural states - that of austenite and martensite is shown. One can see that both spectra have 2 intensive absorbtion bands which are divided by a deep minimum. The band localized in the visible region (1.2-4.5ev) does not change its energy state by MT and preserves the elements of its structure. The absorbtion-edge is much more clearly out in austenite. The maximum by the energy of 3ev is transformed in martensite into the shoulder, the high-energy part of the band is narrowed to 0.2ev. The infra-red part of the spectrum where the second band is localized is changed cardinally by MT. In austenite $\sigma(\omega)$ is growing steadily by the reducing of the energy, displaying the peaks of the interband absorbtion, which are absent in martensite, up to the lowest energies including. In martensite a new intense band of an assymetrical shape with the maximum at the energy 0.52ev appears. The growth of $\sigma(\omega)$ at $\hbar\omega < 0.2$ev is probably caused by the fraction from the free carriers of the Drude-Zinner-type. The presence of 2 bands divided by a clear cut minimum in the spectrum of optical conductivity

may testiy to the presence of 2 groups of electrons in TiNi valency spectrum, one of which is localized in the region E_F. The origin of the intense interband absorbtion in the infra-red region in austenite is due to the transitions between the bands which closely approach E_F. The analyses of the results received in the model of direct transitions on the basis of the energy bands TiNi [4] showed that the infra-red part of the absorbtion spectrum can't be described on the basis of this model. As for the visible part of the spectrum it is described satisfactory enough. For the analyses of optical conductivity in the model of mostly indirect transitions we used the curve of the density of states N(E) calculated in [5]. The structure N(E) in the occupied part of the valency band is determined by d-states localized on the nickel atoms. The fraction of d-states of titanium is considerably lower. Using the curve N(E) we calculated the theoretical optical conductivity $\sigma_T(\omega)$ by the formula Berglund-Spaiser supposing the constant matrix-element approximation $W(E)$

$$\sigma_T(\omega) = \frac{1}{\hbar\omega} \int_{E_F}^{E_F - \hbar\omega} W(E) N(E) N(E - \hbar\omega) dE \qquad (1)$$

From fig.3a one can see that there are 2 absorbtion lines in the spectrum $\sigma_T(\omega)$ as well as in the spectrum $\sigma_{exp}(\omega)$. The infra-red band in $\sigma_T(\omega)$ arises from the electronic transitions in the region E_F and gives the information concerning mostly d-states localized on the nickel atoms. The structure of $\sigma_T(\omega)$ band in the visible region is well divided and renders the peculiarities of $\sigma_{exp}(\omega)$. The maximum A' in $\sigma_T(\omega)$ is caused by the electronic transitions from the areas of the points X_5 and $\Gamma_{25'}$ and also by ($X_{5'}$, Γ_{12}) on E_F and transitions from the Fermi edge to the peak C (the eleventh band in the directions Z and Σ). A good qualitative description of $\sigma_{exp}(\omega)$ in the indirect transition model in the whole investigated energy interval testifies to the fact that the indirect transitions can give a large fraction into the spectrum of optical absorbtion in TiNi. But the spectrum $\sigma_T(\omega)$ completely lack the peak at the energy of 2.16ev. It may be connected either with the fact that it was caused exclusidely by the direct transition $X_3 - X_5$ or by the fact that the spectrum $\sigma_T(\omega)$ is shifted relative to $\sigma_{exp}(\omega)$ to 0.5ev. One may get a full accordance in the localization of the bands in $\sigma_T(\omega)$ and $\sigma_{exp}(\omega)$ if one shifte the peaks B and C on the curve N(E) 0.5ev nearer to E_F. The observed displacement $\sigma_T(\omega)$ calculated in the model of indirect transitions relative to $\sigma_{exp}(\omega)$ may be connected with the inaccuracy of nonselfconsistent calculation N(E). The self-consistence in the case of TiFe(CsCl) results the considerable lowering of the energy of states Γ_{12} ($\sim$ 0,6ev) as well as the redistribution of the bands near X [4]. Such a lowering of d-states (Γ_{12}, $X_{5'}$) in the TiNi case will cause their

getting on E_F. The localization of E_F in the region of the narrow peak makes it possible to suggest the approach to the analyses of the probable reason of the B2 structure in TiNi instability analogous to that developed in the compounds with the structure A-15. In the most of the models explaining MT in these compounds, peak N(E) near E_F series as a necessary condition of the structural instability realization. The place of E_F in the immediate proximity to the peak N(E) in TiNi determines the tendency to the instability of B2.

Now we shall pass to the discussion of the results of the investigation in the structure B19'. The greatest changes of $\sigma(\omega)$ by MT are observed in the infra-red region which testifies to the considerable change of the Fermi surface during the transition B2-B19'. By the given MT the deep states and also the states higher than E_F forming the bands at the energy of 2.16 and 2.65ev in the structure CsCl change a little. The absence of the visible changes in the localization of the minimum of $\sigma_{exp}(\omega)$ and also in the place of the band in the visible part of the spectrum makes it possible to suggest that if E_F shifts during MT this shift is insignificant. By methods photoelectron spectroscopy we established that the shift E_F by MT B2-B19' is not more then 0.2ev. The disappearance of the most length-waved bands in the infra-red part of the spectrup in martensite and the appearance of the intense peak of absorbtion at the energy of 0.52ev testifies to the fact that in the region E_F in the great part of the Brillouin zone one gap is made in some directions. The minimum of the density of states around E_F is formed by this. The observed changes of optical conductivity speaks for the fact that the changes of the electronic structure by the given MT shouldn't be treated in the model of the rigid band, which suggests the stability of the N(E) form as it was supposed in the ref. [6]. The change of $\sigma(\omega)$ by heating, fig.4, shows that already in the martensitic phase the elements of electronic structure, typical of austenite, are formed. All the results received confirm the hypothesis of F.E.Wang about the electronic nature of MT in TiNi.

References

I V.N.Khachin, Yu.I.Paskal, V.E.Gunter, L.A.Monasevich: Fiz. Metallov i Metallovedenie 46 (I978)
2 I.I.Sasovskaja: Dissertation, I974, Sverdlovsk
3 D.A.Papaconstantopoulos: Phys.Rev., 11B (I975, 480I
4 D.A.Papaconstantopoulos, D.J.Nagel: I.J.Quantum Chemistry, 5 (I97I), 5I5
5 D.A.Papaconstantopoulos, J.M.Caffrey, D.J.Nagel: J.Phys. F.Met.Phys., 3 (I973) I 26
6 M.A.Mitchell, F.E.Wang, J.R.Cullen: J.Appl.Phys., 45 (I974).

Table I.Contributions of constituents G_1, P, φ

	G_1	P	φ
B2	76.5	22.4	I.I
$B_{19'}$	73.4	25.6	I.I

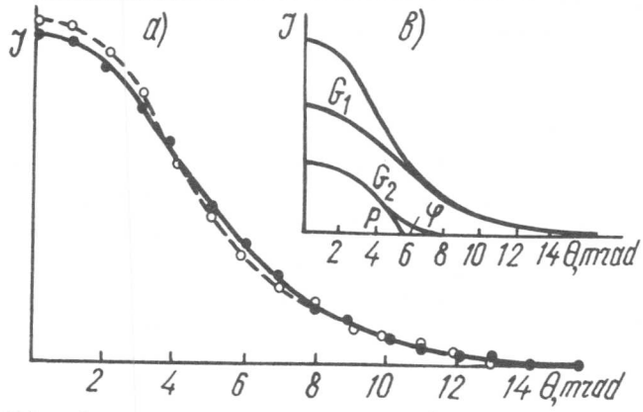

Fig.1. ADAP of TiNi a) in B19' at the T=20°C (continuous line) and by the T=75°C (dotted line), b) two ways of expanding into its constituents G_1+G_2 , $G_1+P+\varphi$

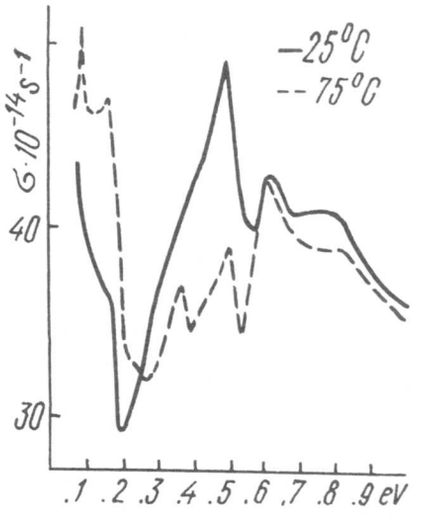

Fig.4. IK part σ (w) of TiNi in the B19' structure

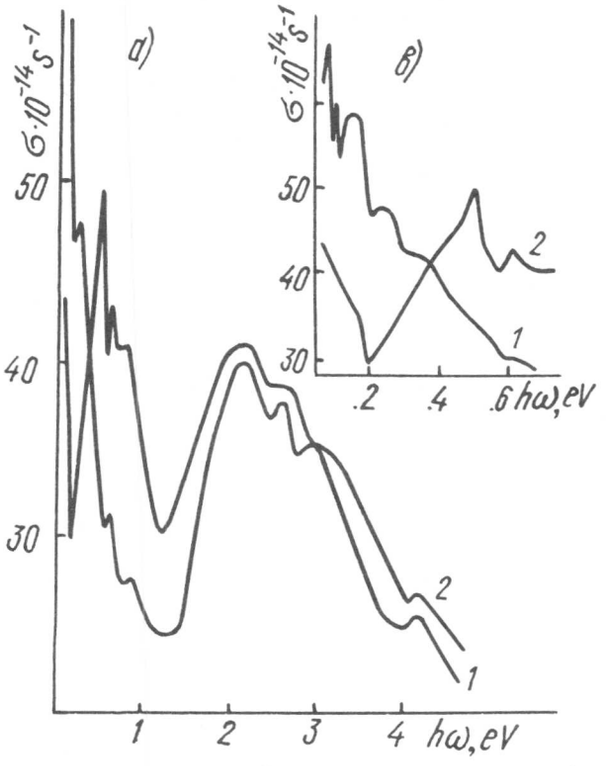

Fig.2. Optical conductivity σ (w) of TiNi in the structure B2(1) and in the B19'(2) structure; b) IK-part σ (w) of TiNi in the B2(1) and B19'(2) structures

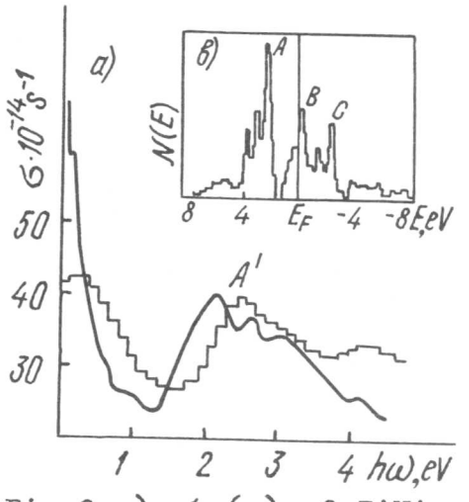

Fig.3 a) σ (w) of TiNi in the B2 structure (continuous line-experiment, stepped-calculation on N(E), b) N(E) from ref. [5]

DENSITY-OF-STATES AND ELECTRON-PHONON-INTERACTION EFFECTS RELATED TO THE MARTENSITIC TRANSFORMATION IN NiAl and Ti (Ni,Co) CUBIC B_2 ALLOYS

Daniel ABBE*, René CAUDRON* and Paul COSTA*

In several cubic systems the electronic specific heat coefficient γ, which increases when close to the concentration which corresponds to the onset at OK of a displacive transformation, is then reduced by the occurrence of this new phase. This effect can be associated to a reduction of the one-electron density of states at the Fermi level. We have found such a behaviour on two families of cubic B_2 alloys showing a martensitic transformation, on which we have performed low temperature specific heat and magnetic susceptibility experiments : $Ni_{1+x}Al_{1-x}$ alloys and TiNi ordered alloys in which cobalt has been partly substituted to nickel in order to reduce the martensitic transformation temperature. The results show that a large phonon enhancement of the specific heat occurs, as expected in the vicinity of a displacive transformation since strong electron-phonon coupling effects are to be found. Beyond this remark, the results are altogether consistent with the former explanation in terms of Fermi density-of-states effects.

I – INTRODUCTION

Several models have been put forward to explain in terms of one-electron-state energy the displacive phase transformations that may occur in metallic systems. A first class of models has been invoked for transformations which lead to a reduction of the phase symmetry, but no increase of the volume of the primitive cell (fig. 1) : if a degenerate van-Hove anomaly of the one-electron density of states is present near the Fermi level and if the reduction in symmetry suppresses the degeneracy, one may expect, when the transformation progresses, a reduction of the density of states at the Fermi level, together with an energy lowering –the total energy being taken as a sum of individual electron-energies–. This type of effect called band Jahn-Teller effect has been invoked in particular for the phase transformations in A_{15} alloys [1] and also in several hydrides [2]. Similar effects can also be expected in relation with phase-transformations generated by a non-homogeneous displacive process ; the argument is of the same nature as in the Peierls transformation [3].

Such density-of-states effects could be detected either through low-temperature specific heat or magnetic susceptibility measurements. As usual, the main intricacy of the problem comes from the electron-phonon and electron-electron mass-renormalisation effects which modify the value of the electronic specific heat. Similar difficulties occur in the interpretation of the paramagnetic susceptibility, mainly in the case of Stoner-enhanced transition systems.

The work which is presented below deals with two cubic B_2 systems which undergo a displacive transformation : the $Ni_{1+x}Al_{1-x}$ and the Ti(Ni, Co) families. In both cases, near the critical concentration for the onset at OK of the transformation, is found a large increase of the phonon term of the specific heat. In relation to this effect an important phonon enhancement of the electronic specific heat is found, which precludes any interpretation in terms of density of bare states. On the opposite, information can be drawn from the susceptibility measurements : in both cases the displacive transformation leads to a reduction of the Fermi-level density of states, in agreement with the former models.

* *ONERA, 29 avenue de la Division Leclerc, 92320 Châtillon, FRANCE.*

II – Ni_{1+x} Al_{1-x} ALLOYS

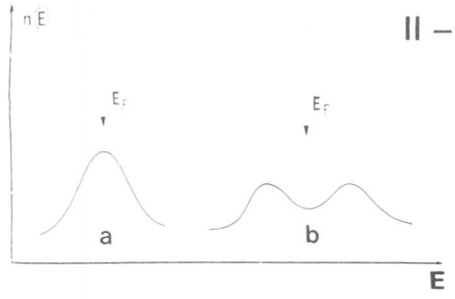

Figure 1 Density of states in the higher symmetry phase (a) and in the lower symmetry phase (b). E_F : Fermi level.

For $x \geqslant 0.2$ these alloys transform into a $L1_0$ type (Cu Au I) martensite [4]. Specific heat experiments between 1.2 and 20 K, and magnetic susceptibility experiments between 4 and 300 K, for a series of alloys ranging from $x = 0$ to $x = 0.24$, were performed. The main results are summarized on figure 2. The values of the β phonon coefficient, deduced from the specific heat measurements in the 1.2 - 7 K range, show a gradual increase in the cubic phase with increasing x values, in relation with the reduction of the elastic constant C' [5]. This effect is linked to the anomalies in the phonon spectrum at $q = 0$. Moreover, strong deviations of the phonon specific heat from the low temperature βT^3 asymptotic behaviour are found in the 5 - 20 K range, in the vicinity of the critical concentration for the onset of the martensitic transformation (fig. 3). This behaviour is related to the occurrence of anomalies at $q \neq 0$ (lowering of frequencies into the range of values which contribute to the low temperature specific heat). Similar effects have been described and interpreted in relation with the phonon spectrum as deduced from neutron inelastic diffusion experiments for the $B_2 - 9R$ transformation in Cu Zn Al alloys [6, 7]. In consequence in the vicinity of the critical concentration the plotted β values are larger than those that would have been deduced from a correct analysis. Nevertheless the general trend is correct, as ascertained by the computed β values deduced from the OK-extrapolated elastic constant values by Rusović [5] and Enami [8], showing a pathological behaviour in the critical region.

The variations of the γT electronic term should be red in parallel with the magnetic susceptibility in order to be understood. For the latter the values given in table 1 and figure 2 do not show any anomalous variation ; they were obtained after subtraction of an estimated value of the diamagnetic term (-20×10^{-6} emu/at.) and deduction of the Curie-Weiss like term associated to anti-structure Co, Fe and Mn impurities. A more extensive description of this analysis could be found in a more thorough paper to be published [9]. On table 1 is also given the ratio of this susceptibility to the γ coefficient expressed in reduced units (i.e. equivalent in terms of Fermi-level density of states). With increasing nickel concentration one may observe as a general trend an increase of this ratio, which should be related to an increase of the Stoner exchange enhancement factor (the system approaches the condition for the onset of intinerant ferromagnetism, as expected if it is recalled that Ni_3Al belongs to this class of ferromagnetic materials). Superimposed to this trend one might see a reduction of the observed ratio in the vicinity of the critical concentration, in the region where the phonon specific heat is very large. This effect should be understood as an increase of the phonon enhancement of the electronic specific heat.

Beyond these remarks the main effects to be found on figure 2 are :

1. the simultaneous increase of the electronic specific heat coefficient and of the susceptibility with increasing nickel content, in the cubic phase ;
2. the reduction of the susceptibility associated to the displacive transformation for values of x beyond the critical value.

Both results are consistent with the model presented in the introduction : with increasing values of x, the Fermi level gets closer to a singularity of the density of states, up to a point where the transformation occurs, which reduces the Fermi-level density.

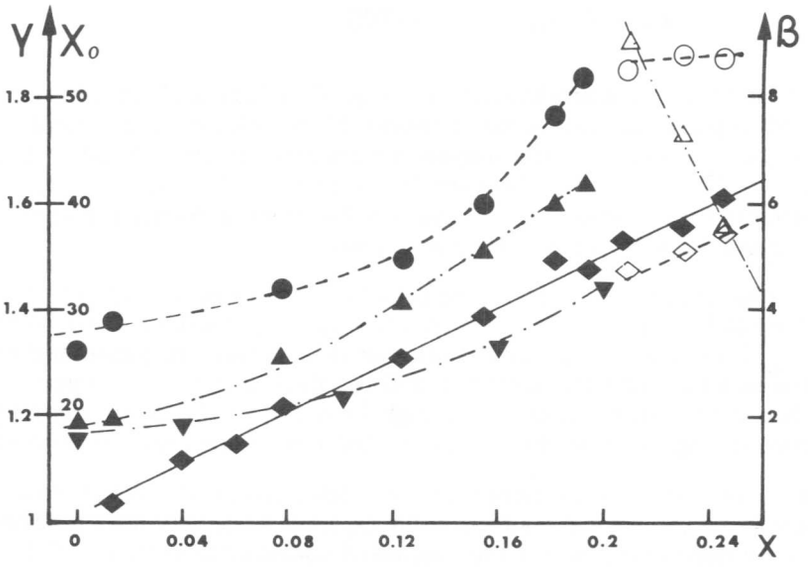

Figure 2 Values of γ (● ○) *and* β (▲ △) *specific heat coefficients (units :* 10^{-3} J/K^2 *atom and* 10^{-5} J/K^4 *atom) and* χ_0 (◆ ◇) *residual magnetic susceptibility (units :* 10^{-6} *emu/atom). (full dots correspond to the cubic phase, empty dots to the martensitic phase).* ▼ *: computed values of* β *deduced from* [5] *in the cubic phase.*

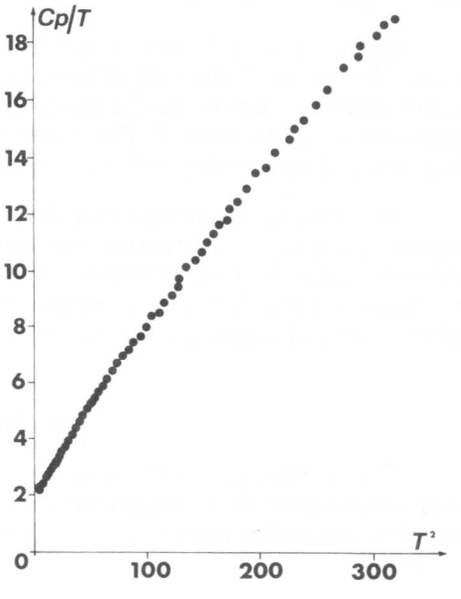

Figure 3 Low temperature specific heat of $Ni_{1+x}Al_{1-x}$ *(x = .19). (Units :* C_p/T *:* 10^{-3} J/K^2 *atom ;* T^2 *:* K^2*).*

x	0	0.014	0.078	0.123	0.154	0.181	0.193	0.219	0.230	0.245
γ	1.32	1.38	1.44	1.5	1.6	1.77	1.84	1.85	1.88	1.87
χ_0	30	31.5	41.5	45.5	49.5	53	54	44	46	48
R	1.68	1.68	2.12	2.24	2.29	2.20	2.15	1.74	1.8	1.89
	(cubic phase)							(mart. phase)		

Table 1 Values of electronic specific heat coefficient γ *(units :* $10^{-3}J/K^2$ *atom) and magnetic susceptibility* χ_0 *(units :* 10^{-6} *emu/atom), after deduction of diamagnetic term, versus x, for* $Ni_{1+x}Al_{1-x}$ *alloys. R : ratio of this susceptibility to the* γ *coefficient expressed in reduced units for these alloys.*

III – Ti (Ni, Co) ALLOYS

TiNi undergoes a martensitic transformation (Ms $\simeq$ 50° C) which leads to a distorted B19 structure [10]. When cobalt is substituted to nickel, Ms is reduced. The critical cobalt concentration for the suppression of the martensitic transformation in $Ti(Ni_{1-x}Co_x)$ alloys falls between $x = 0.25$ and $x = 0.5$. This result has been checked both by low temperature X-ray diffraction experiments and by susceptibility experiments which showed irreversible behaviour above 50 K in the $x = 0.25$ specimen.

The specific heat and susceptibility results are presented on figure 4. The experiments were performed on compositions which were shifted towards a slight excess of titanium ($Ti_{0.502}(Ni_{1-x}Co_x)_{0.498}$), in order to reduce the number of antistructure nickel and cobalt atoms. Indeed, the latter at least are magnetic, and the Pauli susceptibility cannot be measured properly when their concentration is too high (it is overshadowed by the magnetic term). Similar difficulties show up in the analysis of the low temperature specific heat.

As in the former system, one should notice the very large values of β which have been found in the vicinity of the critical concentration (x_0). Besides, very strong deviations to the βT^3 law have been observed for the specimens corresponding to $x = 0.5$ and 0.25 (fig. 5). No correct analysis can be given, due to the magnetic contribution.

Besides, near the critical composition, the electronic specific heat term is also maximum. The ratio of the susceptibility value, –after deduction of the diamagnetic* and the Curie-Weiss like term– to the electronic specific heat coefficient value, expressed in reduced units are given on table 2. The decrease of this ratio near the critical concentration proves the onset of very strong electron-phonon coupling effects.

One should also notice that the large reduction of the magnetic susceptibility associated to the $B_2 \rightarrow$ martensite transformation is again consistent with the above-given interpretation in terms of one-electron-state energies. But in this case no conclusion can be drawn on the Fermi-level density of states, because of simultaneously large electron-phonon and electron-electron coupling effects.

ACKNOWLEDGEMENTS

The authors are indebted to Dr. Lapierre (Strasbourg) who kindly performed the low-temperature X-ray experiments, and to Dr. Wang (Naval Ordnance Laboratory) who supplied alloys for preliminary experiments. This work has been supported by a DGRST contract.

REFERENCES

[1] J. LABBÉ and J. FRIEDEL, J. Physique, 27 (1966), 153.
[2] F. DUCASTELLE, R. CAUDRON and P. COSTA, J. Physique, 31 (1970), 57.
[3] R. PEIERLS, Quantum theory of solids (Clarendon Oxford) (1964), 108.
[4] K. ENAMI, S. NENNO and K. SHIMIZU, Trans. JIM, 14 (1973), 161.
[5] N. RUSOVIC and H. WARLIMONT, Phys. Stat. Sol. (a), 44 (1977), 609.
[6] G. GUÉNIN, S. HAUTECLER, R. PYNN, P.F. GOBIN and L. DELAEY, Scripta. Met. to be published (June 1979).
[7] D. ABBÉ, R. CAUDRON and P. COSTA, J. Physique, Colloque C_6, 39 (1978), C_6-1033.

---

* $-20 \cdot 10^{-6}$ emu/atom.

[8] K. ENAMI, J. HASUNUMA, A. NAGASAWA and S. NENNO, Scripta Met, 10 (1976), 879.
[9] D. ABBÉ, R. CAUDRON and P. COSTA, to be published.
[10] K. OTSUKA, T. SAWAMURA and K. SHIMIZU, Phys. Stat. Sol. (a), 5 (1971), 457.

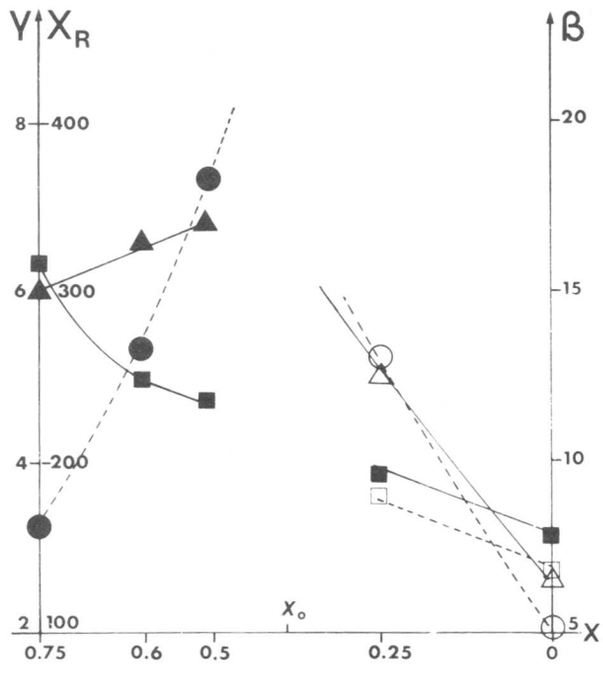

Figure 4 Values of γ (▲ △) and β (● ○) specific heat coefficients (units : 10^{-3} J/K² atom and 10^{-5} J/K⁴ atom) and χ_R (■ □) residual magnetic susceptibility (units : 10^{-6} emu/atom). (Full dots correspond to the cubic phase, empty dots to the martensitic phase).

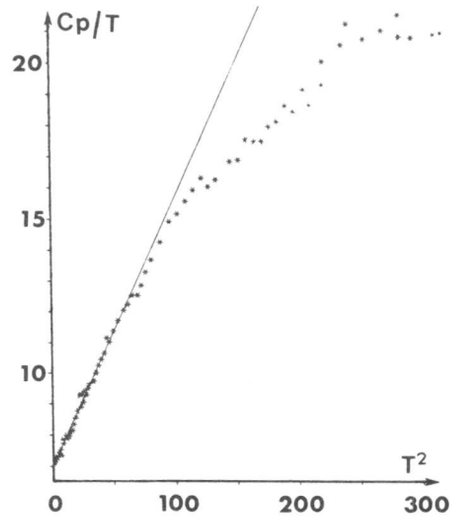

Figure 5 Low temperature specific heat of $TiNi_{0.5}Co_{0.5}$ (units : C_p/T : 10^{-3} J/K² atom ; T^2 : K²).

	x_o				
x	0	0.25	0.5	0.6	0.75
γ	2.5	5	6.75	6.62	5.95
χ_R	130	180	236	247.5	318
R	3.83	2.65	2.58	2.76	3.94
	(mart. phase)		(cubic phase)		

Table 2 Values of electronic specific heat coefficient γ (units : 10^{-3} J/K².atom) and magnetic susceptibility χ_R (units : 10^{-6} emu/atom), after subtraction of diamagnetic term, versus x, for $Ti(Ni_{1-x}Co_x)$ alloys. R : ratio of this susceptibility to the γ coefficient expressed in reduced units for these alloys.

Lattice Instability, Martensitic Transformations, Plasticity and Anelasticity of TiNi.

V.N. Khachin, V.E. Gjunter,
V.P. Sivokha and A.S. Savvinov

The character of structure transformations, shape-memory effects, superelasticity, internal friction, shear modulus and plasticity were investigated within a wide range of temperature, stress and composition changes. It was found that in TiNi from one to three martensitic transformations are realized, viz. B2 $\rightleftarrows$ R (the transformation near to the second type), R $\rightleftarrows$ B19' and B2 $\rightleftarrows$ B19' (transformations of the first type), where B2 is the initial phase, R is rhombohedral distortion B2 and B19' is orthorhombic martensite with monoclinic distortion. The number and succession of transformations are determined by the composition and thermomechanical treatment of the alloy. Transformation B2 $\longrightarrow$ R is found to be effected under the conditions of developing mechanical instability of lattice ("softening" of shear modulus) and is probably the consequence of it. Here the trend to unstable state of lattice causes the anomaly of high plasticity of the alloy in premartensitic region. Clear indications of developing structure instability and anomalous properties were not found before two other transitions. Every martensitic transformation is shown to be accompanied by shape-memory, superelasticity and high damping anelastic effects of their own, differing from others in hysteresis, magnitude and temperature of development. It was established that ability of alloys to developing these anelastic effects, martensitic transformation type and plastic properties of the material are interdependent. Proceeding from this optimum conditions (composition, heat treatment, initial phase state) are determined for the most clear developing of one or another effect of anelasticity and plasticity.

I. Introduction

Anelasticity (effects of shape-memory, superelasticity, high damping modulus defect) and plasticity of a number of alloys including TiNi are due to martensitic transformations, which in their turn can be the results of the loss by the crystal lattice of its stability at

Siberian Physico-Technical Institute,
Tomsk State University, Tomsk, USSR.

definite temperature, pressure and composition. In this paper complex investigation of aforesaid properties and structure of TiNi and TiNi doped with iron up to 5 at % instead of nickel. All the alloys had been annealed at the temperature 800°C for one hour and cooled together with the furnace. The composition of the studied alloys is given in the table.

II. Structural Transformations.

Using the results of the preceding paper [1] by the methods of roentgenography and electrical resistivity for binary TiNi and ternary TiNi Fe alloys diagrams for martensitic transformations in the process of cooling (Fig. 1a, b) were built. As an example the character of changing structure and electrical resistivity in cooling the alloy Ti + 49 at.% Ni + 1 at.% Fe. was shown in Fig.2. As seen from Fig. 1a, b the initial B2 phase depending on the composition undergoes three different sequences of martensitic transformations. It alloys enriched with titan one transformation $B2 \rightleftharpoons B19'$ is observed. In alloys enriched with nickel and doped with iron there are two martensitic transformations, i.e. $B2 \rightleftharpoons R$ and $R \rightleftharpoons B19'$. Finally in alloys near to stoichiometry three structural transformations take place: $B2 \longrightarrow B2 + B19' \longrightarrow R + B19'$ B19'. The martensitic transformation $B2 \rightleftharpoons R$ possesses a very narrow hysteresis and two-phase region (2-3°C) and is a transformation close to the second type. On the contrary the two other transformations $R \rightleftharpoons B19'$ and $B2 \rightleftharpoons$ B19' possess a wide hysteresis and two-phase region (20--50°C) and are definitely transformations of the first type. One should note that the transformation $B2 \rightleftharpoons R$ occurs by stages which will be described in another paper. Moreover B19' in further cooling may undergo additional distortions of the lattice [2]. In the given paper only the three pointed out martensitic transformations will be considered.

III. Lattice Instability.

The trend to mechanical instability of lattice on approach to the point of phase transformation shows itself in anomalous behaviour of elastic constant of the alloy $C' = 1/2 (C_{11} - C_{12})$ or elastic anisotropy $A = C_{44}/C'$ ($C' \longrightarrow 0$, $A \longrightarrow \infty$). The latter is closely connected with the shear modulus G [3] . Therefore the investigation G (T) (or frequencies of natural oscillations of the sample since $G \sim f^2$) enables to obtain objective information on developing the process of lattice instability.

In the state B2 one can observe a wide region of anomalous dependence G(T) ($dG/dT > 0$) which precedes the martensitik transformation $B2 \longrightarrow R$, i.e. the transformation which is near to the second type. After this the shear modulus transformation behaves normally up to

M_s(R → B19') (Fig. 3, curve 1). It is important to note that at the moment of transformation greater or less decrease of oscillations frequency occurs. However this process does not show the true behaviour of G(T), but it is due to the modulus defect. The modulus defect is caused by developing anelastic deformation by displacement of interphases. The same modulus defect is also responsible for a high internal friction in martensitic transformation. After the completion of transformation a relative.contribution of the modulus defect to the change of G(T) is small and it does no longer distort the path of curve in monophase R and B19' states.

Formally "softening" of the shear modulus is observed also before the transformation B2 → B19' a transition of the first type. However total results of all investigated alloys and available information on the character of premartensitic phenomena [4,5] enable us to draw the following conclusion. All the anomalies of properties and structure in the state B2 are associated with the preparation of the material to transformation B2 → R, but not with premartensitic state B2 → B19'. The transformation B2 → R, however, does not always have time to realize. In stoichiometric and enriched with titan alloys it is preceded by another martensitic transformation B2 → B19', to which aforesaid indications of structure instability bear no relation. It should be pointed out that a mechanical instability of lattice caused by anomalously great plastic anisotropy of the alloy is meant here. Other indications reflecting preparation and the mode of structural rearrangement of the lattice are likely to take place in transformations of the first type. In this paper they have not been investigated and they are not discussed.

In spite of the fact that the developing of "soft" mode in B2 does not bear a direct relation to the transformation B2 → B19', it can affect the final crystallographic structure of the martensitic phase. In particular an additional distortion B19 can be just the consequence of "freezing" the "soft" mode in an orthorhombic phase which did not have enough time to do it in the state B2.

IV. Plasticity

With the approach to the point of martensitic transformation B2 → R plasticity of the alloy grows, and after the completion of transformation it reduces (Fig. 3, curve 2). Within the range of temperatures preceding the second transformation R → B19' where shear modulus behaves normally premartensitic anomyly of plasticity was not detected. Therefore relatively high plasticity of intermetallid TiNi and its very great anomaly before martensitic transformation is the result of developing lattice instability.

V. Anelasticity

It is found that a definite complex of anelastic effects of shape-memory, reversible shape change, superelasticity and high damping corresponds to each of the three martensitic transformations. Here anelastic effects in B2 $\rightleftarrows$ R transformation naturally differ from those in R $\rightleftarrows$ B19' and B2 $\rightleftarrows$ B19 transformations by hysteresis, the magnitude and temperature of developing. In Fig. 4a, the effect of reversible shape change is presented as an example in successive realization of two martensitic transformations B2 $\rightarrow$ R (with T_R) and then R $\rightleftarrows$ B19 (with M_S). The first transformation is practically without hysteresis, the hysteresis of the second transformation is about 50°C. Of special interest is the precess of developing martensitic transformations upon loading and particularly the conditions of developing the effect of superelasticity. It is found that higher than B2 $\rightarrow$ B19' martensite is formed under stress only in the immediate neighbourhood (not higher than 20-30°C) from M_S(B2 $\rightarrow$ B19'). Here contribution of anelastic deformation to the joint deformation of the alloy quickly reduces with dropping the loading temperature from M_S (Fig. 4a). On the contrary higher than R $\rightarrow$ B19' one may manage to bring about a martensitic reaction by external stress even 200°C before M_S(R $\rightarrow$ B19') and the share of anelastic deformation at it remains on a high level (Fig.4 c, d). The reason for this difference is the following. The mobility of the martensitic transformation temperature upon loading M_S^σ is determined by the value of the coefficient $d\sigma/dT = \Delta H/\varepsilon_m T_c$, where ΔH is a specific enthalpy, ε_m is a shear in martensitic transformation, T_c is the temperature of equilibrium of phases. It turmed out that above B2 $\rightarrow$ B19' the value of $d\sigma/dT \sim 1.2$ kG/mm^2 grad., and that above R $\rightarrow$ B19 the value is only ~ 0.3 kG/mm^2 grad. As a result of this upon loading higher than M_S(B2 $\rightarrow$ B19') critical stresses at the beginning of martensitic transformation soon go beyond the limit of alloy elasticity and the plastic flow process becomes more preferable than phase transition. At the same time low value of the coefficient above M_S(R $\rightarrow$ B19') provide a wide temperature interval $\Delta T = M_S^\sigma - M_S$ before the plastic flow of the metal starts. Hence, in particular, it is clear why superelasticity effect in stoichiometric and enriched with titan alloys is absent and why it is clearly developed in other compositions of this system. By using a preliminary plastic flow combined with annealing at the T° 300-550°C, one may change the succession of martensitic transformations from B2 $\rightleftarrows$ B19' into B2 $\rightleftarrows$ R $\rightleftarrows$ B19' and simultaneously increase the elastic properties of the alloy. In this case the effect of superelasticity is observed in alloys containing more than 50 at. % of titan.

In conclusion we shall point out that in deformation in the state R one can observe two different effects of

superelasticity. First a reversible rearrangement of the domain structure of rhombohidral phase takes place and this process defines the first not large effect of superelasticity (Fig. 4d, in the first upper corner). Then a monodomainized rhombohedral structure undergoes martensitic transformation and this process gives the main effect (Fig. 4d).

These problems will be considered in detail and published in [6,7].

References

1 V.N. Khachin, V.E. Gjunter, L.A. Monasevich, Ju.I. Paskal, Dokl. Akad. Nauk SSSR 234, 1059 (1977).

2 L.A. Monasevich, Yu.I. Paskal, Fiz. Metallov i Metallovedenie (in print).

3 V.S. Postnikov, Vnutr. trenie v metallakh, M., Metallurgiya, 62 (1974)

4 G.D. Sandrock A.S. Perkins, R.F. Hehemann Met. Trans., 2 (1971), 2769.

5 S. Vatanayon and R.F. Hehemann. Shape-mem.Eff. in Alloys, N-Y-Lid. 1975, 115.

6 V.N. Khachin, Yu.I.Paskal, V.E. Gjunter, L.A.Monasevich, V.P. Sivokha, Fiz. Metallov i Metallovedenie (1978).

7 V.N. Khachin, V.P. Sivokha, A.S. Savvinov, V.E. Gjunter Fiz. metallov i Metallovedenie (in print).

Table

alloy		1	2	3	4	5	6	7	8	9	10	11	12
The composition, at%	Ti	51,5	51,0	50,5	50,0	49,5	49,0	48,5	50,0	50,0	50,0	50,0	50,0
	Ni	48,5	49,0	49,5	50,0	50,5	51,0	51,5	49,0	48,0	47,0	46,0	45,0
	Fe								1,0	2,0	3,0	4,0	5,0

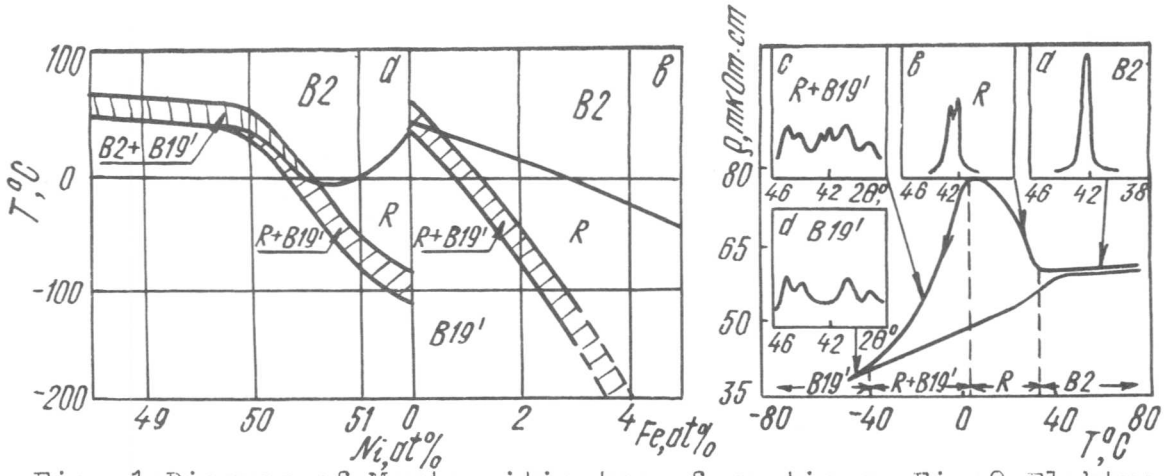

Fig. 1 Diagram of Martensitic transformations. Fig.2 Elektro· resistance (1) and difractograms (a-d) Alloy N 8.

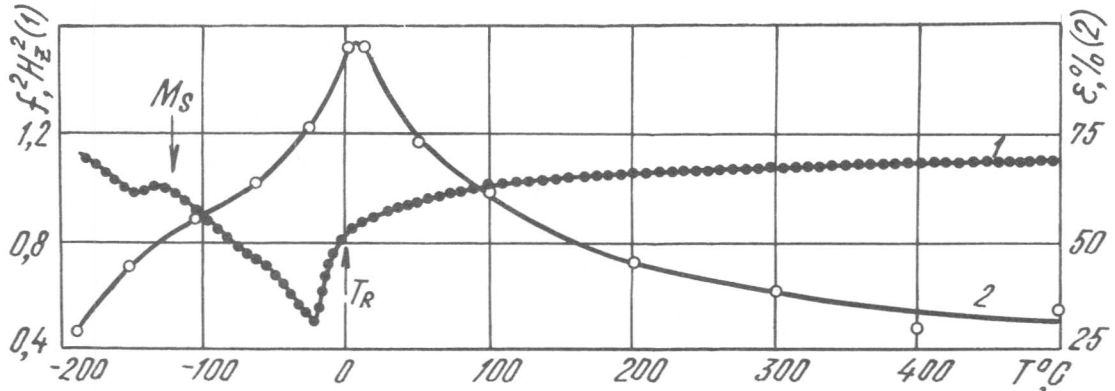

Fig. 3 The square of oscillations frequency (1) and maximum deformation before destruction (2). Alloy N 10.

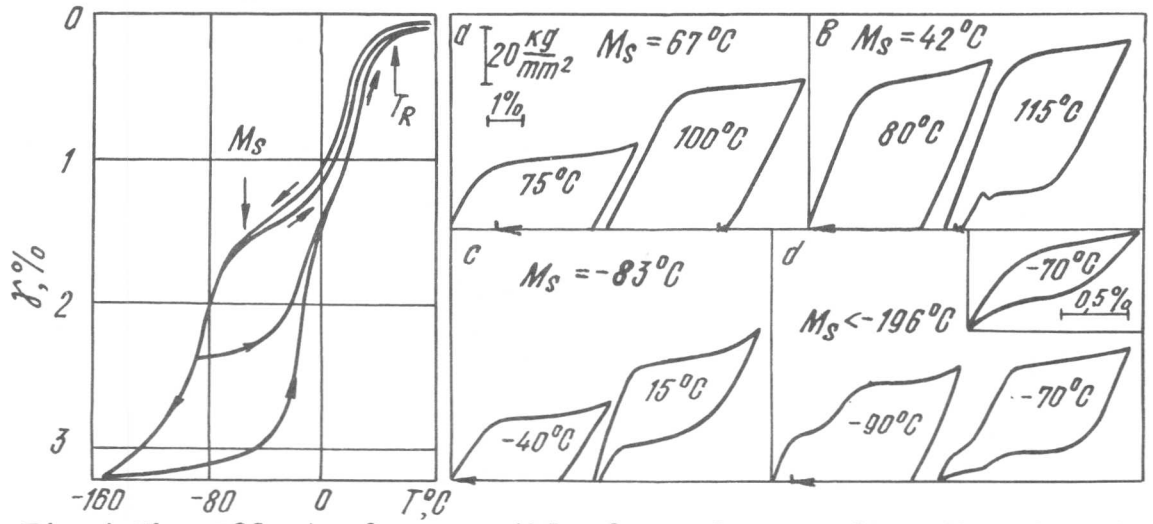

Fig.4 The Effect of reversible form change after the plastic flow at 350°C by 6%. Alloy N6. Fig.5 a) alloy N3; b) alloy N3 after the plastic flow and annealing at 550°C for 15 min; c)alloy N 6; d)after the plastic flow and annealing at 550°C for 15min.The arrows show the deformation recovered in heating

The "martensite-martensite" transformation in NiTi

L. A. Monasevich, J. I. Paskal

The X-ray examination of TiNi-base alloys with varying nickel contents has been carried out. In the alloy with 49,8% Ni the broadening of certain B19' structure reflections was observed in course of cooling below Mf, the final temperature of B2 → B19' transition. This is due to transition from monoclinic B19' phase to triclinic B19'' phase. The B19' → B19'' transition occurs in the monoclinic phase formed only from the cubic B2. In the alloys with 50,0; 50,3 and 50,75% Ni where B19' phase formed from the rhombohedral R the broadening of the same reflections was not observed up to - 196°C. The B19' → B19'' transition, as well as B2 → R, is similar to the second-order transition. The atomic displacement transforming B19' to B19'' are like the ones which transform B2 to R. It is supposed that the physical factors causing B2 → R transition continue to act in the monoclinic structure when this transition does not realize but, instead, the first-order B2 → B19' transition occurs. These factors cause the B19' → B19'' transition in Ti - 49,8% Ni alloy. On the contrary the realization of the same factors as a result of B2 → R transition leads to the conservation, by further cooling, of the B19' phase formed from R.

The crystallography of martensite transformation in TiNi-base alloys has been extensively studied by many authors [1 - 6]. It was established that "austenitic" high-temperature phase in these alloys has B2 (CsCl-type) structure and is transformed by cooling to low-symmetric martensite phase directly or through an intermediate rhombohedral phase. The majority of authors have supposed that the low-symmetric martensite structure is of a B19-type with additional monoclinic or triclinic distortion. A simultaneous formation of the two transformation products of the same (monoclinis [3]) or different (triclinic and hexagonal [4]) structure is possible.

It has been shown in [5] that in TiNi-base alloys depending on their composition and pretreatment the following transition sequences (TS) take place:

Tomsk State University, Tomsk, USSR

TS1: $B2 \rightarrow B2 + B19' \rightarrow B19'$

TS2: $B2 \rightarrow R \rightarrow R + B19' \rightarrow B19'$

TS3: $B2 \rightarrow B2 + B19' \rightarrow R + B19' \rightarrow B19'$

Here R designates the rhombohedral phase and B19' designates the B19 structure with additional monoclinic distortion.

The alloys Ti-49,8; Ti-50,3 and Ti-50,75% Ni (all in atomic %) were melted from iodid titanium (99,9) and electrolitic nickel (99,9) in high-frequency induction furnace under an argon atmosfere. The ingots were subjected to six-fold arc-remelting. The weight loss during the preparation procedure was negligibly small and hence the alloy ingots can be assumed to possess the nominal composition. After remelting and homogenisation the ingots were hot-rolled in sheets of 1 millimeter thick. The specimens were annealed for 1h at 600°C.

X-ray diffraction examination was made by using a diffractometer DRON-2 with Cu-K_α radiation. The high-temperature and low-temperature devices were used to examine the intensity and profile of X-ray lines during cooling and heating through the temperature region of direct and inverse martensite transformations.

In Ti-49,8% Ni alloy martensite transformation occurs during the first cycle accordingly to TS1. In course of cooling below $M_s = 85°$ the reflections of low-symmetric product appears and their intensity grows. Simultaneously the intensity of "austenitic" reflections falls without any broadening or splitting. The structure of this transition product is well deseribed as monoclinic with parameters which were established in paper [6]

$$a = 2,89\text{Å};\ b = 4,12\text{Å};\ c = 4,62\text{Å};\ \beta = 96,8°$$

The formation of the structure with these lattice parameters may be Bain deformation that transforms b.c.c. B2 structure to monoclinic B19' and of the additional shear $(100)_{B19}\ [001]_{B19}$ that creates a monoclinic distortion of B19. Here we discuss a crystallgeometry of martensite transformation regardless of shuffles (in this case along $(100)_{B19}\ [001]_{B19}$). The $\{110\}_{B2}$ - type plones are transformed to planes (002), $(11\bar{1})$, (020), (111) of the monoclinic martensite B19'. One can seen it from matrix equation

$$\begin{pmatrix} h \\ k \\ l \end{pmatrix}_{B19'} = \begin{pmatrix} 0 & 0 & \bar{1} \\ \bar{1} & \bar{1} & 0 \\ \bar{1} & 1 & 0 \end{pmatrix} \begin{pmatrix} h \\ k \\ l \end{pmatrix}_{B2}$$

The results of examination are shown in fig.1. It is seen that in course of cooling below 0°C (this temperature

is lower than M_f for the B2 → B19' transition in Ti -49,8 % Ni alloys a broadening of reflection $(111)_{B19'}$ starts. Simultaneous broadening of other reflections originated from the $\{110\}_{B2}$ does not take place.

The broadening of only one of these reflections may be explained solely by the structure phase transition from the monoclinic B19' structure to tryclinic B19''.

Inasmuch as the displacement of X-ray reflections, i.e. variation of interplanar distances due to the B19' → B19'' transition within the method accuracy does not exceed the temperature dependance of the lattice parameters we may suppose that in the course of this transformation the parameters a,b,c and ß remain constant and the observed broadening of the $(111)_{B19'}$ reflection is due to the deflections of α and γ angles from 90°.

We find from the constancy of the width of $(\bar{1}11)_{B19'}$ reflection, i.e. from condition $\sin^2\theta_{\bar{1}11} - \sin^2\theta_{11\bar{1}} = 0$, and from the broadening of $(111)_{B19'}$ reflection, $\beta = 2\theta_{111} - 2\theta_{1\bar{1}1}$, that α and γ varys from 90° to 90,5° and 90,2° respectively. The variation of the width of $(111)_{B19'}$ reflection occurs gradually without jump and is completely reversible without hysteresis. One can suppose that the B19' ⇄ B19'' transition as well as B2 ⇄ R is similar to the second-order transition.

The same analysis of the alloys containing 50,0;50,3 and 50,75% Ni in course of cooling below Mf (the final temperature for the B2 → B19' transition) does not show any sign of reflection broadening. Up to - 196°C the structure of these alloys remains monoclinic and may be deseribed by the parameters established in paper [3] within the same accuracy as a martensite structure in the Ti-49,8% Ni alloy.

This different low-temperature behaviours of different alloy compositions are comarable to difference of the transition sequences studied earlier [5]. In the Ti-49,8% Ni alloy the monoclinic martensite B19' is formed from the cubic B2 phase (TS1), in the Ti-50% Ni mostly (TS3) and in the Ti-50,3% and the Ti-50,75%% Ni completely (TS2) from the rhombohedral phase R. Thus, monoclinic martensite phases formed from the cubic B2 and rhombohedral R have different behaviours by cooling below Mf.

One should drow attention to the fact that the B19' ⇄ B19'' transition is similar to the B2 ⇄ R transition. Both of them represent a transition from an initial high-symmetric structure to a final low-symmetric structure by means of a gradual small distortion, without a jump.

The R-phase structure is like ω-phase structure [8]. Theprincipal and primary component of the lattice deformation is the shuffle of planes $\{112\}_{B2}$ along $\langle 111\rangle_{B2}$ lit is equivalent to mutual displacements of $\{111\}_{B2}$ planes in certain sequences [7]). The shuffle is accompanied by observed rhombohedral distortion of an elementary cell.

It is known that the premartensitic states in TiNi is characterized by diffraction effects that may be inter-

preted as local dynamic or static displacements along $\langle 111 \rangle_{B2}$ [8]. These displacements are precussors of the ω-type structure formation. Thus, the premartensitic state diseussed here is in essence a prerhombohedral state.

In TS1 the tendency to form the R-phase is not realised due to the B2 $\rightarrow$ B19' transition. It is a well-defined first-order transition and is due not to mechanical instability of the B2-phase, but to more complicated thermodynamical reasons. Unlike the above the B19'' structure may be formed from the B19' by means of a certain small displacement in the direction neur to one of the $\langle 111 \rangle_{B2}$ direction. Fig 2 shows four directions originated from tse different $\langle 111 \rangle_{B2}$-type directions by means of the B2 - B19' transition. The distortion in the two of these directions ($[\bar{1}0\bar{1}]$ and $[\bar{1}01]$) changes the monoclinic angle and the one in two others ($[\bar{1}\bar{1}0]$ and $[\bar{1}10]$) transforms the monoclinic structure to triclinic.

This enables us to suppose that the physical factors causing premartensitic (prerhombohedral) state and the B2 $\rightleftarrows$ R transition are conserved in the monoclinic structure. When the TS1 is realized and the B2 $\rightarrow$ R transition does not occur these factors result in the B19' $\rightarrow$B19'' transition. On the contrary, the realization of these factors as a result of the B2 $\rightarrow$ R transition causes the conservation (by further cooling) of the B19' phase formed from R.

REFERENCES

[1] A. Nagasawa: J. Phys. Soc. Japan 31 (1971), 136.
[2] S. P. Supta, N. A. Johnson, K. Mukherjel: Mat. Sci. Eng. 2 (1973), 43.
[3] A. S. Sastri, M. J. Marcinkowski, D. Koskimaki: Phys. Stat. Sol. 25 (1968), K 67.
[4] F. E. Wang, S. J. Pickart, H. A. Alperin: J. Appl. Phys. 43 (1972), 97.
[5] V. N. Khachin, V. E. Guenter, L. A. Monasevich, J. I. Paskal: Doklagy Acad. Nauk USSR 234 (1977), 1059.
[6] K. Otsuka, T. Sawamura, K. Shimizu: Phys. Stat. Sol. A5 (1971), 457.
[7] J. I. Williams, D. de Fontaine, N. E. Paton: Met. Trans. 4 (1973), 2701.
[8] Q. D. Sandrock, A. I. Perkins, R. F. Hehemann: Met. Trans. 2 (1971), 2769.

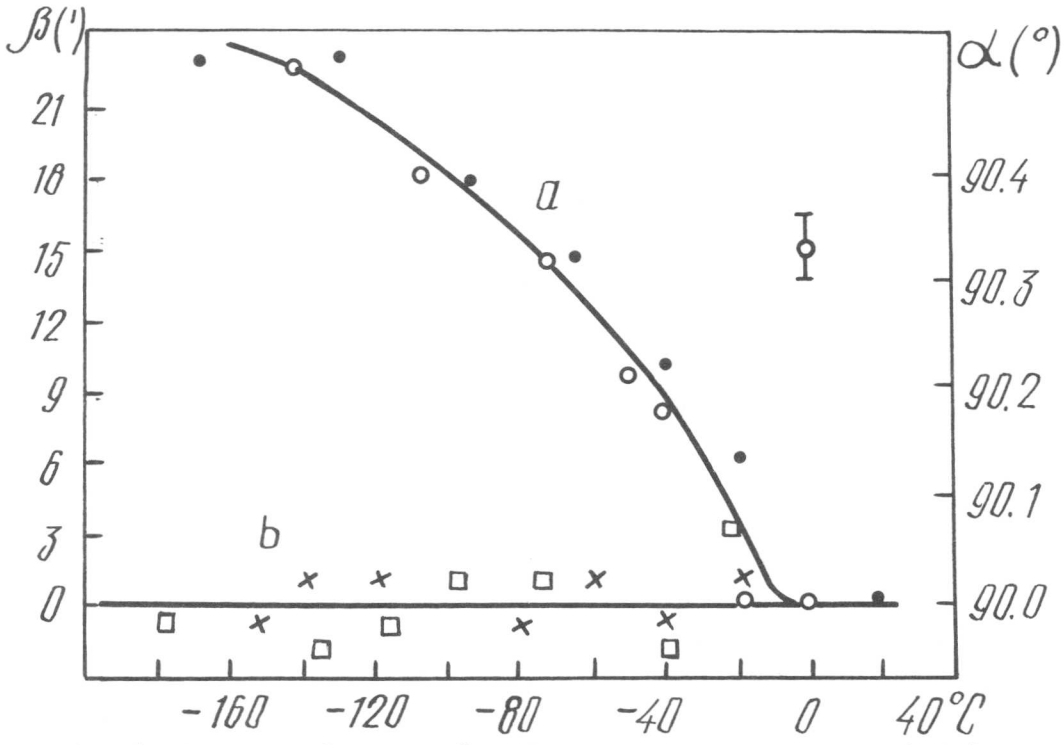

Fig.1.The broadening β of X-ray reflections (111) (curve a),(11$\bar{1}$) (curve b) and of ongle α (curve coincide with a) VS temperature.

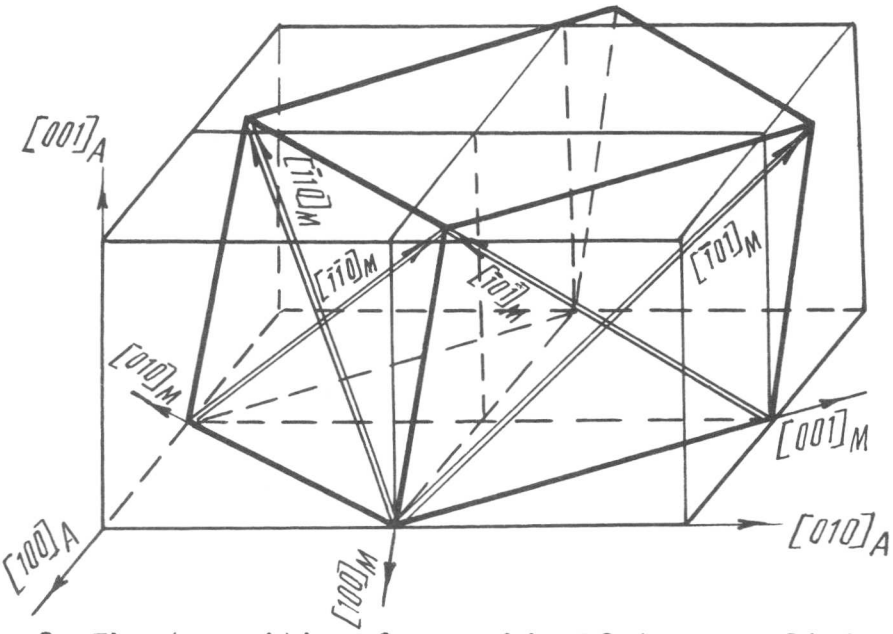

Fig.2. The transition from cubic B2 to monoclinic B19 structure (without Bain deformation).The directions near to $\langle 111 \rangle_{B2}$ are shown.

Martensitic Transformation and Precursor Phenomena in Fe_3Pt

M. FOOS*, C. FRANTZ* and M. GANTOIS*

Premartensitic effects have been revealed in the long range ordered Fe_3Pt alloy by means of X-ray diffraction and transmission electron microscopy at low temperature. It has been found that these effects correspond to a tetragonal distorsion of the austenite due to the simultaneous action of two shears $\{011\}_\gamma\langle 01\bar{1}\rangle_\gamma$ on two planes lying at 60° from each other. The origin of these phenomena might be due to the existence of an internal driving force acting on a metastable softened austenite lattice. A microscopic model based upon the observed shears describes a possible path for the transformation of austenite into martensite.

I. Introduction

First, we shall recall the results obtained by X-ray diffraction and electron microscopy at low temperature which show unambigously the existence of premartensitic effects in the long range ordered stoechiometric Fe_3Pt alloy [1].

Then, we shall interprete these phenomena and try to explain their origin. We know that such effects have already been observed in several alloys, particularly in β alloys of the CsCl type [2-4], and they were often interpreted by soft modes [5-7 for example]. However, there is no evidence that such soft modes exist in Fe_3Pt in the full sense of the word : only a softening of certain elastic constants is well established [8-9]. Therefore, we shall consider the appearance of the premartensitic effects in Fe_3Pt in terms of an internal driving force wich operates on a softened metastable system.

Finally, we shall present a microscopic model which is consistent with our experiments and explains how the $L1_2$ austenite phase could transform into a b.c.t. martensite through the medium of transitory stages whose first steps are revealed experimentally.

II. Experimental Procedure

The studied alloy, prepared in an induction furnace under helium from platinum and iron with purities of 99,997 % and 99,95 % respectively, is stoechiometric and exhibits a long range order parameter of about 0.70. It is a one phase alloy. Its M_s temperature is near - 170°C and its Curie temperature near 130°C. The b.c.t. structure of the martensite can be deduced from the $L1_2$ austenite structure by the Bain distorsion [10].

The X-ray lines are either established discontinuously by numeration or sometimes recorded continuously. The radiation used corresponds to the $K\alpha_1$-$K\alpha_2$ doublet of the cobalt. The diffractometer is equipped with a cooling

---

* Laboratoire de Génie Métallurgique - Ecole des Mines de Nancy - 54042 NANCY-CEDEX (France)

device permitting to reach the temperature of liquid hydrogen. The samples are either bulk specimens or platelets of fine compressed powder.

The specimens for transmission electron microscopy are first electrolytically jet-thinned by a 85-15 aceto-perchloric mixture and then by ion bombardment. The electron microscope can work up to the temperature of liquid nitrogen.

III. Results and Discussion

The X-ray lines, characteristic of a $L1_2$ structure at room temperatur are modified when the temperature decreases (figures 1-3). This becomes obvious from - 155°C (figure 3), about 15°C above M_s. The lines of the non transformed austenite are very broad at - 195°C (figures 2-3) and split in two, except the $(111)_\gamma$ and $(222)_\gamma$ ones. They exhibit an enhancement of the intensity near the angle corresponding to the initial line at room tempera ture. This enhancement indicates the existence of a small amount of non af fected austenite as it can be shown by the extrapolation to - 195°C of the lattice parameter measured in a temperature range where the lines broadening is imperceptible.

By transmission electron microscopy, relrods appear at low temperatur on the electron diffraction patterns and striations are associated on the micrograph. These striations are well in contrast in the dynamical regions of the foils near the extinction bends. Whether the relrods lie or not on the observation plane (figures 4d-4a), their orientations are parallel to the $<110>^*_\gamma$ directions and the corresponding striations on the micrograph are parallel to the traces of the $\{110\}_\gamma$ planes. We do not observe individual domains on the micrograph which would characterize the existence of two distinct phases.

All these effects observed by radiocrystallographic analysis or by transmission electron microscopy are reversible and reproducible at each thermal cycle.

The X-ray lines broadening suggests that the austenite, initially cubic, becomes tetragonal from a temperature T'_δ = - 155°C higher than M_s of about 15°C. The tetragonal austenite would be a transitory phase between the parent and the product phase. It would exhibit a broader and broader distribution of the lattice tetragonality parameter $q = \frac{c}{a}$ as the temperature decreases (figures 2 and 3), its structure approaching the martensite one.

This interpretation is consistent with the small broadening and the unicity of the $(111)_\gamma$ and $(222)_\gamma$ lines : the corresponding reflecting planes are identically sollicitated and as the calculation shows, their interplanar distances are weakly affected by the tetragonal distorsion of the initial cubic lattice. In the same way, the sense and the amplitude of the other interplanar distances variations explain the splitting and the broadening of the corresponding X-ray lines. The X-ray lines geometrical broadening is estimated from the room temperature measurements and thus, can be eliminated. The unicity and the small broadening of the $(111)_\gamma$ and $(222)_\gamma$ lines subsequently justify that the influence of other factors, such as the dimensions of diffraction domains or the existence of eventual elastic stresses, is neglected. In these conditions, if we only consider the

distribution of the tetragonality parameter as the origin of the lines broadening, the q values lie between 1 and 0.93 at - 195°C and between 1 and 0.85 at - 253°C. The q average values corresponding to the center lines are respectively 0.96 and 0.92 for the two previous temperatures. Figure 5 describes the evolution with temperature of the parameter $\eta = 1-c/a$ which can be chosen as the order parameter of the $L1_2$ into b.c.t. lattice transformation. It shows that the austenite tetragonal distorsion seems to be a second order structural transition.

The relrods and the associated striations can be explained by the appearance of small deformations due to $\{011\}_\gamma \langle 01\bar{1}\rangle_\gamma$ shears. Such effects too have already been observed for the case of nucleation and growth transformations [11] as well as for the case of martensitic transformations [2-12-13-14]. According to [14], due to the elastic anisotropy, the observed relrods may be described in terms of fluctuation transverse waves of displacements propagating along $\langle 110\rangle_\gamma$ and polarized along $\langle \bar{1}10\rangle_\gamma$ which, by local ordering of shifts of $\langle 110\rangle_\gamma$ linear atomic chains, give rise to atomic planes displacements containing these directions. In Fe_3Pt, they are the $\{110\}_\gamma$ planes sheared along $\langle \bar{1}10\rangle_\gamma$. It should be pointed out, as for every disorder displacement, there is no diffuse intensity at the reciprocal lattice origin.

According to [8][9] who studied the $Fe_{72}Pt_{28}$ alloy which however never transforms into martensite, our observations show a loss of rigidity of the austenite lattice with respect to $\{011\}_\gamma \langle 01\bar{1}\rangle_\gamma$ shears. [8] and [9] suggest that the lattice softening could be due to a magneto-elastic coupling : the anisotropy constant $A = \frac{C_{44}}{C'}$ increases as soon as the temperature is lower than T_c. The loss of rigidity becoming important well below T_c, this could explain that no effect has been observed in the long range disordered Fe_3Pt alloy where M_s is near T_c. If the stoechiometric Fe_3Pt alloy exhibits the same behaviour as that of the $Fe_{72}Pt_{28}$ alloy, the elastic constants do not cancel at M_s and the premartensitic effects do not indicate a true soft mode in austenite. The lattice softening, if it is not at the origin of the martensitic transformation, contributes nevertheless to make its nucleation easier. The driving force associated with the tetragonal distorsion of the austenite begins to act from an equilibrium temperature T_o lying between M_s and A_f. It gives the necessary energy to the shear deformation of the matrix, provided that its elastic limit is high enough to can accommodate reversibly the corresponding stresses. The driving force increasing from T_o, the lattice is soft enough at T'_o, between T_o and M_s (figure 5), to be deformed preferentially by $\{011\}_\gamma \langle 01\bar{1}\rangle_\gamma$ shears whose amplitude continuously increases with the decrease of the temperature. The reversibility of the premartensitic phenomena is explained by the elastic nature of the deformations.

We know that most of the microscopic models, giving a possible crystallographic path for the f.c.c. → b.c.c. or b.c.t. transformation, are based upon a double shear mechanism [15-16-17]. The first shear being always along $(111)_\gamma$, these models differ from each other in the magnitude of the first shear and in the nature of the second shear which happens either on a potential twinning plane $(112)_{\alpha'}$ or on a compact plane $(110)_{\alpha'}$ of the martensite. These models account for the usually observed crystallographic relationships but not for the habit plane. Taking into account the nature of the first shear, they cannot explain the premartensitic effects observed in Fe_3Pt which rather suggest that austenite becomes tetragonal by the action of $\{011\}_\gamma \langle 01\bar{1}\rangle_\gamma$ shears.

Considering that the initial lattice can be deformed before the appearance of the first martensite platelet, the $L1_2$ lattice can become b.c.t. by the simultaneous action of two $\{011\}_\gamma\ \langle 01\bar{1}\rangle_\gamma$ shears of same amplitude g, the shear planes lying at 60° from each other. This transformation is accompanied by a rigid body rotation around a $\langle 110\rangle_\gamma$ axis. The lattice tetragonality parameter $q = \frac{c}{a}$ can be expressed in terms of the shears magnitude. In Fe_3Pt, with S = 0.70, g is included between 0 and 0.046 at - 195°C and between 0 and 0.1 at - 253°C ; its average values are respectively 0.026 and 0.054 at these two temperatures. We suppose that the shears magnitude continues to increase till the final lattice is quasi b.c.c., without the elastic limit of austenite is reached. The moduli of the base vectors describing the new lattice are respectively 0.795 a_o , 0.793 a_o and 0.795 a_o (with a_o, the initial $L1_2$ lattice parameter) and their angles : 90°06 , 86°67 and 88°88. The shuffles, necessary to describe the final martensitic lattice, have a small magnitude. During the whole distorsion, the $(111)_\gamma$ plane and the $[\bar{1}10]_\gamma$ and $[11\bar{2}]_\gamma$ directions stay parallel to their transforms $(011)_{\alpha'}$, $[100]_{\alpha'}$ and $[01\bar{1}]_{\alpha'}$, respectively. The crystallographic relationships existing between the initial and the final lattice are consistent with the Nishiyama-Wasserman relations. Although the $(111)_\gamma$ plane stays parallel to its transform $(011)_{\alpha'}$, it is however distorded and cannot be considered as an invariant plane of the transformation.

However, the internal stresses associated with the double shear will become so high that, in certain regions of the alloy, they will be largely accommodated by transformation plasticity. Thus, some martensite will appear and interfaces will be created by internal shear of martensite on $(112)_{\alpha'}$ planes [20]. This martensite shear is very likely energetically favourable because it happens on planes which correspond to the austenite $(011)_\gamma$ plane.

According to the mathematic theory of the martensitic transformation [18-19], it appears that the deformation matrix associated with the proposed double shear mechanism corresponds, neglecting some small shuffles, to the product of the Bain distorsion B by a rigid body rotation R. As the determinant of the matrix is unity whatever is the shear magnitude, the proposed deformation takes place without any volume change. This is consistent with experiments, particularly in the case of the stoechiometric Fe_3Pt alloy whose long range order parameter is at least equal to 0.60 and which exhibits a thermoelastic martensitic transformation [10][21][22].

IV. Conclusion

The $L1_2$ austenite lattice of the long range ordered Fe_3Pt alloy exhibits, about 15°C above M_s, premartensitic effects which are revealed by X-ray and electron microscopy experiments. These effects are interpreted by a tetragonal distorsion of the austenite due to the joint action of two shears $\{011\}_\gamma\ \langle 01\bar{1}\rangle_\gamma$, the shear planes lying at 60° from each other. These effects might find their origin in the existence of an internal driving force increasing from a temperature T_o, between M_s and A_f, and becoming efficient at a temperature T_δ' between T_o and M_s, when it applies on a metastable system which is soft enough : in this case, the Curie temperature is much higher than T_δ'.

A microscopic model based upon these two previous shears give a possible path for the $L1_2$-b.c.t. transformation and anticipates the N.W. lattice relationships : it is consistent with the observed premartensitic

effects which can be expressed according to the phenomenological theory of the martensitic transformation, by the beginning of the deformation due to B×R, where B is the Bain distorsion and R the rigid body rotation.

References

[1] M. Foos, C. Frantz and M. Gantois : Scripta Met., 12(1978), 795
[2] G.D. Sandrock, A.J. Perkins and R.F. Hehemann : Met. Trans., 2(1971), 2769
[3] L. Delaey, R.V. Krishnan, H. Tas and H. Varlimont : J. Mat. Sci., 9(1974), 1521
[4] K. Enami, J. Hasunuma, A. Nagazawa and S. Nenno : Scripta Met., 10(1976), 879
[5] Proc. of the Symp. on *"Shape Memory Effects in Alloys"*, Ed. by Jeff Perkins, Plenum Press, New-York, (1975)
[6] *"New Aspects of Martensitic Transformation"*, JIMIS I KOBE, (1976)
[7] *"Martensitic Transformation"*, ICOMAT, Kiev, (1977)
[8] G. Hausch : J. Phys. Soc. Japan, 37(1974), 819
J. Phys. F. - Metal Phys., 6(1976), 1015
[9] K. Tajima, Y. Endoh and Y. Ishikawa : Phys. Rev. Lett., 37(1976), 519
[10] O. Herbeuval, C. Frantz and M. Gantois : Mem. Sc. Rev. Met., 10(1974), 647
[11] L.E. Tanner : Phil. Mag., 14(1966), 111
[12] M.O. Aboelfotoh, H.A. Aboelfotoh and J. Washburn : J. Appl. Phys., 49(1978), 5230
[13] Yu.D. Tyapkin, V.G. Pushin, R.R. Romanova and N.N. Buynov : Fiz. Metal. Metalloved, 41(1976), 1040
[14] V.G. Pushin, R.R. Romanova, Yu.D. Tyapkin, N.N. Buynov and V.V. Kondrat'yev : Fiz. Metal. Metalloved, 43(1977), 826
[15] G. Kurdjumov and G. Sachs : Zeit. Phys., 64(1930), 325
[16] Z. Nishiyama : Sci. Rep. Tohoku Univ., 3(1934), 637
Sci. Rep. Tohoku Univ., 25(1936), 79
[17] A.J. Bogers and W.G. Burgers : Acta Met., 12(1964), 255
[18] J.S. Bowles and Mackenzie : Acta Met., 2(1954), 129
[19] M.S. Wechler, D.S. Lieberman and T.A. Read : Trans A.I.M.E., 197(1953), 1503
[20] Tsugio Tadaki and Ken'ichi Shimizu : Trans. J.I.M., 11(1970), 44
[21] M. Foos, C. Frantz and M. Gantois : Mem. Sc. Rev. Met., 1(1977), 55
[22] D.P. Dunne and C.M. Wayman : Trans A.I.M.E., 4(1973), 137

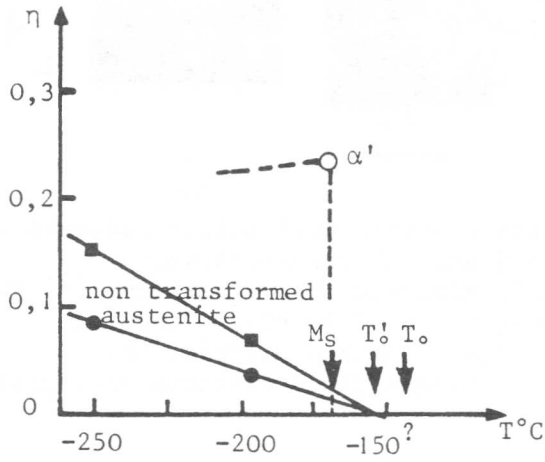

Fig. 5 : Evolution of the order parameter η of the transformation versus temperature.

■ maximal values,

● average values.

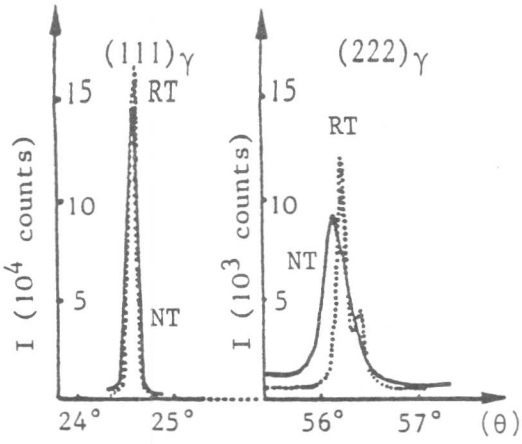

Fig. 1 : The $(111)_\gamma$ and $(222)_\gamma$ X-ray lines are little affected at - 195°C.

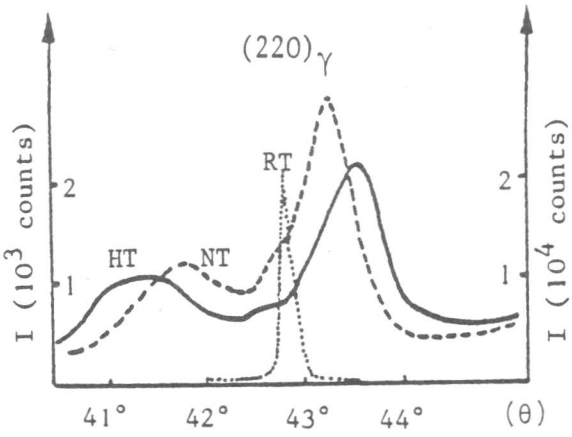

Fig. 2 : Evolution versus temperature of the $(220)_\gamma$ X-ray line. The distribution of the tetragonality parameter becomes wider as the temperature decreases (RT = 25°C , NT = - 195°C , HT = - 253°C).

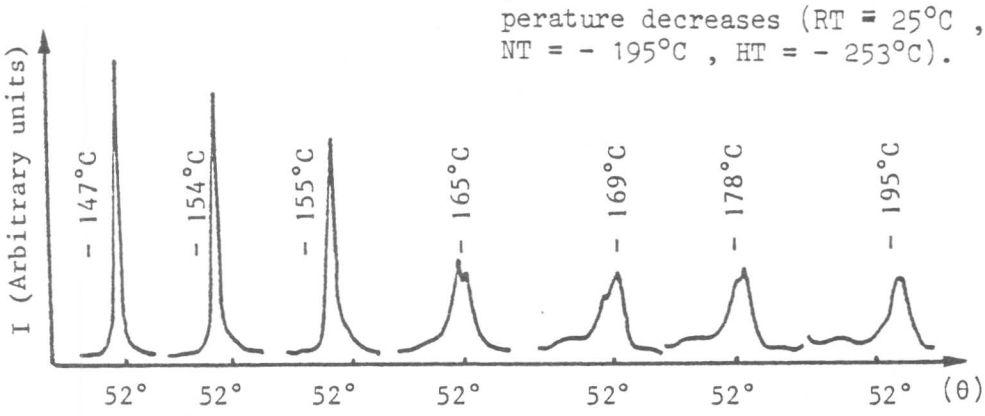

Fig. 3 : Evolution versus temperature of the $(311)_\gamma$ line. The austenite tetragonal distorsion appears distinctly from - 155°C, the fraction of affected phase increases as the temperature decreases.

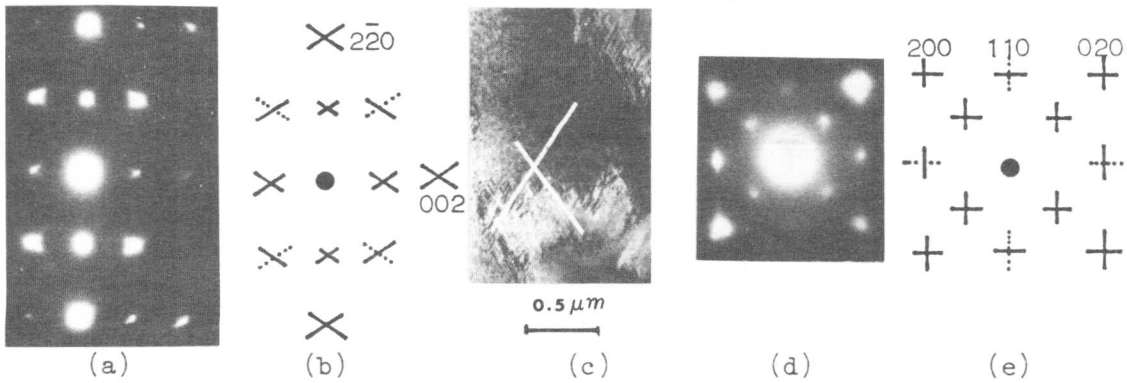

Fig. 4 : (a) and (d) : austenite electron diffraction patterns at low temperature with zone axis [110] and [001] respectively.

(b) and (e) : schematic diagrams of the patterns (a) and (d) respectively. Full lines correspond to $\{011\}_\gamma\langle 01\bar{1}\rangle_\gamma$ shears, Dotted lines are due to double diffraction.

(c) : Striations on the bright field electron micrograph ω associated to the pattern (a).

The Mössbauer Effect Study of Martensite Transformation of Thermoelastic Fe_3Pt Alloy

Ryuichiro Oshima, Katsuro Adachi and Francisco E. Fujita

The ^{57}Fe Mössbauer effect measurements are performed for Fe-Pt alloys in the neighborhood of the composition of Fe_3Pt. The area of Mössbauer absorption is measured as a function of temperature, and lattice softening is observed in the ordered Fe_3Pt alloy in the vicinity of the M_s temperature. Rather negative temperature dependence of recoil-free factor during the process of thermoelastic martensite transformation indicates the large looseness of coupling of atoms, or the deviation from the harmonic oscillation of atoms occur in the lattice.

The internal magnetic field distribution is also obtained as a function of temperature. The austenite of ordered alloy shows a broad distribution curve similar to that found in Fe-Ni Invar alloy and different from that in Pt rich Fe_3Pt Invar alloy. Two peaks appear in the distribution curve of ordered martensite corresponding to two kinds of Fe sites, while a single peak distribution is seen in the disorderd martensite.

I. Introduction

Ultrasonic measurements in V_3Si[1] and Nb_3Sn[2] have indicated a remarkable drop in the elastic moduli and a lattice softening upon cooling to the phase transition temperature at which a β-W type cubic structure changes martensitically to a slightly distorted tetragonal structure. Since then, a Mössbauer spectroscopy[3] and an inelastic neutron scattering experiment[4] also showed the appearance of soft phonon mode in Nb_3Sn. Many recent works on the martensite transition of noble metal alloys have revealed that the soft phonon mode is a precursor of the thermoelastic martensite transformation. For ferrous alloys, most of which undergo a burst type martensite transformation, it has not been so clear whether a lattice softening exists as a premonitory phenomenon of the transformation. However, Suzuki et al.[5] reported that a resonant frequency of ultrasonic attenuation for a polycrystalline Fe-28%Ni alloy remarkably decrease just above the M_s temperature. Recently Oshima et al.[6] observed some premartensitic effect and an intermediate phase during the martensite transformation process of Fe-Mn-C alloy. Among ferrous martensite alloys Fe_3Pt alloy is a unique material. The austenite of this alloy has an order-disorder transition around 700°C. The morphology of martensite depends on the order parameter. A disordered Fe_3Pt alloy shows a typical burst type martensite transformation, while an ordered Fe_3Pt alloy exhibits a thermoelastic martensite transformation. The M_s temperature also remarkably falls from above room temperature to below -196°C as the order parameter increases. Taking into consideration of the characteristic thermoelastic martensite transformation of the alloy, the ordered Fe_3Pt is a suitable material to investigate the lattice softening in iron alloys.

Since the Mössbauer spectroscopy provides the information of the dynamical behavior of Mössbauer atoms in the lattice, the ^{57}Fe Mössbauer resonance in Fe_3Pt alloys are investigated during the process of martens-

Department of Material Physics, Faculty of Engineering Science, Osaka university, Toyonaka, Osaka, Japan 560

ite transformation in the present study. From the total area of Mössbauer absorption the recoil-free factor, f , is measured as a function of temperature, because the f-factor directly reflects the rigidness of a lattice, and it is found that a lattice instability exists in the wide temperature range between just above the M_s and the M_f.

The fcc Fe_3Pt alloy is also famous for its Invar behavior. A magnetic heterogeneity is reported to be required for the Invar behavior, while a recent Mössbauer spectroscopy of Fe-Pt alloy does not suggest the magnetic heterogeneity. So the internal magnetic field distribution in the specimen is also determined. The result shows that iron atoms with small internal magnetic field do exist in the wide range of temperature below the Curie temperature, indicating the magnetic heterogeneity as in the Fe-Ni Invar alloy.

II. Experimental

Fe_3Pt alloy used in this study is prepared from electrolytic iron and sheets of a platinum plate of 99.9% purity. It is melted in an induction furnace in argon+5%H_2 atmosphere. After homogenized, it is cold-rolled to 30 μm thick. The foils of specimen are annealed for various period at 650°C to obtain an ordered structure. The order parameter (s) is determined by comparing the intensity of a normal and an order relection of an X-ray diffraction pattern. The transformation temperature of M_s, M_f, A_f and A_s is examined by the electrical resistance measurement. The Mössbauer spectroscopy is carried out with transmission geometry between 20°C and -196°C using 14.4 kev γ-ray from ^{57}Co source dissolved in copper.

III. Results and Discussion

(I) Area of Mössbauer Absorption

In the present work Fe-24%Pt alloy is mainly used, because all of the transformation temperature M_s, M_f, A_s and A_f of the ordered alloy of this composition are between room temperature and -196°C, and that is convenient to the Mössbauer spectroscopy.

A disordered specimen quenched to 20°C water from 1100°C shows a burst type martensite at room temperature, while an ordered specimen exhibits a thermoelastic martensite transformation. The ordered specimen also reveals a remarkable shape memory effect. The crystal structures of austenite and martensite of an ordered alloy are shown in Fig.1. There are two kinds of iron atom site in the martensite of which nearest neighbor configurations are 4 Pt - 4 Fe, and 8 Fe, respectively. The ordered martensite is a tetragonal structure, but the disordered martensite has a cubic symmetry.

The transformation temperature of the ordered specimen of the present case was

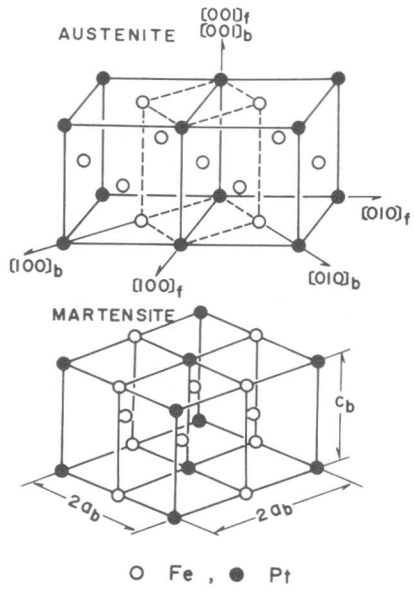

Fig.1 Crystal structures of austenite and martensite of an ordered Fe_3Pt alloy.

M_s=-118°C, M_f=-175°C, A_s=-157°C and A_f=-100°C. The variation of Mössbauer pattern is shown as a function of temperature in Fig.2. The pattern obtained at room temperature apparently consists of complex peaks. This pattern is similar to that of an Invar type pattern. The Curie temperature of this specimen is determined by the magnetic balance method and the central peak counting rate of the Mössbauer absorption. The obtained Curie temperature is 97°C, and the specimen must be ferromagnetic at room temperature. Nevertheless, the specimen has small internal magnetic field, which is quite different from the ferromagnetic component at low temperatures. As the temperature is lowered, the small internal magnetic field component decreases. When a Lorentzian function is considered for a Mössbauer spectrum, the area of a resonant peak is expressed as

$$S = \frac{\pi}{2} \frac{f_s D}{2} \Gamma_{exp} \quad , \qquad (1)$$

where f_s is a recoil-free fraction, D is the effective thickness of the specimen, and Γ_{exp} is the half-width of observed peak. The area of absorption is proportional to recoil-free fraction, and the latter is given by

$$f_s = \exp\{-\frac{4\pi^2}{\lambda\gamma^2} <u>^2\} \quad , \qquad (2)$$

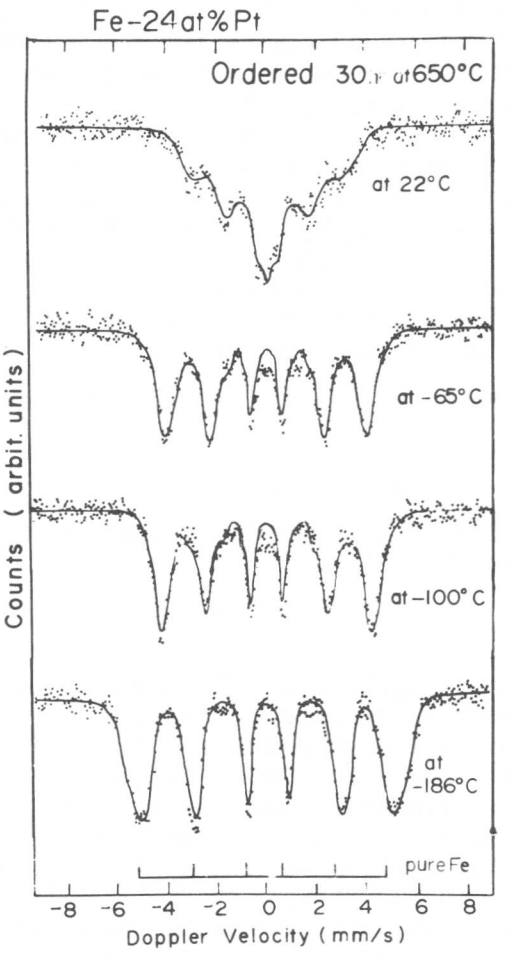

Fig.2 Mössbauer spectra obtained with an ordered Fe-24%Pt alloy at several temperatures.

where $\lambda\gamma$ is a wave length of γ-ray, and $<u>^2$ is a mean square displacement of Mössbauer atoms. Generally, $<u>^2$ reflects the thermal shift of atoms, which will determine the Debye characteristic temperature. However, if a lattice softening occurs when a soft phonon mode is excited, $<u>^2$ will become large in the special crystallographic direction and f_s factor will be reduced. The reduction of f_s is also caused by the deviation of the mode of atomic vibration from a harmonic oscillation. Thus, the temperature dependence of f_s factor measurements can provide a good check on the lattice dynamical behaviors. Although the measurement of absolute value of f_s factor is difficult, the relative change of it can be obtained by the evaluation of the total area of a Mössbauer resonance spectrum as a function of temperature. Fig.3 is the temperature dependence of the absorbed area which is normalized by the value of room temperature. Around the M_s temperature, the area remarkably decreased, and does not change so much between the M_s and M_f. This fact suggests that a lattice softening appears around the transition temperature, and the lattice is

unstable between the M_s and the M_f where the austenite and martensite coexist. The area of the single phase of martensite has a larger absorption area than that of austenite corresponding to higher Debye temperature. The lattice instability between the M_s and the M_f is confirmed by the following analysis.

Taking α as the volume fraction of martensite and β the volume fraction of austenite, we have

$$\begin{aligned} &\alpha = 1, \quad \beta = 0 \quad T \leq M_f \\ &\alpha + \beta = 1 \qquad M_f \leq T \leq M_s \\ &\alpha = 0, \quad \beta = 1 \quad M_s \leq T \end{aligned} \tag{3}$$

Accordingly the absorption area S(T) can be written as

$$S(T) = \alpha(T)\, S_M(T) + \beta(T)\, S_A(T), \tag{4}$$

where $S_M(T)$ and $S_A(T)$ are the total Mössbauer resonant area at temperature T of martensite and austenite, respectively. The $\alpha(T)$ and $\beta(T)$ are experimentally determined by taking the peak intensities of X-ray diffraction pattern at T. Fig.4 shows the variation of $\alpha(T)$ and $\beta(T)$ estimated from the peak intensity change of $(112)_M$ and $(022)_A$ reflection of the same specimen which is used for the present Mössbauer spectroscopy. By using this result the temperature dependence of S(T)/S(RT) is calculated as indicated by the solid line in Fig.5. $S_M(T)$ of the ordered Fe_3Pt at room temperature is not available, because the specimen does not transform to martensite at this temperature. Therefore, instead of it $S_M(T)$ of disordered Fe-24.5%Pt with M_f above room temperature is examined at room temperature and -196°C. At the same time, in order to check the temperature dependence of the absorbed area of austenite, an ordered Fe-24.5%Pt alloy is also measured at room temperature and -196°C, which is shown in Fig.3 and 5 together with the data for disordered Fe-24.5%Pt. Comparing Fig.5 with Fig.3, it is clear that the measured absorption area of the Fe-24%Pt specimen is

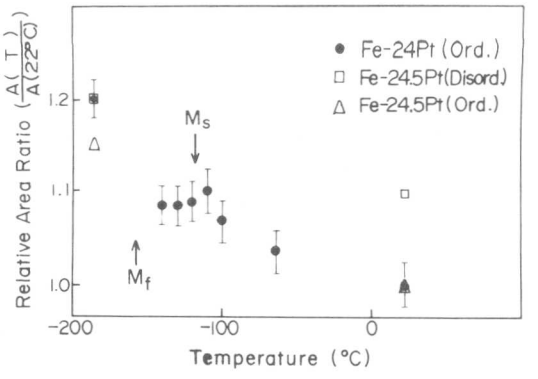

Fig.3 Temperature dependence of the Mössbauer absorbed area of Fe-Pt alloy.

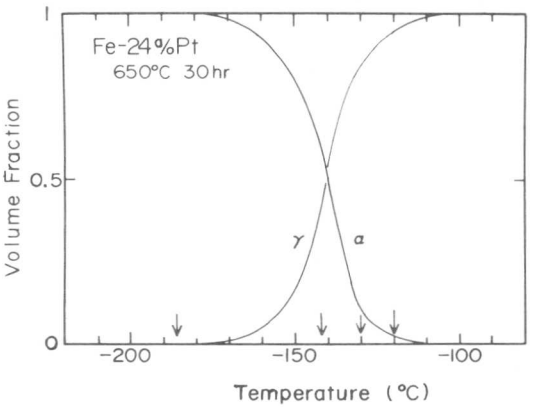

Fig.4 Change in volume fraction of austenite and martensite of ordered Fe-24%Pt alloy.

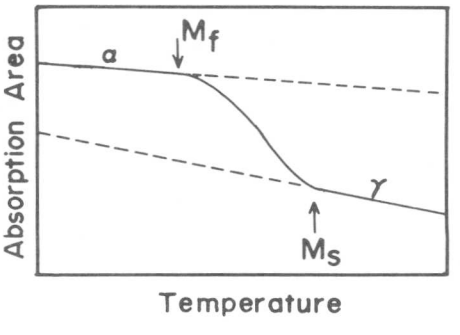

Fig.5 Schematic representation of the temperature dependence of the Mössbauer absorption area.

remarkably small between the M_s and the M_f. This means that the state of the Mössbauer atoms is unsteady during 10^{-8} sec life time of γ-ray, that is, the lattice is very unstable between the M_s and the M_f. Hausch[7] studied elastic constant of a disordered $Fe_{72}Pt_{28}$ alloy and found a large anomaly of elastic anisotropy below the Curie temperature. He also found that Young's modulus of ordered Fe_3Pt becomes very small at -196°C. He concluded that it is not due to the soft phonon mode excitation but due to the magnetic elastic effect. However, since the result of the Mössbauer experiment directly indicate the rigidness of the lattice, the present result clearly shows the softness of austenite lattice at around the M_s temperature.

The excitation of soft phonon mode has not been reported in Fe_3Pt alloy. The present Mössbauer experiment first shows that low recoil-free fraction exists in wide temperature range between just above the M_s temperature and the M_f temperature. Notwithstanding that the volume fraction of martensite increases when the temperature decreases below the M_s temperature, the area of Mössbauer absorption slightly decreases in that temperature range. This indicates that rather negative temperature dependence of f-factor appears in the two phase region, suggesting anharmonic coupling of atoms in the lattice.

(II) Internal Magnetic Field Distribution

The fcc Fe_3Pt alloy shows Invar behavior as well as the Fe-Ni alloy. The coexistence of two magnetic states has been considered as the origin of Invar behavior of Fe-Ni system. However, no experimental evidence of the magnetic heterogeneity is obtained from the typical Invar composition of Fe-35%Ni alloy. Sumiyama et al.[8] studied both the ordered and disordered states of the $Fe_{72}Pt_{28}$ Invar alloy by the Mössbauer effect and NMR experiments, and found no indication of the coexistence of two magnetic states. They concluded that thermal expansion and magnetization anomalies are not due to the inhomogeneity, but are attributable to a fundamental property of the ferromagnetic fcc alloy. In this respect it is interesting to examine the internal magnetic field distribution on the alloy used in the present experiment. The computer fitting is carried out by using some fitting parameters such as the range of internal magnetic field distribution, the number and species of nearest neighbor atoms, and the spin orientation parameter. The isomer shift is also taken into consideration. The internal field distribution is thus obtained by the Fourier analysis by computer. The temperature dependence of internal magnetic field is shown in Fig.6. The shapes of the curves do not substantially change by the parameters used. At room temperature which corresponds to 0.79 Tc, the internal magnetic field distribution curve has three peaks, as was seen in the Fe-Ni Invar alloy. Although such widely spread internal

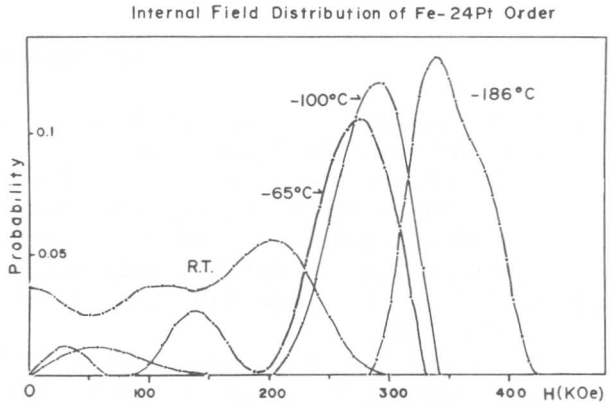

Fig.6 Internal field distribution curves of ordered Fe-24%Pt alloy at several temperatures.

field distribution is difficult to explain, the result clearly indicates the magnetic inhomogeneity in the austenite lattice. As the temperature decreases, the three peaks shrink to a broad single peak. Sumiyama et al. reported that the paramagnetic central peak in the Mössbauer spectra of the ordered and disordered $Fe_{72}Pt_{28}$ alloy already disappeared at 0.90Tc. In the present case of the lower Pt concentration it still remain at 0.79Tc, in consistent with the case of Fe-Ni alloy.

The internal magnetic field distribution curve of the ordered martensite consists of two peaks. The peaks must arise from the two kinds of Fe sites; one with 8 nearest neighbor Fe atoms and the other with 4 nearest neighbor Fe and 4 nearest neighbor Pt atoms. The first peak of 340 kOe corresponds to the Fe site with 8 nearest Fe atoms,and the second peak of 370 kOe to the Fe with 4 nearest Fe and 4 nesrest Pt atoms. The smaller second peak can be expected from the deviation of the alloy concentration from the stoichiometric composition and that of the order parameter from the complete ordering.

IV. Conclusion

Lattice softening has been observed in ordered Fe-24%Pt alloy by means of the Mössbauer effect. The total area of the Mössbauer absorption begins to decrease just above the M_s temperature, and has rather negative temperature dependence between the M_s and M_f. The results suggest that large looseness of coupling of constituent atoms occurs in the lattice in that temperature range.

The internal magnetic field is also determined for the austenite and martensite from the Mössbauer spectra, and widely spread distribution is obtained. This is consistent with the case of Fe-Ni Invar alloy, but not with the Pt rich Fe-Pt Invar case. The internal magnetic field of 340 kOe and 370 kOe are obtained from the ordered Fe_3Pt martensite, corresponding to the two kinds of Fe site with 8 nearest neighbors,and 4 Fe and 4 Pt neighbors, respectively.

Acknowledgment

The authors are grateful for being partly supported by the Grant-in-Aid from the Ministry of Education.

References

[1] L. R. Testardi, T. B. Bateman, W. A. Reed and V. G. Chirba: Phys. Rev. Letters, **15**(1965), 250.
[2] K. R. Keller and J. J. Hanak: Phys. Rev., **154**(1967), 628.
[3] J. S. Shier and R. D. Taylor: Phys. Rev., **174**(1968), 346.
[4] G. Shirane and J. D. Axe: Phys. Rev. Letters, **27**(1971), 1803.
[5] T. Suzuki and W. Wuttig: Acta Met., **23**(1975), 1069.
[6] R. Oshima, H. Azuma and F. E. Fujita: Proc. First JIM Symposium, (1976), 293.
[7] G. Hausch: J. Phys. Soc. Japan, **37**(1974), 819. 824.
[8] K. Sumiyama, M. Shiga, K. Tachi and Y. Nakamura: J. Phys. Soc. Japan, **40**(1976), 1002.

Martensite Pretransition Phenomena in Fe-Ni Alloys: Analysis Technique of Diffuse X-ray Scattering

R. J. Comstock and J. B. Cohen*

The first order nature of the martensite transition implies the presence of anharmonic interactions in the parent phase. The anharmonicity implies interactions among phonons (i.e. atomic displacements). Such displacement interactions could take place throughout the solid near M_s, but be amplified at imperfections which then are the actual nuclei. If these effects do occur for most of the atoms they can be observed in an X-ray scattering experiment. A technique has been devised to separate the third and fourth order atomic displacement contributions from the total X-ray diffuse scattering thereby providing an experimental means of examining the nature of the anharmonic terms prior to the transformation. Measurements are being made of the diffuse X-ray scattering in an Fe-31Ni sample as the M_s temperature is approached.

Introduction

Recent work has suggested that lattice vibration modes may provide the means by which a martensite embryo is formed. Since the martensite transformation is first order, higher-order displacement terms would appear important in understanding the nature of the transformation.

Clapp[1] has used this concept by expanding the elastic free energy to third order in strain. By doing so, he demonstrated that the strain required to produce a lattice instability was only a few percent and that the mode of strain causing the instability was very close to the Bain strain.

Suzuki and Wuttig [2] approached the problem of martensite nucleation by considering both third and fourth order displacement terms in a model involving the forces on atoms. They showed that the anharmonic terms could produce "martensite-like" regions in computer simulations.

Thus, anharmonic lattice vibrations can lead to instability in the structure which results in the transformation of the parent phase to martensite. Following that line of reasoning, it is suggested here that the third and fourth order displacement terms in a diffuse X-ray scattering experiment which would arise only for such anharmonic interactions be measured as the sample is cooled to the M_s temperature. The results of such an experiment would be twofold. First, since X-rays "see" only the average atom, one could determine if the anharmonic effects are localized (such as around defects on free surfaces) or are

*Department of Materials Science and Engineering, Northwestern University, Evanston, Illinois 60201, U.S.A.

occurring for all atoms. If the effects are localized, there would be no change in the higher-order displacement contributions to the diffuse intensity as the M_s temperature is approached. But, if the anharmonic effects involve most atoms, then whether it is due to the third or fourth order interactions in the martensite transformation can be determined. In fact, there have been reports of changes in the diffuse scattering near M_s [3].

Theory

The method to be described here to separate the diffuse scattering into various components is based on a suggestion by Tibballs [4] and implemented by Georgopoulos and Cohen [5]. The total diffuse scattering from a binary cubic solid can be expanded in powers of interatomic displacements from the average lattice. Inclusion of third and fourth order terms results in a total of 100 terms for the diffuse scattering as compared to the 25 terms Georgopoulos and Cohen obtained by terminating the expansion at second order in displacements. Since the terms are periodic in reciprocal space, total diffuse intensities at 100 (or more) equivalent positions could in principle be measured and then the set of equations could be solved exactly (or by least squares) to obtain the 100 components of the diffuse scattering. However, in practice, such a procedure is unworkable as it is unlikely that 100 points could be reached in reciprocal space and the time required for such measurements would be prohibitive. Therefore, a means must be developed to reduce the number of terms to a manageable size.

Following the development of Georgopoulos and Cohen but including third and fourth order displacement terms, the diffuse intensity from a binary AB alloy having atomic concentrations of C_A and C_B can be written as,

$$\begin{aligned} I_D(h_1,h_2,h_3) = {} & I_{SRO} + h_1\eta Q_x^{AA} + h_1\xi Q_x^{BB} + h_2\eta Q_y^{AA} \\ & + h_2\xi Q_y^{BB} + h_3\eta Q_z^{AA} + h_3\xi Q_z^{BB} + h_1^2\eta^2 R_{x^2}^{AA} + h_1^2\eta\xi R_{x^2}^{AB} \\ & + h_1^2\xi^2 R_{x^2}^{BB} + \text{additional second, third, and fourth} \\ & \text{order terms,} \end{aligned} \tag{1}$$

where $\xi = f_B/(f_A-f_B)$, $\eta = f_A/(f_A-f_B)$, and f_A is the atomic scattering factor of atom A. The first term is the short range order intensity and remaining terms represent contributions to the diffuse scattering from atomic displacements. The subscript on the displacement components refer to the direction and the order of the average relative displacements between an A-A, A-B, or B-B pair of atoms as designated by the superscript. The components of the diffuse scattering (such as I_{SRO}, Q's, R's and higher order terms) are periodic functions in reciprocal space as shown by the following equations for I_{SRO} and Q_x^{AA}:

$$I_{SRO} = \sum_{\ell}\sum_{m}\sum_{n} \alpha_{\ell mn} \cos 2\pi h_1 \ell \cos 2\pi h_2 m \cos 2\pi h_3 n$$

$$Q_x^{AA} = -2\pi \sum_{\ell}\sum_{m}\sum_{n} \{(\frac{C_A}{C_B} + \alpha_{\ell mn}) \langle x_{\ell mn}^{AA} \rangle \sin 2\pi h_1 \ell \cos 2\pi h_2 m \cos 2\pi h_3 n\}$$

where $\alpha_{\ell mn}$ is the short range order parameter and $\langle x_{\ell mn}^{AA} \rangle$ is the average relative displacement in the x direction between two A atoms separated by a lattice vector $\ell\underline{a}_1 + m\underline{a}_2 + n\underline{a}_3$. Details of the algebra involved in obtaining equation (1) are given by Schwartz and Cohen [6]. It should be noted that the terms of Q_x^{AB}, Q_y^{AB}, and Q_z^{AB} have been eliminated from the equation by using the fact that the average displacements of A-A, A-B, and B-B pairs are related since there is an average lattice. The relation allows Q_x^{AB} to be written in terms of Q_x^{AA} and Q_x^{BB}.

The second, third and fourth order terms include contributions from A-A, A-B, and B-B displacements. A typical example is the following three third order terms,

$$h_1^2 h_2 \eta^2 U_{x^2y}^{AA} + h_1^2 h_2 \eta\xi U_{x^2y}^{AB} + h_1^2 h_2 \xi^2 U_{x^2y}^{BB}.$$

These three terms can be rewritten in the following way, $h_1^2 h_2 \eta\xi \bar{U}_{x^2y}$, where

$$\bar{U}_{x^2y} = 4\pi^3 \sum_{\ell}\sum_{m}\sum_{n} \{\frac{\eta}{\xi}(\frac{C_A}{C_B} + \alpha_{\ell mn})\langle (x^2y)_{\ell mn}^{AA} \rangle + 2(1-\alpha_{\ell mn})\langle (x^2y)_{\ell mn}^{AB} \rangle + \frac{\xi}{\eta}(\frac{C_B}{C_A} + \alpha_{\ell mn})\langle (x^2y)_{\ell mn}^{BB} \rangle\} \cos 2\pi h_1 \ell \sin 2\pi h_2 m \cos 2\pi h_3 n.$$

$\bar{U}_{x^2y}$ will be periodic in reciprocal space provided the coefficient of the trigonometric functions is independent of h_1, h_2, h_3. The only dependence the coefficient has on h_1, h_2, h_3 is through the scattering factor ratios η and ξ. For an Fe-Ni alloy irradiated with MoK_α radiation, it can be shown that the coefficients vary little with h_1, h_2, h_3 and therefore $\bar{U}_{x^2y}$ can be approximated very well as being periodic in reciprocal space.

By combining the remaining A-A, A-B, and B-B terms of second, third, and fourth order, the number of diffuse scattering terms can be reduced from 100 to 38. Written out explicitly, the diffuse intensity in Laue units is the following:

$$I_D(h_1,h_2,h_3) = I_{SRO} + h_1\eta Q_x^{AA} + h_1\xi Q_x^{BB} + h_2\eta Q_y^{AA} + h_2\xi Q_y^{BB} + h_3\eta Q_z^{AA} + h_3\xi Q_z^{BB} + h_1^2\eta\xi \bar{R}_{x^2} + h_2^2\eta\xi \bar{R}_{y^2} + h_3^2\eta\xi \bar{R}_{z^2} + h_1h_2\eta\xi \bar{S}_{xy} + h_2h_3\eta\xi \bar{S}_{yz}$$

$$+ h_3h_1\eta\xi\bar{S}_{zx} + h_1^3\eta\xi\bar{T}_{x^3} + h_2^3\eta\xi\bar{T}_{y^3} + h_3^3\eta\xi\bar{T}_{z^3}$$

$$+ h_1^2h_2\eta\xi\bar{U}_{x^2y} + h_2^2h_1\eta\xi\bar{U}_{y^2x} + h_2^2h_3\eta\xi\bar{U}_{y^2z}$$

$$+ h_3^2h_2\eta\xi\bar{U}_{z^2y} + h_3^2h_1\eta\xi\bar{U}_{z^2x} + h_1^2h_3\eta\xi\bar{U}_{x^2z}$$

$$+ h_1h_2h_3\eta\xi\bar{V}_{xyz} + h_1^4\eta\xi\bar{W}_{x^4} + h_2^4\eta\xi\bar{W}_{y^4} + h_3^4\eta\xi\bar{W}_{z^4}$$

$$+ h_1^3h_2\eta\xi\bar{X}_{x^3y} + h_2^3h_1\eta\xi\bar{X}_{y^3x} + h_2^3h_3\eta\xi\bar{X}_{y^3z} + h_3^3h_2\eta\xi\bar{X}_{z^3y}$$

$$+ h_3^3h_1\eta\xi\bar{X}_{z^3x} + h_1^3h_3\eta\xi\bar{X}_{x^3z} + h_1^2h_2^2\eta\xi\bar{Y}_{x^2y^2}$$

$$+ h_2^2h_3^2\eta\xi\bar{Y}_{y^2z^2} + h_3^2h_1^2\eta\xi\bar{Y}_{z^2x^2} + h_1^2h_2h_3\eta\xi\bar{Z}_{x^2yz}$$

$$+ h_2^2h_3h_1\eta\xi\bar{Z}_{y^2zx} + h_3^2h_2h_1\eta\xi\bar{Z}_{z^2yx}. \qquad (2)$$

The diffuse scattering components can be obtained by solving in a least squares sense a set of m equations in n unknowns where $m \geq n$. The m equations should be of the form of equation (2) where the left hand side of the equations will be determined by measuring the diffuse intensity at m symmetry related points. The n unknowns correspond to the components of the diffuse scattering. (As Georgopoulos [7] has successfully carried out such a procedure with 25 terms and up to $\sim$ 50 measurements several times in reasonable intervals, this is entirely feasible.)

Experimental

Measurements are being made of the diffuse scattering from an Fe-31Ni sample using monochromated MoK_α radiation from a pyrolitic graphite monochromator. MoK_α enables a large region of reciprocal space to be measured thereby providing a sufficient number of symmetry related points for the separation of the various terms in equation (2). Fe-31Ni was chosen for the experiment as its M_s temperature is below room temperature and the contributions to the diffuse scattering from short range order is small because the scattering factors are similar ($I_{SRO} \propto (f_A - f_B)^2$).

Acknowledgements - This research was sponsored by the U.S. National Science Foundation under Grant No. DMR-76-80662.

References

1] P. C. Clapp: Phys. Stat. Sol. (b) 57, 561 (1973).
2] T. Suzuki and M. Wuttig: Acta Met. 23, 1069 (1975).
3] Y. D. Tyapkin et al.: Fiz. Metal. Metalloved. 41, 1040 (1976).
4] J. E. Tibballs: J. Appl. Cryst. 8, 111 (1975).
5] P. Georgopoulos and J. B. Cohen: J. de Phys. C7, 191 (1977).
6] L. H. Schwartz and J. B. Cohen: Diffraction from Materials, Academic Press (1977).
7] P. Georgopoulos: Ph.D. Thesis, Northwestern University, Evanston, Illinois (1979).

Loss of Lattice Rigidity in Austenite*

Nicholas DeCristofaro† and Roy Kaplow††

Mössbauer spectra were taken at and below room temperature in iron -2.4 wt.% nitrogen samples containing various amounts of stabilized martensite and austenite ($M_s \simeq 260K$). The intensities of the martensite spectra increase with decreasing temperature as expected from the normal thermal variation of the recoilless fraction. Conversely, the intensities of the austenite spectra are smaller below room temperature and M_s, and decrease with decreasing temperature. This corresponds to a decreasing recoilless fraction, which is associated with a lessening of lattice resistance to excitations caused by the transference of the gamma-ray recoil momentum. This behavior is thought to be related to lattice instabilities in the austenite phase, possibly related to its transformation to martensite. The magnitude of the effect indicates that, although the excitations in themselves may be localized, these instabilities are characteristic of the bulk material and cannot be explained in terms of the conventional theory of pre-existing martensitic embryos.

I. Introduction

Recently, the concept that various crystal lattices become structurally unstable on cooling has assumed an important role in models for martensitic or displacive transformations. In this context, a number of anomalous effects occurring in the parent (austenite) phase at temperatures above M_s have been reported. Electron microscopic effects [1-5], softening of elastic constants [6,7], and resistivity and magnetic anomalies [8,9] have been observed. Mössbauer studies of Fe-Ni and Co-Fe systems [10-12] show a decrease in the recoilless fraction of the parent phase as the temperature is lowered to M_s. It has been argued that these "premartensitic phenomena" intensify as the temperature is lowered to M_s [1] and continues to exist in the retained austenite at temperatures below M_s [13].

These effects have been associated with the martensitic transformation in a variety of ways. Models exist in which specific phonon modes in the parent phase related to the martensitic structure [14,15] become unstable and eventually trigger the transformation through their own stress fields [16-18]. Other interpretations speculate two step processes including either the slight distortion of the parent lattice [5] or the precipitation of a transitory phase [3,4] preceding the actual transformation. In many instances, the model for martensitic trans-

---

* This paper is based in part on the Ph.D. thesis of N.D. The work was sponsored by the Office of Naval Research, under Contract No. N00014-76-C-0171, NR031-795.

† Corporate Development Center, Allied Chemical Corporation, Morristown, NJ 07960.

†† Department of Materials Science and Engineering, Massachusetts Institute of Technology, Cambridge, MA 02139.

formation involves inhomogeneously distributed "embryos" based on (a) spatially localized, "soft" vibrational modes [19], (b) static atomic displacement waves [10], or (c) particular configurations of defects (e.g. dislocations) [21].

II. Experimental Procedure

Samples of iron 2.4 wt.% nitrogen (8.9 at.%) austenite (M_s approximately 260°K) [22] were produced by nitriding iron foil (0.025 mm thick) in flowing mixtures of NH_3 and H_2 at 973°K and rapidly quenching directly from the nitriding atmosphere.

Mössbauer spectra were measured on a constant acceleration spectrometer with a gamma-ray source of ^{57}Co embedded in a copper matrix. The austenite absorber was mounted in a low-temperature dewar on this spectrometer so that its temperature could be controlled in situ, without disturbing the source-sample-detector geometry.

The austenitic sample was cycled a number of times between room temperature (295°K) and 183°K. The total time spent at 183°K exceeded 24 hours and the total time at room temperature following the first quench exceeded one week. This process served to ensure that the martensite formed was stabilized both in amount and with respect to short term room temperature aging for this temperature range. The first data set, following this treatment, comprised a sequence of Mössbauer measurements at 295, 183 and 295°K. The spectrum recorded at room temperature is illustrated in Figure 1; it indicates the presence of approximately 40% martensite (the complex, spectrum labeled M), and 60% austenite, (the spectrum labeled A).

The sample was then quenched to 82°K and cycled between this temperature and room temperature in a manner similar to that described above. Following this treatment, another series of Mössbauer spectra were recorded at 295, 183, 82 and 295°K. The spectrum measured at room temperature indicated that during the additional cooling from 183°K to 82°K, the amount of martensite increased to approximately 55%.

III. Analysis of Mössbauer Spectra

The recoilless fraction, which determines the absolute magnitude of the relevant spectra, is related to a recoil energy, R, that would be transferred to a single free and motionless atom when its nucleus absorbs a gamma-ray, and to the effective, quantized energy increment for available lattice excitations, E*, in the form: [23]

$$f_T = \exp\ (-\ R/E^*) \qquad (1)$$

For the vibrational excitation of a Debye solid:

$$E^* = (1/6)\ k_B\ \theta_D/\{1/4 + (T/\theta_D)^2 \int_0^{\theta_D/T} \frac{x\ dx}{e^x - 1}\ \} \qquad (2)$$

where k_B is Boltzmann's constant, θ_D the Debye characteristic temperature, and T the absolute temperature. On the basis of ordinary temperature-dependent vibrational behavior, the recoilless fraction should increase with decreasing temperature. This temperature dependence, expressed in terms of f_T/f_{295}, predicted by Equation (1) and (2), is illustrated as the solid curve in Figure 2. The value of $\theta_D \sim 411°K$, taken as an average and from interpolation and extrapolation of various data [24,25] is appropriate for both phases.

The theoretical intensity of a Mössbauer absorption peak, $P_{th}(E_s)$, is related to the recoilless fraction, f_T, through the convolution: [26]

$$P_{th}(E_s) = \int_{-\infty}^{\infty} I(E, E_s)\,[1 - \exp(-f_T\, n\, \sigma(E))] \qquad (3)$$

where $I(E,E_s)$ is the nominally Lorentzian energy distribution of the gamma-ray source, n is the effective thickness of the absorber in nuclei per cm^2, and $\sigma(E)$ is the cross section for resonant absorption. In practice, the proper absorption intensities and shapes are obtained through the convolution of the theoretical intensity with a Gaussian curve to compensate for instrumental broadening [17]. Since the nuclear parameters are constant, the temperature variation of the magnitude of resonant absorption in each phase is dependent only on f_T.

When the argument of the exponential term in Equation (3) is small, the depth of the Mössbauer peaks is also small and may be approximated as being directly proportional to f_T. This is the case for the ferromagnetic martensite spectra. For the austenite spectrum, where the exponent is larger, the more rigorous nonlinear treatment of Equation (3) must be applied.

IV. Experimental Results

The first series of Mössbauer measurements, on 40% martensite stabilized at 183°K, were recorded at 295, 183 and 295°K again. The martensite peaks showed increased intensity at the low temperature by the amount expected from the thermal increase in f_T. The austensite peak, however, showed a decrease in intensity corresponding to a decrease in f_T of approximately 9%.

The second series of measurements, on 55% martensite stabilized at 82°K, were recorded at 295, 183, 82 and 295°K again. As in the first series, the martensite peaks were observed to increase with decreasing temperature in the expected manner while the austenite showed a continuous decrease in f_T with decreasing temperature. In both series of measurements, all peaks returned to their original room temperature intensities when the sample was reheated to 295°K.

The measured relative recoilless fractions are compared to the theoretical values in Figure 2. An important aspect of these results is that the f_T value for austenite at 183°K is the same, within precision, for both series of measurements.

IV. Discussion

The reduced value of the recoilless fraction in the austenite at low temperature implies an increase in the probability that a gamma-ray will create a lattice excitation, i.e., that it will be absorbed in a non-recoilless manner. This increasing probability reflects a lessening of lattice resistance to excitation. The energy available from the gamma-ray to create an excitation is, at most, the free atom recoil energy, R. R is determined by the gamma-ray energy and the atomic mass of the atom, and equals 3.1348×10^{-15} joules (1.9567×10^{-3} ev) for the Mössbauer transition in ^{57}Fe [28]. This value is an order of magnitude less than thermal energy at room temperature.

Since at temperatures below M_s there is a driving energy for the transformation of austenite to martensite which increases with decreasing temperature, such lattice excitations formed in the austenite structure might be related to the martensitic transformation. Without distinguishing between excitations in the form of static distortions or vibrational displacements (such as of soft normal modes) one can conceive of an excitation causing a localized change in the atomic configuration toward the martensitic structure. The behavior of the recoilless fraction of the austenite with decreasing temperature is consistent with such a proposition. The essential independence of the recoilless fraction of the austenite from both the amount of martensite already formed and the immediate tendency to form more martensite indicates that it is at least primarily an intrinsic property of the austenite. This does not necessarily mean that prior treatment (e.g., the formation of the additional amount of martensite at 82°K) does not change the excitation probability at all, but only that such effects (e.g., as may be due to strains, etc.) are small in comparison to the intrinsic effect.

If the localized excitations are normal vibrational modes enhanced by a lessening of certain elastic constants, a decreasing f_T would imply a decrease in the vibrational characteristic energy required to create the excitation (e.g., the Debye excitation energy given in Equation (2)). If the excitations are different from the normal modes and independent of them, the probability of a recoilless event would take the form:

$$f_T = f_N f_S \tag{4}$$

where f_T is the measured recoilless fraction at temperature T, f_N is the probability that the gamma-ray absorption will not create a normal thermal excitation, and f_S is the probability it will not create a special excitation. If we assume that $f_S = 1$ at 295°K and f_N is the Debye value at all temperatures, the temperature variation of f_S and E^*_s can be estimated (where E^*_s is the characteristic energy associated with the special excitation and $f_S = \exp(-R/E^*_s)$). These values are given in Table I. Although the value E^*_s decreases with temperature the probability of such excitations existing through thermal effects, estimated through the Boltzman factor, $\exp(-E^*_s/kT)$, does not increase, since the thermal energy, kT, decreases more rapidly. If we were to assume that the austenite tendency toward instability onsets well above M_s the absolute values of the f_T's would be slightly lower. This alternate assumption has only

minor effects on the derived values.

The anomalous decrease in f_T, which amounts to 27% at 82°K, is too large to be explained in terms of localized instabilities at small metastable regions ("embryos") which are postulated to serve as nucleation centers for martensite. Based on estimates of their size (10^6 atoms) and density ($10^7/cm^3$)[29], "embryos" would comprise only 10^{-10} of the material. Even if all atoms in an "embryo" behaved as if $f_T = 0$, they could not in themselves cause the observed behavior. Thus, the loss of lattice rigidity in the austenite must be a bulk effect, reflecting the overall mechanical instability of this phase at low temperatures.

VI. Summary

The anomalously decreasing recoilless fraction of the austenite with decreasing temperature below ambient is associated with lattice instabilities of this phase, possibly related to its transformation to martensite. The magnitude of the effect indicates that, although the excitations themselves may be localized, they are characteristic of the bulk material and cannot be explained in terms of the conventional theory of pre-existing martensitic embryos. It is unknown whether the gamma-ray induced excitations are stable or unstable. However, in the course of each Mössbauer measurement, it is certain than an appreciable amount of additional martensite has not been formed.

References

1. G. D. Sandrock, A. J. Perkins and R. F. Hehemann: Met. Trans., 1971, vol. 2, p. 2769.
2. K. Chandra and G. R. Purdy: J. App. Phys., 1968, vol. 39, p. 2176.
3. C. L. Corey and K. M. Tatteff: Scripta Met., 1976, vol. 10, p. 909.
4. E. Gillam and D. V. Wield: Scripta Met., 1976, vol. 10, p. 965.
5. A. Nagasawa, A. Gyobu, K. Enami, S. Nenno and K. Nakanishi: Scripta Met., 1976, vol. 10, p. 895.
6. S. Zirinski: Acta Met., 1956, vol. 4, p. 1323.
7. K. Enami, J. Hasunuma, A. Nagasawa and S. Nenno: Scripta Met., 1976, vol. 10, p. 879.
8. C. M. Wayman, I. Cornelis and K. Shimizu: Scripta Met., 1972, vol. 6, p. 115.
9. J. E. Hanlon, S. R. Butler and R. J. Wasilewski: Trans. A.I.M.E., 1967, vol. 239, p. 1323.
10. Ye. Ye Yurchikov and A. Z. Men'shikov: Phys. Metal. Metallog., 1971, vol. 32, No. 1, p. 169.
11. Ye. Ye Yurchikov, A. Z. Men'shikov and V. A. Tzurin: Conference on the Application of the Mössbauer Effect (Tihany, 1969), p. 413.
12. B. S. Bokshtein, Yu. B. Voitkovskii, G. S. Nikol'skii and I. M. Razumoyskii: Sov. Phys. JETP, 1973, vol. 37, p. 283.
13. I. Cornelis, R. Oshima, H. C. Tong and C. M. Wayman: Scripta Met., 1974, vol. 8, p. 133.
14. R. F. Hehemann and G. D. Sandrock: Scripta Met., 1971, vol. 5, p.801.
15. L. Delaey, J. Van Paemel and T. Struyve: Scripta Met., 1972, vol. 6, p. 507.
16. J. Perkins: Scripta Met., 1974, vol. 8, p. 31.
17. J. Perkins: Scripta Met., 1974, vol. 8, p. 439.

18. J. Perkins: Scripta Met., 1974, vol. 8, p. 975.
19. P. Clapp: Phys. Stat. Sol. (b), 1973, vol. 57, p. 561.
20. D. deFontaine, N. E. Paton and J. C. Williams: Acta Met., 1971, vol. 19, p. 1153.
21. G. B. Olson: Ph.D. Thesis, M.I.T., 1974.
22. T. Bell and W. S. Owen: Trans. A.I.M.E., 1967, vol. 239, p. 1940.
23. V. I. Goldanskii and R. H. Herber: Chemical Applications of Mössbauer Spectroscopy, Academic Press, Inc., New York, 1968.
24. International Tables for X-Ray Crystallography, p. 241, Kynock Press, Birmingham, England, 1965.
25. Y. Tanji: J. Phys. Soc. Japan, 1971, vol. 30, p. 133.
26. S. Hanna and R. Preston: Phys. Rev., 1965, vol. 139, 3A, p. 722.
27. N. DeCristofaro and R. Kaplow: Met. Trans., 1977, vol. 8A, p. 35.
28. A. Muir, K. Ando and H. Coogan: Mössbauer Effect Data Index 1958 - 1965, Interscience, New York, 1966.
29. S. R. Pati and M. Cohen: Acta Met., 1969, vol. 17, p. 189.

TABLE I: Estimated Values of f_S and E_S^*

T °K	f_T	f_D	f_S	E_S^* (joules)	$\exp(-E_S^*/kT)$
295	0.778	0.778	1.0	---	0.0
183	0.720	0.846	0.851	$1.95*10^{-14}$	0.463
82	0.661	0.901	0.734	$1.01*10^{-14}$	0.409

FIGURE 1: 295°K Mössbauer Spectrum of Fe-2.4 wt.%N.

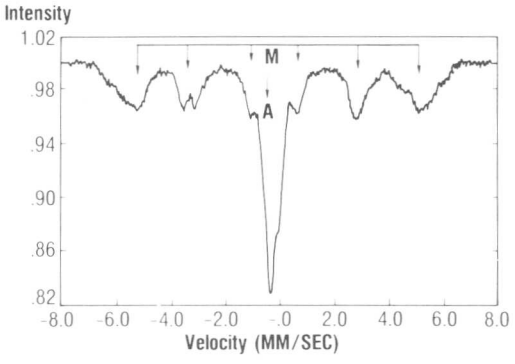

FIGURE 2: Temperature Dependence of the Recoilless Fraction; Debye Theory (—) and Experiment.

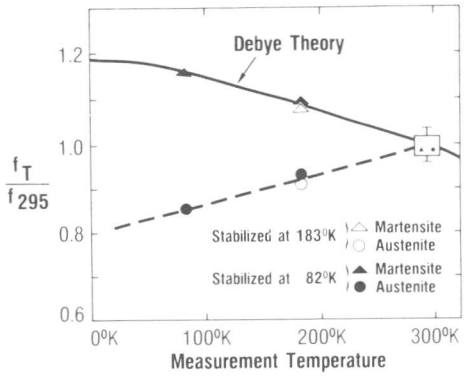

The Study of the Stability of the γ-Phase at the Martensitic Transformation

E.I. Estrin and V.H. Serebryakov *)

The elastic constant $C' = 1/2\ (c_{11}-c_{12})$ (determining the stability of the γ-phase) has been measured by ultrasonic echo-pulse method on the monocrystalline samples of the alloys Fe-33. 7% Ni (I) and Fe - 5.9% Ni - 4.4% Mn - 0.48% C (II) in the close vicinity of the martensitic points. It has been found that during slow cooling no transformation occurred up to 4.2 K in the samples of alloy (I), which had been stabilized by heat treatment. At fast cooling or warming the "burst" martensitic transformation take place in the same samples at temperatures ranging from 35 to 75 K. In this connection it was possible to measure C' for such samples during slow cooling from 200 to 4.2 K, i.e. at a temperature range involving the martensitic point. It has been established that C' has a finite value essentially different from zero and does not show any singularities when approaching the temperature at which the "burst" martensitic transformation takes place. In alloy samples (II) with a martensitic point at 266.5 K, C' is measured at temperatures from 292 to 267.5 K. In such samples C' has a normal temperature dependence (the constant rises as the temperature decreases). Hence, in alloys (II) C' shows no signs of anomaly when approaching the martensitic point and there are no tendencies towards a loss of the lattice stability. Consequently, the martensitic transformation in the alloys examined is not related to the full loss of the γ-phase stability.

I. Introduction

Martensitic polymorphic transformation, which can proceed at very low temperatures, with a high velocity ("athermally"), is a well-known process in crystalling solids.

Ziner [1] propose that such transformations may be associated with the loss of the mechanical stability of the crystalline lattice. The prove of this assumption is a principal problem. There exists experimental evidence of this hypothesis in the case of transformations close to transformations of the second kind (in V_3Si, Nb_3Sn, In-Te alloys [2]). However, for typical transformations of the first kind there are no data for allowing one to make an unambiguous conclusion [2].

---

*) Central Scientific Research Institute of Ferrous Metallurgy, Moscow

In the case of a fcc → bcc transformation stability of the initial γ-phase is determined by magnitude of elastic constant $C' = 1/2\ (c_{11}-c_{12})$ (i.e. by magnitude of corresponding second derivative of thermodynamic potential).

Total loss of stability means vanishing $C':C' \to 0$. The elastic constant C' in Fe-Ni alloys decrease with the drop in temperature, but near the martensitic point (T_M) it remains finite [3, 4]. In reference [4] the constant C' (T_M) lowers monotonously with T_M decreasing. Therefore, it is quite possible that at a very low position of the martensitic point the corresponding C' (T_M) value appears close to zero.

Besides references [5, 6] indicate that a sharp decrease in the elastic constant is possible in the immediate vicinity of the martensitic point.

In this connection a study has been carried out by us on phase transformation of the first kind, fcc → bcc ($\gamma \to \alpha$) in Fe-Ni alloys regarding the temperature dependence of the shear constant C', with the martensitic point positions being as low as possible (when it is unlikely possible to overcome the energy barrier at the expense of thermal fluctuations) and with the temperature being as close as possible to T_M [7]. The behaviour of C' in Fe-Ni-Mn-C alloy also has been studied.

II. Material and Methods

The investigation was carried out on a single crystal alloy Fe - 33.7 wt % Ni, size Ø 38x40 mm, grown according to Bridgeman's method. Samples of 5x10x10 mm was cut out and oriented in the direction of [110]. The elastic constant C', was calculated from the measurement of velocity of the shear ultrasonic wave (frequency ~ 4 M c/s) propagating in the direction of [110] and polarized along [1$\bar{1}$0], using the echo-pulse method. The accuracy of the relative measurement was not worse than 0.1%. The sample was cooled by slowly immersing it into a Dewar transport helium vessel, capacity 25 l. The temperature of the sample was taken with a copper-constant thermo-couple. The cold thermo-couple junction was inserted in liquid nitrogen. The temperature gradient along the sample length under the cooling conditions employed, did not exceed 0.6 K.

III. Super-cooling Phenomenon of "Birst" Martensitic Transformation

To reduce the martensitic point the stabilization γ-phase phenomenon was used as a result of chilling the samples to a temperature close to T_M and subsequent annealing at 500°C [8].

In our case the single crystals of the alloy under investigation was subsequently cooled to temperatures 120, 110, 100, 90 and 80 K and annealed after each cooling at 500°C for one hour. Thanks to such a treatment it was possible to observe a super-cooling phenomenon of "burst" martensitic transformation [9].

For a long time the martensitic transformation was regarded as an athermal process which could not be supercooled. In 1948 G.V. Kurdyumov supposed [10] and later G.V. Kurdyumov and O.P. Maksimova [11, 12] experimentally revealed the possibility of a partial and then a full supercooling of martensitic transformation.

In recent years research, carried out into kinetic of the martensitic transformation and the morphology of its products, has allowed one to get insight into the existence of two kinds of martensitic transformation - isothermal and athermal, each of which is characterized by kinetical and morphological peculiarities [13-18]. In accordance with this elucidation the athermal martensitic transformation as distinct from isothermal, proceeds at a rapid rate (often burst-like) at all temperatures and does not supercool. Typical representatives of alloys with athermal martensitic transformation are Fe-Ni alloys of a high percent of nickel (> 31%), low T_M and a "burst" nature of transformation.

It was in this kind of alloy that a possibility was found for supercooling the "burst" transformation. It turned out that the single crystal undergoing stabilization treatment can be cooled slowly down to 4.2 K and slowly heated up to room temperature without transformation. The results of measurements of the elastic constant C', carried out during cooling and heating coincide fully (Fig. 1), thus testifying to the absence of transformation during slow cooling. In subsequent accelerated cooling or warning of the same single crystals or in the process of isothermal treatment there occurs a "burst" transformation.

For instance, a "burst" martensitic transformation took place in one of the single crystals, that had undergone a cycle of slow cooling down to 4.2 k without transformation and a slow warming up to room temperature, at repeated accelerated (30 deg/min) cooling in a temperature range of 75-35 K. The relief arises on the preliminarily ground faces (110) of the single crystal is illustrated in Photo 1.

The same "burst" transformation at accelerated cooling of crystals which did not undergo transformation at slow cooling to lower temperatures was observed in two more samples. In the first one the transformation occurs

at a temperature in the vicinity a little lower than 77 K, although before that the single crystal was slowly cooled to 4.2 K and warmed to room temperature. In respect of the second one the procedure was the following: the single crystal was slowly cooled to 98 K, heated it 101 K for 10 minutes and then brought down to room temperature after which a "burst" transformation took place during repeated accelerated (10 deg/min) cooling at 113 K, i.e. at a temperature 15 K higher than the temperature that was used when the crystal was cooled without transformation in the previous slow cooling process.

In the fourth single crystal of the same composition the "burst" martensitic transformation did occur during accelerated warming process after slow (0.3 deg/min) cooling to 110 K and held at this temperature for 2 min. One more case of "burst" transformation was observed to occur in the single crystal with a composition close to the previous one during isothermal treatment (for 9 min) at T = 150 K.

Thus, the "burst" transformation in Fe - 33.7% Ni single crystal alloys described above took place at temperatures much higher than the lowest temperature to which these crystals were preliminary cooled. This testifies to the possibility of supercooling the "burst" (athermal) martensitic transformation at slow cooling of the single crystalline samples and, likely, to the casual fluctuational character of nucleation during this kind of transformation.

IV. Temperature Dependence of Elastic Constant C' and γ-phase Stability in Martensitic Transformation

The supercooling "burst" martensitic transformation phenomenon has enabled measuring the γ-phase elastic constant, C', at temperatures not only close to the vicinity of the "burst" martensitic transformation temperature, but also below it.

It follows from Fig. 1 that the temperature dependence of C' assumes a curve with a smooth minimum at 25 K, where $C' = 1.78 \cdot 10^{11}$ dynes/cm^2. Such a character of change in C' coincides with the data obtained in [19] on single crystal alloy Fe-Ni of invar composition. After these measurements one of the crystals was annealed at 1100°C for 1.5 hours in vacuum after which measurements of constant C' was repeated at slow (1.1 deg/min) changing of the temperature. The measurement was made up to 75.0 K. With further decreasing the temperature at 74.8 K the "burst" martensitic transformation took place. Thus, in this run of experiments it was possible to measure the elastic constant C' to the temperature standing at 0.2 K from the transformation starting point. The data obtained as a result of repeated cooling, are illustrated in Fig. 2. The

same figure presents the curve (thin line) plotted from the results of the first cooling. It issued from Fig. 2 that the temperature dependence of constant C' of the annealed single crystal repeats totally the temperature dependence of constant C' of the crystal subjected to stabilization treatment, which has not undergone a transformation up to 4.2 K. No changes in the behaviour of C' were observed near "burst" martensitic transformation starting point.

The same results were obtained for the three single crystal samples observed in the supercooling "burst" transformation phenomenon described above. The measurement of constant C' for two of them were made to 4.2 K. The transformation at a more faster repeated cooling in one of them happened near 35 K, in the other near 77 K. In the third one measurement of C' was made down to 110 K, the transformation took place when warmed from this temperature. Thus, the measurements of the elastic constant C', in these three cases were actually made at temperatures lower than that of the "burst" transformation. However, no changes took place in the behaviour of C' when approaching to transformation.

The data obtained showed no association of the "burst" martensitic transformation in alloy Fe - 33.7% Ni with the total loss of the γ-phase lattice stability.

V. Behaviour of C' in Fe-Ni-Mn-C Alloy System

We studied the temperature dependence of modulus C' in the single crystal of an Fe - 5.9%, Ni - 4.4%, Mn - 0.48% C alloy subjected to "burst" transformation at a temperature below 0° C [20].

The samples of a 7 mm thick pellet were cut out of a single crystal, Ø 10 mm, 60 mm long, grown in a Tamman furnace by cooling from the melt in a temperature gradient.

To follow the development of transformation the sound velocity measurement was made simultaneously with that of the sample magnitization. The sample together with the cemented quartz single crystal and heater were inserted into a Duar vessel (external diameter of 20 mm) which was incorporated in an inductance coil immersed in liquid nitrogen. The inductance coil was switched to the bridge circuit.

The measured elastic constants values at room temperature were:

$$C' = 3.702 \times 10^{11} \text{ dynes/cm}^2$$

$$C_{44} = 11.23 \times 10^{11} \text{ dynes/cm}^2$$

$$(C_{11} + C_{12} + 2C_{44}) = 24.76 \times 10^{11} \text{ dynes/cm}^2$$

The elastic constants C' values were determined under cooling conditions at a rate of 1.5 deg/min from 292 K to 267.5 K (Fig. 3). At 266.5 K the "burst" martensitic transformation took place. It is distinctly fixed on the thermal effect on the cooling curved, and on the "burst" enhancement of magnetization.

The C' measurements show that the temperature dependence of this shear constant is of a normal kind. The elastic constants increases linearly with the decrease of temperature up to the temperature standing 1 K from the onset of transformation.

Thus the alloy specimen under study does not reveal anomalies associated with approaching the transformation temperature, moreover there is no tendency observed toward a loss of the crystal lattice stability.

VI. Conclusion

A. Data obtained on the single crystals of alloy Fe - 33.7% Ni show that:

1. The elastic constant of γ-phase, C', has a finite value substantially different from zero at all temperatures up to 4.2 K and does not reveal any peculiarities associated with approaching the temperatures at which a "burst" martensitic transformation takes place. The martensitic transformation in the alloy under investigation and, probably, in other Fe-Ni alloys is not associated with the full loss of the γ-phase stability;

2. With slow cooling the γ-phase can be cooled (up to 4.2 K) without any martensitic transformation; the "burst" martensitic transformation occurs with subsequent accelerated warming or with accelerated cooling after slow warming, or in the process of isothermal heating. Hence, the "burst" martensitic transformation in the alloy under investigation can be supercooled.

B. Alloy Fe - 5.9%, Ni - 44%, Mn - 0.48% C does not reveal any tendency toward a loss of stability

Analysis of the experimental data available shows that practically a full loss of lattice stability is seen only in those cases when the deformation of the lattice during transformation is small (V_3Si, Nb_3Sn, In-Tl, Au-Cu-Zn). The loss of stability in these cases in a natural consequence of similarity to the transformation of the second kind and fully coincides with the prediction of Landau's theory.

When approaching the starting point of transformation (as per composition, temperature, or pressure), one observes in most of the rest of cases (β-alloys on Cu, Ag, Au bases, alloys Ni-Al, Fe-Ni, alkaline halogenides CdS, InSb and others) a more or less pronounced tendency toward a

stability loss (low value of elastic constant corresponding to transformation and its further anomalous decreasing upon approaching the transition point and an increasing anisotropy of the lattice), however no total loss is observed at the onset of transformation; moreover, no tendency towards a stability loss is seen in Fe-Ni-Mn-C system of the alloy under investigation or in Li and Na [21, 22].

References

1 C. Zener: Elasticity and anelasticity of metals, Chicago (1948).
2 Roitburd A.L., Estrin E.I.: "Itogi nauki i tekhniki. Metalovedenie i termicheskaya obrabotka 1968", Moscow (1970), 5.
3 Salama K., Alers G.: J. AppL Phys., 39 (1968), 4857.
4 Hausch G., Warlimont H., Acta Met., 21 (1973), 401.
5 Suzuki T., Wutting M.: Met. Trans., 3 (1972), 1555.
6 Suezawa M., Sumino K.: Scripta Met., 10 (1976), 789.
7 Serebryakov V.H., Alshevsky Yu.L., Estrin E.I.:Fizika Metallov i Metalovedenie, 46 (1978), 646.
8 Maksimova O.P., Nemirovsky V.V.: Doklady Akademii Nauk SSSR, 177 (1967), 81.
9 Serebryakov V.H., Estrin E.I.: ibid 237 (1977), 322.
10 Kurdyumov G.V.: Journal Tekhnicheskoy Fiziki, 18 (1948), 999.
11 Kurdyumov G.V., Maksimova O.P.: "ProblemyMetalovedenijy i Fiziki metallov", Vol. 2, Moscow (1951).
12 Maksimova O.P.: ibid, Vol. 3.
13 Bokros J.C., Parker E.: Acta. Met., 11 (1963), 1291.
14 Brook R., Entwisle A.R.: J. Iron Steel Inst., 203 (1963), 905.
15 Nemirovsky V.V.: Fizika metallow i metalovedenie, 25 (1968), 900.
16 Georgjeva I.J., Isotov V.I., Nikitina I.I., Handarev P.A., Ibid, 27 (1969), 1129.
17 Georgjeva I.J., Isotov V.I., Doklady Akademii Nauk SSSR, 186 (1969), 85.
18 Maksimova O.P., Zambrjisky V.N., Panarina I.J.: ibid, 224 (1975), 323.
19 Hausch G.: J. Phys. F., 6 (1976), 1015.
20 Serebryakov V.H., Kushnir I.P., Estrin E.I.: Doklady Akasemii Nauk SSSR, 244 (1979), № 2.
21 Slotwinski T., Trivisonne I.: J. Phys. Chem. Sol., 30 (1969), 1276.
22 Martinson R.H: Phys Rev , 178 (1969), 902.

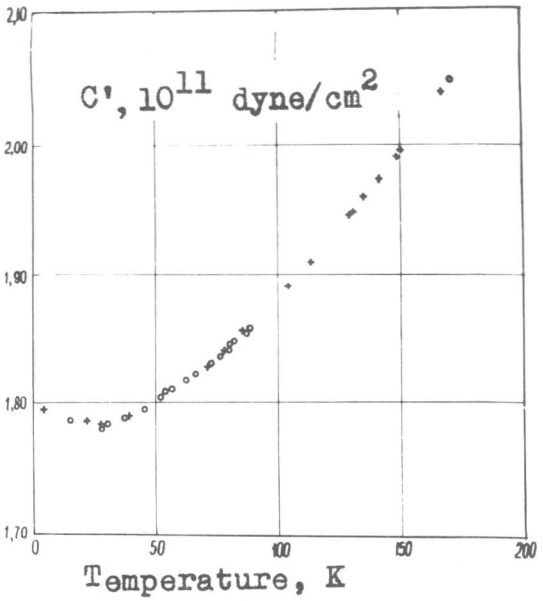

Fig. 1. Elastic constant C' of the Fe - 37.7%Ni crystal undergoing stabilization treatment
+ cooling; o - warming

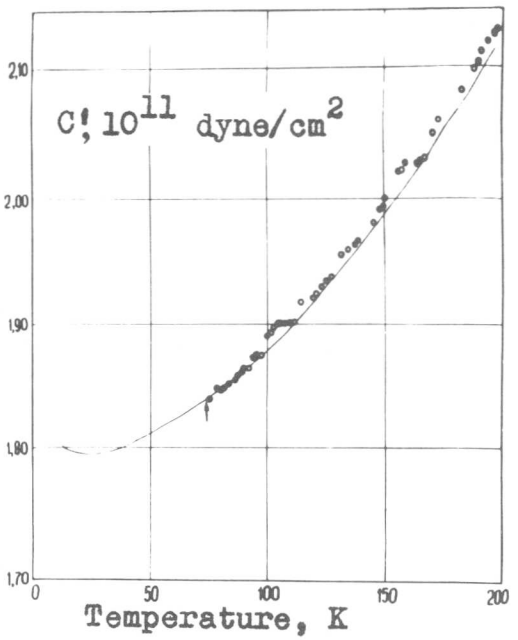

Fig. 2. Elastic constant C' of annealed at 1100°C Fe - 33.7%Ni crystal. Thin line shows behaviour of C' of the same crystal before annealing

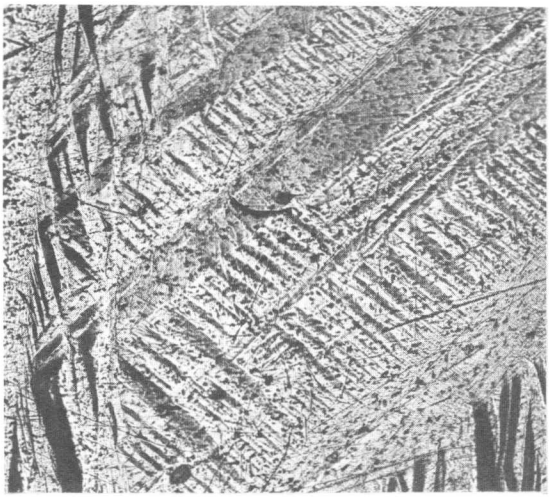

Photo 1. Relief on the (110) plane of the Fe - 33.7% Ni crystal after "burst" transformation

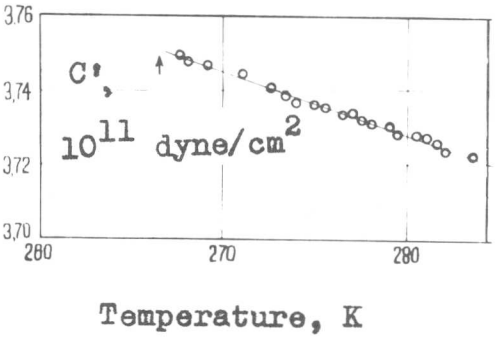

Fig.3 . Elastic constant C' of the Fe-Ni-Mn-C crystal

A Theory of Streaming

Manfred Wuttig* and Tetsuro Suzuki*+

Electron microscopical observations of alloys at temperatures close to but above the martensite transformation temperature show the by now well-established shimmering or streaming.[1,2] The effect manifests itself as a periodic change of contrast propagating in a wave-like manner across the field of view. This paper presents a theory of this effect.

The starting point of the theory is the realization that the electron beam constitutes a strong mechanical excitation of the foil. This excitation brings about the baining-unbaining transitions which are the source of the variations of contrast. The martensitic transformation of the alloys for which streaming has been observed is of first order. Furthermore, energy is dissipated in the foil during the formation of the coherent martensite nuclei. Thus, the theory develops and explores the equation of motion of finite displacements of an anelastic solid.

The solution of this equation shows that at sufficiently high excitation, the motion of the foil will be modulated whenever the foil alloy possesses a metastable state. The modulation frequency is zero at the limit of the metastability and increases as the temperature is lowered. It is proposed that this modulation manifests itself as streaming.

The Nonlinear Anelastic Solid

The standard linear anelastic solid can be modeled by the well-known equation[3,4]

$$\sigma + \tau_\varepsilon \dot{\sigma} = c_r \varepsilon + c_u \tau_\varepsilon \dot{\varepsilon} \qquad (1)$$

where σ and ε denote the stress and strain, c_r and c_u the relaxed and unrelaxed elastic constants, and where τ_ε represents the relaxation at constant strain. This equation describes the solid satisfactorily, as long as the strains are sufficiently small. For large, or more precisely, finite strains such as encountered in first order martensitic transformations, equation (1) must be extended. This may be done by expanding the elastic constants c_r and c_u into Taylor series in the strain. Equation (1) then reads

$$\sigma + \tau_\varepsilon \dot{\sigma} = \sum_{i=2}^{n} c_{ri} \varepsilon^{i-1} + \tau_\varepsilon \dot{\varepsilon} \sum_{i=2}^{u} c_{ui} \varepsilon^{i-2} \qquad (2)$$

---

*University of Missouri-Rolla, Rolla, Missouri 65401; +Visiting professor from Yokohama City University, Yokohama, Japan

where c_{ri} and c_{ui} denote the elastic constants of order i.

The Equation of Motion

The derivation of the equation of motion of a one-dimensional solid may start with the differential equation

$$\rho\ddot{\varepsilon} = \sigma_{xx} \tag{3}$$

where ρ is the density and the double index, xx, denotes the partial differentiation with respect to x. Substituting the characteristic (1) of a linear anelastic solid into this differential equation yields

$$\rho\ddot{\varepsilon} + \tau_\varepsilon\rho\dddot{\varepsilon} = c_r\varepsilon_{xx} + c_u\tau_\varepsilon\dot{\varepsilon}_{xx}. \tag{4}$$

For small values of the damping, as commonly observed in metallurgical observations, the solution of equation (4) is given by

$$\varepsilon(x,t) = \varepsilon_o\exp[-\tfrac{1}{2}\tau_\varepsilon k^2\rho^{-1}(c_u-c_r)t]\cos[k(c_r/\rho)^{\frac{1}{2}}t]\sin kx. \tag{5}$$

It can be seen from equation (5) that all oscillations of small amplitude are attenuated since it is known that $c_u > c_r$.[4] This is not necessarily so for a nonlinear anelastic solid. As will be seen below, in the vicinity of a martensitic transformation, the Taylor expansion in equation (2) needs to be extended to terms i=6. In this case, the equation of motion obtained in the same manner as equation (4) reads

$$\rho\ddot{\varepsilon} + \tau_\varepsilon\rho\dddot{\varepsilon} = \sum_{i=2}^{6} c_{ri}\varepsilon_{xx}^{i-1} + \tau_\varepsilon\dot{\varepsilon}_{xx}\sum_{i=2}^{6} c_{ui}\varepsilon_{xx}^{i-2}. \tag{6}$$

This equation may be solved by a method given first by van der Pol.[5] The solution is

$$\varepsilon(x,t) = \varepsilon_o M(t)\cos[k(c_r/\rho)^{\frac{1}{2}}t - \xi(t)]\sin kx \tag{7}$$

where the amplitude and phase functions, M(t) and $\xi(t)$, are solutions of the differential equations

$$\dot{M}(t) = -\tfrac{1}{2}k^2\rho^{-1}\tau M(t)[(c_{u2}-c_{r2}) + (9/16)c_{u4}M^2(t) + (25/64)c_{u6}M^4(t)], \tag{8}$$

$$\dot{\xi}(t) = k(\rho c_{r2})^{-\frac{1}{2}}[(9/32)c_{r4}M^2(t) + (25/128)c_{r6}M^4(t)]. \tag{9}$$

Only unrelaxed and relaxed elastic constants of even order figure in euqations (8) and (9). Uneven order constants drop out in the process of solving equation (6). This explains the inclusion of terms up to i=6, because the martensitic transformation must be modeled by unrelaxed and relaxed elastic potentials,

$$F_{u,r}(\varepsilon) = (1/2)c_{u,r2}\varepsilon^2 + (1/4)c_{u,r4}\varepsilon^4 + (1/6)c_{u,r6}\varepsilon^6. \qquad (10)$$

In the vicinity of the transformation, the potentials (10) have two minima. Hence, $c_{u,r4}$ must be negative. Therefore, it follows from equation (8) that at sufficiently large amplitudes, $\dot{M}$ can become positive. Existing oscillations of this amplitude will thus be amplified and not attenuated. This amplification does not lead to infinitely large amplitudes, though, because the constant, c_{u6}, in equation (8) is positive.

Automodulation

The amplification of oscillations in a certain range of amplitudes leads to the phenomenon of automodulation. Suppose a solid characterized by elastic potentials of the type (10), i.e., one close to a martensitic transformation, is mechanically excited to an amplitude sufficiently large so that $\dot{M} > 0$. This will excite another stable oscillation. The frequency of this second oscillation will be different because its amplitude is larger than the amplitude of the driving oscillation. This follows from equations (7) and (9). The superposition of the two oscillations leads to a modulation of the exciting oscillation. Since this modulation is brought about by a self-excitation of the second oscillation by the special characteristics of the solid, it is called automodulation. It can be shown[6] that the frequency of the automodulation is given by

$$\omega = (1/4)[c_{r4}/c_{r2} + (c_{r6}/c_{r2})(c_{u4}/c_{u6})](1-\Delta)^{1/2}k(c_{r2}/\rho)^{1/2} \qquad (11)$$

$$\Delta = (400/81)(c_{u2}-c_{r2})(c_{u6}/c_{u4}^2).$$

Streaming

Streaming manifests itself as a periodic change of contrast propagating in a wave-like manner across the field of view of an electron microscope if the observation is made at high-beam currents. If the high-beam current is interpreted as representing a large amplitude mechanical excitation, the streaming oscillations may constitute an automodulation. The crystallographic features, the wavelength and the frequency of the streaming agree qualitatively with what is to be expected in that case. The elastic constants c_{ui} are matrices. Hence, the streaming will depend on the crystal orientation, which it does.[1,2] If flexural oscillations are excited, the wavelength of the streaming should be of the order of the thickness of the sample, which it is.[1,2] Finally, the frequency of the automodulation will be low, because the quantity $(1-\Delta)$ in equation (11) becomes real and is small as the transformation is approached. This agrees semiquantitatively with the observed streaming frequencies of the order of 10 sec^{-1}. It is therefore proposed that streaming represents an externally excited, large amplitude mechanical oscillation which is
modulation arises from the special anelastic properties which the sample has in the vicinity of the martensitic transformation.

References

1. H.C. Tong and C.M. Wayman, Phys. Rev. Letters 32 (1974), 1185-1188.
2. I. Cornelius, R. Oshima, H.C. Tong and C.M. Wayman, Scripta Met. 8 (1974), 133-144.
3. C. Zener, "Elasticity and Anelasticity," University of Chicago Press, Chicago (1948).
4. A.S. Nowick and B.S. Berry, "Anelastic Relaxation in Crystalline Solids," Academic Press, New York (1972).
5. B. van der Pol, Phil. Mag. 7-3 (1927), 65.
6. M. Wuttig and T. Suzuki, Acta Met., to be published.

Diffraction and Shimmering Effects in the β-Cu-Zn-Al Shape Memory Alloys

L. Delaey[o], G. Van Tendeloo[x], J. Van Landuyt[x] and Y. Murakami[xx]

The electron diffraction patterns of the β-Cu-Zn-Al phase contain apart from the usual bcc (DO_3) β-spots many supplementary diffraction spots as well as streaking. In the corresponding images shimmering effects are observed upon heating slightly above room temperature. High angle tilting experiments on $(110)_\beta$ foils of a β single crystal show that the observed phenomena are not due to a bulk precipitation, but the supplementary spot in the $[011]^*_\beta$ diffraction patterns which is located at 2/3 $[\bar{4}\bar{4}4]^*_\beta$ has to be identified as the $\bar{3}20$ reflection of a finely dispersed 9R transformation product which has thus the same structure as the bulk martensite. The macroscopic shear associated with the supplementary 9R phase is nearly parallel to the foil surface. The shimmering effect observed in bright as well as in dark field taken with one of the supplementary spots is thus related with the appearance of these supplementary 9R-phase.

INTRODUCTION

β-Cu-Zn and β-Cu-Zn-Al contain, apart from the fundamental and superlattice bcc spots, supplementary diffraction spots as well as relrods along the $\langle 110\rangle_\beta$ and relplanes or walls on the $\{111\}_\beta$ planes [1,2]. Moreover, streaking occurs due to faulting and to size effects of the supplementary phase [3,4]. The reciprocal lattice of the β-phase with its supplementary spots has been constructed in literature by assembling the various <hkl> zone axis diffraction patterns taken from various thin foil orientations. In doing this, a possible loss of a cubic symmetry due to surface precipitation or relaxation effects can hardly be detected or accounted for. In a recent study it was shown that, although the diffraction patterns could be better explained by a (β + orthorhombic) than by a (β + ω) mixture, some doubts remain about the bulk character of the observations [4]. For this reason high angle tilt experiments on single specimens were made in the present study. Moreover, the present study should allow us to verify the observations and interpretations made by Nagasawa [5]. He observed supplementary spots in the $[100]^*_\beta$ diffraction patterns upon cooling, which he attributes to a phase intermediate between β and the 9R martensite. The electron microscopic images corresponding to the diffraction patterns with supplementary spots are characterized by a mottled or tweed-like structure [1]. In a similar alloy, β-Cu-Zn-Sn [6], fluctuations in contrast (shimmering or streaming) have been observed and attributed to a premartensitic phenomena. Since, in other alloy systems shimmering has been observed which are attributed to a pretransformation phenomenon (Fe-6 Mn- 1 C [7], $AlPHO_4$ [8], quartz [8]

[o] Departement Metaalkunde, Katholieke Universiteit Leuven (Belgium)
[x] Centrum voor Hoogspanningelektr. mikr., Univ. of Antwerp (Belgium)
[xx] Departement of Chemistry, Kyoto University, Kyoto (Japan)

as well as in systems which do not at all transform (graphite and Cu [9] and γ_2-Cu-Al [10]. Some new aspects on shimmering in β-Cu-Zn-Al will be presented in the present paper.

EXPERIMENTAL PROCEDURE

A Cu-27,3 wt % Zn - 4 wt % Al alloy was prepared by induction melting followed by hot extrusion. An extrusion bar was vacuum sealed in a quartz tube and a single crystal was grown by a modified Bridgman-method. After annealing at 973 K the single crystal was water quenched in order to retain the β-phase. The M_s-temperature of the alloy is about 233 K. 3 mm diameter discs with a $(0\bar{1}1)_\beta$ foil orientation were prepared. TEM observations were made with a JEM 120 kV microscope equipped with a low angle double tilt goniometer or a heating stage, with a Philips EM 300 equipped with a high angle tilt stage (± 60°) and with a JEM 100 C microscope equipped with a dynamic recording system using a Plumbicon-tube.

RESULTS AND DISCUSSION

Dark field electron micrographs, taken with the supplementary spot which is clearly visible in a diffraction pattern slightly tilted away from $[011]_\beta$, show the supplementary phase which is characterized by striations (Photo 1 a-b-c). There are two variants of the supplementary phase, spot 1 and 2 on photo 1b belong resp. to variant 1 and 2. The striations are similar to those previously observed (see fig. 1b of ref. [11]). Photo 2a, a $[011]^*_\beta$ pattern, shows the pattern corresponding to the foil normal whereas the other diffraction patterns are obtained by tilting around a $[001]_\beta$ axis about 45° in both directions. Photo 2b and 2c which are exactly at 90° from each other show that the cubic symmetry is lost. Both patterns show streaking along $<110>_\beta$, but sharp maxima at the 1/3 and 2/3 positions are only visible in Photo 2b. These maxima correspond to those observed by Nagasawa : slight tilting reveals the presence of two 9R variants (Photo 2d), whereas in Photo 2f no spots due to 9R variants are present. The corresponding bright and dark field images reveal finely dispersed particles of the two variants but no well developed martensite plates. A stereographic analysis was carried out in order to determine habit plane of the two martensite variants which correspond with the orientations of the two 9R variants shown in Photo 2d. From figure 1 it can be concluded that the positions of the habit planes which are indicated by H_1 and H_2, are located closely to that of the foil surface (011). The angle between the two corresponding basal planes (B_1 and B_2 in figure 1) corresponds with the angle between the $[009]^*_{9R}$ directions in Photo 2d. The most important conclusion that can be drawn from figure 1 is that a $(\bar{1}\bar{1}1)$ pole of the β-phase coincides with the $(\bar{3}20)$ pole of the 9R structure. From Photo 1a and Photo 2a it follows that the reciprocal direction pointing to the supplementary spot coincides with the $[\bar{4}\bar{4}4]^*_\beta$ and $[4\bar{4}\bar{4}]^*_\beta$ direction, which is in complete accordance with figure 1. If the 9R structure is slightly monoclinic the $[\bar{3}20]_{9R}$-spot will deviate a few degrees from its ideal position. This would explain why the supplementary spot is more intense in Photo 1b. The position of the $(\bar{3}20)_{9R}$ spot is moreover unaffected by the exact sequence of the close packed (009) basal planes. This explains why in all $[110]^*_\beta$ type diffraction patterns published in literature a supplementary spot is observed at that same position. Figure 1 shows also that the

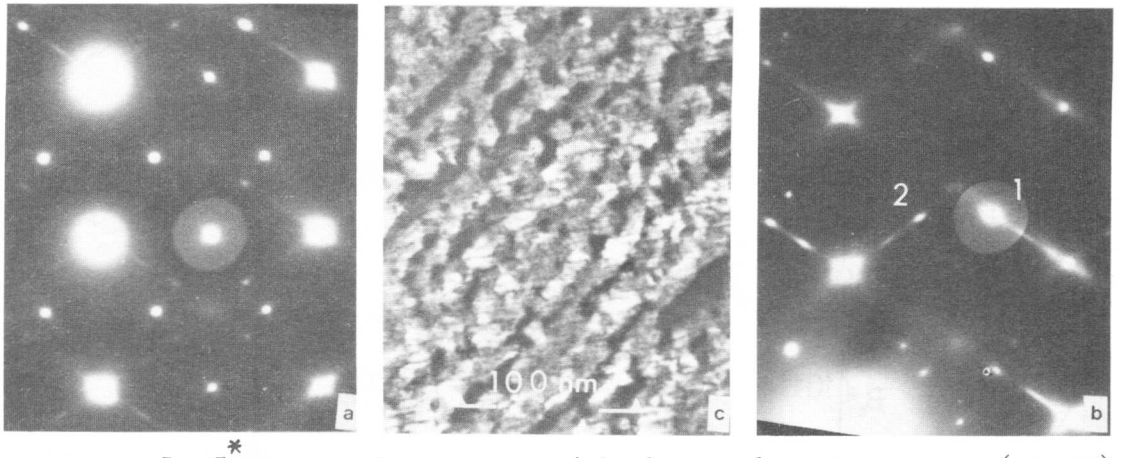

Photo 1 : $[011]^*$-diffraction pattern with the supplementary spots (arrows) and the corresponding dark field taken with one of the supplementary spot.

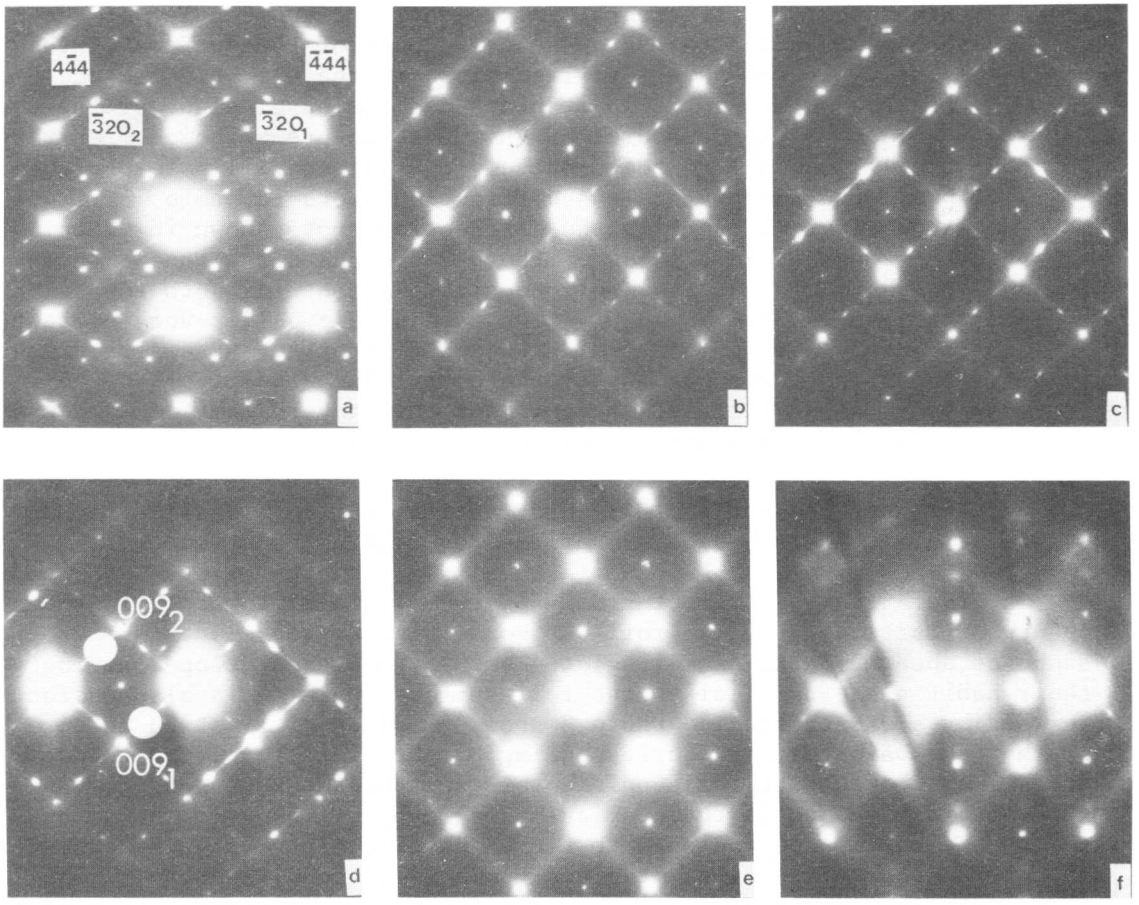

Photo 2 : Diffraction patterns taken from the same sample area after various tilting and rotation. [011]-zone (a); ∿ [010]-zone after 45° tilt (b), 43° tilt (c) and 41° tilt (d), ∿[001]-zone after - 45° tilt (e) and - 50° tilt (f).

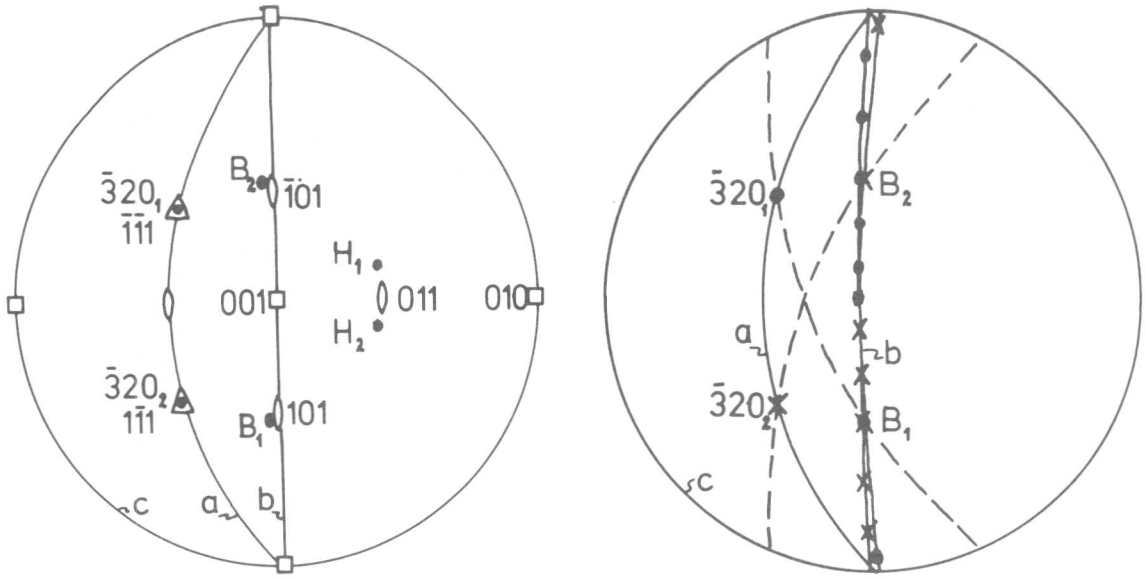

Fig. 1 : Standard (001) stereographic projection of some poles of the bcc β-phase and the 9R phase. The pole of the surface of the single crystal thin foil lies close to the 011-pole. H and B are the poles of the habit plane and the basal plane of the two variants. The $\bar{3}20$-poles of the 9R-structure coincide with resp. the $1\bar{1}1$ and $\bar{1}\bar{1}1$ of the β-phase. The $1\bar{1}1$ and $\bar{1}\bar{1}1$ poles correspond with the $4\bar{4}4$ and $\bar{4}\bar{4}4$ diffraction spots in photo 2a. The zone circle a contains the diffraction spots shown in Photo 2a, the zone circle b those of Photo 2 b,c and d and zone c those of Photo 2 e and f. The zone circle a contains both supplementary spots $\bar{3}20_1$ and $\bar{3}20_2$. The zone circle b lies very close to the zone circles containing the most important 9R diffraction spots and corresponding to Photo 2d. The zone circle c contains no 9R diffraction spots and only a very limited number of spots lies in a zone circle close to it.

two variants are present in $[011]^*$ diffraction, but not in all other $\langle 110\rangle^*$ patterns. This has been confirmed by tilting experiments.

In order to have a direct proof for the origin of the spot in the observed position, a $(011)_\beta$ foil was heated inside the electron microscope at about 250 °C. Some isolated bainite plates developed having their habit plate parallel to the foil surface (bainite is also characterised by a 9R-stacking). Photo 3 shows a $[011]^*_\beta$ diffraction pattern of the (β + bainite), the corresponding bright field image and the dark field image taken with the supplementary spot at the same position as the spot referred to in the previous paragraph. It clearly shows that the supplementary spot belongs to the 9R bainite plate. It can thus be concluded that for the present given geometrical conditions, a $(110)_\beta$ thin foil, the supplementary phase consists of two 9R martensite variants with their habit planes parallel with the foil surface and not due to a ω- or Sato phase.

Under certain conditions transmission electron microscopy observations of these alloys reveal a so-called "shimmering-effect". The origin of these effects being still rather vague we have paid particular

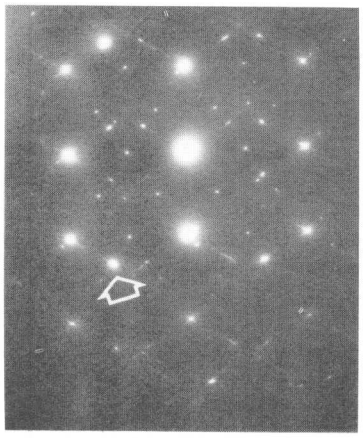

Photo 3 : Dark field image of a bainite plate and the corresponding electron diffraction pattern.

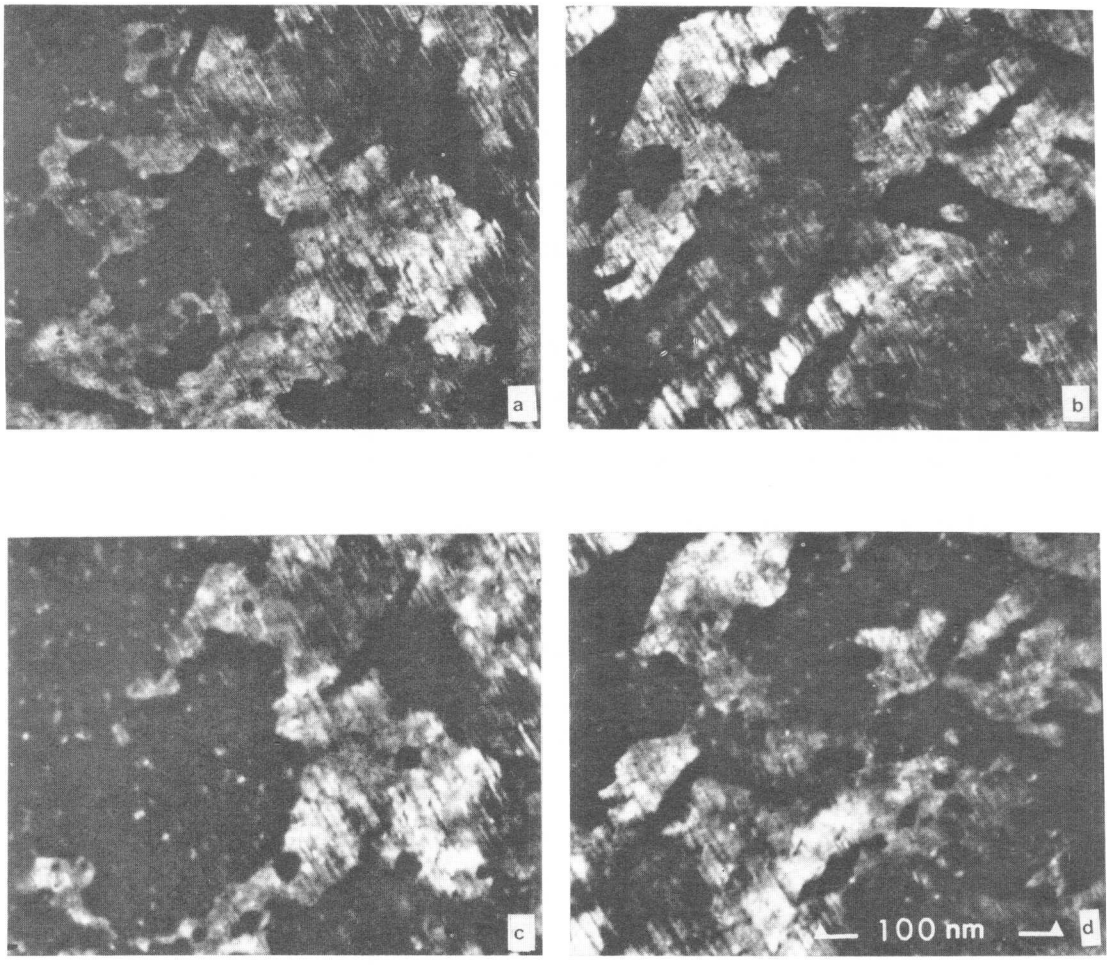

Photo 4 : Dark field electron micrographs taken with the supplementary spot. Photos b and d are taken from the same area as Photos a and c but one minute after the Photos a and c were taken.

attention to the microstructural aspects of the phenomenon, and report here some experimental aspects. The amplitude of the intensity fluctuations becomes more important upon increasing the beam current by e.g. removing a condensor aperture. The phenomenon is not observed in dark field images from B_2 or DO_3 superlattice reflections. The defects observed under these conditions are perfectly stable (e.g. antiphase boundaries). On the contrary dark field images in the 9R-reflections of a $[011]^*$-section do reveal certain instabilities upon heating slightly above room temperature. In these images one variant appears brighter, and at high magnifications small domains are distinguished containing numerous planar defects (Photo 4). These are probably stacking faults with respect to the 9R-stacking lying in the $(009)_{9R}$ planes. These stacking faults have an orientation parallel with the electron beam, and vibrate continuously, sometimes changing position or even disappearing. Also the configuration of variants changes but only after longer time lapses (Photo 4). Similar defect and twin mobility was observed close to the $\alpha \rightarrow \beta$ phase transition in quartz [8]. In the present case the defect mobility is only clearly observed if the defects are parallel with the electron beam. However, after heat cycling the specimen area several times, the fluctuations become less important and finally even vanish. These two kinds of dynamic phenomena i.e. the shimmering observed in the low magnification bright field images, and the defect mobility observed at high magnification in the 9R dark field images are probably due to the same physical process. Although it is difficult to prove because of the different modes of observations it is our strong opinion that they have the same origin i.e. the defect instability related with stacking modifications.

REFERENCES

[1] L. Delaey, A.J. Perkins and T.B. Massalski, J. of Mat. Science 7 (1972) 1197.
[2] K. Otsuka, C.M. Wayman and H. Kubo, Met. Trans.
[3] K. Takezawa and S. Sato, J. of Japan Inst. of Metals 37 (1973) 793.
[4] Y. Murakami, L. Delaey and G. Smeesters-Dullenkopf, Trans. Jap. Inst. Metals 19 (1978) 317.
[5] A. Nagasawa, J. Phys. Soc. Japan 40 (1976) 1021 and A. Nagasawa et al. Scripta Met 10 (1976) 895.
[6] I. Cornelis, R. Oshima, H.C. Tong and C.M. Wayman, Scripta Met 8 (1974) 133.
[7] R. Oshima, H. Azuma and F.E.Fujita, Suppl. Trans JIM 17 (1976) 293.
[8] G. Van Tendeloo, J. Van Landuyt, S. Amelinckx, Phys. Stat. Sol (a) 33 (1976) 723.
[9] C.M. Wayman, AIME Proceedings 1979.
[10] J. Van Landuyt, G. Van Tendeloo, M. Van Sande and S. Amelinckx, AIME Proceedings.
[11] L. Delaey and H. Warlimont in "Shape Memory Effects in Alloys", ed. J. Perkins, Plenum Press (1975) 89.

Premartensitic Effects in Marmem Alloys

W.M. Stobbs

There is a considerable amount of evidence that the parent phase of many materials undergoing martensitic transformations exhibit precursor transitional "structures". There appears, however, to be some confusion over whether such effects are correctly described as a progressive amplification of a distortion of the matrix, or as the precipitation of a discrete second phase.

The extent to which a variety of imaging techniques in electron microscopy can be used to clarify this point is discussed using the Ni-Ti and Ni-Ti-Cu systems as examples but with some reference to the NiAl and Cu-Al-Ni thermoelastically transforming alloys. It is demonstrated that combinations of lattice fringe imaging and dark field stereographic techniques allow specific classification in terms of discrete precipitation or "standing distortional packets". Such a classification in thin foils has only indirect relevance to the path followed by a transformation in bulk because of the relaxation resultant upon the proximity of the foil free surfaces. However the way in which the foil can relax and the consequent structural changes can, in some cases, be linked with the presumed phonon distribution in bulk material and is thus useful in interpreting the transformation mechanism. In particular the relevance of the $\langle 110 \rangle_q$ $\langle 1\bar{1}0 \rangle_\varepsilon$ transverse distortional waves, common to all the above alloys, as well as the potential coupling of these waves to give locally locked distortions is argued to be of fundamental importance in the interpretation of both the martensitic transformation and the variety of competitive reactions which can occur in b.c.c. material.

I. Introduction

"Premartensitic" phenomena have been studied by a wide variety of techniques including X-ray and electron diffraction, neutron diffraction and Mössbauer spectroscopy. Wayman [1] has recently reviewed some of these results and the reader is referred to his article for general references. While neutron diffraction is extremely useful in delineating the scattering which can be associated with phonon disturbances of the b.c.c. matrix, the careful use of electron microscopy can provide added information on the various types of local and non local distortions which can arise in thin foils. Perhaps the most important point to realise is that any real space information obtained necessarily from the examination of a very thin electron microscope specimen is strongly dependent on the proximity of the stress free surfaces of the foil. This need not however be considered a disadvantage: if for example one were to imagine the b.c.c. matrix just prior to a tranformation to contain specific phonons; these would be liable to be locked in a thin foil as distortions which would show forms which, though a function of the foil surface geometry,

Department of Metallurgy and Materials Science, Cambridge University, England.

would necessarily indicate at least related bulk phenomena. The now well known <110> diffuse stacking in β-phase alloys is generally associated with a low frequency $\langle 110 \rangle_q$ $\langle \bar{1}10 \rangle_\varepsilon$ transverse phonon mode [2-4] and the main interests are now: the origin of this phonon, its relation, or lack of it, to the transformation and how it otherwise affects the parent b.c.c phase. For some time I, like many others, have been of the impression that the fundamental link in the whole process ought to be understandable by examination of the 2/3{222} "ω like" reflection which tends to occur in not only the thermoelastically transforming alloys but also appears in alloys such as Zr-Nb where it is well known [5] that there is a longitudinal distortion of the matrix in <111> directions. The modelling of the ω-transformation is well established (see for example the work of Cook [6] or Sanchez and de Fontaine [7]). The relevant point is that not only is it relatively easy to imagine the associated wave vector of the phonons to be associated with appropriate charge density waves linked with the relatively flat area of the Fermi surface in the <111> direction but also antiphase anharmonic coupling of such phonons could easily provide at least localised shears across {110} planes and thus nucleate the transformation. Anharmonic coupling is not unlikely in bulk in the displacement fields of defects and in a thin foil as a result of the irregular free surfaces of the foil. Indeed it has been established [8] that in the dichalcogenides "soft" phonons can give rise, in thin foils, to distortions, which, though not characteristic of bulk material, can be used to gain a greater understanding of the bulk phonon distribution. It is consequently with some surprise that I have been forced to the conclusion that at least in NiAl [3] and Cu-Al-Ni [4] the scattering near $2/3\{222\}_{bcc}$ is associated with a predominantly transverse rather than longitudinal distortion and for that matter that the <112> streaks can be naturally interpreted as the result of localised coupling of $\langle 110 \rangle_q$ $\langle 1\bar{1}0 \rangle_\varepsilon$ waves which appear to be the more fundamental phonons of the bcc material. In many materials, reflections appearing at or near 2/3{222} are genuinely associated with second phase precipitation effects rather than with instabilities of the b.c.c. parent phase and these have lead to considerable confusion in the literature [1]. It would appear that such precipitation effects, certainly in Cu-Al-Ni, Cu-Zn-Al and Ni-Al are competitive rather than precursory relative to the martensitic transformation [3,4].

Further evidence that any simple link between charge density waves and periodic lattice distortions is extremely unlikely to explain any incipient tendency for the b.c.c. matrix to transform comes from the recent results of Bricknell et al. [9]. These authors have established that large atomic fractions of Ni may be replaced by Cu in Ni-Ti alloys with little effect on the transformation temperature. With this result in mind I have recently commenced a systematic electron microscopical examination of the bcc phases of Ni-Ti and Ni-Ti-Cu alloys and present here preliminary results.

II. Results

Electron diffraction patterns of Ni-Ti and Ni-Ti-Cu show, in general, the characteristics common to Cu-Zn-Al, Cu-Al-Ni and Ni-Al of transverse $\langle 110 \rangle_q$ $\langle 1\bar{1}0 \rangle_\varepsilon$ distortions. One of the more interesting normals to examine

is {110} and a diffraction pattern obtained at this orientation is shown in figure 1. The characteristic <112> streaking is clear, as is the tendency for the streaks more nearly transverse to the main beam to be stronger than those pointing towards it. This is as would be expected for locally locked distortions, as inferred for NiAl and Cu-Al-Ni, by the addition of appropriate $<110>_q$ $<1\bar{1}0>_\varepsilon$ waves. The strengthening of these streaks near to 1/3(112) and thus near ω positions is not as in the above alloys however, in that there is a tendency for a rotation of the streak or a flattening with normal <114>. This tends to mean that the intensity near to the 2/3(222) position tends to lie on the adjacent 112 side of the 222 direction. These strengthened regions of diffuse intensity are sometimes further linked to give added relatively localised reflections near 2/3{002} (see figure 2). Images obtained using {001}, and the local diffuse streaks from 002 but excluding the latter reflection are interesting. In situations when the link mentioned above is strong images show not only relatively regular fringes of approximately 5Å spacing indicative of interference between 001 and the strengthened part of the <112> streaks specifically at $\sim$ 1/3(114) but also more irregular fringes of spacing nearer 9Å with normal near the cube direction. The appearance of these fringes is very reminiscent of the distortions seen in thin foils of IT_2TaS_2 [8] and in that material associated with the coupling of periodic lattice distortions. There is certainly no evidence of precipitation. More conventional lattice fringe images of NiTi are equally intriguing. In very thin areas there is abundant evidence for large local rotations (see figure 4) and optical diffraction patterns show the spread of orientation as about 7 to 10° (see figure 5) with, usually, no evidence of the presence of martensite though a very slight change in spacing (compare results on NiAl and Cu Al-Ni [3,4]). A possible mechanism for these rotations is that local areas have transformed to martensite and then reverted to the bcc phase after local plastic relaxation in the thin foil [10]. The effect is not always seen however, and in foils which have perhaps never transformed there is only the tendency to a variable spacing in the <112> directions as seen in other alloys [3,4], (see figure 6 and note the distortions with 112 normal).

NiTiCu alloys tend to show a greater tendency to retain very small apparently martensitic regions in thin areas (figure 7) and the changed spacing of the reflecting planes of the product is readily demonstrated by optical diffraction patterns (figure 8). Images obtained using the "ω" reflection, 2/3<222>, tend to show more localised speckle than in NiTi and for both alloys stereo microscopy would appear to demonstrate local domains of distortions within the foil. The speckle is however very sensitive to deviation parameter (in particular in the streaking with normal in the <112> direction, as in CuAlNi, (not in the <111> direction as for "ω" in Zr-Nb alloys) and thus this conclusion is tentative. Since such regions of locally amplified distortion could well be nucleation sites for the martensitic transformation further experimental classification is required using the techniques used to delineate the form of short range order [11,12,13]. (see figure 9).

III. Conclusion

It would appear that NiTi and Ni-Ti-Cu alloys show local thin foil

distortions which can in general, as in CuAlNi and NiAl alloys, be interpreted as the result of the local locking and anharmonic addition of phonons. The differences between the alloys is surprisingly small though perhaps in NiTiCu the size of the distorted regions seen in "ω" reflections tends to be smaller than in Ni-Ti. The NiTi alloys show less tendency than CuAlNi or NiAl to undergo competitive precipitation or faulting reactions though the reason for this is not understood.

A disadvantage of using electron microscopy to investigate the thin foil distortions is that, since they are amplified and altered by the proximity of the free surfaces, it is unlikely that any change in amplitude of the inherent phonons could be inferred. It is thus difficult to answer the basic question as to whether or not the distortions associatable with anharmonic coupling of the phonons near defects in bulk are truly precursory to the transformation and variable as a function of temperature. While it would seem unlikely that they are not, other techniques must be used to answer this question.

As a final point, it has been suggested [1] that effects apparently similar to those discussed here for NiTi and for other alloys elsehwere [3,4] might be associated with spinodal decomposition; I see no reason to invoke this interpretation for the locally variable yet essentially crystallographically specific thin foil distortions described; though a thin foil, if aged, might well show such a decomposition as a secondary effect to relax the locally variable distortions.

References

[1] C.M. Wayman, IV Phase Transformations, York (1979) p.1.
[2] K. Otsuka, C.M. Wayman and H. Kubo: Met. Trans. 9A (1978) 1075.
[3] R. Portier and W.M. Stobbs, ICOMAT 1979, ibid.
[4] W.M. Stobbs, R.J. Henderson and A. Crossley, ICOMAT (1979) ibid.
[5] T.S. Kuan and S.L. Sass: Phil. Mag. 36 (1977) 1473.
[6] H.E. Cook: Acta Met. 22 (1974) 239.
[7] J.M. Sanchez and D. de Fontaine: J. Appl. Cryst. 10 (1977) 220.
[8] W.M. Stobbs: Phil. Mag. 35 (1977) 1001.
[9] R.H. Bricknell, K.N. Melton and O. Mercier: Met. Trans. A (1979) in press.
[10] R.H. Bricknell and W.M. Stobbs: to be published.
[11] W.M. Stobbs and J.P.A-A Chevalier: Acta Met. 26 (1978) 233.
[12] J.P.A-A Chevalier and W.M. Stobbs: Acta Met. 27 (1979)285.
[13] J.P.A-A Chevalier and W.M. Stobbs: Acta Met. 27 (1979) in press.

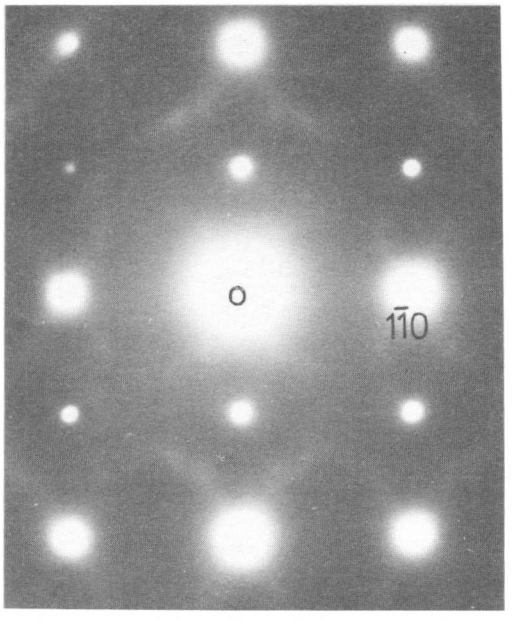

Fig.1 (110) normal Ni-Ti.

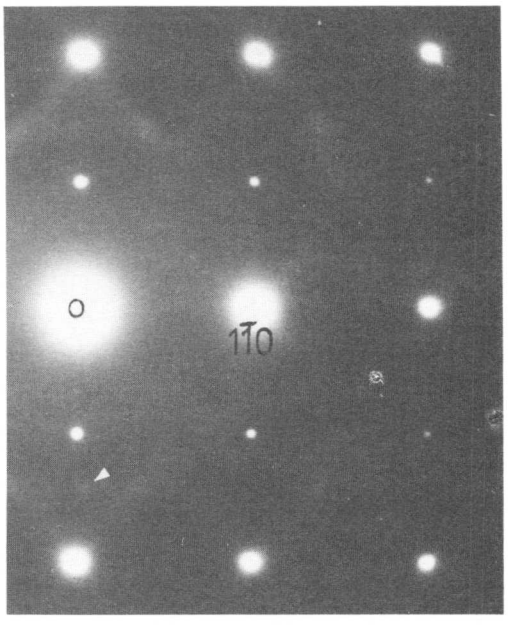

Fig.2 (110) normal Ni-Ti note extra link near 2/3(002) marked.

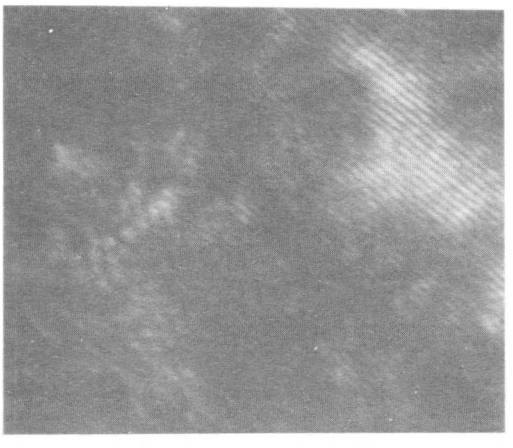

Fig.3 Dark field image with (001) and 2/3(002) ∿ horizontal Ni-Ti.

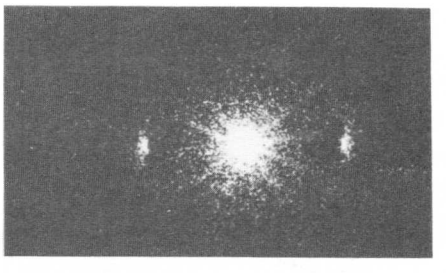

Fig.5 Optical diffraction pattern of area as figure 4.

Fig.4 Non-axial 1$\bar{1}$0 lattice fringe image: Ni-Ti.

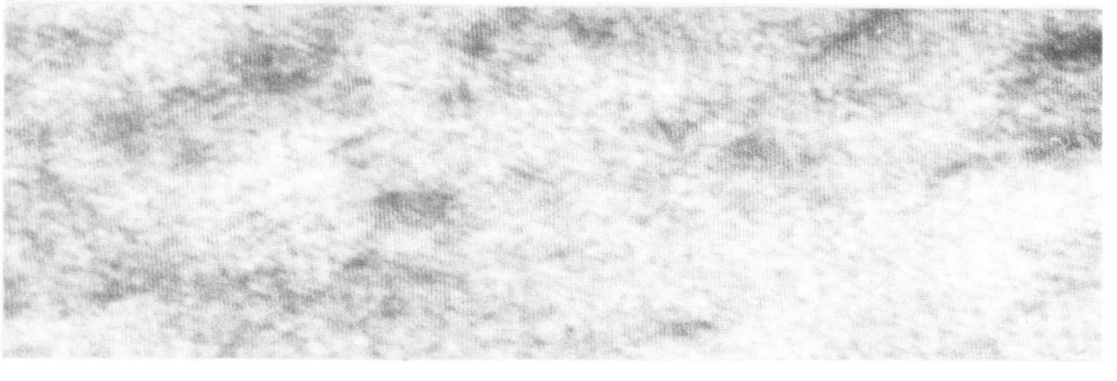

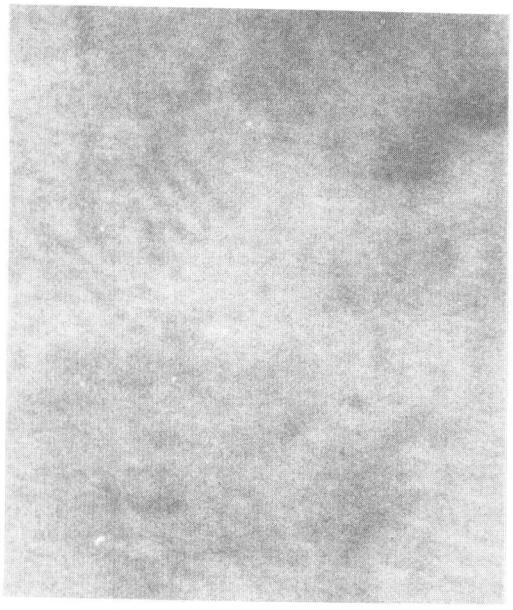

Fig.6 Ni-Ti lattice fringes $(1\bar{1}0)$ (non-axial)

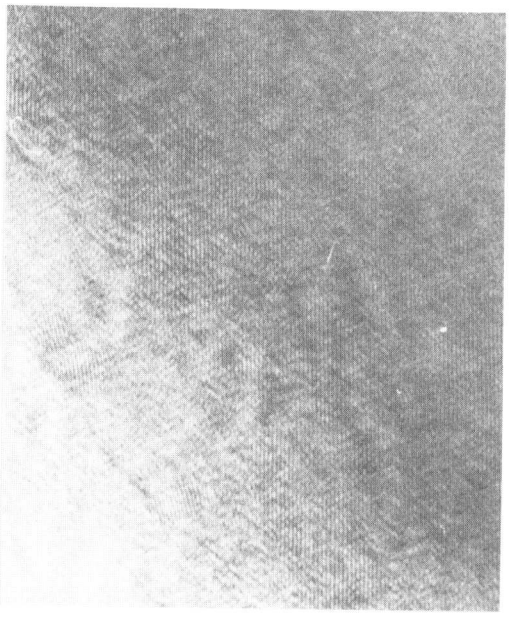

Fig.7 Ni-Ti-Cu lattice fringes $1\bar{1}0$ and small regions of thin foil "martensite".

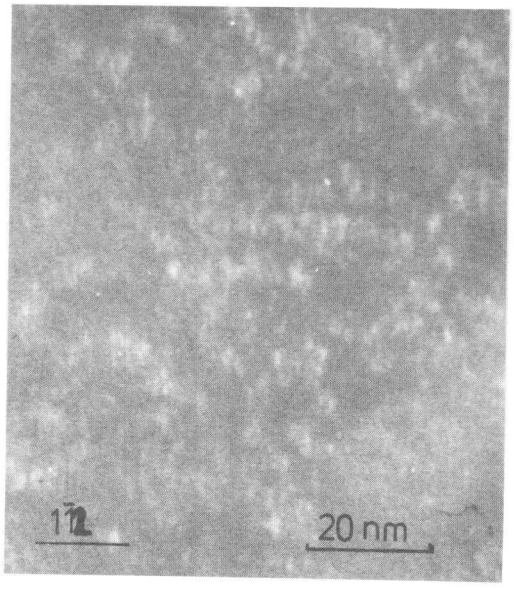

Fig.9 ω reflection at 110 and $1\bar{1}1$ direction marked.

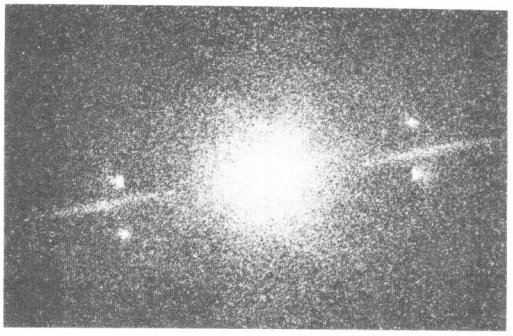

Fig.8 Optical diffraction pattern of area in figure 7.

9R-Type Phase, 2H-Type Phase and Martensite Formation in β-Brass

H. Kubo* and C. M. Wayman**

The electron diffraction patterns of quenched β-brass often show "extra" reflections. A structural analysis of the metastable phases which give rise to such extra reflections has been carried out. It is found that two kinds of metastable phases, one having a 2H-type and the other having a 9R-type structure, are formed depending upon foil orientation of the specimen. In a thin foil with $[001]_\beta$ normal, no metastable phase is found. It is confirmed experimentally that the metastable phases have nothing to do with the subsequent martensitic transformation.

I. Introduction

Various anomalous reflections such as "extra" spots and diffuse streaks are found in the diffraction patterns of the matrix phase of noble metal alloys which undergo a martensitic transformation on subsequent cooling [1]. In the case of the quenched β phase of a Cu-Zn alloy, which is of present concern, three kinds of anomalous reflections have so far been reported: one is streaks or rel rods along $\langle 110\rangle^*_\beta$ directions, which are recently confirmed to result from the presence of a low frequency transverse acoustic phonon mode [2], $\langle 110\rangle^*_\beta\langle \bar{1}10\rangle_\beta$; the other two are extra spots, one set of which is interpreted as resulting from the ω-phase [3], and the other is indexed as the 2H-type structure [4]. The presence of metastable phases are often claimed as proof for a tendency of instability of the matrix phase and as premartensitic or premonitory effects for a subsequent martensitic transformation. But there is no direct proof for such claims.

Recently, Murakami et al. [5] and Otsuka et al. [6] analyzed the extra reflections in quenched Cu-Zn-Al and Cu-Al-Ni alloys, respectively. They both claim that all the extra reflections are more appropriately explained by the 2H-type structure rather than the ω-type, although they could not completely deny the presence of the ω-type phase. The purpose of the present paper is, therefore, to analyze the extra spots, to identify the crystal structure of the metastable phases and to clairfy whether or not they play an important role in a subsequent martensitic transformation.

II. Experimental Procedure

A Cu-39.6 wt.% Zn alloy was melted in an evacuated quartz capsule and then single crystals were made by the Bridgman method. The rods of single crystals were homogenized at 850°C for 24 hr. The specimen

* The Institute of Scientific and Industrial Research, Osaka University, Yamadakami, Suita, Osaka 565, Japan.
** Metallurgy and Mining Engineering Department and Materials Research Laboratory, University of Illinois, Urbana, Illinois 61801 U.S.A.

orientation was determined by the back reflection Laue method. The crystal rods were then cut into slabs with $[001]_\beta$, $[011]_\beta$ and $[111]_\beta$ normals. Heat treatment was carried out at 850°C for 5 min. and specimens were quenched into 10% NaOH at -15°C. 3 mm diameter discs were polished to electron transparency using the jet method followed by final polishing using an H_3PO_4-CrO_3 solution. A Hitachi H-500 electron microscope equipped with side entry stage which can be tilted to ±45°C and cooled to -140°C was used.

III. Results and Discussion

3.1 No extra spots in diffraction patterns from a $(001)_\beta$ foil

Figure 1 is a series of electron diffraction patterns taken from the same area of a specimen. The foil normal is $[001]_\beta$. From (a) to (b), the foil is tilted around $[110]_\beta$ by an angle of 25° and from (a) to (c) around the $[200]_\beta$ axis by 45°. In order to avoid an aging effect, special care was paid to shorten the total time from heat treatment to observation of the specimen, which takes at least 2 hr. It should be noticed that these diffraction patterns have no "extra" spots, and especially that the $[0\bar{1}1]_\beta$ zone (c) does not exhibit any ω-type or 2H-type extra spots. Extensive analysis of various diffraction patterns taken from $(001)_\beta$ foils was carried out to confirm the above result.

Two possible but conflicting conclusions may be derived from the above experimental results: one is that there is not any metastable phase in a bulk specimen; and the other is that, by thinning the specimen, the metastable phase has disappeared. However, the latter is less probable, because a metastable phase may appear more easily in a thin film than in a bulk specimen due to a stress relaxation effect. Therefore we may conclude that there is not any metastable phase in a bulk specimen.

3.2 9R-type metastable phase

When $(0\bar{1}1)_\beta$ foils were examined, they always exhibited extra spots in the diffraction patterns without any exception. Figure 2(a) is a typical diffraction pattern showing the $[0\bar{1}1]_\beta$ zone taken from a $(0\bar{1}1)_\beta$

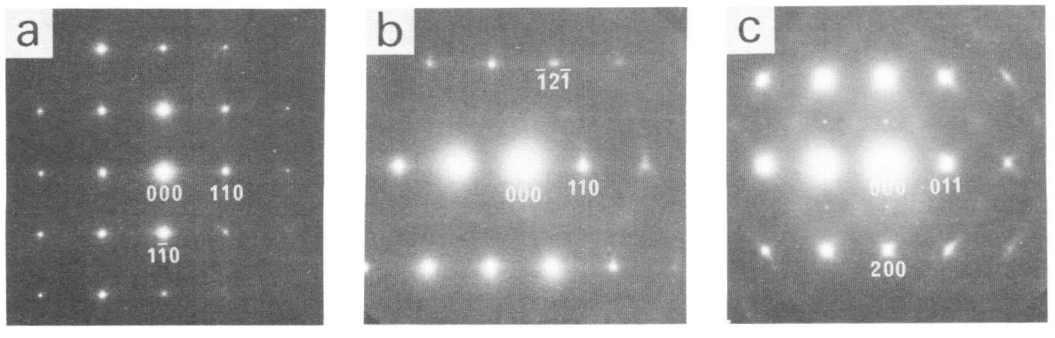

Fig. 1. A series of electron diffraction patterns taken from the same area of the specimen with $[001]_\beta$ normal. (a) $[001]_\beta$ zone. (b) $[1\bar{1}3]_\beta$ zone. (c) $[0\bar{1}1]$ zone.

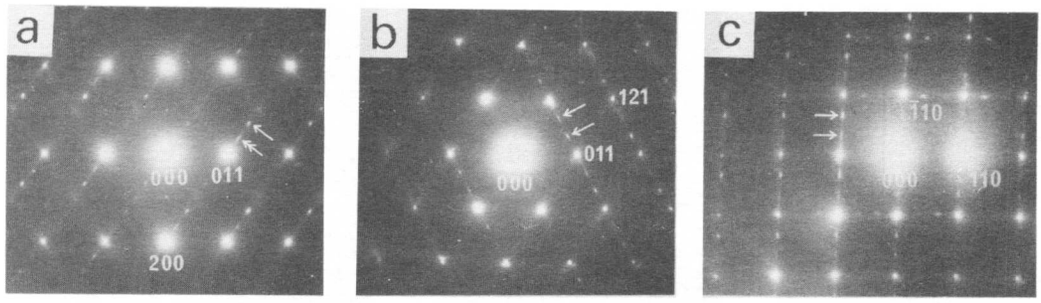

Fig. 2. A series of electron diffraction patterns taken from the same area of the specimen with $[0\bar{1}1]_\beta$ normal. (a) $[0\bar{1}1]_\beta$ zone. (b) ~ $[1\bar{1}1]_\beta$ zone. (c) ~ $[001]_\beta$ zone.

foil. The foil was again examined soon after quenching. Comparing this pattern with (c) in Fig. 1, the difference between the two is apparent. The spot indicated by a single arrow is sometimes interpreted as ω-phase [3,7] or 2H-type phase [4-6] and the one indicated by a double arrow is explained by an intersection of streaks associated with extra spots of the 2H-type structure with the Ewald sphere [4-6]. However for the present case, the intensity of the latter is too strong to be explained in such a way. By tilting the specimen around $[011]_\beta$ by 35°, the diffraction pattern (b) is obtained, where the extra spots divide the distance between matrix spots into thirds. The same kind of extra spots appears when the specimen is tilted around the $[002]_\beta$ axis by 45° as shown in (c). It is to be noted that the extra spots lie on a single streak and that the distance between the nearest extra spots along the streak is about one-third of that of the matrix fundamental spots. Thus, it may be concluded that a 9R-type phase is present in the $(0\bar{1}1)_\beta$ foil specimen. Assuming the 9R-type structure with the same basal plane as that of the 2H-type structure proposed by Takezawa and Sato [4], the extra spots in (a) can be consistently explained. But as to the intensity of the extra spots, more rigorous analysis is necessary. A dark field image using extra spots usually does not show any sharp bright area or regions when the specimen is not aged. The relative intensity of extra spots to that of fundamental spots becomes weak with an increase of the specimen thickness. This strongly suggests that the 9R-type metastable phase might be formed on the surface of the specimen or in a thinner region of the specimen. As mentioned above, if a bulk specimen does not contain any metastable phase, the 9R-type phase is probably formed on thinning the specimen.

3.3 2H-type metastable phase

As pointed out by Otsuka et al. [5] and shown in Fig. 1 extra spots are usually absent in the diffraction patterns of $\langle 001\rangle_\beta$, $\langle 113\rangle_\beta$ and $\langle 111\rangle_\beta$ zones. But they have occasionally been observed as shown by the arrows in Fig. 3. They most likely result from precipitates formed by the diffusion of atoms. Several experimental results support the above conclusion. The $(001)_\beta$ foil specimen which did not show any extra spots was annealed at 150°C in an electron microscope. Many small particles appeared in the specimen after an incubation time of 5 to 6 min. When they had grown to a size of about 100 A, stacking faults were clearly visible in the particles. The diffraction pattern from the specimen was

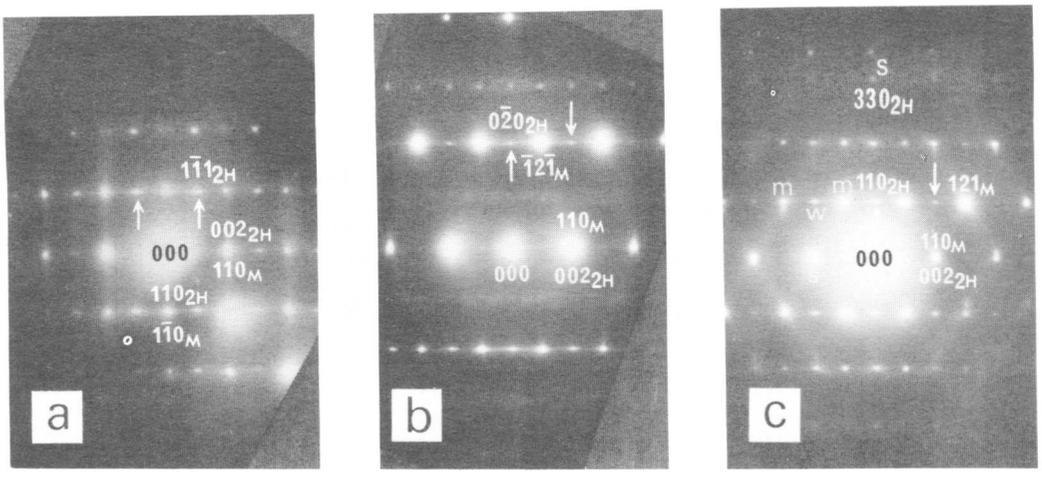

Fig. 3. Electron diffraction patterns exhibiting 2H-type extra spots. (a) ~ $[001]_\beta$ zone. (b) ~ $[1\bar{1}3]_\beta$ zone. (c) ~ $[1\bar{1}1]_\beta$ zone.

very similar to Fig. 3(a); that is, extra spots with streaks which are perpendicular to stacking faults and nearly parallel to the $\langle 110\rangle_\beta$ direction were revealed in the diffraction pattern. Similar experiments were carried out on $\{1\bar{1}1\}_\beta$ foils. The thin foils were kept at room temperature for a week. A diffraction pattern very similar to Fig. 3(c) was obtained from such foils, which contained rather large (~ 2000 Å in diameter) precipitates. This result is published elsewhere [8].

The extra reflections in Fig. 3 can not be accounted for by the 9R- or ω-type structure but by the 2H-type structure proposed by Takezawa and Sato [4]. In the $[1\bar{1}1]$ zone (c), the estimated intensity of extra spots by calculating the structure factors for the 2H-type phase is represented by s (strong), m (medium) and w (weak), which are in qualitative agreement with the observed intensity of the spots. Thus we may conclude that 2H-type phase appears in the quenched β-brass as a result of aging.

3.4 Aging effect at room temperature

Depending upon the foil orientation and the aging temperature, the aging effect is different as mentioned below. In the case of $\{001\}_\beta$ foils, spinodal decomposition takes place at first by aging at room temperature (r.t.) and then the 2H-type phase appears in the spinodally decomposed phase [8]. {111} foils are, as explained in the above section, easily decomposed to a mixture of β and 2H-type phases at r.t. [8]. Figure 4(a) is a diffraction pattern slightly off the $[0\bar{1}1]$ zone taken from a specimen which had been kept at r.t. for a week after thinning, and (b) is a dark field image taken by using the arrowed spots which can not be explained by the 2H- or ω-type structure but by the 9R-type structure. Many particles are observed with faults in the contrast image (b). This clear contrast image was never observed in a fresh specimen, i.e., the dark field image using the same 9R-type spots is very vague. In contrast to the change of image with aging time, a particular change in the diffraction pattern was not recognized in the $\langle 011\rangle_\beta$ zone.

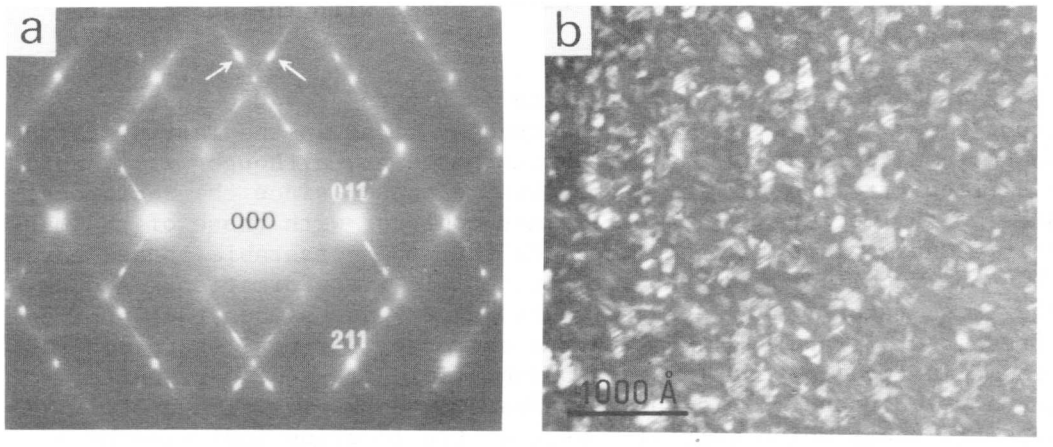

Fig. 4. (a) represents diffraction pattern, slightly off $[0\bar{1}1]_{\beta}$ zone taken from $(0\bar{1}1)_{\beta}$ foil. (b) is corresponding dark field image taken by arrowed spots representing 9R-type structure.

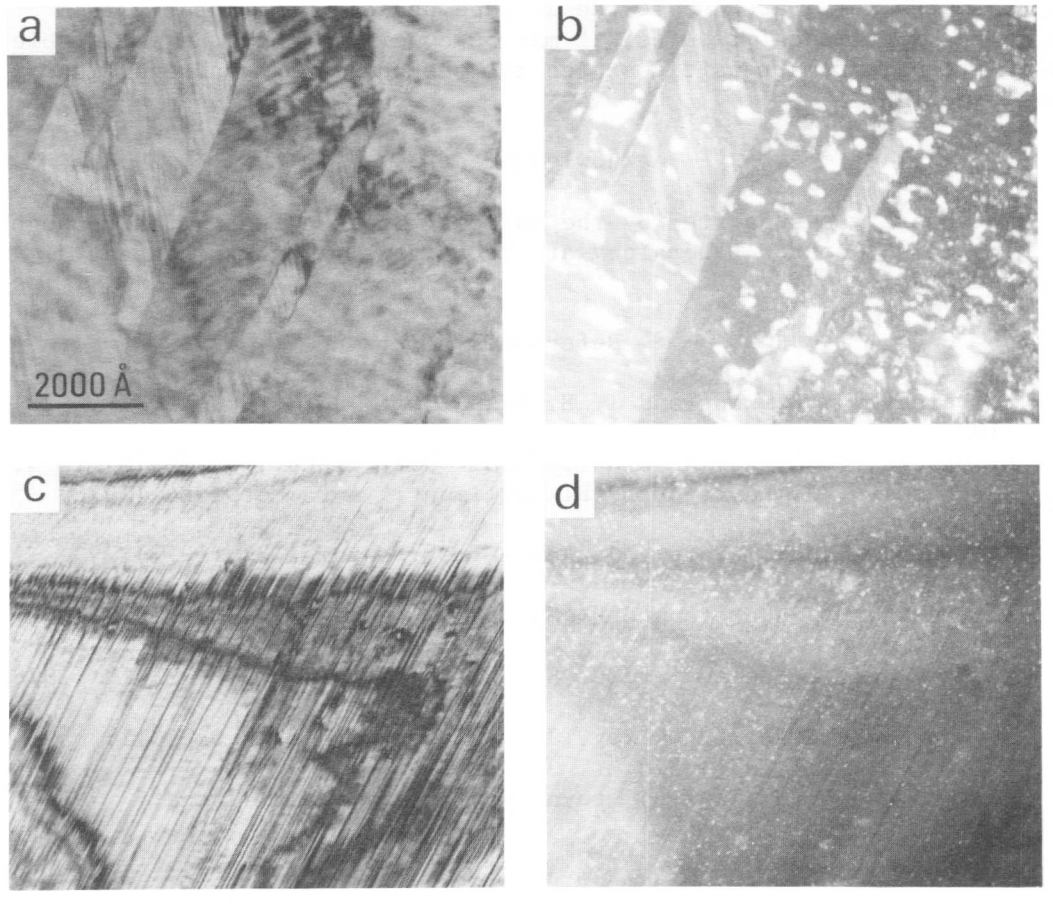

Fig. 5. (a) is bright field image of martensite and (b) is dark field image taken by 9R-type extra spot. (c) is martensite with $\sim [010]_{9R}$ normal and (d) is corresponding dark field image taken by $1\bar{1}1_{2H}$ spot.

3.5 Relation between 9R-type or 2H-type phase with the subsequent martensitic transformation

On cooling a specimen, martensite is formed at -40°C in the present alloy. The extra spots observed at first in the matrix diffraction patterns persist in the martensite patterns, although extra spots are difficult to observe in the martensite phase, since the reciprocal planes of the metastable phases are not coplanar with those of the martensitic ones. This strongly suggests that the metastable phases have nothing to do with the subsequent martensitic transformation. A dark field image taken with the extra spots is very vague when the specimen is fresh, but in an aged specimen the extra spots reveal sharp contrast as shown in Fig. 5 where (a) is a bright field image of martensite taken at -100°C and (b) is the corresponding dark field image using 9R-type extra spots which initially were at the location indicated by a single arrow in Fig. 2(a). It is clearly shown that the 9R-type particles remain in the martensite. (c) and (d) are respectively a bright field image of martensite and the corresponding dark field image taken by a $1\bar{1}1_{2H}$ spot, where the foil orientation is very close to the $[010]_{9R}$ zone of martensite which is nearly parallel to the $[001]_{\beta}$ zone. The bright spots in (d) are due to the 2H-type phase. Consequently from the above experimental results, it may be concluded that the metastable phases are not premartensitic states for the subsequent martensitic transformation.

Acknowledgement

This work was supported by the National Science Foundation through the Materials Research Laboratory at the University of Illinois at Urbana-Champaign.

References

[1] L. Delaey, J. Perkins and T. B. Massalski: J. Mat. Sci., 7 (1972) 1192.
[2] K. Otsuka, C. M. Wayman and H. Kubo: Met. Trans., 9A (1978) 1075.
[3] A. Prasetyo, F. Reynaud and H. Warlimont: Acta Met., 24 (1976) 1009.
[4] K. Takezawa and S. Sato: J. Japan Inst. Metals, 37 (1973) 793 (in Japaneses).
[5] K. Otsuka, H. Sakamoto and K. Shimizu: to be published in Trans. JIM.
[6] Y. Murakami, L. Delaey and G. S. Dullenkopf: Trans. JIM, 19 (1978) 317.
[7] M. Chandrasekaran, L. Delaey, J. V. Paemel and R. Rapacioli: Z. Metall., 67 (1976) 323.
[8] H. Kubo and C. M. Wayman: to be published in Met. Trans.

ELECTRON DIFFRACTION ANOMALIES PRIOR TO THE MARTENSITIC TRANSFORMATIONS IN In-Tl ALLOYS

Alain LASALMONIE[+] and Paul COSTA[+]

In Tl alloys have been examined in electron microscopy at temperatures above M_s.

It is shown that the diffused intensity observed in the diffraction patterns does not increase when the C' modulus decreases. The anomalies are attributed to static defects. The shimmering effect occuring on the images is attributed to the heating of the foil by the electron beam.

I - INTRODUCTION

Numerous papers have described the electron microscopy anomalies, observed in B2 compounds in the vicinity of the martensitic transformation.

These anomalies consist in a mottled contrast on the images and in diffused intensity along $\langle 110 \rangle$ in the diffraction patterns.

These anomalies are generally described as premonitory effects which result from the softening of the elastic modulus $C' = 0.5\ (C_{11} - C_{12})$, the static or dynamic nature of the phenomenon is not yet clear.

The shimmering effect described by Cornelis et al. [1] seems to be an indication of dynamical fluctuations propagating in the specimens.

The premartensitic origin of the anomalies is however a matter of controversy in most B2 alloys [NiAl [2], β Brass [3]] which are often chemically metastable ; the formation of small precipitates is difficult to avoid and could be responsible for the observed effects.

In-Tl is a more convenient alloy for the study of premartensitic effects since :

a) no precipitation can occur

b) there is a complete softening of C' as the temperature goes to M_s [4,5]. The change in the structure is from f.c.c. to f.c.t. and can be totally described by a set of $(1\,1\,0)\langle 1\bar{1}0 \rangle$ shears.

This work summarizes the observations made on three alloys : In-24%Tl ($M_s = 220°K$) , In-28%Tl ($M_s = 100°K$) and In-30%Tl ($M_s \simeq 0°K$).

[+]ONERA, 29 avenue de la Division Leclerc 92320 Châtillon (France)

Images and diffraction patterns were made on thin foils in the electron microscope. The temperature of the experiments could be adjusted between 77°K and 300°K in the cooling stage of the microscope.

II - EXPERIMENTAL RESULTS

1°) Reciprocal lattice : diffused intensity streaks are visible on the diffraction patterns ; for instance in the (001) plane, ‹110› streaks are observed (Fig. 1). A systematic study shows that the intensity is diffused in the (110) planes around the ‹110› directions.

2°) Bright field images : a mottled contrast is observed (Fig. 2) ; some shimmering occurs when the beam is focused ; the shimmering effect fades with the time, it is also of much smaller amplitude when the accelerating voltage of the electrons is one million volts.

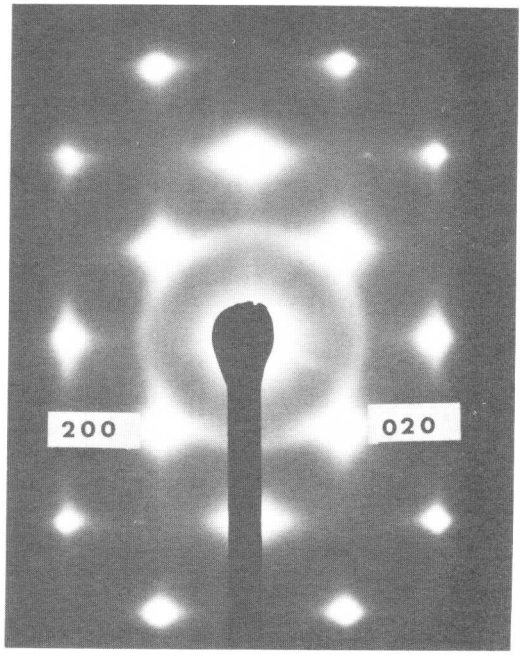

Fig. 1 : (001) diffraction pattern of In-24Tl at 300°K.

Fig. 2 : mottled contrast in In-28Tl at 300°K.

3°) Influence of the temperature : in the three alloys, no increase of the diffused intensity has been witnessed when the temperature was lowered towards M_s.

III - CONCLUSIONS

1°) The anomalies in In-Tl are much smaller than in the B2 compounds, although the C' modulus takes much lower values. The diffused intensity is also more isotropic in In-Tl than in NiAl or Brass, which however have a smaller anisotropy ratio around M_s in the vicinity of M_s : 30 for In-Tl [6] 10 for NiAl [7] and β Brass [8] . In InTl diffused intensity does not vary strongly when C' goes near zero.

It is thus inferred that no simple correlation exists between the strength of the anomalies and the softening of C'. On the basis of the observations made on InTl the very strong ⟨110⟩ streaks observed in B2 compounds seem rather surprising and cannot be due only to the anomaly in the shear modulus.

2°) The fact that the diffused intensity was found to be temperature independent 100°K and 300°K even in In-30Tl, where C' remains almost a constant, indicates that the phenomenon is not thermally activated.

3°) The shimmering effect originates in the local heating of the foil by the electron beam.

REFERENCES

[1] J. CORNELIS, R. OSHIMA, N.C. TONG, C.M. WAYMAN - Scripta Met. 8, p. 133, 1974.
[2] A. LASALMONIE - Scripta Met. 11, p. 527, 1977.
[3] H. MORIKAWA, K. SHIMIZU, Z. NISHIYAMA - Trans. Jap. Inst. Metals, 8, p. 145, 1967.
[4] N.G. PACE, G.A. SAUNDERS - Proc. Roy. Soc. London A, 326, p. 521, 1972.
[5] P.J. GUNTON, G.A. SAUNDERS - Solid state comm. 12, p. 569, 1973.
[6] D.B. NOVOTNY, J.F. SMITH - Acta Met 13, p. 881, 1965.
[7] K. ENAMI, J. HASUNUMA, A. NAGASAWA, J. NENNO - Scripta Met. 10, p. 879, 1976.
[8] A. PRASETYO, R. REYNAUD, H. WARLIMONT - Acta Met. 24, p. 651, 1976.

Electron Microscopical Observations of a thermoelastic Ni-Al Alloy

R. Portier, D. Gratias and W.M. Stobbs[+]

Nickel rich Ni-Al alloys have been examined, using electron microscopy, in the premartensitic state. A number of effects were observed, notably the apparently surface precipitation of a second phase as well as general distortions of small regions of the b.c.c. material. These small regions tended to be extended perpendicular to <112> directions and lattice fringe images showed the {110} lattice fringes to be disturbed. It is argued that this latter result can be interpreted in terms of the displacements occuring in thin foils as a result of the presence of the $\langle 110 \rangle_{q}$ $\langle 1\bar{1}0 \rangle_{\varepsilon}$ transverse acoustic phonons well known in alloys of this type. Further consideration is given to the variety of local displacements which might result through the anharmonic coupling of these phonons, in either the strain field of a crystal defect or in a thin region.

I. Introduction

There are two main problems associated with the investigation of instabilities of the b.c.c. lattice in alloys which undergo themoelastic transformations. Firstly the very fact that the lattice is unstable tends to mean that a number of potentially competitive reactions can occur and secondly, the course which transformations follow is bound to be strongly dependent on the geometry of the thin foil examined when using transmission electron microscopy. This latter point need not mean however that all thin foil results should be discarded: provided that account is taken of the likely effects of the presence of the local free surfaces the resultant amplification of some of the reactions of the material can provide useful information on what is likely to happen in bulk.

B2 Ni-Al will undergo thermoelastic transformations over an extended temperature range as a function of the binary composition and there is extensive evidence [1] for the shear stiffness $(C_{11}-C_{12})/2$ decreasing while its temperature coefficient becomes positive with increasing Ni concentration. The crystallography of the transformation has also been thoroughly investigated [2] so the alloy should be suitable for the electron microscopical investigation of any precursory effects associated with the martensitic transformation. Furthermore there has been some recent controversy [3,4,5,6] about the origin of certain electron diffraction anomalies in the alloy and this itself is suggestive of the materials instability and potential tendency to show perhaps competitive reactions in thin foil form. We have consequently undertaken a high

---

C.E.C.M./C.N.R.S., 15 Rue Georges Urbain 94400-Vitry/Seine, France.
+ Dept. of Metallurgy and Materials Science, Cambridge, England.

resolution electron microscopical investigation of the state of thin foils of B2 Ni-Al near to their martensitic transformation temperature and give an interpretation of our results in terms of the displacements associated with $\langle 110 \rangle_q$ $\langle 1\bar{1}0 \rangle_\varepsilon$ transverse acoustic phonons.

II. Results

NiAl alloys were prepared by R.F. melting of 4N Nickel and Aluminium with a subsequent fast quench. Foils for examination in the electron microscope were made by electropolishing in $HClO_4/C_2H_5OH$ or $HClO_4$/Butyl alcohol with additional ion beam thinning in one instance. The electron microscopical observations, using a JEOL 120CX machine with an objective lens with C_s of 2.5mm, were concentrated on alloys containing 58; 62; 62.5 wt%Ni which showed no bulk martensite at room temperature.

A systematic study of the streaking associated with <110> reflections indicated, in agreement with other authors [3,6], that these streaks could attributed consistently to the presence of $\langle 110 \rangle_q$ $\langle 1\bar{1}0 \rangle_\varepsilon$ transverse acoust phonons. Interesting effects which can be associated with these phonons are best observed in diffraction patterns obtained at {110}. A pattern obtained from a rather thin foil region is shown in figure 1. A ring pattern may be seen with the second ring of $\langle 110 \rangle_{bcc}$ spacing and the third of $(200)_{bcc}$ spacing. The relative size of the first ring and the apparent {111} texture indicated by the third ring is strongly suggestive of an fcc or hexagonal phase with surprisingly accurate correspondence of $\langle 220 \rangle_{fcc}$ and $\langle 200 \rangle_{bcc}$. Images taken using the spot marked A in figure 1 are indicative of a rather irregular morphology of precipitation which appeared to be associated with the surfaces of the foil (figure 2). Ion beam thinned fields showed a stronger ring pattern and more intense precipitation. The apparent lattice spacings are not consistent with any oxide such as Al_2O_3 which might be expected. The presence of the "surface phase" and in particular the proximity of reflections from it to the $2/3(222)_{fcc}$ "ω" reflection made examination of contrast effects associated with this latter reflection difficult; however images obtained using apertures including the adjacent 111 reflection showed not only the variab orientation of the surface phase but also in some regions fringes which might be associated with interference of 2/3 222 with A (see figure 1) at a spacing of approximately 5Å (figure 3).

The further streaking of reflections in <121> directions as seen in figure 1 is characteristic of the alloy. Note the way in which tangential streaks (associated with a given reflection) are stronger than radial streaks. This suggests an essentially transverse component of the displace ments associated with the streaking and in an attempt to gain a further understanding of the origin of the scattering, lattice fringe images were obtained with the optic axis at $1/2(1\bar{1}1)$ and $1\bar{1}0$, 001 and $1\bar{1}1$ equally excited. The images were variably modulated with however a distinct tendency to show regions perpendicular to $1\bar{1}2$ and $\bar{1}12$, suggestive of local misorientations or variable lattice spacing. The general appearance of such images is indicated by figure 4 and the region marked B is shown at a higher magnification in figure 5. The <112> streaking indicating variability of at least the lattice fringes associated with the $[1\bar{1}0]$ lattice spacing (2Å) is demonstrated by the optical diffraction pattern

shown in figure 6. It should be noted that while some of the fringes seen in figure 4 are undoubtedly associated with the surface precipitate the variable spacing of the banding as well as the marked variation in the extent though not of the direction of the streaking in optical diffraction patterns is not consistent with either moiré effects or the sort of elastic strain field distributions which might be expected for the surface precipitates. Given the locally changing contrast of the lattice fringes it is difficult to relate their variable spacing, characteristically in regions elongated in <111> directions, with any specific lattice spacing variability. At the same time it is also however difficult to imagine any other origin for the effects observed.

A consistent interpretation for such a variable lattice spacing can be arrived at by considering how the $\langle 110\rangle_q$ $\langle 1\bar{1}0\rangle_\varepsilon$ transverse acoustic phonons might interact in thin regions of the foil where surface relaxations could lead to their being locked and anharmonically coupled. For example the in phase coupling of $\langle 101\rangle_q$ $\langle \bar{1}01\rangle_\varepsilon$ with $\langle 0\bar{1}1\rangle_q$ $\langle 011\rangle_\varepsilon$ would result in a row of atoms along the $1\bar{1}\bar{1}$ direction being displaced in the $\bar{1}12$ direction. Other rows in the $(1\bar{1}2)$ plane suffer other displacements (all in the $(1\bar{1}\bar{1})$ plane) as a function of the magnitude of $\underline{q}$ however the displacements above would tend to be the most extensive and the greatest for small $\underline{q}$. This type of addition is thus consistent not only with the variable lattice fringe spacing seen here, but also with the morphology of the apparently distorted regions seen in Cu-Al-Ni alloys in which no other precipitation effects are observed at least in the rapidly quenched state [7]. Such anharmonic coupling of phonons could also occur in bulk in the strain fields of defects and it would be surprising if this type of interaction were not important in the transformation.

III. Discussion

If the implication of the anharmonic coupling of phonons, as suggested above, is in fact of any relevance to the transformation behaviour of an unstable b.c.c. phase it is worthwhile considering other possible classes of addition and examining the evidence for their existence or otherwise. The addition of $\langle 10\bar{1}\rangle_q$ $\langle 101\rangle_\varepsilon$ and $\langle 101\rangle_q$ $\langle 10\bar{1}\rangle_\varepsilon$ would give longitudinal distortions which would be largest in the 100 direction in local regions elongated in the 001 plane in 010 directions. There is some evidence for thin foil effects in Ni-Ti suggestive of this type of distortion giving intensity at approximately 2/3(200) [8]. Another general type of distortion could be produced by the coupling of three waves: for example $\langle 1\bar{1}0\rangle_q$ $\langle 110\rangle_\varepsilon$, $\langle 10\bar{1}\rangle_q$ $\langle 101\rangle_\varepsilon$ and $\langle 01\bar{1}\rangle_q$ $\langle 011\rangle_\varepsilon$ would give regions of maximum longitudinal distortion which would be of alternative compressional and dilatational form and localised along the 111 direction. This is suggestive of the "ω" distortion well documented in Zr-Nb alloys. Again the addition of the three waves with q vectors in the (111) plane can result in regions again elongated in the 111 direction but with transverse displacements and suggestive of the apparently transverse nature of the "ω like" 2/3(222) reflection seen in Cu-Al-Ni alloys [7].

It should now be clear that interpretation of the local displacements in terms of the various apparently possible phonon additions leads to a high degree of flexibility. It is thus instructive to consider the

contraints on the thermoelastic transformation which can be understood by the application of group theory. Using the notation described elsewhere [9] and generally available crystallographic data [2] any one orientation of parent can give 24 martensitic variants:

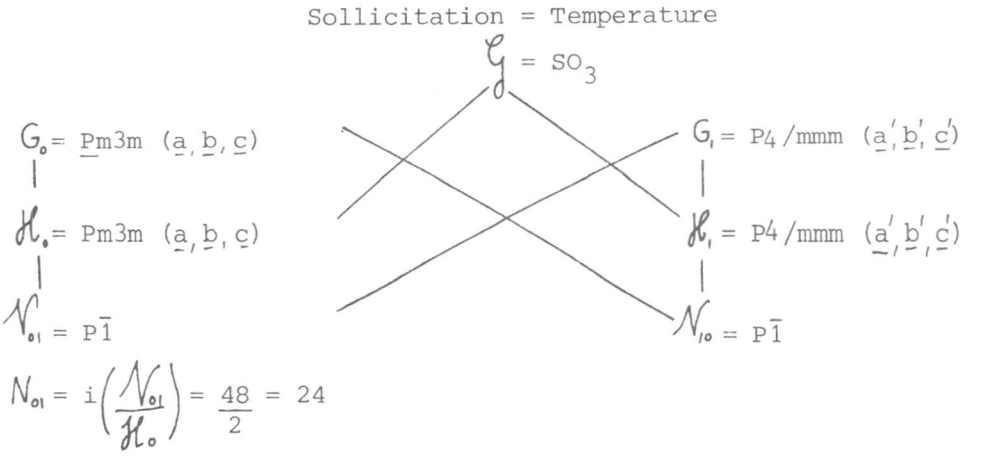

$$N_{01} = i\left(\frac{\mathcal{N}_{01}}{\mathcal{H}_0}\right) = \frac{48}{2} = 24$$

However, given that the transformation is thermoelastic, reversion to the b.c.c. form must give the initial variant of parent. Further the transformation occurs by the migration of interphase boundaries. Thus, in this situation, the specific b.c.c. product from the martensite reversic is determined by the nature of the group intersection of any two variants of the martensites formed in the forward transformation. Here these intersection groups (P$\bar{1}$) are subgroups of the group of the parent phases and cannot generate other orientations of the parent phase.

IV. Conclusion

While we have not observed the bulk precipitation phenomena described by some other authors in b.c.c. B2 Ni-Al [4,5] we have characterised a number of thin foil effects which occur in the b.c.c. phase. These include the surface precipitation and localised distortion of the b.c.c. matrix which we suggest can be interpreted in terms of the displacements associated with the $\langle 110 \rangle_g$ $\langle 1\bar{1}0 \rangle_\varepsilon$ transverse acoustic phonons. We further suggest that the coupling of such modes in bulk in locally variable elastic strain fields could result in a number of the well known apparently competitive reactions to the martensitic transformation which an unstable b.c.c. phase can undergo including the production of "ω distortions".

References

[1] N. Rusović and H. Warlimont: Phys. Stat. Sol. 44(a) (1977) 609.
[2] S. Chakravorty and C.M. Wayman: Met. Trans. 7A (1976) 555.
[3] K. Enami, J. Hasunuma, A. Nagasawa and S. Nenno: Scripta Met. 10 (1976) 879.
[4] A. Lasalmonie: Scripta Met: 11 (1977) 527.
[5] F. Reynaud: Scripta Met. 11 (1977) 765.
[6] K. Enami, A. Nagasawa and S. Nenno: Scripta Met. 12 (1978) 223.
[7] W.M. Stobbs, R.J. Henderson and A.M. Crossley, ICOMAT 79.
[8] W.M. Stobbs, ICOMAT 79.
[9] D. Gratias and R. Portier ICOMAT 79.

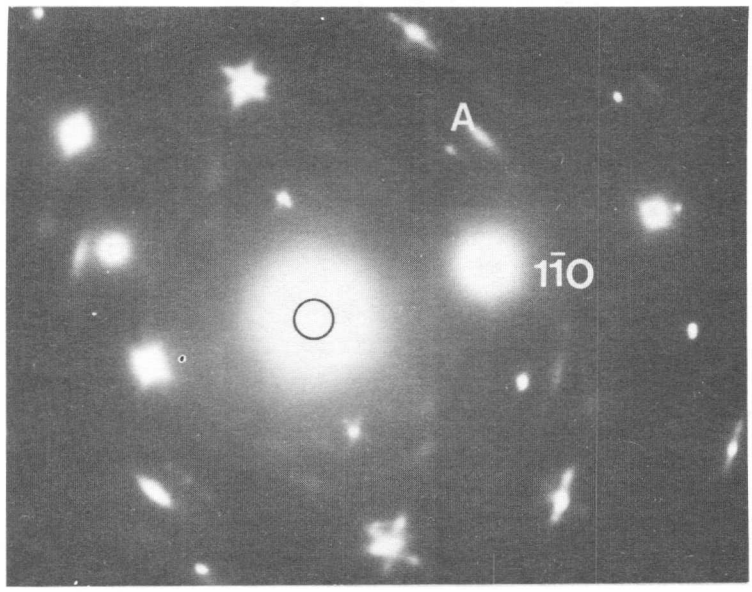

Fig.1
(110)diffracting
pattern

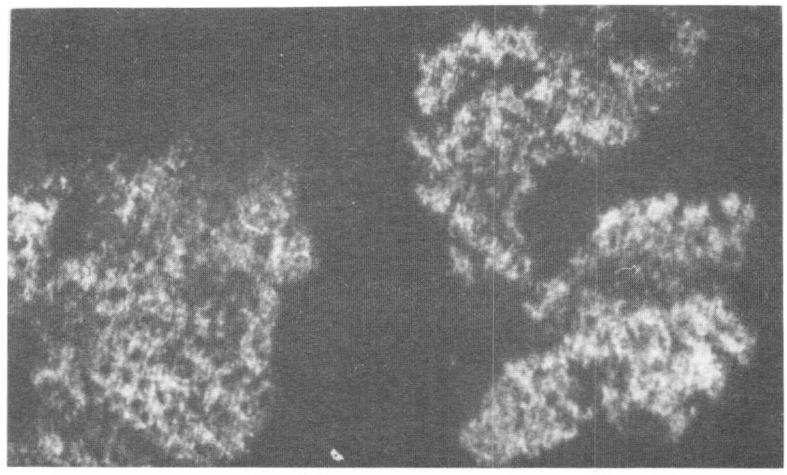

Fig.2
Dark field =
ring (A)

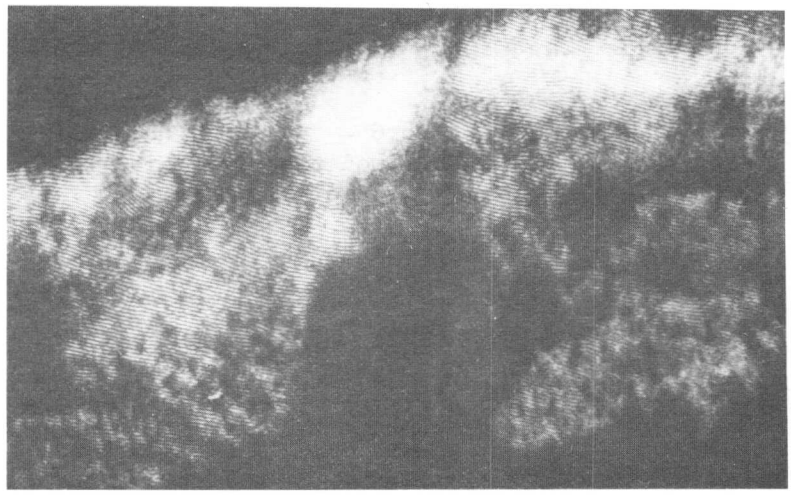

Fig.3
Dark field =
$\omega+1\bar{1}1$+ring(A)

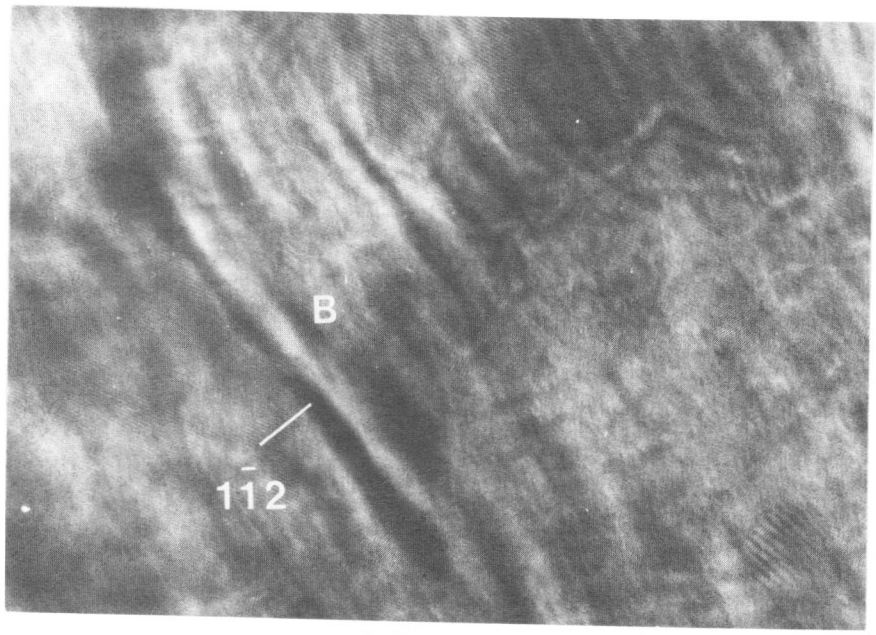

Fig.4
lattice fringe image using $1\bar{1}0$,001, $1\bar{1}1$,000

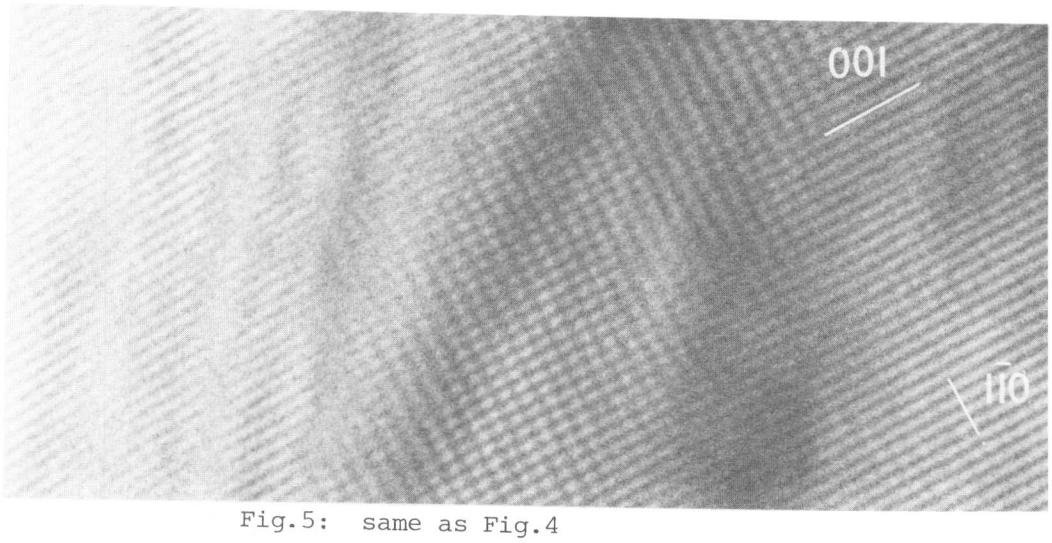

Fig.5: same as Fig.4

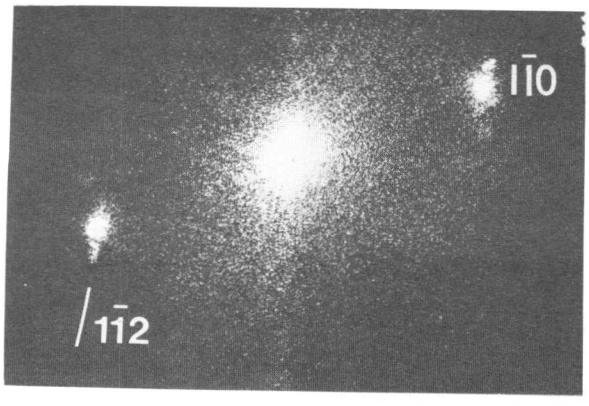

Fig.6
optical transform of area like B of Fig.4.

Preaging Austenite and Post-Aging Martensite - A Review of Recent Results

P. G. Winchell

The effect of preaging austenite on the lattice of the corresponding martensite is restricted by symmetry and has been determined in two alloy systems: Fe-Ni-Ti, which clusters, and Fe-Pt, which orders, and additional data is available in Fe-Al-C and Fe-Ni-C alloys. A formalism for describing mean lattice strains caused by point defects is available. The effect of post-aging of martensite is especially significant in carbon-bearing martensites even for subambient aging temperatures. Modern TEM, Mössbauer, and X-ray diffraction studies show that during aging carbon-rich regions develop with increased local displacement of metal atoms but no change in mean strain. Martensites in which not all atoms are located by a homogeneous correspondence with the austenite behave differently. Examples include Fe-Mn-C martensite in which a low as-quenched c/a ratio increases during subambient aging, and Fe-Ni-Ti martensites in which clusters have grown to coherent precipitates of sufficient size to locally resist martensitic transformation.

Introduction

The effects of aging on iron-base martensite are significant and have been the subject of many interesting reports. Work is far from complete and the present contribution is merely a partial review of an area in which future developments may change our perspective. Aging may be carried out either before or after transformation and the resulting effects in martensite are significantly different. Aging of austenite may result in short-range or long-range ordering or in precipitation. Upon transformation the structure in austenite may be swept atom-by-atom into a corresponding structure in martensite or it may stick in its present structure and force transformation to pass it by. These two processes have significantly different consequences in the microstructure and lattice of the resulting martensite. On the other hand, aging freshly formed martensite may result in ordering, clustering, or precipitation directly in the martensite with attendant changes in its properties. In the important case of carbon-bearing martensite, the term aging is used to describe the early stage of tempering before formation of a distinct carbide phase. Special consideration will be given to this process. Reverse martensite transformation requires the transfer of the age-induced structure in the martensite to the austenite with attendant modification of its properties.

School of Materials Engineering, Purdue University, West Lafayette, Indiana 47907

The preaging of austenite is considered first. The resulting structure, which has the point symmetry of austenite, can correspond to a structure which restricts the symmetry of martensite. The rules of this symmetry reduction are of interest as are experimentally observed examples of aging treatments and alloying additions which produce such reductions in symmetry. Some experimental observations are available for austenite aged to produce structures which do not transform to the corresponding structures in martensite but instead lose coherency during transformation.

The post transformation aging of carbon-bearing martensite will be considered second. Although many substantial questions remain, a significant beginning has been made in understanding this important process and some data indicate a regime which may precede aging in some alloys.

Preaging Austenite

Theoretically the distortion of martensite formed from preaged austenite is supposed to follow certain rules. These rules apply to martensite whose structural features have transformed atom-by-atom into the corresponding martensite. John Cahn's [1] theory is that the minimum point symmetry of martensite, M, is a subgroup of the point symmetry of the austenite A_e and that of the lattice strain, S. We shall assume it is the largest such subgroup. A quantitatively special lattice strain applied to "simple" austenite, i.e., austenite with one equivalent atom at each lattice point, results in a substantial increase in the symmetry of the transformation product from M to M_e, i.e., M_e is a supergroup of M formed for a special A by a special S. The relationship is shown in Fig. 1A in general and is illustrated for the Bain strain of face-centered cubic austenite to body-centered martensite in Fig. 1B. The loss of symmetry when supergroup formation is not achieved is substantial, but the deviation in size and shape from the highly symmetric unit cell of M_e is often small, i.e., using the symbols M and M_e to represent the lattices

$$M = (I + \varepsilon)M_e \tag{1}$$

where the strain components ε_{ij} are commonly less than 0.1.

One way of discussing the source of these strains is to characterize by a distribution of point defects the deviation of austenite from the "simple" structure referred to above [2]. This point of view then allows the (at least formal) assignment of the strain to the strength of the point defect represented in the linear approximation by double force strengths, P_α and to their concentration, C. According to Kroner [3] in the Voight notation

$$\varepsilon_\alpha = \sum_{\beta}^{6}{}_{1} S_{\alpha\beta} P_\beta C \tag{2}$$

where $S_{\alpha\beta}$ are the martensite crystal compliances. One may imagine that a given martensite could have one, two, or more different kinds of point defects present and the resulting deviation of the M lattice from M_e will be due to the superimposed strains each calculated according to Eq. (2) and the total strain exhibiting the point symmetry of M. In fact the existence of several sources of martensite tetragonality has been suggested by several authors [4,5,6,7,8,9,10,11,12,13] and since many of these sources are developed by preaging, some experimental results will be presented below.

Probably the best known point defect in "simple" austenite is the carbon atom. It is present (by popular acclaim supported by film-recorded X-ray intensity measurements [14]) in the octahedral site in austenite and the corresponding site in martensite is the "c" oriented octahedral, c-O, site in the martensite. For iron-carbon alloys of 0.6 wt.pct C or higher, the linear variation of the martensite tetragonality with carbon content indicates linear behavior. Tetrahedral and octahedral sites for carbon both have tetragonal point symmetry and interstitials in either site might lead to tetragonality of the lattice, but the reasonable assumption must be that a carbon atom has a significantly smaller energy in one of these sites than in the other. X-ray attenuation [15,16,17] and neutron diffraction studies [18] strongly favor the c-oriented octahedral site, c-O, but the last result might be interpreted on the basis of some appreciable number of carbon atoms in other sites. Quantitative agreement of better than ten percent between tetragonal lattice distortions of iron-carbon martensite and strength of stress-induced Snoek damping in carbon-bearing ferrite given in Table I [19] coupled with the above data, points to occupation of the c-oriented octahedral sites by nearly all the carbon atoms in iron-carbon martensite as present at room temperatures soon after quenching. This is not to say that immediately following quenching due to a local perturbation of the correspondence, other sites may not be temporarily occupied or may be occupied in local (and coherently diffracting) regions. Indeed some evidence for such behavior in high carbon and in some alloy steels has been reported [11,17,20]. If such sites are distributed thoughout the structure they appear to be unstable and even at rather low temperatures carbon atoms jump and increased population of the c-O sites occurs [21].

The clustering of substitutional solutes in austenite either during quenching or during aging has resulted in additional sources of tetragonality. Fe-Ni-Ti alloys near 25 atomic pct. Ni and with 0 to 6 atomic pct. Ti have been fairly carefully examined [6,22,23,24,25,26]. Among the more recent contributions, Hall's work stands out because he was able to separate clearly the formation of coherent γ' preprecipitates as seen by X-ray satellite formation from the earlier formation of clusters which caused tetragonality in the subsequently formed martensite. His interpretation is that tetrahedral clusters of Ni_3Ti form in the austenite and transform to the corresponding cluster in martensite. The tendency of such tetrahedra to remain regular, i.e., to locally resist the Bain strain, accounts for the increase in tetragonality of the resulting martensite observed due to clustering. That tetragonality increases with titanium content and increased aging for short aging times. According to other work [23], heat treatments producing clustering also

account for a significant decrease in M_S, possibly due to the decreased stability of the less symmetric martensite which results [25,27]. The hardness of the martensite is not much affected by the clustering or the later precipitation.

Continued preaging of Fe-Ni-Ti austenite results in preprecipitate formation as revealed by the appearance of satellites in the austenite X-ray diffraction pattern [22,25] and by transmission electron microscopy, TEM [22,28]. As a result of this process the martensite tetragonality is substantially reduced [25] and the X-ray lines from the martensite are broadened. Very broad γ' X-ray diffraction maxima are found and these exhibit particle size and strain broadening as well as peak shifts which indicate faulting. TEM also shows γ' and shows it to be rotated by several degrees with respect to the austenite matrix due to the rotation accompanying martensite formation [28]. Not only do the incoherent γ' particles cause inhomogeneous strain but they also are responsible for large residual shear strains in the martensite (a shear angle of 2% was recorded in a Fe-Ni-6% Ti alloy aged 710°C for 1 hr)[29]. Such strains and rotations are not due to lattice distortions alone and consequently do not follow the scheme outlined in Fig. 1. Rather they represent an interaction between the γ' particles and the microscopic strain accompanying transformation. Their development may impose limitations on mechanical properties to be expected from such martensite.

Other alloy systems in which such clusters and preprecipitates form may well behave in an analogous way and some data is available on Fe-Ni-Nb and Fe-Ni-Al alloys [10,30]. These coupled with Fe-Ni-Ti results given above indicate that the M_S is further decreased during early preprecipitation, which is accompanied by continued clustering, that hardness of the martensite is not much changed, and that austenite formed by reversal of such martensite is substantially strengthened [31].

Larger particles embedded in transforming austenite prevent martensite formation locally [32]. The particles cast "shadows of austenite" extending away from the plate midrib. The orientation of these shadows is taken to indicate the direction of motion of the transformation front and on that basis shows that martensite/austenite transformation proceeds from the midrib outward during the formation of the plate.

Another alloy system involving increased martensite tetragonality due to formation of clusters during quenching and aging is Fe-Al-C [7, 33,8,34]. The fact that austenites containing 4 to 8 percent aluminum transform to martensite which has greater tetragonality than would be observed in Fe-C martensite at the same C-level appears to be due to the formation of clusters of $FeAl_3C$, which is the Perovskite-type carbide present at equilibrium in this system. Preprecipitates have been observed by TEM [33], but maximum tetragonality may again precede preprecipitate formation. Some work on martensites which form from these aged austenites shows that as-quenched martensite has an even higher tetragonality [34]. A complete study of aging effects in Fe-Al-C is not yet available. Of particular interest will be the way enhancement of tetragonality varies with aging time. One might expect a behavior not totally different from that observed in Fe-Ni-Ti alloys. The enhanced tetragonality in Fe-Ni-C martensite may have a source analogous

to that in Fe-Al-C [35,36]. Consideration of this literature is complicated by several reports of long-range order near Fe_3Ni but such order due to ordinary heat treatment is not confirmed (see below).

Alloys which order a substantial portion of the austenite and subsequently transform according to the Bain lattice strain produce martensite which inherits the corresponding order. The remarkable effects of long-range ordering of binary alloys on both tetragonality and transformation behavior are documented for Fe-Pt near Fe_3Pt [12,13, 37,38,39] and more interesting results may be expected soon [40]. Increasing the ordering in Fe_3Pt by preaging at 550°C to 650°C results after transformation in a change from martensite with 2 pct. tetragonality to one with more than 10 pct. A depression of the M_s is also observed and a very marked depression of the A_s [38,39]. This latter depression appears to be the result of a discontinuous change in the reversal kinetics, and may reflect a change in the reversal process associated with the onset of thermoelastic behavior. Cahn has suggested this possible consequence of prevention of supergroup formation [1], but other factors may also be important [39]. The suggestion has been made that Fe-Ni martensite is tetragonal because of short-range order in the austenite [9,41] but by normal heat treatment procedures the generation of long-range order does not occur [41,42,43].

The discussion of the effects of preaging austenite on the lattice and properties of the resulting martensite has been predicated on the assumption that the same lattice strain is applied throughout the transforming region. Only transformed austenite structures or austenite structures which resisted transformation have been considered. Evidence that the lattice correspondence is not everywhere the same has been put forward [44,45,11,21,46,47,48,49,50,51]. Iron-manganese-carbon austenite transforms to martensite which exhibits tetragonality below that of iron-carbon martensite of equal carbon content [46]. Fe-Re-C behaves similarly [50]. Moreover this tetragonality reduction is even more marked in martensite never brought above about -100°C. The several explanations of this behavior all involve the perturbation of the lattice strain accompanying the transformation. The perturbations put carbon atoms in "a" or "b" octahedral sites by (011)[01$\bar{1}$] twinning [52] or in tetrahedral sites by transformations involving shuffles [49] or by transformation involving previous formation of hexagonal close-packed martensite [53]. Some evidence of (011) twinning is available from TEM observations of very high carbon steels [54]. In evaluating the significance of evidences of deformation in martensite whose lattice parameters have changed since its formation, due account should be made of the necessity of accommodating such strains. Such strain does not produce local stress if it is homogeneous when viewed on a fixed basis, e.g., volume change occurring homogeneously, but otherwise, e.g., for tetragonal changes in strain, local plastic deformation may result from lattice parameter changes rather than be its cause.

In summary a rough outline of some of the main effects of austenite preaging is gradually emerging as a result of a significant amount of careful experimental work and some interesting concepts. Although many desirable experiments remain to be carried out, a preliminary

summary of the pattern appears possible on the assumption that the lattice strain in most ferrous martensite is the Bain strain. The carbon atoms are usually in the "c" octrahedral sites. Very small atom clusters, short-range order or long-range order present in the quenched austenite are swept atom-by-atom into the corresponding structure in martensite and this structure prevents cubic symmetry and results in tetragonal symmetry. The strains so produced are not small compared to those of carbon (or nitrogen) and the correct structural interpretation of changes in parameters requires careful evaluation of all such sources [35].

Aging Martensite

This review will be confined to the low temperature tempering of carbon-bearing martensite, the upper temperature range of this regime is often referred to as aging and we will call the lower temperature regime recovery.

The recovery regime encompasses changes occurring in the temperature range up to about -50°C. In this temperature range the carbon atom in a normal c-O site is immobile during the time of an experiment [55,56,57]. Changes in tetragonality which are observed in Fe-2% C, Fe-Mn-C, Fe-Re-C, and Fe-Al-C [47,50,34] have been hypothesized to be due to carbon swept by transformation into high energy sites. The occupancy of such sites could be a consequence of local and perhaps even regular perturbations in the lattice strain or of dislocations. The observation of Mössbauer spectra of iron $\sim$ 2% carbon alloys in this same temperature range indicate a rather small change [58], which has been interpreted in agreement with the above hypotheses. Speculation on the nature of the high energy sites temporarily occupied by carbon atoms in these alloys depends on the alloy. Tetragonality is increased upon reheating in Fe-Re-C and Fe-Mn-C martensites whereas it is decreased upon reheating Fe-Al-C martensite. In the former case as mentioned previously, the hypothesized high-energy defect is either carbon in the tetrahedral site, trapped there because of a local or perhaps, even periodic shuffling of the lattice, or carbon in the a, b octahedral sites, forced there by (011), [0$\bar{1}$1]twinning which results in twins too narrow to produce coherent diffraction. In the case of Fe-Al-C martensites a possible defect is the 001 carbon atom pair where both atoms occupy c octahedral sites. The formation of this pair should be favored by formation of Fe_3Al-C clusters. The pair should have a high positive interaction energy and the effect on tetragonality of its disappearance would probably be a reduction in tetragonality because its double force strength would be larger than twice the double force characterizing a single c-O carbon atom.

In the aging regime much more data is available and some conflicting hypotheses to explain the results have been presented. Mössbauer spectra from high carbon martensite formed in Fe-C, Fe-Mn-C, and Fe-Ni-C all exhibit qualitatively the same changes [58,59,60,61, 62,63,20,49] but the interpretation of these changes varies with the

investigator. Fujita [20,49] interprets the changes as representing the change of dissolved carbon from 50% in tetrahedral, T, sites and 50% in c-O sites to a much higher proportion in c-O sites and another group agrees with this concept [60]. Kaplow and co-workers [61,62,57] interpret the differences in the spectra rather than the spectra themselves and from the development during aging of a spectrum like that of pure iron, Kaplow concludes that carbon clustering is occurring. Two other new six line spectra arise; they are hypothesized to be due to iron atoms in carbon clusters -- iron atoms supposed to differ in their magnetic moments and hence supposed to be components of Fe_4C structurally isomorphous with Fe_4N. Other investigators conclude from the spectra themselves that carbon clustering in octahedral sites is occurring but without identification of Fe_4C [59,58]. The kinetics of the changes observed during aging are compatible with its interpretation as carbon clustering [59,57].

Significant diffuse electron scattering develops during aging [64,65,66] and more results may be expected soon [67]. A cone of scattering is observed about the 001 axis through each selected area diffraction spot. The cone angle is less than 30° and the intensity within the cone is strongest along 10,2 reciprocal lattice directions originating at the spot. An interpretation [68] has been given which accounts for the pattern on the basis that this scattering is just due to scattering from c-O carbon atoms which interact elastically. The more intense spots which develop during aging have been interpreted as Fe_4C in the form of plates 10Å thick along $(10,2)_M$ and dark field images have been obtained using these spots which show partially periodic arrays [64,65,66]. More information in this area can be expected shortly [67]. Recently X-ray diffuse scattering near the 002 reciprocal lattice peak and near the 001 reciprocal lattice direction has been detected, Fig. 2 [17]. This scattering is more intense on the side nearer the origin and in view of the small atomic scattering factor of X-rays by carbon is certainly due to metal atom displacement. This same X-ray work by P. C. Chen has also clearly shown that in an 18 Ni, 1 pct. C alloy, martensite freshly quenched and aged between -50°C and +40°C no change in the 200, 020, or 002 interplanar spacing occurs until carbon depletion due to precipitation starts at about 40°C (1 hr tempering time). This result shows unambiguously that a significant change in interstitial site occupancy does not occur in this alloy in this key temperature range, i.e., no change from tetrahedral to octahedral occupancy occurs. If generalization to higher carbon contents holds, this new evidence weighs against the interpretations of Mössbauer spectra in terms of tetrahedral to octahedral site occupancy. Rather the c-O carbon cluster produce no change in the average metal atom displacement but produce an increase in the RMS metal atom displacement in the 001 direction and hence a decrease in the intensity of the 002 peak [17] as expected [73].

In this discussion I have interpreted experimental results on the basis that (with some possible exceptions) the carbon in Fe-C martensite is quenched into the "c" octahedral sites and stays in such sites during the aging process. Thus, the tetragonality of iron-carbon martensite is supposed to be due to such point defects. Previous work

has shown that, if the M_S is suppressed by nickel, similar tetragonality is maintained to very low carbon levels [69,70]. A question is why doesn't carbon redistribute equally among the a-O, b-O, and c-O sites? This question is especially pressing in view of the expectation that with each diffusion jump carbon atom tries out a differently ordered octahedral site. Khachaturyan [71] has offered a reason for this behavior which I paraphase here. He suggests that the residual stress inherent in the transformation favors the "c" sites and may hold the carbon there during their initial jumps until clustering occurs the local carbon level is increased and the carbon atoms support each other [72,73]. Some indirect indication that residual stress may be important in determining the occupation by carbon of octahedral sites is provided by the recent comparison of the X-ray 002 peaks (in an 18% Ni 1% C alloy) from martensite formed in austenite polycrystals and from that formed in austenite single crystals. The martensite formed in polycrystals has a much broader 002 peak but the 020, 200 peaks are about the same [17]. Some extra intensity exists between the 002 and the 200, 020 peak in martensite from the polycrystal and this intensity can be approximated as a broad peak from some nearly cubic martensite. Such a variable situation is not unexpected, due to the stress variations in and near martensite plate intersections if residual stresses influence the c-O site occupancy.

In summary, the aging of carbon-bearing martensite often consists of clustering of carbon atoms which occupy c-octahedral sites. These sites are favored by residual stresses arising during transformation and by the clustering process itself. Clustering results in very small carbon-rich plate shaped domains on $(102)_M$. In very high-carbon steel and in some alloy steels (Mn, Re, Al) some high energy sites are occupied by carbon in freshly quenched martensite. These sites probably depopulate rapidly in a recovery stage preceding or overlapping aging.

Summary

Preaging austenite can produce structural changes which if swept atom-by-atom into martensite result in martensite tetragonality comperable in magnitude to that produced by carbon. Long-range order has this effect. More extensive aging which causes formation in austenite of precipitates that do not transform produces reduced tetragonality and large elastic shear strains in martensite and severe distortion and rotation of the precipitate.

Aging carbon-bearing martensite, which may be preceded by a depopulation of high-energy carbon sites, often consists of the clustering of carbon atoms in c-oriented octahedral sites. Aging occurs rapidly at room temperature.

Acknowledgements

The support of the National Science Foundation DMR 77-08688 is greatfully acknowledged. Helpful results were supplied to me in the MIT Sc.D. thesis of A. Sherman, A. K. Sachdev, and H. C. Ling, and the Purdue Ph.D. thesis of P. C. Chen.

References

[1] J. Cahn: Acta Met., 25(1977), 721.
[2] P. G. Winchell and G. R. Speich: Acta Met., 18(1970), 53.
[3] E. Kroner: Kontinuums theories der Versetzunger und Eigenspannungen, Springer-Verlag, Berlin, Germany, (1958), 158.
[4] N. J. Petch: J. Iron and St. Inst., 147(1943), 221.
[5] K. H. Jack: Proc Roy Soc., A208(1951), 200.
[6] Y. Honnorat, G. Henry, and J. Manenc: Mém. Scient. Rev. Mét, 62 (1965), 429.
[7] M. Watanabe and C. M. Wayman: Scripta Met., 5(1971), 109.
[8] L. I. Lysak, A. G. Drachinskaya, and N. A. Storchak: Phys. Met. Metallogr., 34(1972), #2, 107.
[9] J. W. Cahn and W. Rosenberg: Scripta Met., 5(1971), 101.
[10] J. Manenc, J. Bourgeot, and H. de Buer: Scripta Met., 2(1968), 453.
[11] L. I. Lysak, Yu. N. Vovk, and Yu. M. Polishchuk: Phys. Met. Metallog., 23(1967), #5, 123.
[12] T. Tadaki and K. Shimizu: Scripta Met., 9(1975), 771.
[13] H. Chang, S. Hahn, and S. Sasti: Met. Trans, 7A(1976), 1796.
[14] N. J. Petch: J. Iron and Steel Inst., 145(1942), 111.
[15] H. Lipson and A. M. B. Parker: J. Iron and Steel Inst., 149(1944), 123.
[16] S. C. Moss: Acta Met., 15(1967), 1815.
[17] P. C. Chen: Ph.D. Thesis, Purdue University, May 1979.
[18] I. R. Entin, V. A. Samenkov, and S. Sh. Shilst'shtein: Doclady A. N., 206(1972), 1096.
[19] J. C. Swartz, J. W. Shilling, and A. J. Schwoeble: Acta Met., 16 (1968), 1359.
[20] F. E. Fujita, T. Moriya, and H. Ino: Proc. Int. Conf Science Tech. Iron and Steel, Suppl. Trans. I.S.I.J., 11(1971), 1273.
[21] L. I. Lysak and S. P. Kondrat'yev: Phys. Met. Metallogr., 30(1970), #5, 78.
[22] J. K. Abraham, J. K. Jackson, and L. Leonard: Trans. ASM, 61(1968), 233.
[23] J. K. Abraham and J. S. Pascover: Trans. Met. Soc. AIME, 245(1969), 759.
[24] R. E. Miner: Met. Trans., 2(1971), 1250.
[25] M. M. Hall and P. G. Winchell: Acta Met., 25(1977), 735.
[26] L. P. Gun'ko and V. V. Kokorin: Sov. Phys. Dokl., 23(1978), #5, 340.
[27] J. W. Cahn: Scripta Met., 11(1977), 81.
[28] T. Maki and C. M. Wayman: Acta Met., 25(1977), 695.
[29] V. G. Veeraraghavan and P. G. Winchell: To be published.

[30] E. Hornbogen and W. A. Meyer: Z. Metallkde., 58(1967), 445.
[31] S. Jin, J. W. Morris, Jr., Y. L. Chen, G. Thomas, and R. I. Jaffee: Met. Trans., 9A(1978), 1625.
[32] H. J. Neuhauser and W. Pitsch: Acta Met., 19(1971), 337.
[33] R. Oshima and C. M. Wayman: Met. Trans., 3(1972), 2163.
[34] L. I. Lysak, N. A. Storchak, and A. G. Drachinskaya: Phys. Met. Metallogr., 43(1977), #3, 138.
[35] G. V. Kurdjumov: Symp. on New Aspects of the Martensitic Transformation Supp. to JIM, 17(1976), 9.
[36] G. V. Kurdjumov and L. K. Mikhailova: Sov. Phys. Dokl., 21(1976), #11, 677.
[37] T. Tadaki, K. Katsuki, and K. Shimizu: Symp. on New Aspects of the Martensitic Trans., Supp. to JIM, 17(1976), 187.
[38] S. Kajiwara and W. S. Owen: Met. Trans., 5(1974), 2047.
[39] M. Umemoto and C. M. Wayman: Met.Trans., 9A(1978), 891.
[40] H. C. Ling: Sc.D. Thesis, Mass. Inst. of Tech., June 1978.
[41] V. G. Veeraraghavan, C. F. Eagen, H. R. Harrison, and P. G. Winchell: J. Appl. Phys., 47(1976), 4768.
[42] S. H. Chen and J. W. Morris, Jr.: Met. Trans., 8A(1977), 19.
[43] A. P. Miodovnik and D. Skinner: Pt. Met. Rev., 22(1978), 21.
[44] L. I. Lysak and Yu. N. Vovk: Phys. Met. Metallogr., 20(1965), #4, 63.
[45] L. I. Lysak, Yu. M. Polishchuk, and Ya. N. Vovk: Phys. Met. Metallogr., 22(1966), #2, 119.
[46] L. I. Lysak, S. P. Kondrat'yev, Yu. M. Polischuk: Phys. Met. Metallogr., 36(1973), #3, 85.
[47] L. I. Lysak, V. Ye, Danil'chenko, Yu. M. Polishchuk, and A. I. Ustinov: Phys. Met. Metallogr., 41(1976), #2, 108.
[48] R. Oshima, H. Azuma, and F. E. Fujita: Symp. on New Aspects of Martensitic Trans., Supp. to JIM, 17(1976), 293.
[49] F. E. Fujita and C. Shiga: ibid., 287.
[50] L. I. Lysak and L. O. Andrishchuk: Phys. Met. Metallogr., 28(1969), #2, 166.
[51] L. I. Lysak, Ya. N. Vovk, A. G. Drachinskaya, and Yu. M. Polishchuk: Phys. Met. Metallogr., 24(1967), #2, 95.
[52] A. L. Roytbourd and A. G. Khachaturyan: Phys. Met. Metallogr., 30(1970), #6, 68.
[53] L. I. Lysak and B. I. Nikolin: Phys. Met. Metallogr., 22(1966), #6, 64.
[54] M. Oka and C. M. Wayman: Trans. Met. Soc. AIME, 242(1968), 337.
[55] A. E. Lord, Jr., and D. N. Beshers: Acta Met., 14(1966), 1659.
[56] M. Hillert: Acta. Met., 7(1959), 653.
[57] N. DeCristofara, R. Kaplow, and W. S. Owen: Met. Trans., 9A(1978), 821.
[58] V. N. Gridnev, V. G. Gavrilyuk, V. V. Nemoshkalenko, Yu. A. Polushkin, and O. N. Razumov: Phys. Met. Metallogr., 43(1977), #3, 109.
[59] J. M. Genin and P. A. Flinn: Trans. Met. Soc. AIME, 242(1968),1419.
[60] M. Lesoille and P. M. Gielen: Met. Trans., 3(1972), 2681.
[61] W. K. Choo and R. Kaplow: Acta Met., 21(1973), 725.
[62] N. DeCristofaro and R. Kaplow: Met. Trans. 8A(1977), 35.
[63] P. M. Gielen and R. Kaplow: Acta Met., 15(1967), 49.

[64] V. I. Izotov and L. M. Utevskiy: Phys. Met. Metallogr., 25(1968), #1, 86.
[65] S. Nagakura, K. Shiraishi, Y. Hirotsu, A. Ono, and H. Yotsumoto: 8th Int. Congress on Elect. Mic., Camberra, 1(1974), 664.
[66] S. Nagakura, K. Shiraishi, and Y. Hirotsu: Jap. Inst. Metals, 16(1975), 601.
[67] A. K. Sachdev: Sc.D. Thesis, Mass. Inst. Tech., June 1977.
[68] A. G. Khachaturyan and T. A. Onisimova: Phys. Met. Metallogr., 26(1968), #6, 12.
[69] A. K. Sachdev and P. G. Winchell: Met. Trans., 6A(1975), 59.
[70] P. G. Winchell and M. Cohen: Trans. ASM, 55(1962), 347.
[71] A. G. Khachaturyan and G. A. Shatalov: Phys. Metals Metallogr., 32(1971), #1, 5.
[72] G. V. Kurdjumov and A. G. Khachaturyan: Acta Met., 23(1975), 1077.
[73] D. W. Hoffman and M. Cohen: Acta Met., 21(1973), 1215.

Table I. Rate of Change of Tetragonality with Atomic Ratio Solute for Carbon and Nitrogen Dissolved in Body-Centered Iron. After Swartz, et al. [19].

Technique of Measurement	Alloy	
	Fe C	Fe N
Martensite Lattice Parameters	.94	.90
Ferrite Anelasticity	.87	.80

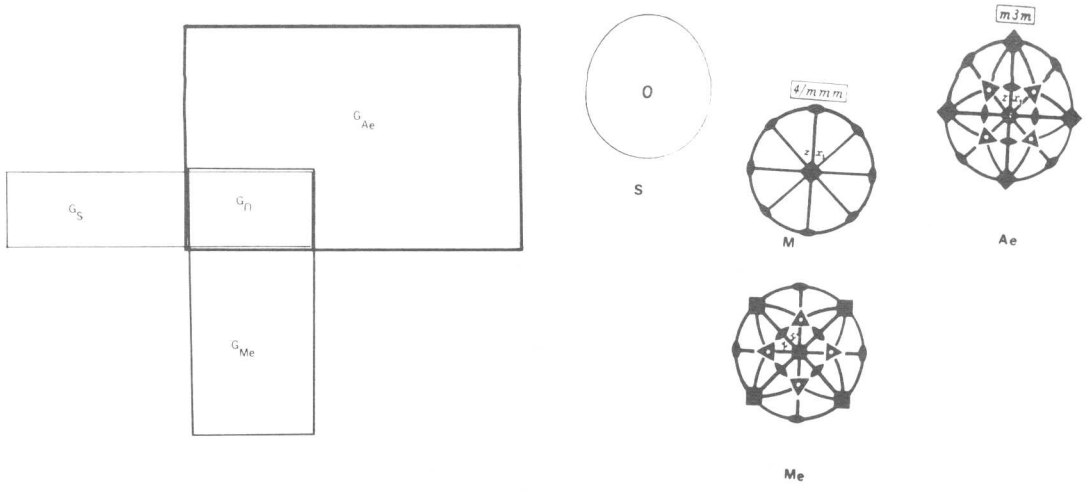

a. b.

Figure 1. a. Point Symmetry of Martensite and Austenite.

Ae = Austenite of Maximum Symmetry
Me = Martensite of Maximum Symmetry
S = Strain
$\cap$ = Intersection and Symmetry of Transformation Product

b. Point Symmetry of Ferrous Martensite formed by the Bain Strain.

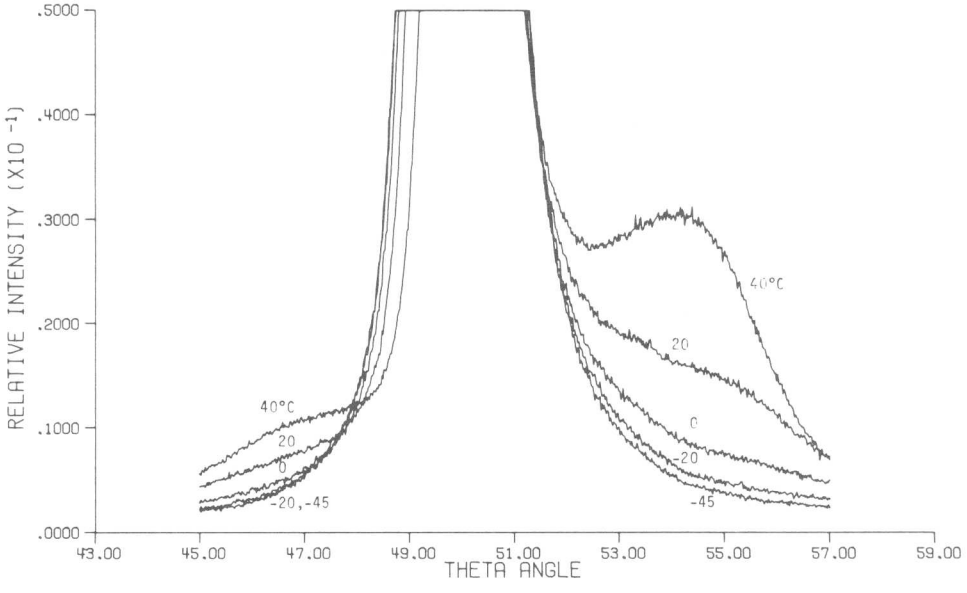

Figure 2. Diffuse CrK_α X-Ray Scattering near the 002 in Fe 18%Ni 1%C Martensite Quenched and Tempered at the Temperature Shown. After P.C. Chen.

Carbon Atom Redistribution During the Ageing and Early Stages of Tempering of Ferrous Martensites

P.A. Beaven, M.K. Miller and G.D.W. Smith

ABSTRACT

The redistribution of carbon atoms during the early stages of ageing of martensite has previously only been studied by indirect methods. The computer-controlled atom probe field ion microscope permits the direct, quantitative determination of carbon concentrations with a spatial resolution of 1nm, and thus all stages of the martensite decomposition process become amenable to direct study.

Detailed analysis of the sequence of ions field evaporated from twinned regions of a high carbon martensite (0.78wt.%C) reveals evidence of carbon segregation to twin interfaces, and of carbon atom clustering in the matrix, after ageing at room temperature. More extensive changes of the same kind are observed after tempering for 1 hour at 160°C. In a low carbon martensite (0.21wt.%C), quenched and tempered for 10 minutes at 150°C, very low matrix carbon levels are found, together with pronounced enrichment of carbon in the region of a lath boundary. Preliminary studies of high-nickel carbon martensite with an M_s temperature of 15°C are also reported.

I. Introduction

The carbon atom redistribution processes occurring during the ageing or low temperature (zeroth stage) tempering of ferrous martensites have been the subject of a large number of investigations in recent years. A wide variety of physical techniques has been used to study the phenomena involved, but there is still disagreement about the nature of some of the processes occurring. Several recent review articles indicate the divergent views which are held [1-4]. In the case of plain, low-carbon martensites, there is a considerable body of evidence which indicates that seqregation of carbon atoms to lattice defects is the dominant ageing process in the temperature range up to about 200°C [5], although the absence of tetragonality in these martensites has also been interpreted in terms of the redistribution of carbon atoms between the various interstitial sublattices of the martensite structure. In the case of higher carbon martensites, a number of additional effects arise. Carbon atom clustering effects, and the early stages of carbide formation, have been widely invoked to explain, e.g., X-ray diffraction data [6-8], dilatometry, electrical resistivity and hardness measurements [8-10], electron microscopy and electron diffraction data [11-16] and Mossbauer spectroscopy results [17-20] from a wide range of martensites. A rather different interpretation of the ageing data for high carbon martensites is offered by Fujita et al. [21-23], in terms of the redistribution of single carbon atoms from octahedral to tetrahedral

Department of Metallurgy and Science of Materials, University of Oxford, Parks Road, Oxford, England.

sites within the martensite lattice. The processes have also been considered by Khachaturyan et al. [2, 12] in terms of an ordering reaction within the martensite structure.

In the present work the distribution of carbon atoms was investigated experimentally using the technique of FIM atom probe time of flight mass spectrometry [24]. The atom probe is particularly suitable to this kind of investigation both because of its high spatial resolution and because of its sensitivity to light elements such as carbon. Since high resolution micrographs can be obtained in conjunction with the recording of mass spectra the interactions between carbon atoms and lattice defects become amenable to direct study.

II. Experimental

The composition of the materials used in the present work are summarised in Table I together with their heat treatments. The iron-nickel alloy used was kindly supplied by the Department of Materials Science, M.I.T., and was taken from the same stock of material as that studied previously by Sherman [15].

The atom probe used for this investigation was a computer-controlled time of flight instrument with an overall flight path of 1.25m. A full account of this instrument may be found elsewhere [25].

The following experimental conditions were used:

a) Base pressure of $<3\times10^{-10}$ torr
b) All analyses made in a vacuum of $<1\times10^{-9}$ torr (i.e. image gas removed)
c) Neon image gas pressure 1×10^{-4} torr
d) Specimen cryostat cooled with liquid nitrogen
e) Pulse fraction 15%
f) Pulse repetition rate 50Hz.

III. Results

Segregation in low carbon martensites.

A neon field ion micrograph of a specimen of low carbon martensite (A) containing a lath boundary is shown in Figure 1. Complementary TEM images of the same boundary are shown in Figure 2. This boundary contained a periodic array of dislocations with a spacing of approximately 8nm. Neither the field ion microscope nor the transmission electron microscope revealed any evidence of carbide precipitation nor the presence of a retained austenite film. Atom probe analyses taken from the matrix and the boundary regions are summarised in Table II, the results clearly indicating that carbon segregates to the boundary. However, these figures underestimate the magnitude of the segregation effect since the area analysed also includes a substantial proportion of atoms from the matrix on each side of the boundary. Assuming the carbon to be present in a single atomic layer at the interface an enrichment factor of 70:1 over the levels of carbon found in the matrix is obtained. This direct observation of carbon segregation to a lath boundary

confirms the interpretation of the resistivity data given by Speich [5].

Segregation in high carbon martensites.

Field ion micrographs of the high carbon (0.78wt.%) martensite are shown for the room temperature aged material (B) and the aged and tempered material (C) in Figure 3. These materials show a series of parallel twin boundaries (spacing 4-12nm) which appear as dark bands in both cases, with the width of the interface being greater in the tempered condition. The results of the atom probe analyses of the boundary and matrix regions are also given in Table II. For the room temperature aged material the degree of enrichment is again underestimated, because of the circular probe aperture, and using the same calculation as before, the local concentration at the boundary is estimated to be in excess of 35at.%C. In the tempered condition carbon levels of up to 20at.% have been measured over regions 2nm in width across the boundary.

Clustering.

Detailed analysis of the ion-by-ion sequence obtained for the 0.78wt.%C steel after room temperature ageing has shown that the distribution of carbon in the matrix is not homogeneous. A high proportion of the carbon atoms desorb as molecular ions C_2 and C_3 and carbon atoms are also observed to desorb on successive high voltage pulses. It is therefore probable that there is a close association between carbon atoms in the lattice. At this stage we cannot completely exclude the possibility that the formation of molecular ions may be an artefact of the experimental technique, arising from the clustering of carbon atoms on the specimen surface just prior to evaporation. However the cryogenic temperature involved and the high incidence of molecular ions makes this possibility seem unlikely. Preliminary experiments using iron-nickel-carbon alloys D and E ($M_S \sim 15°C$) have also given evidence of clustering. In this case the specimen blank was first water quenched to 25°C, at which temperature the field ion specimen was made and then inserted into the atom probe where the final liquid nitrogen quench was carried out. The first sequence of data was then collected immediately. This specimen was then allowed to age at room temperature for 8 hours after which a second sequence of data was obtained. The data were divided into blocks of 25 atoms. The experimental value for the number of carbon atoms within each block was then compared with the value expected under the assumption that the number of carbon atoms followed a Poisson distribution (i.e. a random distribution of carbon in the structure). The resulting histograms, each based on a total of approximately 5000 ions, are shown in Figure 4. In both cases the experimental values show a pronounced deviation from a random distribution, as there is an excess of blocks with 3 or more carbon atoms per block, and also an excess of blocks containing no carbon. This behaviour is consistent with the clustering of carbon atoms in the martensite matrix, although the two sets of data are not markedly different. Experiments with materials of lower M_S temperatures are planned to investigate these effects further.

IV. Conclusion

Atom probe studies of ferrous martensites are still in their infancy, but the above results show the ability of this experimental technique to give valuable and direct information about carbon atom redistribution processes. The segregation of carbon to lath boundaries and twin interfaces has been unequivocally demonstrated, and strong indications have been obtained that carbon atoms cluster rapidly in the matrix, even below room temperature. More sophisticated statistical analysis procedures are currently being developed, which should permit a quantitative approach to the desorption of the clustering and ordering of carbon atoms. The interaction of carbon atoms with individual dislocations should also be amenable to study, as should the interaction of carbon atoms with other solute species such as Si, Cr, V, and Mo.

References

[1] G.R. Speich and W.C. Leslie: Met. Trans., 3 (1972), 1043.
[2] G.V. Kurdjumov and A.G. Khachaturyan: Met. Trans., 3 (1972), 1069.
[3] Y. Imai: Trans. Japan Inst. Metals, 16 (1975), 721.
[4] G.V. Kurdjumov: Met. Trans. Series A, 7 (1976), 999.
[5] G.R. Speich: Trans. TMS-AIME, 245 (1969), 2553.
[6] G. Kurdjumov and L. Lyssak: J. Tech. Phys. U.S.S.R., 16 (1946), 1307.
[7] G. Kurdjumov and L. Lyssak: J. Iron Steel Inst., 156 (1947), 29.
[8] P.G. Winchell and M. Cohen: Trans. A.S.M., 55 (1962), 345.
[9] C.S. Roberts, B.L. Averbach and M. Cohen: Trans. A.S.M., 45 (1953), 576.
[10] H.O. Gerdien: Arch. Eisenhuttenw., 30 (1959), 673.
[11] V.I. Izotov and L.M. Utevsky: Fiz. Metal. Metalloved., 25 (1968), 98.
[12] A.G. Khachaturyan: Fiz. Tverd. Tela, 9 (1967), 2861.
[13] S. Nagakura, K. Shiraishi, Y. Hirotsu, A. Ono and H. Yotsumoto: Proc. 8th Intl. Congress on Electron Microscopy, Canberra, Australia (1974) Vol. 1, p. 664.
[14] S. Nagakura, K. Shiraishi and Y. Hirotsu: Trans. Japan Inst. Metals, 16 (1975), 601.
[15] A.M. Sherman: Ph.D. thesis, M.I.T. (1972).
[16] A.K. Sachdev: Ph.D. thesis, M.I.T. (1977).
[17] J.R. Genin and P.R. Flinn: Trans. TMS-AIME, 242 (1968), 1419.
[18] W.K. Choo and R. Kaplow: Acta Met., 21 (1973), 725.
[19] N. De Cristofaro and R. Kaplow: Met. Trans. Series A, 7 (1977), 35.
[20] N. De Cristofaro and R. Kaplow: Met. Trans. Series A, 9 (1978), 821.
[21] F.E. Fujita, C. Shiga, T. Moriya and H. Ino: J. Japan Inst. Metals, 38 (1974), 1030.
[22] C. Shiga, M. Kimura and F.E. Fujita: J. Japan Inst. Metals, 38 (1974), 1037.
[23] C. Shiga, F.E. Fujita and M. Kimura: J. Japan Inst. Metals, 39 (1975), 1205.
[24] E.W. Muller, J.A. Panitz and S.B. McLane: Rev. Scient. Instrum., 39 (1968), 83.
[25] M.K. Miller, D.Phil. thesis, Oxford University (1977).

Table I.

Composition and Heat Treatment of Alloys

Alloy	Composition	Austenitising Temperature	Subsequent Treatment
A	Fe-0.21 wt.% C	1000°C	WQ + 10 mins at 150°C*
B	Fe-0.78 wt.% C	1200°C	WQ, LNQ + RT*
C	Fe-0.78 wt.% C	1200°C	As B + 1 hr at 160°C*
D	Fe-18% Ni-0.5% C	850°C	WQ* LNQ (in situ)
E	Fe-18% Ni-0.5% C	850°C	As D + RT for 8hrs + LNQ

WQ = Water quenched; LNQ = 78°K quenched; RT = Room temperature aged
* denotes when field ion specimens made (in D and E total time from WQ to LNQ in situ was 20 mins).

Table II.

Summary of Atom Probe Analyses of Martensites
(from regions 2nm in diameter; all analyses in at.%)

Alloy		Matrix Composition	Boundary Composition
A	1%C	0.14 ±0.04%C	2.01±0.2%C
B	3.47%C	2.7±0.2%C	6.9±0.4%C
C	3.47%C	1.5±0.3%C	8.7±0.5%C

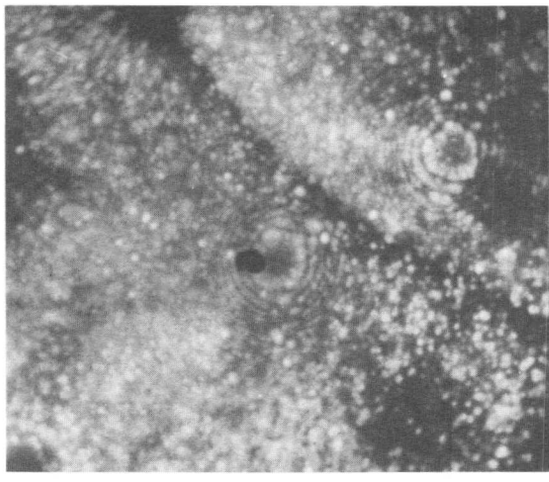

Figure 1. Neon Field Ion Micrograph of a low carbon Martensite specimen (A) containing a lath boundary.

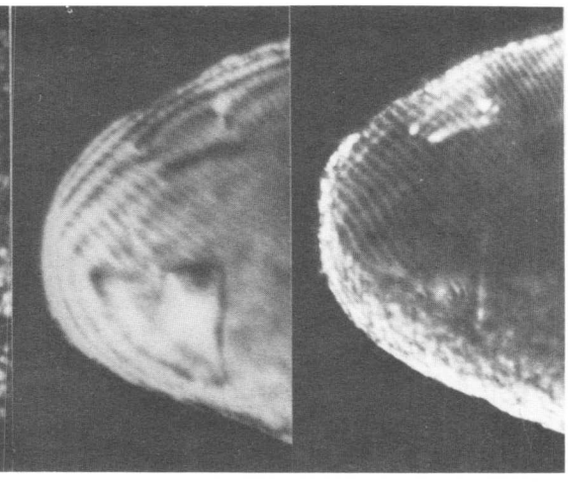

Figure 2. Complementary TEM Micrographs of specimen shown in Fig. 1.

Figure 3a. Neon Field Ion Micrograph of Room Temperature Aged High Carbon Martensite (B)

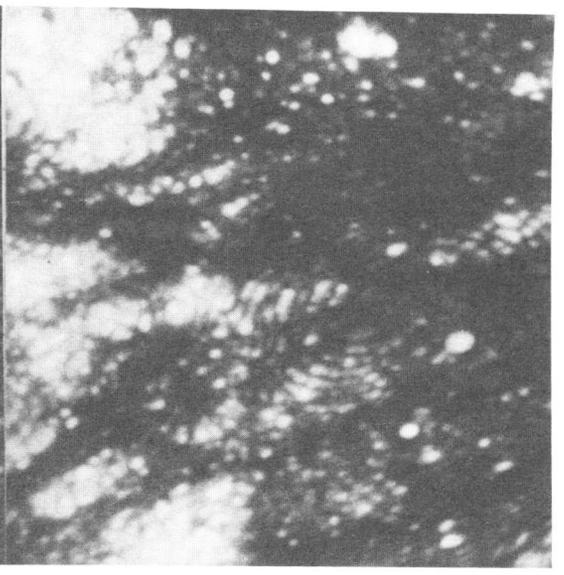

Figure 3b. Neon Field Ion Micrograph of Room Temperature Aged and Tempered High Carbon Martensite (C)

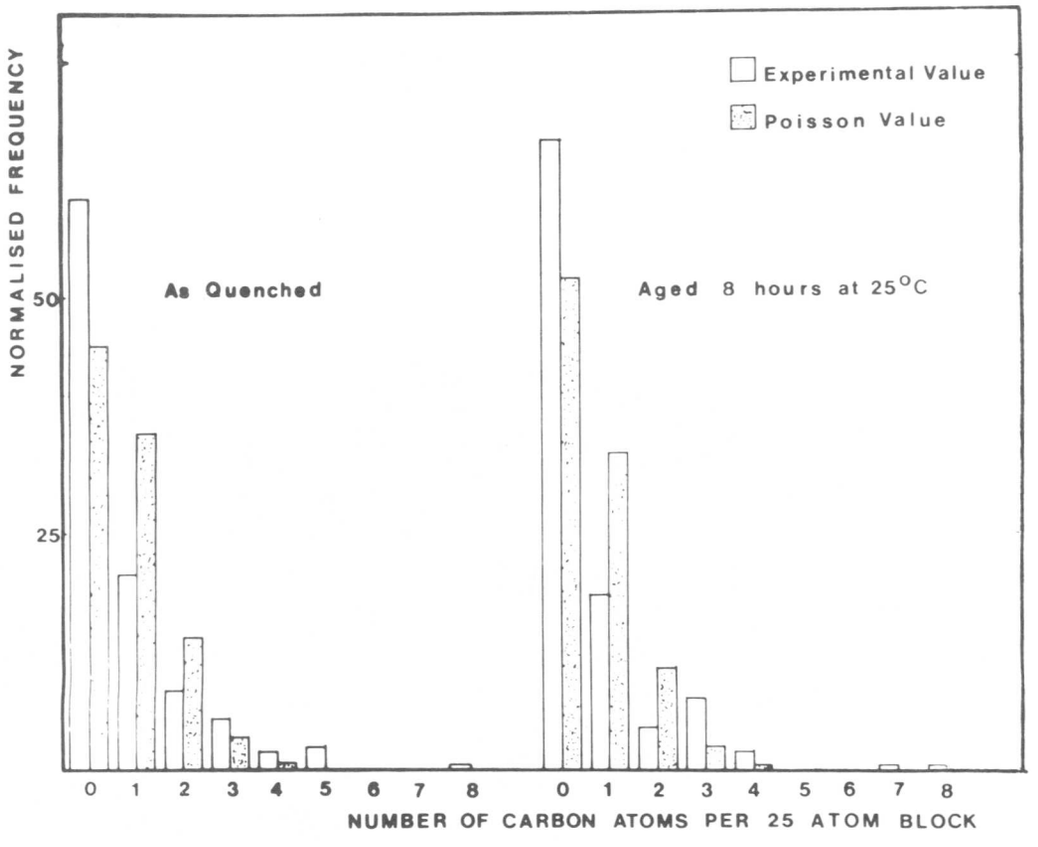

Figure 4. Histograms of the clustering behaviour of carbon in Fe-Ni-C Martensites D and E.

X-RAY DETERMINATION OF THE DISTORTIONS DUE TO CARBON ATOMS IN Fe-Ni-C MARTENSITE

P. C. Chen, B. O. Hall, and P. G. Winchell

ABSTRACT

Measurements of the profile and intensity of 200, 020, and 002 martensite peaks have been made for 1%C 18%Ni martensite formed from single crystalline and polycrystalline austenite as a function of tempering between - 45°C and 400°C. The results show that the effective "size" of the carbon atoms, which are in the 001/2 octahedral sites, increases during subambient aging, and the "first stage of tempering" involves significant reorientation of the martensite--probably by twinning, that martensite formed from polycrystals has finer diffracting domains and/or is more heavily strained than is martensite formed from single austenite crystals, and that an appreciable fraction of the martensite formed in austenite polycrystals is a nearly cubic solid solution of carbon.

(Paper will appear elsewhere.)

Isothermal Decomposition of the β_1' Martensite in Cu-Al. Morphological Study

H.Goldenstein* and I.G.S.Falleiros**

The isothermal decomposition of β_1' martensite of Cu-Al (11,3 to 11,7% Al) was studied in the $\alpha + \gamma_2$ field (520°C); it was observed the partial revertion from β_1' to the high temperature phase β_1 and the "in situ" transformation of β_1 to supersatured α phase. Latter, the γ_2 phase precipitates inside β_1, initially as globules which coalesces to form irregular plates. With long periods of treatment the α/γ_2 boundaries straigthen and becomes smooth, preserving the morphology of martensite and resisting spheroidizing. The results sugests that the α and γ_2 lattices have orientation relationships so as to have α/γ_2 interfaces of low energy in some directions (cusps in the α/γ_2 gama plot). These relationships can be explained as follows: - It is known that the basal plane $(12\bar{8})_{\beta_1'}$ of the martensite form a small angle with the $(110)_{\beta_1}$ plane during martensite revertion; it is probable that the β_1' basal planes become $(111)_\alpha$ planes of the f.c.c. phase during "in situ" transformation; the γ_2^α phases which precipitates coherently with β_1, will then maintain the same orientation relationship with α that the β_1 phase had with β_1'. To check the existence of these relationships the decomposition of β_1' in the $\alpha+\beta$ field (650°C) was also studied, resulting in a $\alpha+\beta$ structure resistant to spheroidizing, produced by the same set of reactions observed in the $\alpha+\gamma_2$ field.

I - Introduction

Tempering of Cu-Al β_1' martensite has been studied for a long time and by several techniques [1] to [6] (Fig.1). Experiments preliminary to this work have shown that the product of decomposition of β_1' in the $\alpha+\gamma_2$ field (520°C) has morphology resistant to spherodization. The objectives of the present work are: 1. To show that the reactions of decomposition of the martensite in Cu-Al alloys (11,3 to 11,7% in mass) may be identified by optical microscopy; 2. Explain the morphological stability of $\alpha+\gamma_2$ structures.

II - Experimental Procedure

Cu-Al alloys with composition between 11,3 and 11,7% Al in mass were induction melt, homogeneized, hot worked, and again homogenezeid. After quenching from 860°C, the structures of the alloys are fully martensitic, β_1'.

Isothermal treatments were made in salt baths. The metallographic specimens were mechanically polished and electrollytically etched with 1% aqueous cromic acid and 6 V tension, with aluminium cathode. This etchant only etches the interfaces between the products of decomposition

* Escola Politecnica da USP; ** Escola Politecnica da USP and Aços Villares S.A. - São Paulo S.P., Brazil, P.O.Box 8174.

of martensite. To reveal martensite, polarized light was used.

III - Results and Discussion

1) Isothermal Decomposition of β_1' at 520°C ($\alpha+\gamma_2$ field).

Isothermal treatments were made, for times between 5 sec and 20 hours.

Between 5 and 40 sec the following reactions were noted: -1) martensite (β_1') revertion to the high temperature β_1 phase. This was originally observed by Nishiyama, in thin foils, above 400°C [2]. The orientation relationship between martensite an reverted phase is $(110)_{\beta 1}$// $(128)_{\beta 1'}$ and $[111]_{\beta 1}$//$[210]_{\beta 1'}$ [2]. Morphologically the reaction is characterized by the formation of fine β_1 lamellae, along interlath boundaries of β_1', sets of parallel β_1 lamellae inside β_1' laths; the regions were martensite laths cross each other is preferential for the formation of β_1 as well (Fig.2). 2) "In situ" transformation of orthorhombic martensite in supersaturated f.c.c. α. Observed by X-Ray difraction in Cu-Zn-Ga alloys [3] and in Cu-Al by optical microscopy [4] and T.E.M. [5], it is a continuous reaction of stacking fault recovery. The reaction competes with the revertion and is identified by optical microscopy through the decrease in optical activity and the characteristic rose color [4] of supersatured α. The habit planes and morphology of martensite are kept. 3) Precipitation of allotriomorphic α crystals in the original β grain boundaries.

The sites where revertion begins suggest that the concentration of elastic stresses, in interfaces between self-accomodated laths and in lath crossings, play a role in the revertion. The set of parallel β_1 lamellae formed inside laths may be the result of nucleation in the internal striations, sites of high concentration of stacking faults, as observed by T.E.M. [6]. In the martensite, the compact planes (basal planes of the orthorhombic system) form a small angle (4°15') with the most compact (110) planes of β_1 and with the twinning plane of β_1'(128) which is the plane of interfaces between martensites laths as well [6]. After "in situ" transformation, the basal planes of β_1' become (111) planes of the α f.c.c. phase and are probably parallel to the (110) planes of the β_1; in this way β_1 has with α the same crystallographic relationships that it kept with martensite. α/β_1 interfaces are possibly low energy interfaces, corresponding $(110)_{\beta 1}$ or $(111)_{\alpha}$, most compact planes in the respective lattices. At 520°C, though, α/β_1 interfaces exist for short times only. α/β interfaces of low energy, are obtained by isothermal treatments of β_1' at 650°C ($\alpha+\beta$ field) as will be described below.

With times longer than 40 sec, the decomposition of β_1' at 520°C, besides the reactions described above, produces γ_2 precipitation. The reaction was originally observed by Cope [4]. The precipitates of γ_2 are isolated nodules at the beginning. The precipitate coalesce forming lamellae with ragged α/γ_2 boundaries. With long times of reaction the lamellae become more perfect, with interfaces more and more smooth, and the morphology of the resulting $\alpha+\gamma_2$ structure resembles clearly the

morphology of the original martensite. The structure is resistant to spheroidizing, at least in the times studied, Figs. (3) to (4).

γ_2 phase is cubic complex (γ brass structure) with lattice parameter 8,77A° while β is c.c.c. with parameter 2,9564A° at 6,72°C [7]. The γ_2 parameter is almost exactly three times the parameters of β and the unit cell of γ_2 if formed by stacking 27 (3^3 cubes) smaller c.c.c. cells, subtracting two atoms and relaxing the 52 atoms left. This suggests the possibility of coherence between β (or β_1) and γ_2, in all directions. The nodular form of γ_2, and the absence of γ_2/γ_2 interfaces support this suggestion.

If, as it seems probable, the α phase has crystallographic relationships corresponding to low energy interfaces with β_1, then γ_2 which is coherent with β_1, must have also low energy interfaces with α. There must be, then, low energy α/γ_2 interfaces in some directions, probably the directions corresponding to the most compact planes in the γ_2 and α lattices. This is the suggested reason for the resistance to spheroidization and the smothness of the α/γ_2 interfaces with increasing time of treatment.

2) Isothermal Decomposition of β_1' at 650°C ($\alpha+\beta$ field).

During isothermal treatment of β_1' at 650°C it was observed: a) - precipitation of α phase alotriomorphs in former β grain boundaries; b)- martensite revertion to β phase; c)- "in situ" transformation to α phase. The last reaction ocurred, in spite the temperature beeing probably higher than the A_f, showing that competition between the reactions with a "difusion mechanism" and the martensite revertion occurs. The volume fraction of α at the beginning is higher than the equilibrium volume fraction.

Between 5 and 30 sec the α/β interfaces becomes unstable and ragged, with the α volume fraction decreasing, until there are only thin α plates in a β matrix. With long periods of treatment (18 h), the α plates coarsen without spheroidizing maintaining straight α/β interfaces. This is evidence of low energy α/β interfaces produced by the same set of reactions observed in the $\alpha+\gamma_2$ field. (Fig. 5).

IV - Conclusions

1) The reactions of decomposition of the martensite in Cu-Al alloys (11,3 to 11,7% in mass) were identified by optical metallography.

2) Both the $\alpha+\gamma_2$ and $\alpha+\beta$ structures obtained by the decomposition of the martensite respectively at 520°C and 650°C resists spheroidizing for the times studied.

3) The resistance to spheroidizing can be explained by the formation of low energy α/γ_2 and α/β interfaces, respectively, in certain directions as suggested by the mechanisms of decomposition of β_1'.

Acknowledgements

This work was supported by FAPESP (Fundação de Amparo à Pesquisa do Estado de São Paulo) through the Grant "Tec. Industriais 73/1026".

References

[1] A.Portevin & G.Arnou: C.R.Ac.Sc. de Paris, V.68 (1912) p.511.
[2] Z.Nishiyama & S.Kajiwara: Jap.Jour.Appl.Phys., V.2 nº 8, (1963), p. 478.
[3] R.K.Govila: Acta Met. V.12 (1964), p.273.
[4] R.G.Cope: Jour.of the Inst. of Met. V.87 (1958), p.130.
[5] L. Delaey & I.Lefever: Metall. V. 11 (1973), p. 1085.
[6] H. Warlimont & L. Delaey: "Martensite Transformations in Cooper, Silver and Gold Based Alloys" Progress in Materials Science V. 18, Pergamon Press (1974).
[7] W. B. Pearson: "A Handbook of Lattice Spacings and Structures of Metals and Alloys" Pergamon Press, (1967).

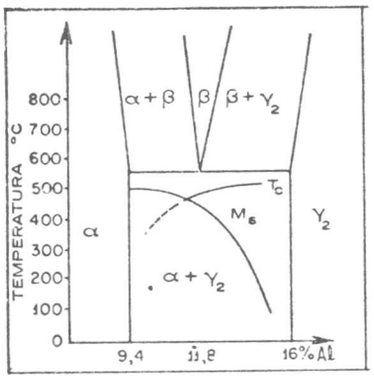

Fig. (1) - Cu-Al phase diagram, with the metastable lines M_s and T_c added.

Phase	Crystal lattice	Comentary
α	f.c.c	Cu terminal solid solution, stable
β	c.c.c	Hume-Rothery phase stable
γ_2	c.c.c., γ brass type	Hume Rothery phase stable
β_1	Ordered c.c.c (DO_3 type)	meta stable, ordered
β_1'	orthorhombic	meta stable, ordered martensite, corresponding to a f.c.c. lattice with structural $\frac{a}{6}\lvert 11\bar{2}\rvert$ stacking faults

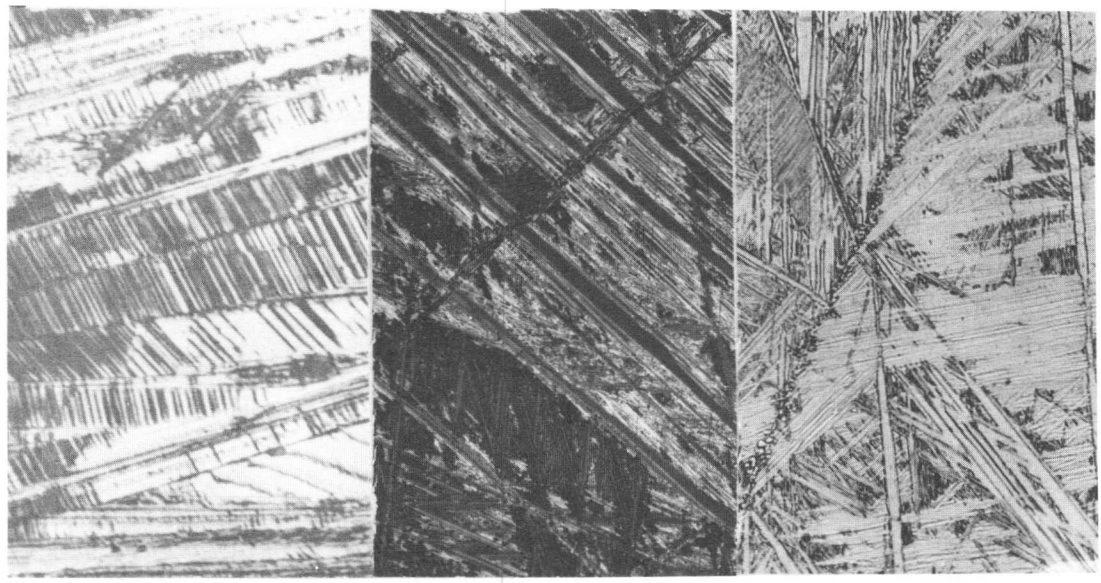

(a) (b) (c)

Fig. 2 - Martensite isothermally treated at 520ºC for a) 5 sec, 400 × (polarized light); b) 10 sec, 100 × (polarized light); c) 15 sec, 250 ×

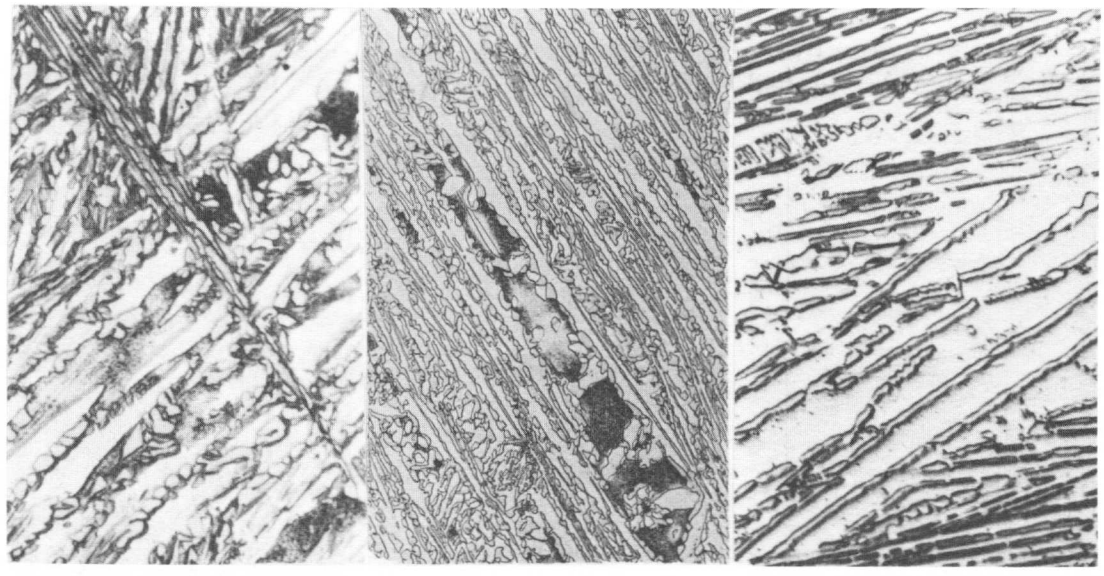

(a) (b) (c)

Fig. 3 - Martensite isothermally treated at 520ºC for a) 60 sec, 500 ×; b) 2 min, 500 ×; 5 min, 400 ×.

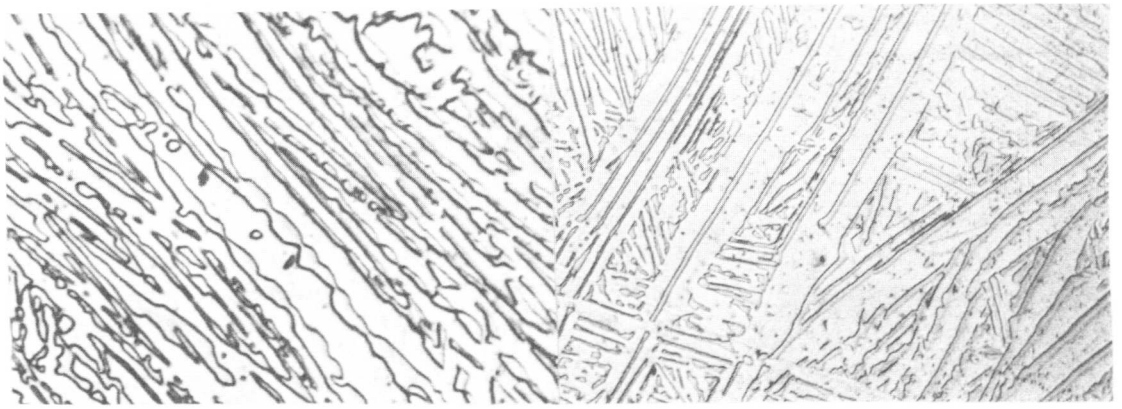

(a) (b)

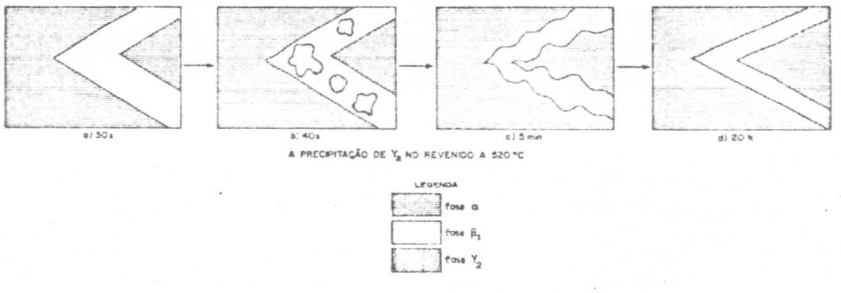

(c)

Fig. 4 - Martensite isothermally treated at 520º for a) 1 h, 630 × ; b) 20 h, 400 × ; c) schematic evolution of the microstructure.

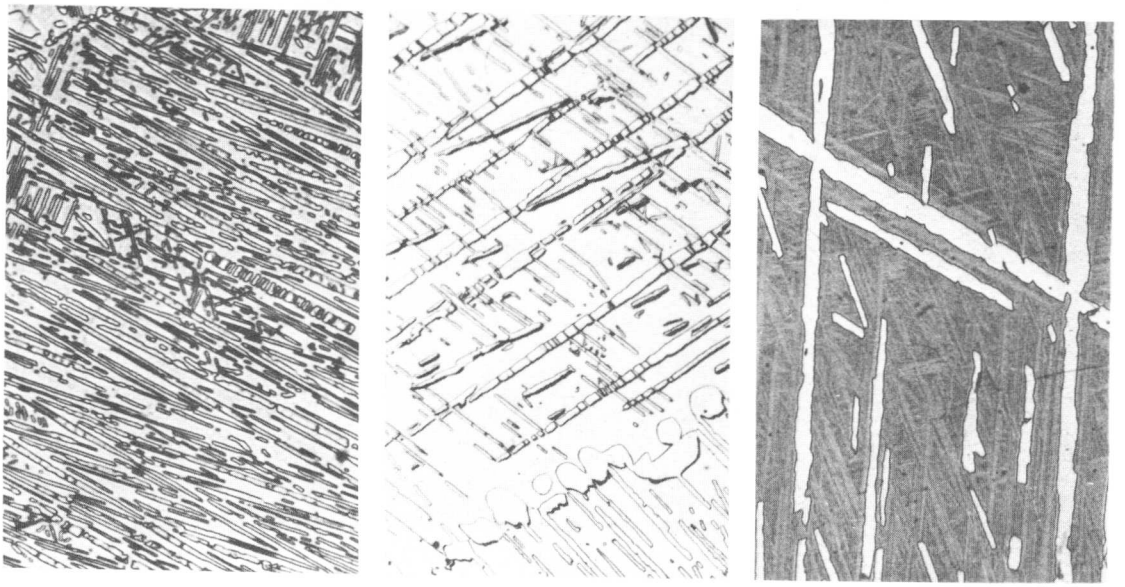

(a) (b) (c)

Fig. 5 - Martensite isothermally treated at 650ºC for a) 5 sec. 100 × ; b) 1 h, 250 × ; c) 18 h, 250 ×

Consequences of the Re-Transformation of Precipitated Austenite in Ferritic Cryogenic Steels

J. W. Morris, Jr.,* C. K. Syn,* J. I. Kim,* and B. Fultz*

The re-transformation of precipitated austenite (γ_R) in Fe-(6-9)%Ni steels has been investigated, with particular emphasis on the influence of transformation characteristics on alloy toughness at cryogenic temperature. In all cases studied the precipitated austenite re-transforms, either during cooling to cryogenic temperature or during deformation prior to fracture of the alloy. When the re-transformation is thermally induced the product martensite tends to form in a variant identical to that present before precipitation of the austenite; no significant refinement of the microstructure is achieved. On the other hand, mechanical transformation of the austenite produces a distribution of martensite variants determined by the local strain, hence preserving a refined microstructure conducive to low temperature toughness.

I. Introduction

Ferritic Fe-Ni steels which are intended for structural use at cryogenic temperatures are given a final intercritical temper, i.e., a temper in the two-phase ($\alpha+\gamma$) region of the phase diagram, which has the effect of precipitating austenite phase along the lath boundaries and prior austenite grain boundaries of the parent martensite.[1-3] The intercritical temper substantially lowers the ductile-brittle transition temperature of the alloy, often by as much as 200°C. This improvement is generally attributed to the retention of a small fraction of precipitated austenite in the product microstructure. However, the mechanism of toughening remains unclear.

Previous research[1-6] on the influence of retained austenite on the toughness of cryogenic steels suggests two qualitative sources for the decrease in the ductile-brittle transition temperature. First, the austenite will getter deleterious species, such as carbon, which segregate to the austenite during the precipitation. Second, the austenite may serve to blunt sharp-fronted cracks in the martensite, preventing them from causing catastrophic failure.

The "gettering" action of precipitated austenite is experimentally verified[4-7] and certainly contributes to alloy toughness. But gettering by itself cannot fully account for the beneficial influence of retained austenite. The introduction of a small fraction of precipitated

---

*Department of Materials, Science and Mineral Engineering, and Materials and Molecular Research Division, Lawrence Berkeley Laboratory, University of California, Berkeley

austenite also decreases the ductile-brittle transition temperature of Fe-Ni alloys which are nominally interstitial-free and chemically gettered.[8] We have, therefore, undertaken research to clarify the "crack-blunting" action of retained austenite. The results of this research suggest that the "crack-blunting" effect is intimately connected to the eventual martensitic transformation of the retained austenite and is particularly sensitive to the orientation of the product phase.

II. Thermomechanical Stability of Precipitated Austenite

Research on the mechanical behavior of intercritically tempered cryogenic steels gives a consistent indication that the beneficial influence of retained austenite is related to its thermodynamic stability.[1-3] The stability of the precipitated austenite decreases if the tempering temperature is too high, which presumably causes the austenite to become relatively lean in stabilizing solutes, or if the tempering time is too long, which leads to an increase in the size of the austenite particles. Both excessive tempering temperature and excessive tempering time cause a rise in the ductile-brittle transition temperature.

The sensitivity of alloy toughness to austenite stability could be easily explained if the austenite were mechanically as well as thermally stable at test temperature, since the relative ductility of austenite islands would serve to blunt propagating fractures. However, recent research conclusively demonstrates that the retained austenite present in tough cryogenic steels is mechanically unstable, and undergoes an essentially complete transformation to martensite prior to fracture.

The mechanical instability of precipitated austenite was first shown by Kim and Schwartz[9] and by Fultz[10] who used Mossbauer spectroscopy to analyse the residual phase distribution near fracture surfaces in cryogenic steels, and found an essentially complete transformation of retained austenite during ductile fracture of both 6Ni and 9Ni steels at cryogenic temperature. These studies were extended by Syn, et al[11] who prepared profile fractographic specimens and conducted transmission electron microscopic studies of the deformed material immediately adjacent to ductile fracture surfaces in 9Ni steel (Fig. 1). They confirmed the mechanical transformation of retained austenite and showed that the transformation product is a dislocated martensite, whose presence in the matrix is not incompatible with high toughness. More recent research on samples pulled in tension at 77°k (Fig. 2) revealed that the transformation of austenite in tough cryogenic steels is strain-induced and completed at relatively modest levels of plastic strain.

The demonstration that the austenite retained in tough cryogenic steels is fully transformed at strains well below those associated with fracture raises a puzzle as to why it is necessary (as it appears to be) that the austenite be present in the first place. The puzzle is compounded by the results of transmission electron microscopic studies (Fig. 3) which show that the austenite which spontaneously transforms on cooling, even near 77°k, yields a dislocated martensite which is apparently identical in substructure to that induced by plastic strain. The resolution of the puzzle appears to lie in a qualitative difference in the orientations of the two kinds of martensite with respect to the

parent matrix, an orientational difference which has its source in the pervasive memory of thermally-induced martensitic transformations in Fe-Ni steels.

III. The Role of Precipitated Austenite in Microstructure Refinement

On quenching, Fe-(5-9)Ni cryogenic steels develop a microstructure which is made up of laths of dislocated martensite which tend to be organized into packets. These packets may be 10-20μm in size and consist of bundles of laths which bear a close crystallographic relation to one another. While the laths themselves may be small (<1μm in diameter) their close alignment in packets has the consequence that the salient mechanical properties of the alloy tend to be controlled by the packet size rather than by the smaller lath size.

The influence of packet alignment on fracture is illustrated in Fig. 4, which shows a profile scanning electron fractrograph of a brittle fracture surface in 6Ni cryogenic steel. Long, flat cleavage traces are apparent; these traverse martensite packets. Crystallographic analysis shows that the facets follow (100) cleavage planes which are nearly common to the packet. Where the packet is not well defined the fracture surface is rough and often locally ductile. Observations such as these suggest that a major goal of the processing of cryogenic steels should be to destroy long-range packet alignment.

An intercritical temper superficially appears to offer an effective means for decomposing aligned packets. During the temper austenite islands nucleate along the lath boundaries and essentially isolate the laths from one another. There is, however, a subtle memory in the austenite precipitation and its reversion to martensite on cooling which vitiates packet decomposition. As illustrated in Figs. 3 and 5 the austenite precipitated within a given packet has a strong statistical tendency to form in a single variant, which is K-S related to the martensite matrix, and, if it re-transforms on cooling, to regenerate the martensite which gave it birth. If the result of an intercritical temper is to precipitate a thermally unstable austenite only slight refinement of the microstructure is accomplished and no significant improvement in mechanical properties should be anticipated. In fact, the transition temperature often rises after such a temper.(12)

If, on the other hand, the intercritical temper leads to the retention of a reasonable distribution of interlath austenite then this austenite remains until it is transformed by plastic strain. Initial studies of mechanically transformed austenite, exemplified by the micrograph shown in Fig. 6, suggest that the martensite variant formed in this case is that most compatible with the local strain, hence tending to be the variant most compatible with the nominal strain of the sample. The product martensite is K-S related to its parent austenite, which is in turn K-S related to the matrix; however, the K-S relationship permits a sufficient number of variants that the martensite will only rarely share a well-oriented cleavage plane with the matrix.

The precipitation of thermally stable austenite hence achieves a decomposition of the packet alignment of martensite laths which is largely retained even if the austenite transforms mechanically prior to fracture.

A substantial decrease in the ductile-brittle transition temperature of the alloy is therefore expected and is usually observed.

IV. Conclusion

The precipitation of austenite during an intercritical temper of Fe-(6-9)Ni martensite will decrease the ductile-brittle transition temperature of the alloy if it breaks up the packet alignment of martensite laths. Because of memory effects in the re-transformation of the precipitated austenite it is necessary that the austenite have sufficient thermal stability for a significant fraction of it to be retained on cooling to the test temperature. Subsequent mechanically-induced transformation of the austenite does not then eliminate its beneficial effect.

Acknowledgment

This research was supported by the Office of Naval Research under Contract No. N00014-75-6-0154 and by the Division of Materials Sciences, Office of Basic Energy Sciences, U. S. Department of Energy under Contract No. W-7405-Eng-48.

References

[1] C. W. Marshall, R. F. Heheman, and A. R. Troiano: Trans. ASM, 55(1962), 135.
[2] T. Ooka and K. Sugiano: J. Japan Inst. Metals, 30(1966), 435.
[3] S. Yano, H. Sukarai, H. Mimura, N. Wakita, T. Ozawa, and K. Aori: Trans. Iron Steel Inst. Japan: 13(1973), 133.
[4] S. Nagashima: "Toward Improved Ductility and Toughness", Climax Molybdenum Co. (1971) p. 353.
[5] S. K. Hwang, S. Jin and J. W. Morris, Jr.: Met. Trans. 6A (1975), 2015
[6] C. Syn, S. Jin, and J. W. Morris, Jr.: Met. Trans. 7A(1976), 1827.
[7] J. I. Kim and J. W. Morris, Jr.: Met. Trans., submitted.
[8] S. Jin, S. K. Hwang, and J. W. Morris, Jr.: Met. Trans. 6A(1975), 1721.
[9] K. J. Kim and L. Schwartz: Mat. Sci. Eng., 33(1978), 5.
[10] B. Fultz, M. S. Thesis, U. C. Berkeley (1978).
[11] C. Syn, B. Fultz, and J. W. Morris, Jr.: Met. Trans., 9A, (1978), 1635.
[12] S. Jin, S. K. Hwang, and J. W. Morris, Jr.: Met. Trans., 6A(1975), 1969.

Fig. 1 Profile TEM fractograph and diffraction pattern in 9Ni steel. The fracture surface (indicated with arrows) was plated with iron (above the boundary indicated with arrows) to prepare thin foils of the fracture surface layer. The diffraction pattern was taken from the central region right below the boundary line. The circled area shows γ_R-like particles which have transformed to α'.

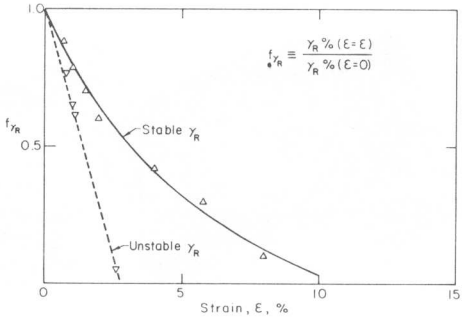

Fig. 2 Martensite Transformation of the termally stable and unstable γ_R in 9Ni steel during tensile tests at 77°K. Remaining fraction of γ_R with respect to the original amount at room temperature was plotted against the tensile strain ε.

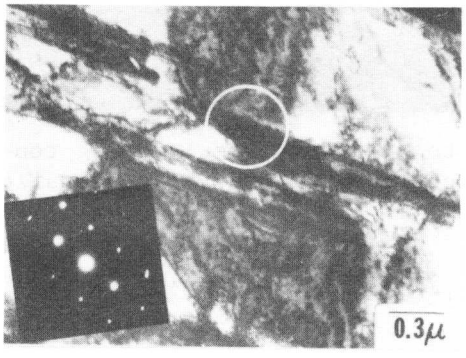

Fig. 3 TEM of the thermally unstable γ_R in 9Ni steel. The γ_R has tranformed to highly dislocated α' on quenching to 77°K from room temperature. It has transformed to the same orientation of the matrix.

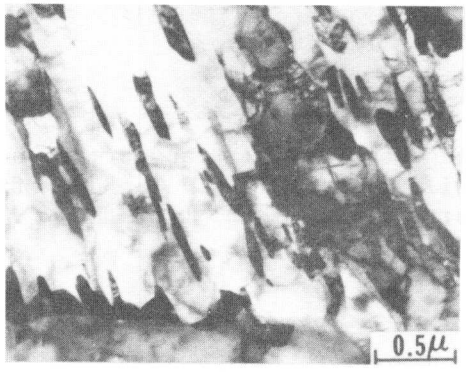

Fig. 5 Typical microstructure of the thermally stable γ_R at 77°K in 9Ni steel. γ_R particles are K-S related to the matrix of tempered α'.

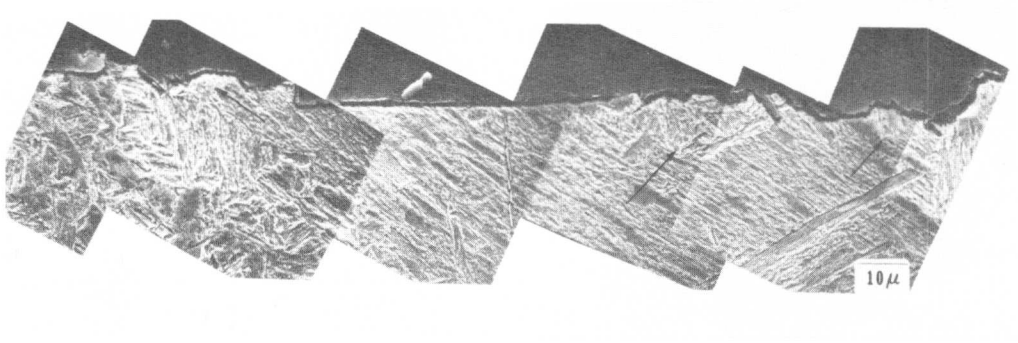

Fig. 4 Profile SEM fractograph showing the lath orientations with respect to the fracture crack path in 6Ni steel. Arrows indicate regions where the crack deviates.

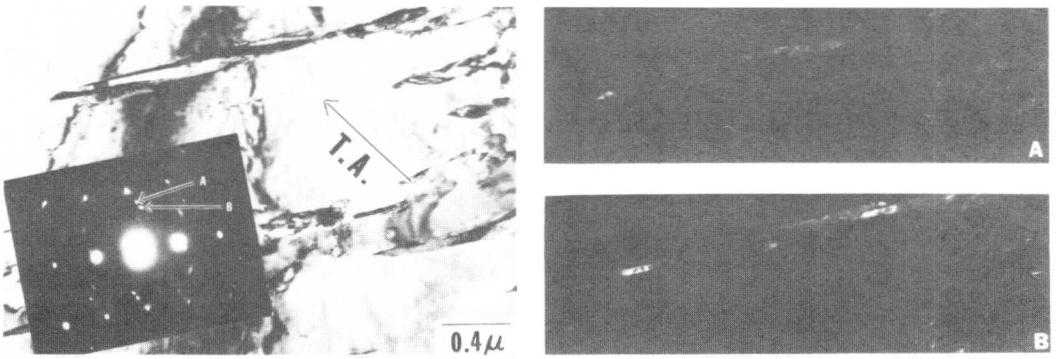

Fig. 6 Partial transformation of γ_R to α' in 9Ni steel during tensile test at 77°K. The dark field pictures show the γ_R and tensile strain-induced α' from the γ_R.

Electron Microscopical Observations of "ω-like" effects in Cu-Al-Ni.

W.M. Stobbs, R.J. Henderson and A.M. Crossley

Spun and bulk quenched alloys of CuAlNi have been shown to have markedly different transformation temperatures. Both the bulk and spun material are also affected by ageing at temperatures in the range between 200°C and 350°C, the martensitic and austenitic transformation temperatures being raised with an increase in thermal hysteresis. The effect of 970°C rebetatisation of the spun material is also to raise the transformation temperature but with, at least for flash anneals, both a reduction in the width of the martensitic transformation peak as seen on a differential scanning calorimeter and in general a reduction in the thermal hysteresis.

Electron microscopy has been used to investigate the form of the alloy in its various states as a function of quench rate and isothermal ageing. It has been found that the spun material exhibits what might be described as a relatively strong "ω-like" distortion of the bcc matrix but no precipitation. The bulk quenched material contains both distortions and an "ω like" precipitate. 250°C ageing of both forms of material gives increasing volume fractions of precipitate while 970°C rebetatisation of the spun material increases the tendency of precipitate formation. The precipitation phenomena is distinct from the formation of martensite and appears to be an essentially competitive rather than premonitory effect.

The thin foil distortions of the b.c.c. matrix are argued to be the result of anharmonic coupling of the $\langle 110 \rangle_{\zeta}$ $\langle \bar{1}10 \rangle_{\varepsilon}$ transverse acoustical phonon modes.

I. Introduction

Cu-Al-Ni alloys which transform thermoelastically have the approximate formula $(Cu\ Ni)_3Al$ and neglecting the influence of Ni they order with the DO_3 structure (β_1). They transform to a 2H distorted orthorhombic martensite (γ_1') though at higher temperatures and with applied stress an 18R acicular martensite can also be formed (β'_1). It has been well known for some years that the transformation temperatures appear to be sensitively dependent on the quench rate from the β phase field [1]. Thus, with a view to understanding this effect and possibly thereby gaining a greater insight into the way in which the martensitic transformation occurs we have recently compared the transformation behaviour of alloys prepared by melt spinning and by conventional water quenching from the β phase field [2,3] as well as investigating the effect of both low temperature (∿ 250°C) anneals and rebetatisation of the spun alloy. The essential results may be summarised: the spun alloy transforms to martensite at a temperature well below that of water quenched 0.5mm thick discs. Ageing both spun and bulk material at 250°C results in increased thermal hysteresis and raised transformation temperatures. Rebetatisation of the spun material initially reduces the range of temperature over which

Department of Metallurgy and Materials Science, Cambridge University, England.

the martensitic transformation occurs, while the transformation temperatures are raised, and generally reduces the thermal hysteresis. 250°C ageing of the rebetatised spun material gives a further increase in the transformation temperatures but now the separation of the peak rate of austenitic and martensitic transformation is increased.

Our purpose here is to describe the results of an electron microscopical investigation of the state of the b.c.c. phase as a function of the various states listed above.

II. Experimental

A range of alloys were examined [2] but all the electron microscopical results described here were obtained on material of composition Cu 81.7wt% Al 14.1wt% and Ni 4.2wt% prepared by argon arc melting of 4N purity components. The details of the melt spinning technique by means of which a thin ribbon is fabricated at quench rates approaching 10^6 Ks^{-1} are described elsewhere [4]. A Dupont 990 thermal analyser with a quantitative scanning system was used to characterise the transformation behaviour and heat treatments were completed in the D.S.C. The 970°C ageing was performed in sealed quartz tubes back filled with argon. A JEOL 100CX electron microscope was used for the structure investigation, specimens being held in a slightly modified top entry tilting holder at a position in the objective lens where the spherical aberration coefficient was approximately 2.5mm.

III. Results

In our discussion we refer the crystallography to the parent bcc structure, despite the DO_3 ordering behaviour, to facilitate comparison between the behaviour of this and B2 ordering materials. A description has recently been published of the diffuse electron scattering in Cu-Al-Ni and Otsuka et al [5] associate the well known <110> streaking with transverse $\langle 110\rangle_q \langle \bar{1}10\rangle_\varepsilon$ phonon modes. They concluded this by an analysis of the way in which a displacement wave of the form $\underline{R}_n = A(q)\underline{\varepsilon}_o \cos 2\pi (\underline{q}.\underline{r}_n - \nu t)$ scatters electrons noting, as did Chandra and Purdy [6], how no streaks are seen if $\underline{g}.\underline{\varepsilon}_o = 0$ {$\underline{\varepsilon}_o$ being the polarisation of the wave of amplitude A and propagation vector $\underline{q}$}. We have used the same interpretative techniques.

The least confusing state of the material was "as spun" and we will describe this first. This material contained no precipitates as viewed some 70°C above its transformation temperature, the <110> streaking was however strong and as described by Otsuka et al [5]. We note however a few further points of interest: Streaking in <112> directions is also strong and apparently at least partly associated with longitudinal as well as transverse displacements. It has been shown in other materials that soft phonons almost certainly associated with charge density waves can be anharmonically coupled both near defects and in a thin foil where the displacement waves can be locked as a result of the proximity of the free surfaces of a foil [6]. We suggest here that a natural explanation for the <112> streaks lies in their being the result of scattering from distortions of the thin foil arising from the addition, in phase, of transverse wa

with q vectors of <110> type 30° above and below the relevant <112> direction. (Discussion of the more general localised distortions which can result from such additions is given elsewhere [7]). Further evidence for this is obtained by examination of a lattice fringe image of the spun material obtained in the 110 normal (figure 1). Particularly near the edges of the foil coarse variably spaced fringes are seen with $<1\bar{1}2>$ normal and an optical transform of such areas shows that the $1\bar{1}0$ lattice fringes have variable spacing in this direction (figure 2). The second point of importance is that while a strong reflection is seen at $\sim$ $2/3\ (2\bar{2}2)$, at the 110 normal, connected by a particularly strong streak to the $1\bar{1}2$ reflection this "ω reflection" becomes well nigh invisible on tilting to the adjacent (121) normal despite the $2\bar{2}2$ reflection remaining excited. The appearance of a reflection at $2/3(2\bar{2}2)$ is in general dependent on there being a strong reflection off the $2\bar{2}2$ systematic row. This implies that the distortion associated with this $\underline{q}$ is transverse and general observation of the intensity of the reflection as a function of orientation suggests that ε_o is in, or close to the $<\bar{1}12>$ direction. The strong assymetric linking streak between reflections such as $1\bar{1}2$ and $2/3(2\bar{2}2)$ at the 110 normal is then explained by the combined strengthening of the scattering from the displacements in the $[1\bar{1}2]$ direction of localised regions elongated in the $1\bar{1}1$ direction, and the strong excitation of the "ω" reflection at $2/3(2\bar{2}2)$ by the adjacent $1\bar{1}2$ reflection. At first sight it is surprising that it is a transverse displacement associated with the $2/3(2\bar{2}2)$ wave vector but the longitudinal components of the distortions in the regions of $[1\bar{1}1]$ major axis perhaps also amplify the $2/3<2\bar{2}2>_q <\bar{1}12>_\varepsilon$ transverse acoustic mode. Further discussion is given elsewhere [7], but it is this which links this description of the distortion patterns with the well known b.c.c distortions found in alloys such as Zr-Nb [8] and generally associated with instabilities of the b.c.c lattice [9,10]. Figure 3 shows a dark field image using the intensity at the 2/3(222) position. The $\sim$100Å banding is indicative of local foil orientation changes, with <112> normal. It is consistent with the locked distortion description given above. No change in microstructure of the as-spun material was observed after 6 months storage at room temperature.

After a flash anneal at 970°C the thin foil banding appeared to become a little more localised, though except at the very edge of the foil no precipitation was observed. Lattice fringe images of "2/3(222)" with 111 serve to show the relatively large misorientations to be expected (fig.4). This material left for a few days at room temperature however exhibited gross precipitation of a heavily faulted (spacing $\sim$ 15Å) species with a reflection just to one side of the 2/3(222) position. At the same time a further competitive reaction of the bcc phase to the distortions within it was gross faulting on (112) planes at spacings between about 3Å and 15Å. This was consistent with the intensification of the <112> streaks in the diffraction pattern (no such faults were observed in the as-spun state).

After ageing for two minutes at 250°C the material, thinned of course after the heat treatment, was shown by stereo microscopy to have both a surface phase in patches and reflecting very near the $2/3(2\bar{2}2)$ position and particles $\sim$ 150Å in size developing through the foil. Lattice fringes now between $3/_2\bar{3}/_2 3/_2$ and $2/_3(2\bar{2}2)$ serve to show the extensive spread in

misorientation, (see figure 5).

Bulk quenched material showed essentially a more developed version of the structure seen in the spun specimens after short 250°C heat treatments: particles extending through the foil but with bigger ones near the surfaces as well as a surface precipitation. Fig.6 shows both the extensive and similar faulting of the two precipitate phases as well as misorientations via lattice fringes with $3/_2\bar{3}/_2 3/_2$ included in the aperture.

Ageing the bulk material at 250°C gave well developed precipitation throughout the foil, an increased tendency for the bcc phase in a thin foil to fault rather than show distortions (fig.7), and regions where martensite had been formed and reverted to bcc (the transformation temperature was near room temperature). Figs.8 and 9 demonstrate that particles and surface phase are lost after reversion to bcc and do not occur in the 2H martensite. Given the correlation of this observation with the tendency to reduced thermal hysteresis on cycling and increased hysteresis on 250° ageing it is inconceivable to think of the particulate phase as a precursor to the formation of 2H martensite. It is clearly a form of a further competitive reaction which the distorted bcc phase can undergo. Amuzingly however analysis of a considerable number of particles indicated that the principal reflection near $2/_3(222)$ with which they were imaged in fact lies between the spots marked for the combined diffraction pattern of 2H martensite and bcc at 110 orientation. This diffraction pattern also serves to demonstrate the close relation between the bcc phase and the 2H martensite and in particular the relevance of the "locked local" distortions in that relation. As a final point it should be noted that no consistent differences were seen in DO_3 A.P.B. separations in any of the above specimens. Further discussion of the importance of the coupling of $\langle 110\rangle_q\langle 1\bar{1}0\rangle_\varepsilon$ displacement waves is given elsewhere [7,11].

IV. Conclusion

It has been demonstrated that the distorted states of a bcc alloy, associated with $\langle 1\bar{1}0\rangle_q$ $\langle \bar{1}10\rangle_\varepsilon$ acoustic phonons, can themselves be linked with a number of competitive reactions which, perhaps as a function of volume dilatations, change the martensitic transformation temperature of the bcc matrix. These reactions include: surface and bulk precipitation as well as both matrix and particle faulting.

R.J. Henderson and A.M. Crossley are supported by Delta Materials Research Ltd. and Standard Telecommunication Laboratories Ltd. respectively, as well as by the Science Research Council. We acknowledge the encouragement of Prof. R.W.K. Honeycombe.

References

[1] K. Otsuka, K. Nakai and K. Shimuzu: Scripta Met. 8 (1974) 913.
[2] J.V. Wood, A. Crossley and W.M. Stobbs: Rapidly Quenched Metals III, Ed. by B. Cantor, The Chameleon Press Ltd. London, (1978) 180.
[3] J.V. Wood and W.M. Stobbs: Phase Transformations April 1979, in press.
[4] J.V. Wood: Proc.Conf. on Solidification (1977) Sheffield, in press.

[5] K. Otsuka, C.M. Wayman and H. Kubo: Met.Trans. 9A (1978) 107
[6] W.M. Stobbs: Phil.Mag. 35 (1977) 1001.
[7] R. Portier and W.M. Stobbs: ICOMAT 79.
[8] T.S. Kuan and S.L. Sass: Phil.Mag. 36 (1977) 1473.
[9] H.E. Cook: Acta Met. 21 (1973) 239.
[10] P.C. Clapp: Phys. Stat. Sol. 57b (1973) 561.
[11] W.M. Stobbs: ICOMAT 79.

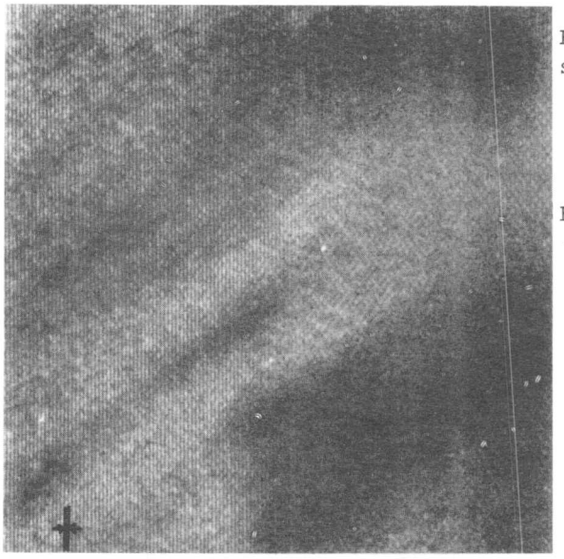

Fig.2 Optical transform of region showing $\langle\bar{1}12\rangle$ trace streaks.

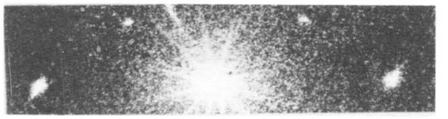

Fig.1 Lattice fringe image showing $\langle 1\bar{1}2\rangle$ trace banding.
$(1\bar{1}0)$ lattice fringes vertical.

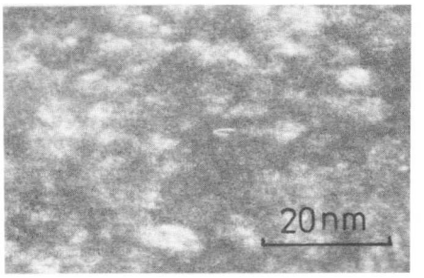

Fig.4 Spun + flash 970°C anneal. "ω" + 111 reflections giving ∿5Å fringes vertical.

Fig.3 As spun "ω" reflection rods lie in 111 direction.

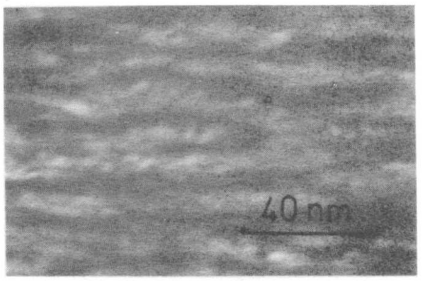

Fig.5 Spun after 2 mins at 250°C. Faulting in particles vertical, fringes ("ω" + 3/2, $\bar{3}$/2, 3/2) ∿ 10Å horizontal.

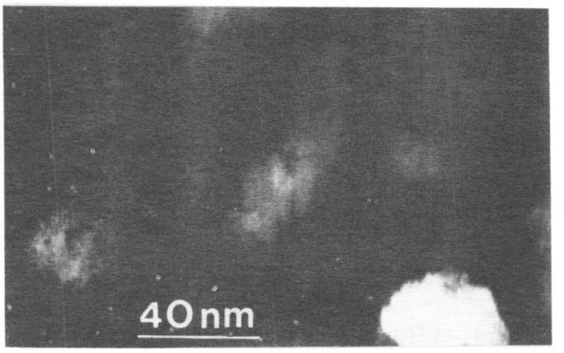

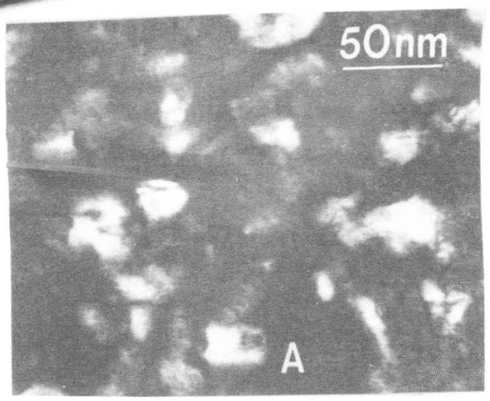

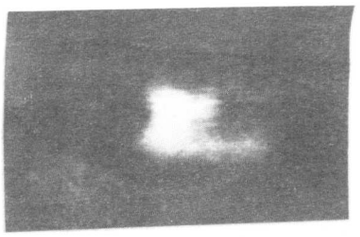

Fig.6 As bulk quenched. "ω"reflection. Area marked A to show faulty and "ω" - 3/2 $\bar{3}$/2 3/2 fringes ∿10Å

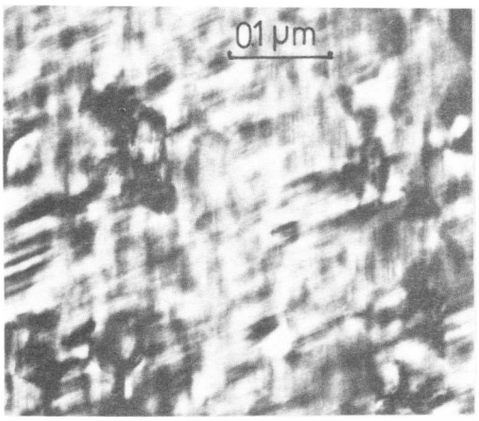

Fig.7 bcc material heavily faulted on (121) planes, trace of (1$\bar{1}$2) vertical, normal (110)

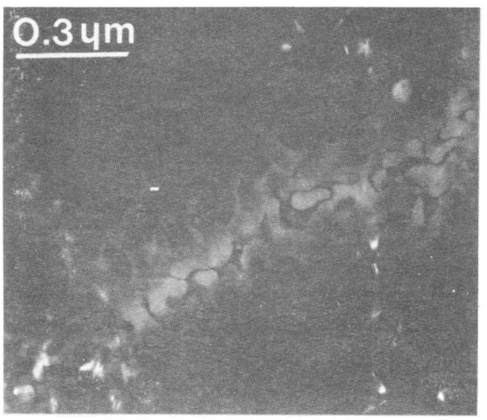

Fig.8 Area reverted from martensite: note no "ω" precipitation.

Fig.9 Retained martensite: no "ω" except in overlap regions.

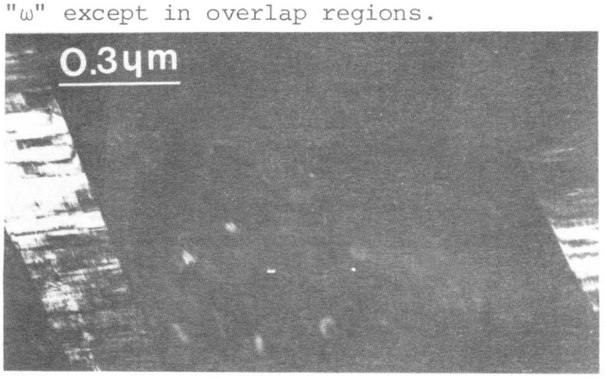

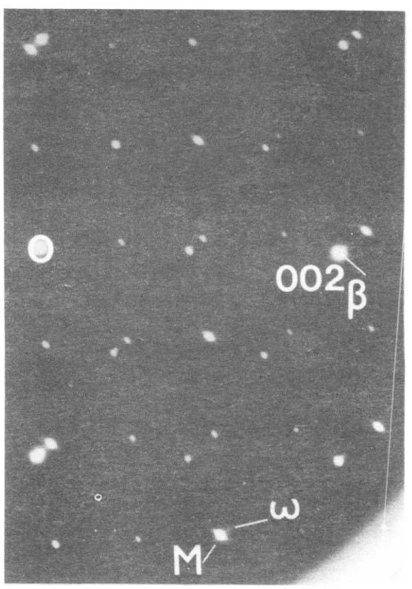

A bcc (110) normal with associated martensite diffraction pattern. Note proximity of "ω" reflection to adjacent martensite spot. Fig.10.

The Effect of Low Temperature Ageing on the Martensitic Transformation in Cu-Zn-Mn Alloys

L. Chandrasekaran+ and A.P. Miodownik*

Low temperature ageing treatments have previously been shown to produce quite marked effects on M_s and A_s temperatures in Cu-Zn-Mn β alloys. Although similar ordering behaviour is predicted thermodynamically for small additions of Al and Mn, the effects observed are quite different as the M_s temperatures move in opposite directions on ageing. Explicit calculations of the effect of ordering on the M_s of binary Cu-Zn alloys can be used to explain the effects observed in Cu-Zn-Mn alloys; it is suggested that the different behaviour of Cu-Zn-Al must lie in the effect of inherited order on the energy of the α phase.

I. Introduction

Ageing effects in Cu-Zn-Al alloys have been studied extensively in recent years, with increasing emphasis on the possible role played by the $B2/DO_3$ ordering transformation [1-3]. The present paper considers some observations and associated theoretical calculations in the related system Cu-Zn-Mn. Manganese was originally selected as a useful alloying addition because (a) the effect of manganese on the M_s is not known in the detail available for many other additions [4], (b) very little information appears to be available on the Cu-Zn-Mn system in general [5-7], and (c) it was hoped manganese might reduce the rate of ordering in the β phase.

Alloys containing between 0.5 and 10 atomic % Mn were investigated by DTA and electrical resistance techniques in order to characterise the M_s and A_s behaviour in the as-quenched and aged conditions. Calculations of the theoretical location of the $B2/DO_3$ transition temperatures were then performed in order to correlate the degree of order with the ageing behaviour and extended to include an explicit calculation of the M_s temperature.

II. Experimental Procedure

Alloys were made by melting copper, zinc and manganese of 99.9% purity in evacuated quartz capsules with a weight loss of less than 0.2%. The as-cast buttons were homogenised for 3 days in the β phase field before being fabricated into wire form. Transformation temperatures were established by the standard four-probe resistance technique and DTA measurements; additional M_s values were obtained from stress strain curves using Ahlers technique [8].

+Metallurgy Dept., Swansea Univ., S. Wales.
*Dept. of Metallurgy, Univ. of Surrey, Guildford, U.K.

III. Results

The effect of manganese on the M_s temperature is shown in (Fig. 1), where the combined effect of manganese and zinc is compared with the effect of zinc alone. Manganese appears to depress M_s by $80\pm2^{o}K$/at%Mn, the same value as for zinc [4]. Also shown are some predicted values for binary Cu-Zn alloys based on calculations outlined later in this paper, and assuming the known small hysteresis of these alloys allows T_o to be equated to M_s [8]. The ageing behaviour of manganese containing alloys is contrasted with aluminium containing alloys in (Fig. 2), where it can be seen that identical treatments lead to opposite effects in the two systems. The entropy change between the parent β phase and martensite as deduced from $\Delta S=\gamma\partial\tau/\partial M_s$ [8] was found to be independent of the ageing treatment, as previously observed in other alloys [9]. This confirms that the α phase inherits its degree of order from the β phase. The value of ΔM_s was found to increase with ageing temperature right up to the temperature where α precipitation interferes with ordering changes, in contrast with Cu-Zn-Al where ΔM_s tends to reach a constant value [1].

IV. Relation of Ageing Behaviour to the $B2/DO_3$ Transition

The $B2/DO_3$ transition temperature for the β phase was calculated using the method of Inden [10,11], the input data being listed in Table I. In the absence of a stable Cu-Mn β phase, the required parameters for BCC Cu-Mn were derived by combining available data for the A2/B2 transformation in ternary Cu-Zn-Mn alloys [7,12] and enthalpy of formation data [20]. A similar procedure for obtaining missing binary data was adopted by Inden for Au-Cu-Zn [11]. It is assumed, following Miedema [21], that the enthalpy for formation for BCC and FCC alloys can be taken to be the same to a first approximation. (Figure 3) shows that the calculated transition temperatures are consistent with inflections found in DSC experiments, and also shows the result of similar calculations for Cu-Al-Zn alloys. Although the two quasibinary sections are not parallel, there is little doubt that the general form of the transition is the same in both systems, so that differences in ageing behaviour cannot be explained by reference to any obvious difference in the ordering of the β phase.

V. Rate of Ordering in Cu-Zn-Mn Alloys

Despite initial hopes that manganese might prove to slow up the ordering reaction, the current results indicate that ordering is still very rapid, as found for the binary alloys [13]. Some disorder can obviously be retained by quenching after ageing [14], but the heat evolved when a quenched β phase is reheated to 300/350 K is only (12-25 J mol^{-1}), in marked contrast to the much larger values found for Cu-Zn-Al (50-150 J mol^{-1}). This is consistent with the idea that greater disorder can be retained in alloys containing trivalent ions rather than ions of lower valency [15]. It is difficult to attribute a specific valency to manganese but the effect on the M_s is consistent with manganese acting like divalent zinc. Such a difference in rate of reordering on quenching from elevated temperatures could explain the absence of any distinctive change in ΔM_s on ageing above and below the

$B2/DO_3$ transition in Cu-Zn-Mn alloys. However the contrast between Cu-Zn-Mn and Cu-Zn-Al shown in (Fig. 2) requires a different explanation involving the associated change in free energy of the martensite on ordering.

VI. Calculation of Free Energy Curves

An explicit calculation of the M_s can be made by combining ordering data for both FCC and BCC phases with a regular solution model and phase stabilities on the lines made familiar by Kaufman [16]. The necessary ordering input data for FCC phases is very sparse, but provisional current estimates are listed in Table II. Space limitations preclude discussion of ternary alloy calculations which will be published elsewhere, but most of the principal conclusions derived from such calculations can be drawn from the much simpler binary case. (Figure 4) shows that the BCC and FCC curves cross three times which, however unexpected it may appear, is in conformity with the known phase equilibrium in Cu-Zn alloys. The ordering parameters x and y and mixing energy listed in Table III arise directly from the data of Tables I and II [10,11]. The variation on the three intersection points with composition clearly reproduces both the retrograde solidus so characteristic of these alloys, and the variation of M_s with zinc content (Inset Fig. 4). The presence of three critical transition points clearly places severe constraints on the input data, and it is surprising that such a good fit can be obtained merely from the ordering data, phase stability information, and a single additional parameter which in the range 35-40% Zn turns out to be a 'destabilisation' of the α phase by $\simeq$440 J mol^{-1}. Such a value is consistent with the magnitude of expected electronic contributions from Brillouin zone effects [17]. Although the intersections of the free energy curves are obviously very sensitive to the entropy difference between the phases, the chosen value of $\Delta S^{\alpha \rightarrow \beta}$ (2.51) J $mol^{-1}K^{-1}$ only differs by 0.83 from Kaufman's value [16], and is virtually identical to the value proposed by Kulkarni (2.80) [18].

VII. Conclusions

1. The effect of Mn on the M_s is essentially the same as for Zn.

2. Because of rapid diffusion, ageing above the $B2/DO_3$ transformation temperature in Cu-Zn-Mn alloys does not produce markedly different structures than ageing at lower temperatures.

3. If the α phase inherits its degree of order from the β phase, any disordering of the β phase will result in a rise of M_s provided the ordering energy of the α phase is smaller than the ordering energy of the β phase. This appears to be the case in binary Cu-Zn and ternary Cu-Zn-Mn alloys.

4. If the M_s is depressed by disordering β, as found in Cu-Zn-Al alloys, the ordering energy of the α phase must be greater than that of the β phase (or some similar secondary effect due to changes of the electronic contribution must occur as a result of ordering). Calculations are in hand to test this hypothesis.

References

[1] D. Schofield and A.P. Miodownik. Metals Society Symposium Copper 77. (In the press.)
[2] S.C. Singh, Y. Murakami and L. Delaey. Scripta Met. 12 (1978) 435.
[3] J.M. Cook and L.M. Brown. Scripta Met. 12 (1978) 949.
[4] H. Pops. Trans. AIME 236 (1966) 1532.
[5] T.R. Graham, R.S. Dean and J.R. Long. Trans. AIME 185 (1949) 675.
[6] M. Gonda, T. Takahashi and H. Watanabe. J. of Jap. Inst. of Metals 36 (1972) 297.
[7] M. Gonda, T. Takahashi and H. Watanabe. J. of Jap. Inst. of Metals 39 (9) (1975) 939.
[8] W. Arnedo and M. Ahlers. Acta Met. 22 (1974) 1475.
[9] N. Nakanishi et al. Scripta Met. 12 (1978) 79.
[10] G. Inden. Z. Metallk. 66 (10) (1975) 577.
[11] G. Inden. Z. Metallk. 66 (11) (1975) 648.
[12] M.M. Shea and N.S. Stoloff. Met. Trans. 5 (1974) 755.
[13] N. Brown. Acta Met. 1 (1959) 210.
[14] S.G. Cupschalk and N. Brown. Acta Met. 15 (1967) 847.
[15] C.S. Barrett and T.B. Massalski. The Structure of Metals 3rd Editio McGraw-Hill (1966).
[16] L. Kaufman and H. Bernstein. Computer Calculations of Phase Diagrams. Academic Press (1970).
[17] T.B. Massalski and U. Mizutani. Progress in Materials Science (3/4) 22 (1978) 256-262.
[18] S.D. Kulkarni. Acta Met. 21 (1973) 1461.
[19] R. Rapacioli and M. Ahlers. Scripta Met. 11 (1977) 1147.
[20] R. Hultgren et al. Selected Values of Thermodynamic Properties ASM (1973).
[21] A.R. Miedema et al. Calphad 1 (4) (1977) 341.
[22] G. Inden. (Private communication)

TABLE I

Ordering and Associated Parameters for BCC Alloys*

System	ΔH Formation C=0.5 kJ mol^{-1}	W_1 kJ mol^{-1}	W_2 kJ mol^{-1}	x	Remarks
Cu-Zn	-10.48	7.51	3.97	0.68	)
Mn-Zn	- 6.30	5.38	1.22	0.78	) This work
Cu-Mn	- 4.20	3.31	1.18	0.75	)
Cu-Al	-17.33	11.86	7.29	0.63	) From
Al-Zn	- 0.65	-0.33	1.31	0.85	) Ahlers [19]

*For the definition of ordering parameters in Tables please refer to Inden [10,11].

TABLE II

Ordering and Associated Parameters for FCC Alloys*

System	ΔH Formation C=0.25 kJ mol^{-1}	W_1 kJ mol^{-1}	W_2 kJ mol^{-1}	x	Remarks
Cu-Zn	-6.4	5.19	1.25	0.82	ΔH from [20]
Zn-Mn	-11.3	9.43	1.16	0.82	ΔH from [21]
Cu-Mn	+2.2	-1.49	-1.00	0.82	ΔH from [20]

TABLE III

Free Energy Contributions in 60/40 Brass*

J mol^{-1}		BCC	FCC	Remarks
ΔG_0	Phase stability	(4916-2.51T)	(736-0.67T)	Combination of Cu & Zn
ΔG_1	Mixing energy	-10070	-8338	Function of W_1W_2 & conc
ΔG_2	Ordering energy	$(18127x^2+5957y^2)$ $-TS^{BCC}_{ord}$	$(6646x^2+3323y^2)$ $-TS^{FCC}_{ord}$	Function of W_1W_2 conc & T
ΔG_3	Additional term		+440	Empirical

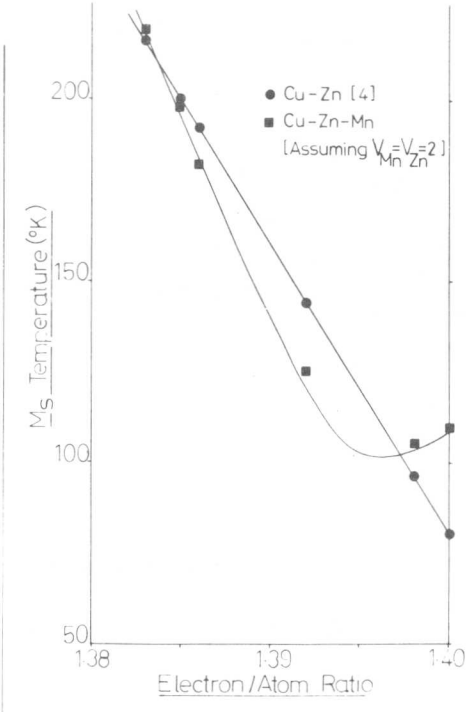

Fig. 1 Variation of M_s with Manganese Content and Comparison with the Effect of Zinc [4] on an Electron Concentration Basis.

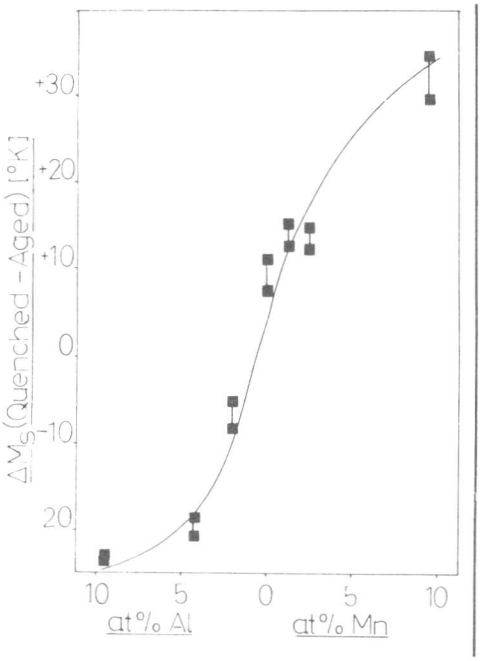

Fig. 2 Variation of ΔM_s with additions of Mn and Al

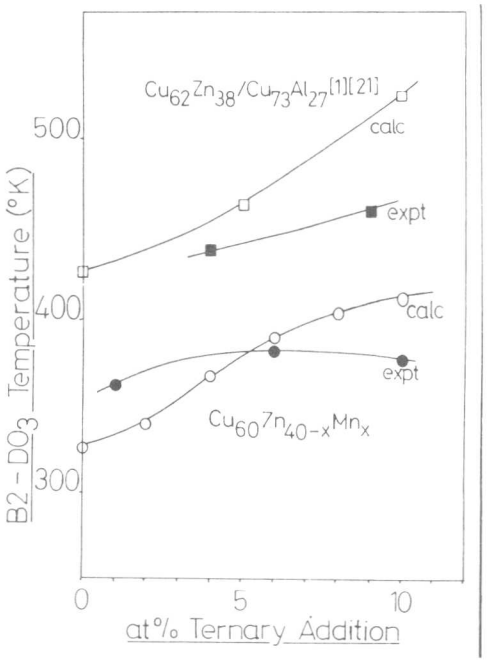

Fig. 3 Comparison of calculated B2/DO_3 Temperatures and Experimental Evidence

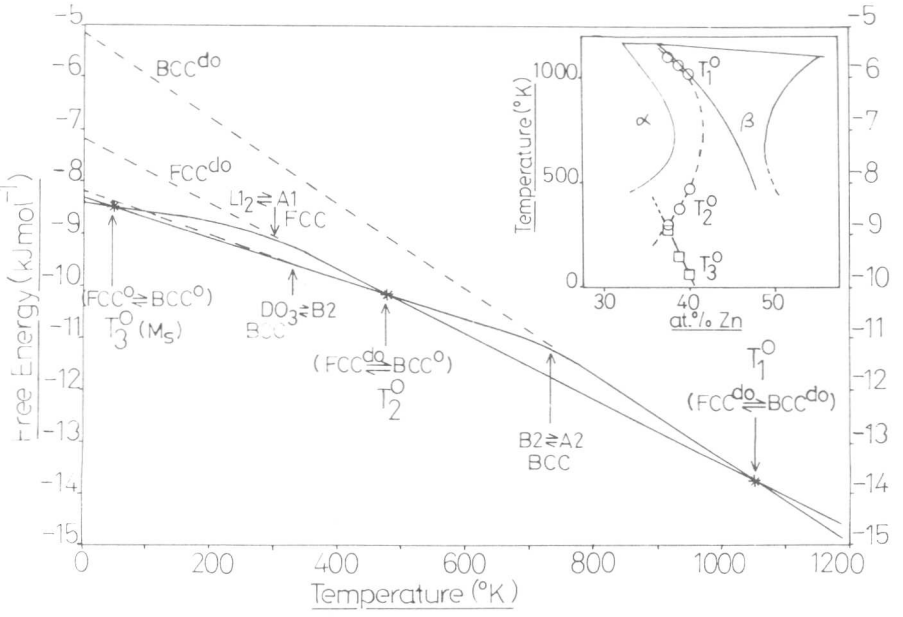

Fig. 4 FCC and BCC Free-Energy Curves for 60/40 Brass

Effect of Temperature on the Martensitic Transformation of CuZnSn Alloys

L. Guzmán[+] and M. Rühle

Martensitic transformations in CuZnSn alloys have been studied by "in situ" observations in a transmission electron microscope fitted with a cold stage. Thin martensite needles appear and grow longitudinally (about parallel to a ⟨112⟩ direction) rather fast. The transverse velocity of growth is 300 times smaller, about $6 \cdot 10^{-2}$ µm/sec. The transverse growth leeds to a final coalescence of adjacent needles. Omega precipitates have been identified. The M_S temperature of the martensitic transformation in thin foils depends on (i) the tin contents of the specimens; (ii) the aging time at room temperature and (iii) the cooling rate in the TEM. Structure and orientation relationship between the martensitic phases and the bcc matrix have been analysed. Some studies were performed concerning the structure of the boundary between matrix and martensite.

I. Introduction

In previous investigations it was tried to determine the variables which control the structure of the martensite formed in a given CuZn alloy. In particular, two sorts of martensite are found in quenched polycrystalline alloys: "thermoelastic" thin needle martensite and "burst" or low temperature martensite [1]. The structure of the thin needle martensite has been recognized to be the same as the structure of low temperature martensite [2], the so-called modified 9R (M9R) structure. The difference between both forms is only morphological, no correlation exists between structure and morphology.

On the other hand it is well known that stress-induced martensite (SIM) grows as narrow parallel bands which coalesce to form thicker bands [3] and eventually a martensitic single crystal. The structure of SIM depends on its mode of formation; it can be identical to low temperature martensite for light deformed specimens, while for higher degrees of deformation it tends to correspond to a more symmetrical structure [4,5].

Max-Planck-Institut für Metallforschung, Institut für Werkstoffwissenschaften, Stuttgart, West Germany

[+]Permanent adress: Instituto de Investigaciones Físicas, Universidad Mayor de San Andrés, La Paz, Bolivia

Little emphasis has been put until now on the kinetics of the spontaneous transformation. The mode of growth should have an important effect on the final morphology and structure of the martensite. It should be possible to follow the nucleation and transformation in a TEM, in which either the temperature of the specimen can be changed or a stress can be applied on the transparent specimen. However, there are experimental reasons why it is not easy to follow the transformation process: (i) The thermal drift of the specimen; (ii) as a consequence of the transformation, the specimen is bent, i.e. the diffraction conditions will be changing during the transformation, and (iii) it is not easy to identify nuclei of the transformation, it may well be that the process starts in an area of the specimen which is not under observation. It may even happen that the martensite does not form at all because of the lack of nucleation sites. This is especially true for thin foils.

The morphology of the martensitic phases observed in CuZnSn alloys does not differ appreciably from the observed one in pure CuZn alloys. Single crystals do not show thin needle martensite, but if the cooling takes place under a small external stress, the burst martensite is preceeded by some thin needles [5]. The kinetics of the transformation seems to be affected by the presence of tin atoms. The burst character can be completely suppressed depending on the cooling rate, also the hysteresis of a transformation cycle is increased and thermal stabilisation phenomena of the β- and the martensitic phase appear.

In this paper TEM observations of the formation, morphology and structure of CuZnSn martensites are reported.

II. Experimental Details

Single crystals of five CuZnSn alloys listed in Table I, were grown by the Bridgman method in sealed quartz capsules, and subsequently quenched from the β-phase region into ice water. Specimens of different orientations and geometries were prepared by spark cutting. Retained martensite could be observed by optical microscopy after aging and straining the specimen, or after a thermal cycle. From the specimens, discs (2.3 or 3 mm diameter) were cut out and thinned electrolytically for TEM work. The same preparation was done with fresh undeformed specimens. The foil normal was parallel to $(100)_\beta$ or $(111)_\beta$.

TEM studies on the strained and precooled ($T < M_s$) specimens were performed in a JEM-200 A electron microscope at room temperature. Retained martensite needles could be identified and analysed. In addition, observations on the formation of martensite were performed in situ in the JEM-200 A fitted with a simple cooling stage, and in a Hitachi

HU-650 high voltage electron microscope, in which a double tilting cooling stage is available and where the cooling rate and the temperature of observation can be controlled.

III. Experimental Results

(1) TEM Observations of the Retained Martensite

Needles of the retained martensite present in pre-strained or pre-cooled specimens of alloy 3 could be observed at room temperature even if the martensitic temperature M_S was much lower than room temperature. The microstructural features of the retained needles produced by both methods are the same. One needle is shown in Fig. 1. From the analysis of the selected area diffraction pattern it can be shown, that the boundary between matrix and martensite (BMM) lies about parallel to a $\{110\}$ plane. Both BMM of one needle are parallel, towards the tip of the needle the two BMM bend together. The direction of the tip is always about parallel to a $\langle 112 \rangle$ direction. In front of the tip a high density of dislocations can be observed. In the BMM parallel dislocations are observed. From contrast experiments (different dark field images) it can be concluded that the strain field of the boundary dislocations is mainly located within the bcc matrix. The SAD pattern of the martensite needle was analysed. The observations are in agreement with the structure proposed by Delaey et al [6]. The fine structure within the needle could be interpreted with the structure of [6]. The microstructure of a martensite needle can best be seen by imaging under dark field condition utilizing a diffraction spot caused by the martensite, Fig. 2. It can be seen that a high density of two dimensional defects is present within the martensite. In some cases, as such presented in Fig. 3, "empty"needles were found. Fig. 3 is a dark field image taken with a martensite reflection. Only the BMM are in contrast. This means that the greatest part of the martensite was removed while along the BMM only a thin layer was retained. In all the specimens, omega phases can be analysed as described by Warlimont et al [7] .

(2) "In situ" TEM Observation of the Formation of Thermal Martensite

Electropolished foils of alloy 5 (Table I) were cooled in the HVEM and the formation of the thermal martensite was observed in situ. It was found, that the temperature at which the transformation starts, M_S, depends on the cooling rate of the thinned specimen. The same specimen was cooled and warmed several times. For a cooling rate $r = 0.2\,^{\circ}C/sec$ M_S was ~130 K while for $r = 1.4\,^{\circ}C/sec$, M_S was ~30 K.

The formation of the martensite follows in two steps. First a thinneedle (with the same orientation relative to the matrix as in III.1) is formed. In front of the tip of the needle moving dislocations are observed. The longitudinal velocity of growth parallel to the tip was determined by evaluating a tape recorded sequence of micrographs. We obtained $v_L \gtrsim 20$ µm/sec. The second step of formation is a growth perpendicular to the original direction of the needle. The velocity of transverse growth is much smaller, $v_T \approx 6 \cdot 10^{-2}$ µm/sec. During the heating the martensite disappears, only a few needles are left, Fig. 4. The temperature of the reverse transformation is close to room temperature.

IV. Discussion

The characteristic temperatures of the martensitic transformation in CuZn and other Cu-based alloys are usually fixed through the composition and the temperatures do not depend on the cooling rates. Only in an aged CuSn alloy, a lowering of the M_s temperature has been reported [8]. This stabilisation of the β-phase in CuSn is explained by the exhaustion of martensite embryos, correlated to the precipitation of a tin rich phase.

We believe that such a precipitation may also be the cause for the rather peculiar behaviour of our alloys. The omega phases which are formed by displacive transformations, are always present in the ß-phases, even in pure CuZn alloys. These omega phases cannot be direct responsible for the stabilisation. We assume that tin rich precipitates which are not identical with the omega have an important interaction with the martensite needles. The precipitates can be observed in foils of orientations different than $\{110\}$. The martensite has the property to dissolve the precipitates in such a way that traces of the needles can still be identified after the completion of the reverse transformation. The transformation itself is never complete and single transformation events continue after the specimen has reached a given temperature. An explanation for retained martensite in the boundaries (Fig. 3) is that the interface movement during the heating may be constrained by the segregation of tin atoms to the boundary.

The velocity of longitudinal growth that we have been able to measure, $v_L \gtrsim 20$ µm/sec, is great respective to the transverse velocity but it is infinitesimal compared with the theoretical prediction, which is 1/3 of the velocity of sound. The slowness of the growth in this alloy may be explained through the pinning of the precursor dislocations, or matrix hardening. The strong dependence of M_s on the cooling rate is the most striking feature. It seems that the transformation needs a certain time to progress, which may not be available during a rapid cooling. The growth may then be limited by the atom mobility. The pure diffusionless character of the transformation is thus questionable.

Acknowledgements

One of the authors (L.G.) is indebted to the Alexander von Humboldt Foundation for providing a grant. We would like to thank L. Bitzek and A. Strecker for their support during the experimental part of the work.

References

1 Pops, H., Trans AIME, 239 (1967), 756
2 Wayman, C.M., Scripta Met., 11 (1977), 1023
3 Wayman, C.M., in "Shape Memory Effects in Alloys", Ed. J. Perkins, N.Y. (1975), 15
4 Flewitt, P.E.J., Metallography, 2 (1969), 277
5 Guzmán, L., Annual Meeting of the Deutsche Gesellschaft für Metallkunde, Innsbruck, 1978, to be published
6 De Vos, J., Aernoudt, E. and Delaey, L., Z. Metallkde., 69 (1978), 438
7 Prasetyo, A., Reynaud, F. and Warlimont, H., Acta Met., 24 (1976), 1009
8 Kennon, N.F., Metal Sc. Journal, 6 (1972), 64

Table I. Composition of the CuZnSn Alloys used (in at %) and their M_s, M_b temperatures (in K)

Alloy	Cu	Zn	Sn	M_s	M_b
1	60	40	-	80	-
2	61	38.5	0.5	-	113
3	61.9	37.1	1	145	136
4	62.9	35.6	1.5	-	170
5	63.9	34.1	2	210	200+

+in fresh quenched bulk specimens

120 K 290 K 300 K

Fig. 4. TEM micrographs showing the reverse transformation of a martensite needle

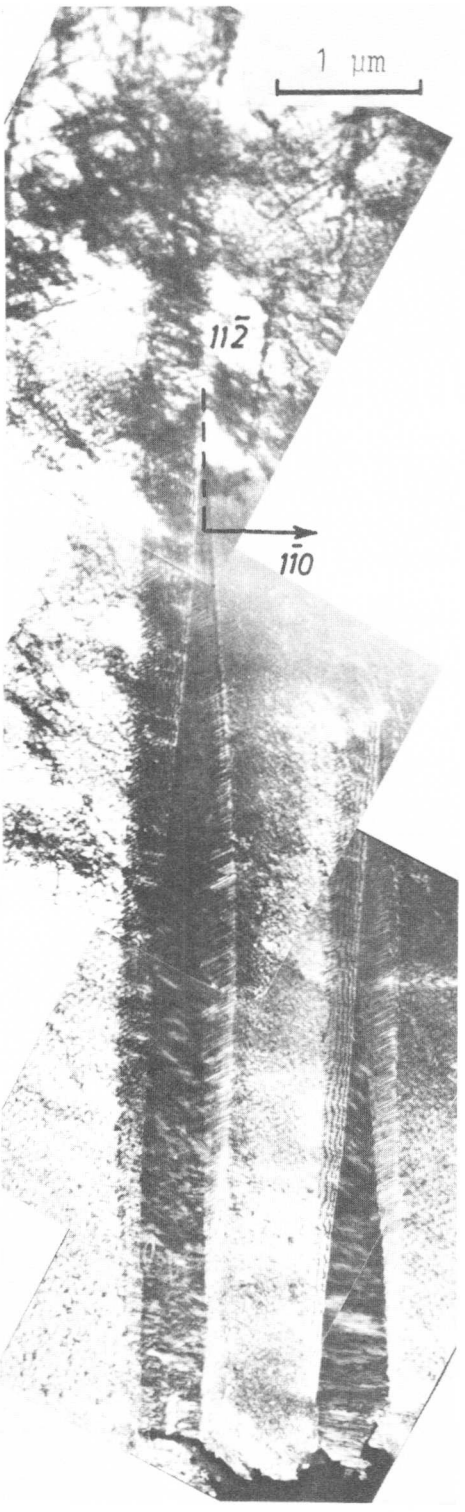

Fig. 1. TEM electron micrograph of a tin martensite needle with dislocations in the surrounding matrix. Foil orientation (111)

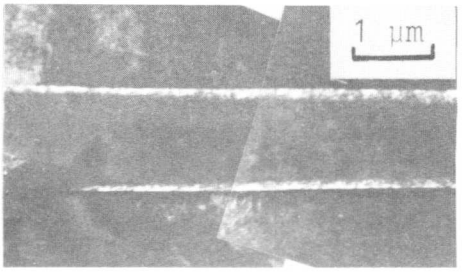

Fig. 3. Dark field image of an "empty" needle

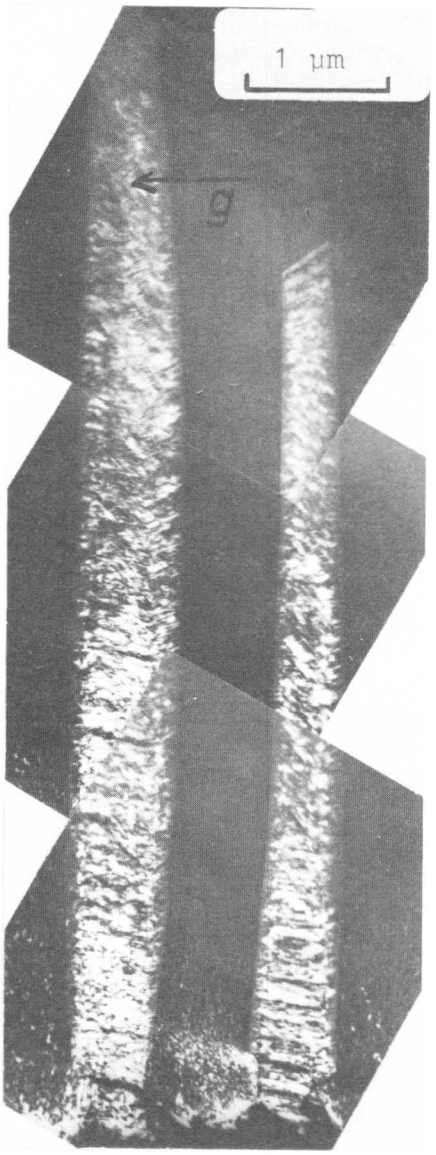

Fig. 2. Dark field of the needle as in Fig.1, showing high density of defects within the martensite

The Influence of Thermal Treatments on Martensitic Transformation in Cu-Zn-Al Alloys

R. Rapacioli* and M. Chandrasekaran*

Abstract: Thermal treatment of β Cu-Zn-Al alloys in the region of β instability (~400°C), immediately following solution treatment and quenching, produce γ precipitates. A widening of the resistance as well as stress hysteresis during subsequent transformation of β to martensite on cooling and stressing respectively is observed in such thermally treated alloys. In addition the M_s-M_f difference on cooling and transformation hardening during stressing are also increased. The utility of the thermal treatments in altering the damping characteristics of the alloy is considered.

I. Introduction

Cu-Zn-Al alloys undergo a martensitic transformation on quenching or after quenching at lower temperatures. Short time thermal treatments at around 250-300°C (flash heating) have been shown to shift to lower values, immediately after the treatment, the temperatures characterising the martensitic transformation. The original pre-treatment values are however recovered on ageing, in the β condition, at temperatures as low as room temperature [1-5]. The thermal treatment has been shown to shift all the characteristic temperatures equally, thereby leaving the hysteresis due to the transformation cycle unaltered.

Recent investigations, which will be reported here, indicate that transformation hysteresis is altered on thermal treatments at a slightly higher temperature. The treatment and the associated changes produced in the alloys are presented in some detail.

II. Experimental Procedure

Cu-Zn-Al alloys were prepared by melting together the component metals of high purity in sealed quartz tubes. Single crystals of the alloys were subsequently grown in quartz tubes by the Bridgman technique. The crystals were then spark machined to two different forms:

i) cylindrical lengths of 20 mm and 2.8 mm diameter to be used for resistance measurements and for providing samples for electron microscopy; and

ii) 2.8 mm diameter and 20 mm gauge length samples with 6 mm shoulders at the ends to serve as samples for tensile testing.

The spark machined pieces were solution treated at 800°C and quenched into iced water at 5°C. After property measurements, the same samples were again solution treated at 800°C, quenched into iced water at 5°C. Immediately after this treatment the samples were heated to around 400°C and maintained at this temperature for 10 seconds, 30 seconds or 3 minutes and then quenched into the iced water.

---

* Centro Atómico Bariloche, Comisión Nacional de Energía Atómica, 8400 S.C. de Bariloche, Argentina

The standard four probe technique was used for resistance measurements. The copper leads were spot welded to the sample as also a chromel alumel thermocouple to the middle part of the sample. A constant current generator was used to drive a current of 100 mA through the sample. The potential drop across the sample was measured by a Keithley 148 Nanovoltmeter that had provisions for zero suppresion and amplification. The amplified output of the Nanovoltmeter after the initial nulling was fed to the y-channel of an x-y recorder; the thermocouple leads were directly connected to the x-channel of the recorder.

The sample with its leads was surrounded by three coaxial glass tubes. The outer tube was then cooled in direct contact with liquid nitrogen in a dewar, and the sample inside could thus be cooled gradually. Lowering the dewar with the liquid nitrogen led to gradual warming up of the tubes and the sample inside it. Cooling and heating rates less than 3°C/minute were possible with this arrangement. Continuous recordings of resistance as a function of temperature were thus obtained with the x-y recorder.

Samples for electron microscopy were obtained by further spark cutting from the 2 cm lengths, slices of 0.2 mm. The resulting discs (2.8 mm diameter and 0.2 mm thick) were first dished by jet polishing with an electrolyte of 20%H_2SO_4 in methanol. Final electropolishing was carried out in a solution of 15%HNO_3 in methanol.

The tensile specimens were tested at room temperature (~20°C) using an Instrom Testing machine.

III. Results

A minimum of 2 days at room temperature (~20°C) was allowed after each thermal treatment prior to measuring the electrical resistance and mechanical behaviour. This was intended to obviate the transient effects that dilute disorder, produced after quenching, has on the M_s and other characteristic temperatures of the transformation [1-5].

Figure 1 shows a comparison of the transformation temperatures and the hysteresis produced in a sample quenched from 800°C and in the same sample after it is subjected to treatment around 400°C for 10 seconds, immediately following solution treatment at 800°C. In figures 2 and 3 are shown the same comparison but for different samples and for differing times of treatment at 400°C, viz., 30 seconds and 3 minutes respectively. The following observations can be made from the figures:

i) the transformation hysteresis is always wider when the sample is subjected to the 400°C treatment than without it;
ii) in samples subjected to 400°C treatment, hysteresis is wider, the longer the time of treatment;
iii) the transformation temperatures and therefore the position of hysteresis after 400°C treatment with respect to that in just solution treated samples are shifted, the direction of shift depending upon the time of treatment at 400°C eg. M_s temperature is shifted to lower values for 10 and 30 second treatments, whereas after a 3 minute treatment M_s is shifted to higher temperatures;
iv) the M_s-M_f difference is increased in samples subjected to the 400°C treatment.

The increase in transformation hysteresis after giving the sample a treatment at 400°C is also evidenced on stress inducing the martensite. Pseudoelastic curves from the same sample with and without the 400°C treatment are shown in figures 4a. and 4b. respectively where the change in hysteresis is clearly observable. The figures also indicate that transformation hardening is enhanced with the 400°C treatment. This is analogous to the increase in M_s-M_f difference on cooling and mentioned earlier.

Electron microscopy of the samples after the 400°C treatment has revealed the presence of precipitates in β matrix. These are shown in figures 5 and 6 for different treatment times, 10 seconds and 3 minutes respectively. The precipitates have been identified as those of γ phase from the characteristic tripling of the cell dimensions of β observed in electron diffraction patterns.

IV. Discussion

It is obvious that hardening during transformation and the increment in transformation hysteresis are to be attributed to the presence of γ precipitates. The manner in which γ effects these changes are however of interest.

Transformation normally occurs in Cu-Zn-Al alloys by the growth of favourable nuclei, that leads to a self accomodating configuration of plates which minimizes shape deformation. If the presence of γ precipitates restricts the growth of some of these favourable nuclei, transformation through growth of alternate variants could lead to a less self accomodated martensite and therefore increased shape deformation. More energy is then to be stored in the material in accomodating the extra strain. This increase in elastic strain energy due to the interaction of less-self accomodating plate variants could then explain the observed transformation hardening.

The factor responsible for the enhanced hysteresis could be the mobility of the β-martensite interface. The γ precipitates may constrain a growing plate to assume an interface that deviates from the usual undistorted habit plane interface, eg., a more lenticular shape. Motion of such interfaces requires more energy which is however dissipated.

These inferences drawn here are consistent with the conclusions of Ahlers et al. [6] concerning the factors responsible for energy dissipation and transformation hardening in β-Brass martensites.

It must be emphasised at this point that the sequence of treatments must be strictly adhered to, in producing γ precipitates. The first quenching from 800°C and the following rapid heating to 400°C are essential in this respect, as it was oberved that direct quenching from 800°C to 400°C did not result in production of γ, even after substantially longer holding times as 60 minutes. It is well known that γ-Brass structure consists of some vacant lattice sites [7] and the production of considerable amount of vacancies during the first quench from 800°C may be responsible at least in enhancing the rate of γ formation.

More work, however, is needed in further understanding these effects, as also the shifts in M_s for longer and shorter treatments at 400°C.

As regards the latter effect, it is possible that the longer 3 minutes treatment at around 400°C produces equilibrium γ with corresponding composition changes in β. This would lead to leaner solute contents in β, thereby accounting for the higher M_s temperature.

The possibility of manipulating the transformation hardening and hysteresis may have some interesting implications regarding the application of this alloy in sound damping devices. It has been shown [8] that damping capacity can be evaluated by the ratio of the area enclosed between the stress-strain curves in loading and unloading, to the total area under the loading curve. Though this ratio can be increased with the thermal treatment suggested here, one must also consider the effect of transformation hardening. In this connection, it may not be possible to enhance the peak damping capacity in the transformation region. However, the transformation hardening and the M_s-M_f difference may be of some help in widening the transformation region at the expense of a decrease in peak damping. This region could then be effectively used for damping at small stress amplitudes. Internal friction studies are at present being conducted to evaluate the damping capacity of the alloys after different thermal treatments. Results of this study will soon be reported.

Acknowledgements: The authors wish to thank Dr. Ahlers for many helpful discussions and a critical reading of the manuscript and Lic. C. Lovey in helping with the electron microscopy. This work was partially supported by the Organization of American States through the Multinational Program of Physics.

REFERENCES

[1] R. Rapacioli, M. Chandrasekaran and L. Delaey, in "Shape Memory effect in alloys", ed. Jeff Perkins, Plenum Press, New York, 1975.
[2] R. Rapacioli and M. Ahlers, to be published in Acta Met.
[3] M. Chandrasekaran, T.A. Bhaskar and R.V. Krishnan. Annual Meeting of the Indian Institute of Metals, Poona, 1976.
[4] D. Schofield and A.P. Miodownik in "Copper 77".
[5] J.M. Cook and L.M. Brown, Scripta Met., 12, 949 (1978).
[6] M. Ahlers, R. Pascual, R. Rapacioli and W. Arneodo, Matts. Sci. Engg. 27, 49 (1977).
[7] C.S. Varrett and T.B. Massalski, "The Structure of Metals", McGraw Hill, New York.
[8] W. Dejonghe, L. Delaey, R. De Batist, and J. Van Humbeck, Met. Sci. J., 11, 523, (1977).

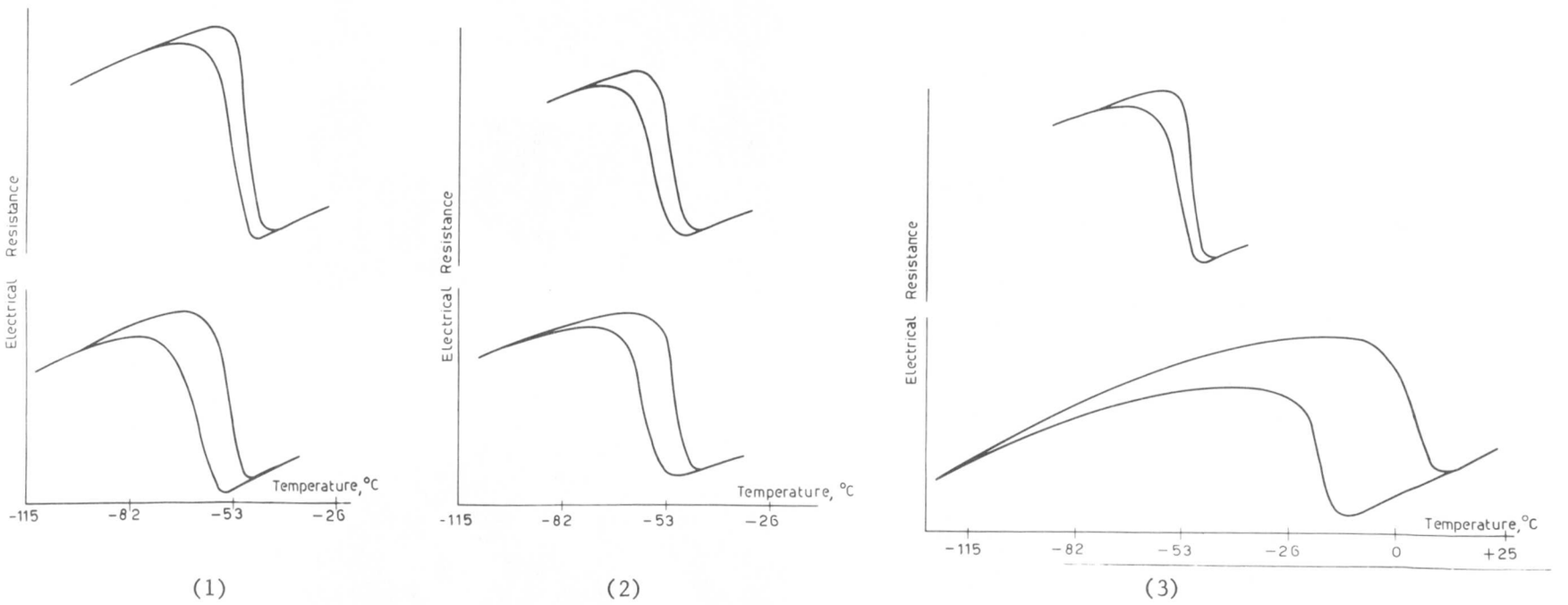

Figures 1 to 3: Transformation hysteresis in samples quenched from 800°C and in the same samples after the 400°C treatment: for 10 seconds (Fig. 1), 30 seconds (Fig. 2) and 3 minutes (Fig. 3).

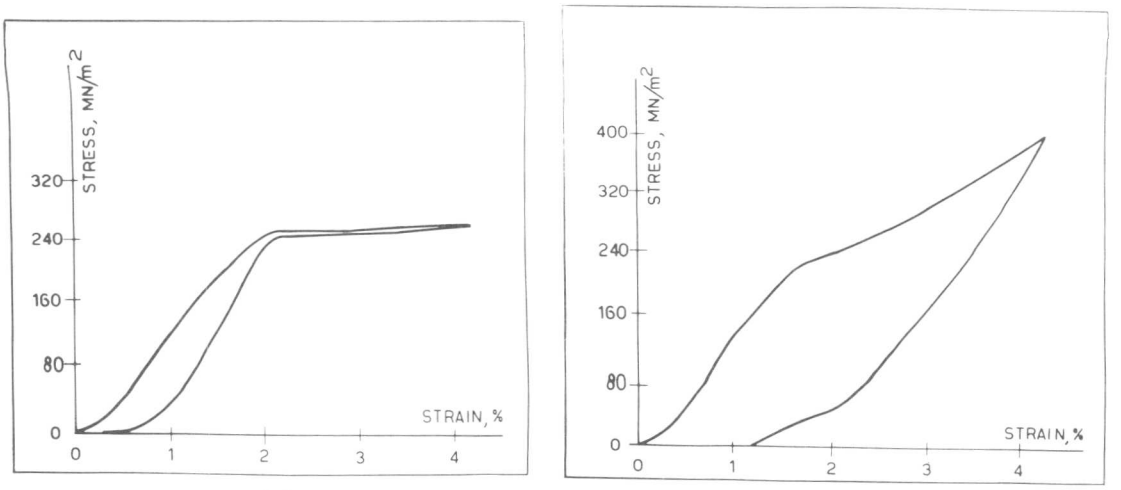

(a) (b)

Figure 4: Stress-strain curves of stress induced martensite in (a) sample quenched from 800°C, (b) sample further subjected to treatment at 400°C for 3 minutes.

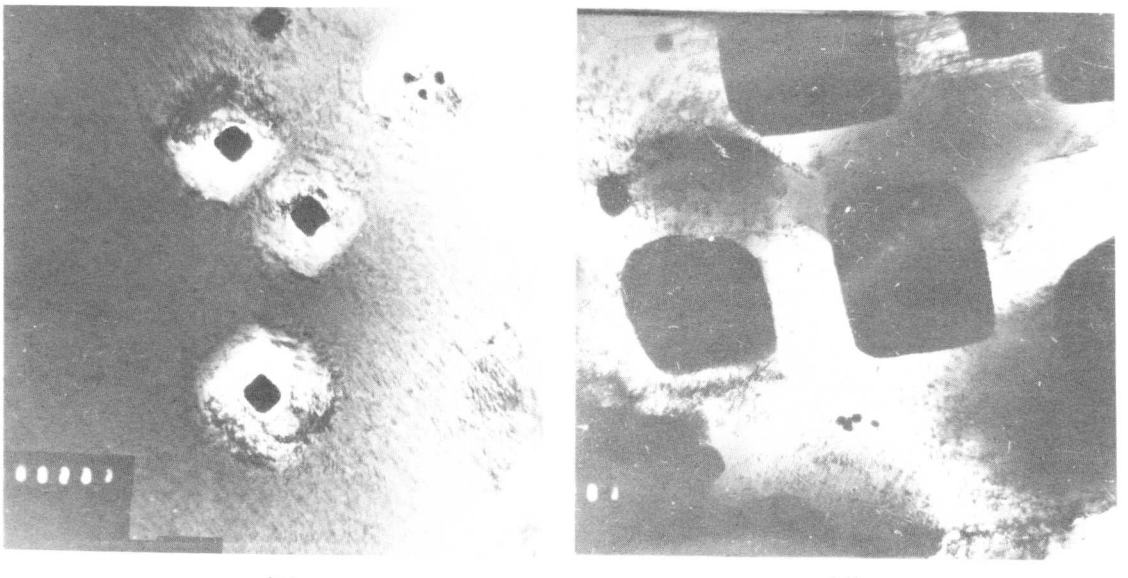

(5) (6)

Figures 5 and 6: γ precipitates in β matrix after treatment at 400°C for 10 seconds (Fig. 5) and 3 minutes (Fig. 6).

Magnification: 1 cm = 1 μ

Formation and Decomposition of Metastable Phases in Some Titanium-Vanadium Alloys

M.H.L. Gomes*, H.M. Flower+, D.R.F. West+

The structure and hardness of Ti-V alloys, containing 7, 12 and 16 wt %V respectively have been investigated after quenching from the β field to room temperature and subsequent ageing. In the 7 %V alloy, quenching produced α' hcp martensite which, on ageing precipitated β with little hardening. The quenched 12% V alloy contained α'' orthorhombic martensite, which decomposed spinodally on ageing, and also showed some reversion to β at 525°C. Ageing produced substantial hardening. The quenched 16% V alloy contained β + ω and ageing led to further ω precipitation with considerable hardening.

I. Introduction

Transition elements, such as Mo, Nb and V, stabilize the β phase of titanium. Some metastable phases (α', α'', ω and β) are formed after quenching the high temperature β phase to room temperature [1]. Complex microstructural changes can occur in such metastable phases upon ageing. The present paper reports an investigation of structural features of these transformations in some Ti-V alloys and the associated hardness changes.

II. Experimental Procedure

Three Ti-V alloys containing 7, 12 and 16 wt %V respectively were prepared by argon arc melting, using high purity titanium sponge and 99.9% pure vanadium. The ingots were rolled at 600°C into 0.65 mm thick sheets. Sheet specimens were mechanically polished, wrapped in Mo foils and encapsulated in silica under argon. They were then solution treated at 1100°C (β field) for 0.5 h and quenched into water, the capsules being broken during quenching. Ageing treatments were performed for times from 10 to 10 000 min, and at temperatures from 375°C to 600°C (α+β field); all the specimens were water-quenched after ageing. Most treatments were repeated twice. The effect of heat treatments was studied by light microscopy, x-ray diffraction, transmission electron microscopy and hardness measurements.

III. Results and Discussion

(1) As-Quenched Specimens

The variation of hardness with composition is shown in Fig 1. Light microscopy revealed that both 7 and 12 %V alloys had transformed martensitically (Figs 2 and 3) while the 16 %V alloy consisted of retained, equiaxed, β grains. (Fig 4).

* CETEC, Belo Horizonte, MG, Brazil
+ Imperial College, London, UK

Martensite Formation: X-ray analysis showed that in agreement with previous work [1] the 7% V alloy consisted of α' hcp martensite, with c/a = 1.585; there was also a small amount of retained β resulting from diffusion during quenching, the Ms temperature being high [2]. The x-ray analysis of the 12% V alloy showed the α' lines split in two (Table I). Considering a distortion of the hexagonal cell to an orthorhombic one [3] all the lines can be accounted for in terms of an α'' martensite (a = 2.91, b = 5.09, c = 4.64A). The detection of orthorhombic martensite in this system has previously proved difficult [1, 4, 5]. Bagariatskii [6] suggested its occurrence in the composition range 9-10 wt %V. Flower et al [7] observed its formation in a Ti-10.6 wt %V alloy and this result together with the present data suggest that α'' occurs in binary Ti-V alloys containing from ∿10 to 12 wt %V. The difficulty in detecting α'' may be due to its composition range being very narrow in the Ti-V system. A similar narrow range of α'' formation is observed in Ti-Mo [7] whereas it has a large compositional range in Ti-Nb [7] and Ti-Ta [8]. The relative stabilities of the α' and α'' forms of martensite have recently been considered in relation to Ti-Mo by Davis et al [9].

Omega Formation: ω was present in the as-quenched 16 %V samples: this accounts for the relatively high hardness shown in Fig 1. The 16 %V alloy showed slight but reproducible age hardening at room temperature (Fig 5). X-ray analysis of this alloy carried out three months after quenching showed a β+ω structure, but with one line, (the first one), not fitting the ω d-spacings (Table I); this line has not been accounted for and electron microscopy revealed the presence of only β and ω. It is believed that room temperature growth of the ω present after quenching may be responsible for the observed hardening.

(2) Aged Specimens

Ti-7 wt %V: This alloy, on ageing, showed only slight hardening followed by overaging (Fig 6). X-ray analysis and electron microscopy indicated that α' martensite decomposed by heterogeneous precipitation of β within α' except at the lowest ageing temperature where homogeneous β precipitation took place.

Ti-12 wt %V: Although relatively soft in the as-quenched condition, this alloy exhibited a strong ageing response (Fig 7). The greatest hardness (∿410 Hv) was achieved at the lowest ageing temperature (375°C). Light microscopy did not resolve the structural changes responsible, but electron microscopy showed the presence of a fine periodic precipitate dispersion within the martensite plates (Fig 8). Similar dispersions in Ti-Mo [10] have been attributed to spinodal decomposition of the α'' phase and the present observations are consistent with this hypothesis. Ageing at 450 and 525°C caused the peak to occur at lower hardness values and shorter times. X-ray examination of overaged specimens at these temperatures showed α and β phases. The 600°C ageing curve is close to that at 450°C. Both light microscopy and x-ray diffraction showed evidence of the reversal of α'' to β at 600°C; hardening is produced by heterogeneous precipitation of α particles from β.

Ti-16 wt %V: Fig 9 shows the variation of hardness with ageing time and temperature in the range 375-600°C. Very high values are attained at 375°C. For t = 10^4 min there are clear diffraction lines of α, β and ω (Table I). ω is hexagonal with c/a = 0.610. Light microscopy shows a greyish surface and hydrides in the β grains (Fig 10) resulting from electropolishing. Hydride formation seriously hampered transmission electron microscopy of material which had been only lightly aged. However, the cuboidal morphology of the ω could be clearly seen in samples aged for longer times (Fig 11). Ageing at 450°C gave relatively little hardening and the overaged specimen showed a fine dispersion of α particles in β. At 525°C the alloy softened without showing any hardening and the light microscopy showed a dense dispersion of α particles in β. At 600°C the overaged alloy showed a coarser distribution of α precipitates, lenticular in shape (Fig 12).

Acknowledgements are made to Professor J.G. Ball for the provision of research facilities at Imperial College. One of the authors (M.H.L.G.) acknowledges the award of a scholarship from the British Council and the financial support from CNPq for attending the ICOMAT-79.

Table I d-spacings (Å) for phases present in some Ti-V alloys

7% V	d	2.54	2.34	2.30	2.23	1.72	1.63	1.48	1.33	1.26
as-	α'planes	100	002		101	102		110	103	112
quenched	β planes			110			200			
12% V	d	2.54	2.48	2.32	2.23	2.20	1.72	1.70	1.48	1.45
as-	α''planes	020	110	002	021	111	022	112	130	200
quenched	(α')	100		002	101		102		110	
16% V	d	2.65	2.29	1.62	1.41	1.33	1.21	1.57	1.03	0.96
as-	β planes		110	200				220	310	
quenched	ω planes	?	110	201	002	121	112	220		302
16% V	d	2.80	2.54	2.30	2.24	1.78	1.72	1.63	1.59	1.41
375°C,	β planes			110				200		
10^4min	ω planes	001		110		111			201	002
	α planes		100		101		102			111

References

[1] J.C. Williams: "Ti Science and Technology", Plenum Press, 3(1973), 1433.

[2] F.R. Brotzen, E.L. Harmon and A.R. Troiano: Trans, ASM, 48(1956), 774.

[3] A. Kelly and G.W. Groves; "Crystallography and Crystal Defects", Longman, London, 1970.
[4] D.W. James and D.M. Moon: "The Science, Technology and Application of Titanium", Pergamon Press, (1969), 767.
[5] M. Oka, C.S. Lee and K. Shimizu: Met. Trans., 3(1972), 37.
[6] In. A. Bagariatskii, G.I. Nosova and T.V. Tagunova: Kristallografiia, 3(1958), 17.
[7] H.M. Flower, R. Davis and D.R.F. West: Proc. 3rd Int. Conf. on Ti, Moscow, 1976.
[8] K.A. Bywater and J.W. Christian, Phil. Mag. 25(1972), 1275.
[9] R. Davis, H.M. Flower and D.R.F. West: J. Mat Sci, 14(1979), 712.
[10] R. Davis, H.M. Flower and D.R.F. West: Acta. Met., 27(1979), 1041.

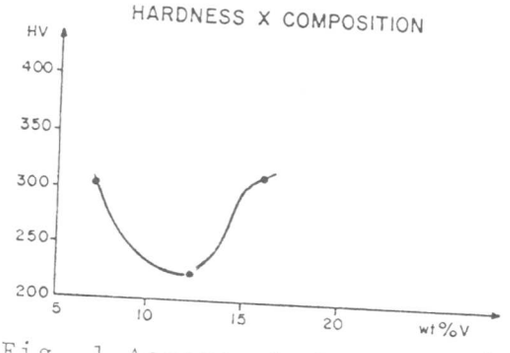

Fig. 1 As-quenched alloys

Fig. 2 Ti-7wt %V, as-quenched

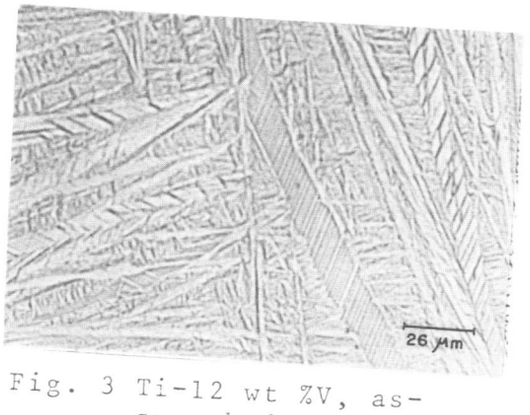

Fig. 3 Ti-12 wt %V, as-quenched

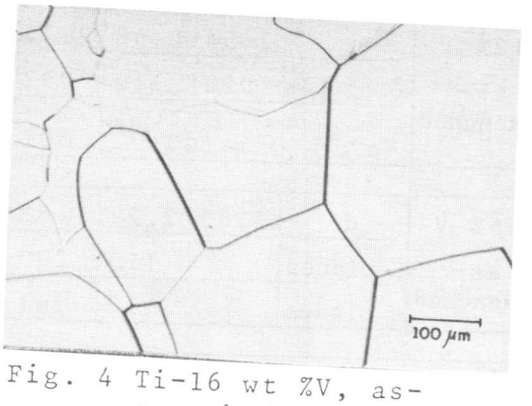

Fig. 4 Ti-16 wt %V, as-quenched

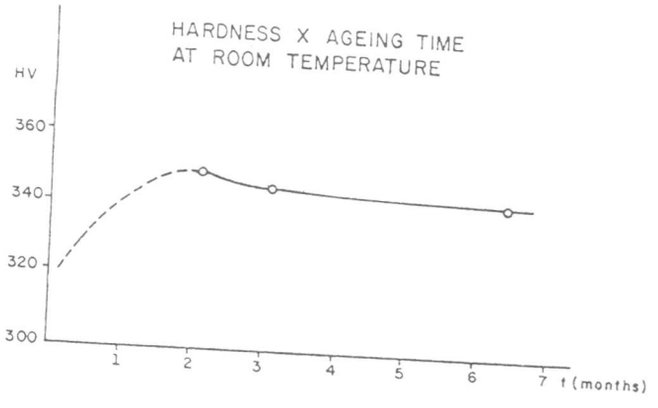

Fig. 5

Ti-16 wt %V, aged at RT